Studies on the Characteristics *of* Tropical Tropopause

Thesis submitted to
Cochin University of Science And Technology

in partial fulfillment for the award of the Degree of

Doctor of Philosophy
in
Atmospheric Sciences

By

Sanjay Kumar Mehta

Department of Atmospheric Sciences
School of Marine Sciences
Cochin University of Science And Technology
Cochin-682016
Kerala, India

April, 2010

Studies on the Characteristics
of
Tropical Tropopause

Thesis submitted to
Cochin University of Science And Technology

in partial fulfillment for the award of the degree of

Doctor of Philosophy
in
Atmospheric Sciences

By

Sanjay Kumar Mehta

COCHIN UNIVERSITY OF SCIENCE AND TECHNOLOGY

Department of Atmospheric Sciences
School of Marine Sciences
Cochin University of Science And Technology
Cochin-682016,
Kerala, India

April, 2010

Dedicated

to

B.V. Krishna Murthy

DECLARATION

I hereby declare that the thesis entitled "**Studies on the Characteristics of Tropical Tropopause**" is an authentic record of the research carried out by me under the supervision of Dr. K. Mohankumar, Department of Atmospheric Sciences, Cochin University of Science And Technology and that no part of it has previously formed the basis for award of any Degree, Diploma, Associateship, fellowship or any other similar title or recognition in any University.

Sanjay Kumar Mehta

Senior research fellow
National Atmospheric Research Laboratory
Dept. of Space, Govt. of India
Gadanki-517502, AP.India

COCHIN UNIVERSITY OF SCIENCE AND TECHNOLOGY
DEPARTMENT OF ATMOSPHERIC SCIENCES
Lakeside Campus, Fine Arts Avenue, Cochin - 682 016, India.

Dr. K. Mohankumar *M.Sc., Ph.D.*
Ex-Dean, Faculty of Marine Sciences
Professor in Atmospheric Sciences

CERTIFICATE

This is to certify that the thesis entitled **Studies on the Characteristics of Tropical Tropopause** submitted by ***Mr. Sanjay Kumar Mehta*** is an authentic record of research work done by the candidate under my supervision in the Department of Atmospheric Sciences, School of Marine Sciences, Cochin University of Science and Technology, Cochin 682 016, India. I further declare that subject matter of his thesis work is original and has not formed the basis for the award of any Degree, Diploma, Associateship or any other similar title in any University or Institution.

I also certify that Mr. Sanjay Kumar Mehta has passed the Ph. D. qualifying examination conducted by the Department of Atmospheric Sciences, Cochin University of Science and Technology in August 2009.

Mohankumar K.

Prof. K. Mohankumar
Supervising Guide

Cochin 682016
April 16, 2010

Tel: 91-484-2372401(Dir), 2353662 (Off.), Fax: 91-484-2374164; Mobile: 9447157370, 2340995(Res.) E-mail: kmk@cusat.ac.in, kmkcusat@gmail.com

Acknowledgements

*First of all I would like to express my sincere gratitude to **Dr. K. Mohankumar**, Ex Dean, Faculty of School of Marine Sciences and Professor, Department of Atmospheric Sciences, Cochin University of Science And Technology (CUSAT), Cochin, Kerala, who was my teacher and became supervisor since the beginning of my study in atmospheric sciences. He devoted his valuable time and provided many helpful suggestions which found to be very helpful in construction of the thesis. Without his constant support, readiness to provide the required facilities, it would have been extremely difficult to finish this work on time. Further, I would like to thank him for writing such a nice book on the Stratosphere-Troposphere interactions which helped me a lot in writing the thesis.*

*I am not right person to write anything about my guide **Dr. B.V. Krishna Murthy**, my knowledge is still very less to express the sincere thanks to him. I am deeply impressed with his sense of humor towards science, his teaching experience and basic knowledge in physics and mathematics. His well focused and sincere attitude leads me to work thoroughly on my topic of research. He had never said no for my any kind of the help and he had always ready to support me. He shows me the way to think in right direction and way to approach scientific problems. I am extremely thankful to him for sparing his valuable time and going through my thesis and making useful corrections and suggestions. Without him, I doubt that this thesis would ever have been written. Also, I would like to express deep sense of gratitude towards Mrs. Krishna Murthy. She loved me as like her own child.*

*I would like to express my deep sense of gratitude to **Dr. M. Venkat Ratnam**, for his invaluable guidance, constant support, and encouragement not only in my research but in personal life also. His techniques and ideas to work gave me lots of learning while working with him. He spends lots of time to discuss the scientific matter, in writing paper and supporting all the way. He provided all kind of the data and material useful for my research. I am extremely thankful to him for sparing his valuable time and going through my thesis and making useful corrections and suggestions. Without his constant support, it would have been extremely difficult to finish this work*

*I would like to express my sincere gratitude to **Prof. K. R. Santosh**, Head, Department of Atmospheric Sciences, School of Marine Sciences, Cochin University of Science And Technology, Cochin, Kerala, for providing necessary suggestions to complete to university requirements.*

*I would like to thank **Prof. A. Jayaraman,** Director, National Atmospheric Research Laboratory (NARL), for providing necessary facilities and supports. I would like to thank him for creating the nice environment for the independent research without any extra load beside the research work, which lead me to focus on my thesis work.*

*I express my deep sense of gratitude to **Prof. D. Narayana Rao**, former Director, NARL for selecting me for my research carrier and assigning me to carry out the research work on the topic which I finished as my thesis.*

*I would like to express my sincere gratitude to **Prof. H. S. Ram Mohan**, Dean, School of Marine Sciences, Cochin University of Science And Technology, Cochin Kerala, for providing necessary suggestions.*

My profound gratitude goes to ***Prof. P. Balarama Rao, Dr. M. Rajeevan, Shri S. Raghavan, Prof. Tsuda, Prof. J. Röttger****,* ***Prof C. J. Pan, and Dr. M. S. Narayanan*** *for their discussions and cooperation in this study.*

I would like to thank ***Dr. A. K. Patra*** *for his well focused attitude towards research that inspired me lot to work in an organized way. I am extremely grateful to* ***Dr. V. K. Anandan, Mr. P. Srinivasulu, Mr. T. V. C. Sarma, Dr. T. Narayana Rao, Dr. T. K. Ramkumar, Mr. Raghunath, Mr. Bhavani Kumar, Mr. T. Rajendra Prasad, Dr. S. Sridharan, Dr. Amit P. Kesarkar, Dr. Alok Taori, Dr. Nirvikar Dashora, Mrs. Yashoda, Mrs. Jyoti Bhate,*** *for supporting me on various way during my research carrier.*

I am extremely grateful to ***Dr. C. A. Babu, Mr. Baby Chakrapani, Dr. Madhu, Dr. Sridevi, Dr. Venu G., Dr. Bindu G.,*** *and all other teaching and non teaching staffs of the Department of Atmospheric Sciences, School of Marine Sciences, Cochin University of Science And Technology, Cochin, Kerala, for helping several way in completion of my thesis work.*

I express my sincere thanks to my senior colleagues ***Dr. K. Kishore Kumar, Dr. Siddarth, Dr. K. Mohan, and Dr. NVP Kiran Kumar*** *for their suggestions during beginning of my research carrier. I express my sincere thanks to my dearest friends and colleagues* ***Dr. N. Venkateswara Rao, Dr. Radha Krishna, Mr. Debashis Nath, Ms. Padma, Dr. K. N. Uma , Dr. D. V. Phani, Kumar, Mr. M. Shravan Kumar, Mr. S. Ghouse Basha, Mr. T. Mohana Satyanarayana, Mr. K. Niranjan Kumar, Mr. S. Satheesh Kumar, Mr. G Hari, Mr. Jayant, Mr. Ravi Kiran, Dr. Abhijeet Chaterjee, Mr. Lalit Mohan Joshi, Mr. Unnikrishnan, Mr. Sai Suman, Ms. Leena, Ms. Madhulatha, Ms. Saikranthi, Mr. Mahesh*** *and S.V.U colleagues* ***Dr. A. Nrendra Babu****,* ***Dr. G. Kishore Kumar, Mr. A. Srikanth, Mr. M. Roja Raman,*** *and CUSAT colleagues****, Dr. Abhilash, Dr. Prasant, Mr. Jhonson, Mr. Rajesh, Ms. Lorna, Mrs. Asha, Mr. Abish, Mr. Vijaykumar, Mr. Nithin, Mr. Sandeep, Mrs. Reshmi and Ms. Aneela*** *for their encouragement and kind assistance throughout the work. The warm support of all my friends enabled me to complete this thesis and have a wonderful time along the way.*

I would like to express my sincere thanks to one and all working in various sections of NARL viz., ***Administration, Accounts, CMD, Canteen,*** *and* ***Security*** *for their kind cooperation in many aspects.*

I would like thank to ***ISRO*** *and* ***NARL*** *for providing me the fellowship under* ***CAWSES-India program*** *to carry out my research work. Also I would like to thank for arranging the necessary documents during my visit for the national as well international conferences.*

My deepest gratitude goes to my family, my parents ***Mr. R. L. Mehta*** *and* ***Sita Devi****, brothers* ***Shyam Mehta*** *and* ***Rajesh Mehta****, and my sisters* ***Supriya*** *and* ***Renu*** *who have encouraged me so much in my life and helped me become the person that I am today. They have showered me with love, kindness and care and have always been supportive of me in perusing my dreams.*

I want to thank my loving wife ***Binita Mehta****. She has the magic to bring a smile on my face and peace in my heart, even in hardest times.*

At last but not least, I would like to thank almighty GOD who always made me stronger during the difficult situations.

Sanjay Kumar Mehta

Preface

The tropopause is one of the most basic features of the temperature structure of the earth's atmosphere. However, it is not clearly understood what exactly determines the height of the tropopause, why tropopause exists in different form such as sharp, broad and multiple in some places. What maintains the tropopause is intimately related to stratosphere-troposphere exchange process which determines the chemistry of both troposphere and stratosphere. This is, however, an important gap in our understanding of the general circulation.

The doctoral thesis entitled "**Studies on the Characteristics of Tropical Tropopause**" contains eight chapters. This thesis presents results on the characteristics of the tropical tropopause parameters such as cold point tropopause (CPT), lapse rate tropopause (LRT), convective tropopause (COT) and topical tropopause layer (TTL) and their association with convections and planetary wave activities over the tropical region, with special emphasis over Indian monsoon region.

To understand the features of the tropical tropopause, the complete account of the factors which affect its properties are briefly presented in Chapter-1. The effect of the solar cycle, El Niño southern oscillation, and quasi biennial oscillations on the annual and intra-annual variation on tropical tropopause is mentioned. Coming down to the scale of variability such intraseasonal variation due to Madden Julian Oscillation (MJO) to short scale variation such as day-to-day variation due planetary waves is also discussed. The stratosphere and troposphere exchange related term such as Brewer Dobson circulation and fountain hypothesis are explained, finally thesis layout are outlined.

Chapter-2 provides a brief introduction to various instruments such MST radar, GPS radiosonde and GPS radio occultations (RO) used for the present study. This chapter also provides in detail about data analysis techniques and methodology, such as wind, temperature and divergence calculation from radar and various atmospheric parameter from RO data.

A comparison between the altitudes of the top of convection identified from MST radar and radiosonde is presented in the Chapter-3. Physical basis of the observed correlation between the altitude of the convective outflow from radar and radiosonde are described in the same. The TTL thickness variation is also discussed.

In Chapter-4, the variability of the tropical tropopause parameters from seasonal to short term scales such as sub daily scales over Indian monsoon region are extensively studied. A detailed analysis for the observed day to day variability and the quantification of the adiabatic and diabatic processes are carried out. The dependence of the various parameters on the convection, especially for sub-daily scale is also brought out. An attempt has been made to study the tidal modulation on the diurnal variability of the CPT. The features of the tropopause parameters over Indian monsoon region are found different from the west Pacific region.

The longitudinal characteristics of the tropical tropopause are discussed in the Chapter-5. A detailed investigation of the various aspects such seasonal variability of tropopause parameters, the annual variation of the temperature anomalies in the UTLS, the influence of the stratospheric temperature into upper troposphere etc are made. Finally, the longitudinal variation of the tropopause parameters in association with convection is discussed. It is well known that the tropical tropopause is well defined; however, there are cases when more than one tropopause structure can be observed in the temperature profile. These are defined as multiple tropopauses.

The characteristics of the multiple tropopauses (MTs) are presented in chapter-6. The occurrence of MT, their seasonal variability and latitudinal variation of the altitude and temperature of the MTs are provided. The possible mechanisms for the occurrence of the MTs due to planetary wave, cirrus occurrence and advection of the air and /or combination of these are briefly discussed.

The planetary wave activity on the modulation of the tropical tropopause is presented in the Chapter-7. Using the advantage of the dense observation from the COSMIC RO data, the CPT modulation due to planetary wave with wave number 1-4 during phases of the QBO are presented. The characteristics of the amplitude and phase of the equatorial wave for wave number 1-4 are briefly discussed. Role of Kelvin wave and Rossby gravity waves in modulating the tropopause in different seasons are brought out. Finally, Chapter-8 contains the brief summary of the present study and recommendations for further studies, emanating from the present research.

Contents

List of Figures

List of Tables

List of Acronyms

ADC	**A**nalog **D**igital **C**onverter
ANT	**Ant**enna
BPF	**B**and **P**ass **F**ilter
BT	**B**rightness **T**emperature
BV	**B**runt **V**aisala
CHAMP	**CHA**llenging **M**inisatellite **P**ayload
COSMIC	**C**onstellation **O**bserving **S**ystem for **M**eteorology, **I**onosphere and **C**limate
COT	**CO**nvective **T**ropopause/ **C**o**n**vective **O**utflow **T**ropopause
CPT	**C**old **P**oint **T**ropopause
CSRT	**C**lear-**S**ky **R**adiative **T**ropopause
DBS	**D**oppler **B**eam **S**winging
DET-SIG	**det**ected **sig**nal
DJF	**D**ecember-**J**anuary-**F**ebruary
E	**E**ast
EM	**E**lectro**m**agnetic
ESF	**E**xperiment **s**pecification **f**ile
GOES	**G**eostationary **O**perational **E**nvironmental **S**atellite
GPS	**G**lobal **P**ositioning **S**ystem
GRACE	**G**ravity **R**ecovery and **C**limate **E**xperiment
IF-AMP	**IF amp**lifier
IF-SIG	**I**ntermediate-**F**requency **sig**nal
IPP	Inter-Pulse-Period
IR	**I**nfra**r**ed
IST	**I**ndian **S**tandard **T**ime
JJA	**J**une-**J**uly-**A**ugust
JMA	**J**apan **M**eteorological **A**gency
LEO	**L**ow **E**arth **O**rbiter
LO	**Lo**cal Frequency

LPF	**L**ow **P**ass **F**ilter
LRT	**L**apse **R**ate **T**ropopause
MF	**M**edium **F**requency
MAM	**M**arch-**A**pril-**M**ay
MJO	**M**adden–**J**ulian **O**scillation
MOD	**Mod**ulated
MST	**M**esosphere-**S**tratosphere-**T**roposphere
MTSAT-1R	**M**ulti-functional **T**ransport **SAT**ellite
N	**N**orth
OLR	**O**utgoing **L**ong wave **R**adiation
OSC	**osc**illator
PRP	**p**ulse-**r**epetition **p**eriod
QBO	**Q**uasi-**B**iennial **O**scillation
QUAD-DET	**Quad**rature **det**ector
Radar	**Ra**dio **D**etection **a**nd **R**anging
RF-SIG	**R**adio-**F**requency **sig**nal
RH	**R**elative **H**umidity
rms	**R**oot **M**ean **S**quare
RS	**R**adio**s**onde
S	**S**outh
SNR	**S**ignal-to-**N**oise **R**atio
SON	**S**eptember-**O**ctober-**N**ovember
SPARC	**S**tratospheric **P**rocesses **a**nd their **R**ole in **C**limate
SST	**S**ea **S**urface **T**emperature
STE	**S**tratosphere-**T**roposphere **E**xchange
STEP	**S**tratosphere **T**roposphere **E**xchange **P**rocesses
STT	**S**econdary **T**ropical **T**ropopause
TBB/BT	**B**rightness **T**emperature
TR	**T**ransmitter **R**eceiver
TRMM	**T**ropical **R**ainfall **M**easuring **M**ission
TTL	**T**ropical **T**ropopause **L**ayer
TTLt	**T**ropical **T**ropopause **L**ayer **t**hickness
TX	**T**ransmitter
UHF	**U**ltra-**H**igh **F**requency
UT	**U**niversal **T**ime
UTC	Universal Time Coordinate
UTLS	**U**pper **T**roposphere and **L**ower **S**tratosphere
UV	**U**ltra **V**iolet
VHF	**V**ery **H**igh **F**requency

W	**W**est
WMO	**W**orld **M**eteorological **O**rganization

List of Symbols

ϕ	Latitude
$\overline{T}$	Average SST
θ_e	Equivalent potential temperature
θ_E	Equivalent potential temperature at 900 hPa
q	Humidity mixing ratio
L	Latent Heat of Condensation
c_p	Specific heat at constant pressure
Ω	Earth's rotational angular velocity
g	Acceleration due to gravity
R	Earth's Radius
y	Meridional distance
N	Brunt Vaisala Frequncy
λ	Wavelength
τ	Pulse width
Θ	Scattering Angle
C_n^2	Refractivity Structure Constant
L_0	Outer Scale of the turbulence
l_0	Inner Scale of the turbulence
P_t	Transmitted Power
G	Gain
A_e	Effective Area of Antenna
f	Radar Frequency
P_r	Received Power
η	Volume Refractivity
$\vartheta_{1/2}$	Half Power beam width
Γ	Adiabatic Lapse Rate
P_w	Water Vapour Pressure
n	Refractive index

ϕ	angle between the ray path and the local radial direction
p	Impact Paramter
R	universal gas constant
R_m	specific gas constant
M_d	mass of the dry air
M_w	Mass and moist air
m_d	Molecular mass of dry air
m_w	Molecular mass of wet air
T_v	Virtual Temperature
S_p	Static Satiability parameter
θ'	Potential temperature lapse rate
J	Rate of heating
u or U	Zonal wind speed
D	Divergence
D	Divergence
E	East
f	Coriolis frequency
g	Acceleration due to gravity
H	Scale Height
h	Planck's constant
H	Density Scale Height
K	Kelvin
k	Wave number
N	North
N	Brunt-Väisälä frequency
º	Degree
P	Pressure
S	South
s	Zonal wave number
T	Temperature
U	Zonal wind velocity
W	West
w	Vertical Velocity
w	Vertical wind velocity
Z	Altitude
Z_C	Altitude of CPT
Z_D	Altitude of maximum horizontal divergence according to definition

Z_L	Altitude of lapse rate minimum according to definition
α	Bending Angle
θ	Potential Temperature
ν	Frequency

Chapter 1

Introduction

1.1. Vertical Structure of the Atmosphere

Temperature varies greatly both vertically and horizontally as well as temporally throughout the atmosphere. However, despite horizontal variations, the vertical structure of temperature characterizes the Earth's atmospheric layers. These variations in temperature are produced by differences in the radiation budget and chemical composition of the atmosphere at different altitudes. Based on temperature changes with altitude, the Earth's atmosphere is divided into mainly four concentric spherical shells, namely, troposphere, stratosphere, mesosphere, and thermosphere. The vertical distribution of temperature in the Earth's atmosphere is shown in Figure 1.1.

The Troposphere: Troposphere is the lowest part of the Earth's atmosphere whose thickness decreases from equator to pole, and is higher in summer than in winter. It extends ~16-18 km at tropics, 10-12 km at mid latitude and 6-8 km at polar region. The greater thickness of the troposphere over the tropics is due to greater solar radiation. The solar radiation heats the surface and the air is warmed by sensible and latent heat fluxes. The warmed surface air which rises aloft to higher altitudes owing to lower density increases the thickness of the troposphere over tropics. The troposphere holds almost ~80% (~90% in the tropics) of the mass of the earth's atmosphere and nearly all the water vapor (~99%). The water vapor raises aloft get condense and then precipitate with release of latent heat which drives the atmospheric phenomena. The density and pressure decreases exponentially with altitude. In the troposphere, temperature decreases linearly with a lapse rate of 6-7 K/km. It may be noted that the tropospheric gases are mostly transparent to the incoming solar radiation which allow it to heat the earth surface. The earth's surface emits long wave radiation which is absorbed and reradiated by the tropospheric gases.

The troposphere is well mixed and highly unstable due to differential heating owing to large land-sea contrasts which are important for monsoonal circulations. However, the latitudinal differential heating is responsible for midlatitude weather systems. The lower troposphere attains convective equilibrium due to release of latent heat during cloud formation and precipitation. Like pressure and density, temperature doesn't decrease continuously but start to increase above troposphere in the stratosphere due to presence of ozone layer, which absorbs almost all the ultra violet (UV) part of the solar radiation. The boundary which separates troposphere and stratosphere is known as tropopause. In this layer temperature is relatively constant (not always, very sharp changes may also occur) with altitude. The tropopause is not a continuous layer, but there are breaks, between midlatitudes and polar tropopause associated with polar front jet streams, and the midlatitude and tropical tropopause associated with subtropical jet streams. The tropopause acts as a lid which resists the exchange of air between troposphere and stratosphere. However, due to greater convection most of the upward exchange of the air takes place through tropical tropopause region. The tropical tropopause and its importance will be discussed in detail in later sections.

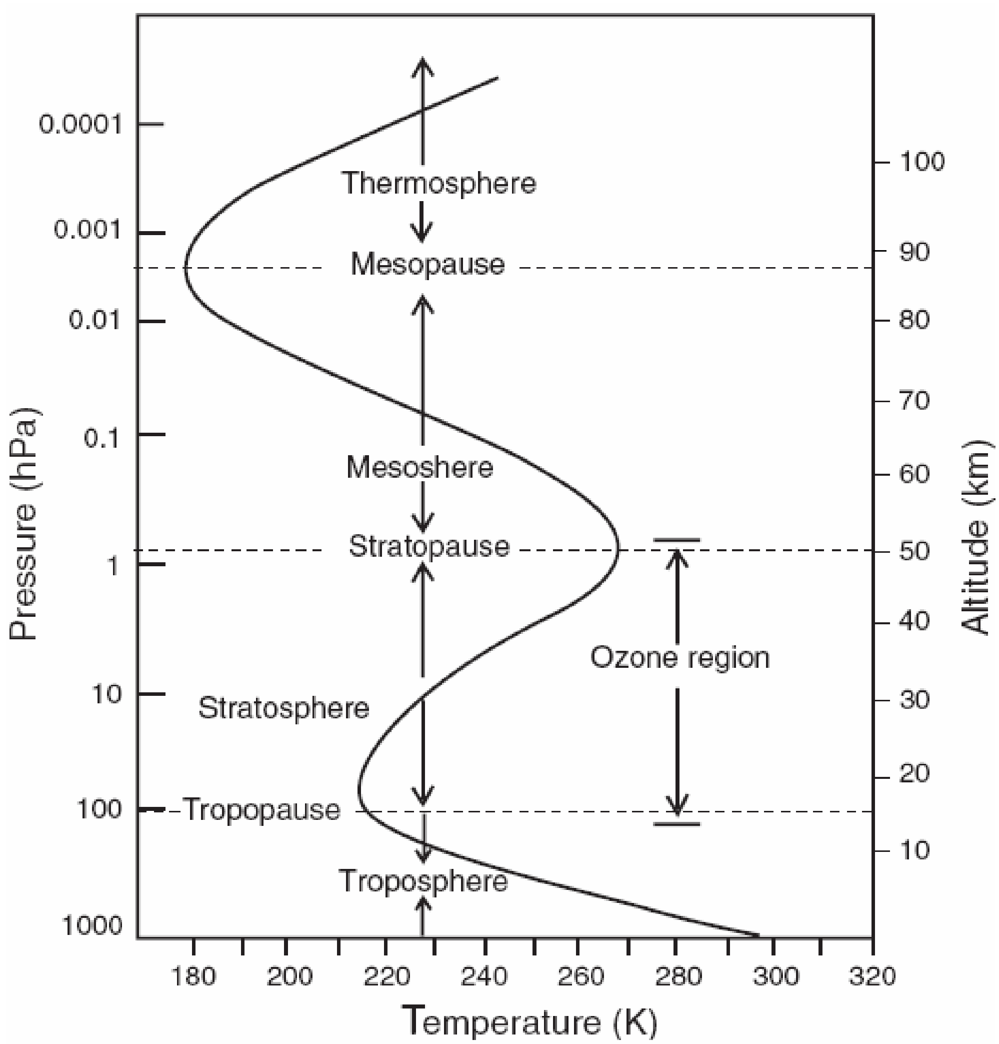

Figure1.1: *Mean vertical thermal structure of Earth's atmosphere.* [*Adapted from G. Brasseur and S. Solomon 1984*].

The Stratosphere: The stratosphere is characterized by high stability and very long vertical mixing time scale in contrast to troposphere. The most significant minor constituent of the stratosphere is ozone which is found maximum at altitude ~ 20-30 km. As mentioned earlier the UV (0.1 μm to 0.35 μm) part of the solar radiation is observed by this layer, which plays the major role in regulating the thermal regime of this layer. The reason for the existence of ozone at these levels is that it is produced here, as a by-product of the photo-dissociation (photolysis) of molecular oxygen, producing atomic oxygen which then combines with molecular oxygen thus:

$$O_2 + h\nu \rightarrow O + O\ ,$$

$$O + O_2 + M \rightarrow O_3 + M$$

where $h\nu$ is the energy of incoming photons (ν is their frequency and h is Planck's constant) and M is any third body. Ozone absorbs UV radiation and with the low densities present at stratospheric altitudes, this absorption is an efficient mechanism of transferring kinetic energy to a relatively small number of molecules causing increase of the temperature from the tropopause to an altitude ~ 50 km. Thus, the –ve lapse rate (~ 3K/km) doesn't allow rapid mixing between the stable layers. The mixing in lower stratosphere takes place in time scale of a month or year. The resulting ozone, through its radiative properties, is the reason for the existence of the stratosphere. It is close to radiative equilibrium. The boundary which separates the stratosphere and mesosphere is known as stratopause, which occurs at an altitude of 45–55 km, the level at which temperature ceases to increase with altitude. The temperature of the stratopause varies in the range 240 K to 290 K over winter pole to summer pole.

The Mesosphere: In contrast to the stratosphere, mesosphere is highly unstable, like troposphere, with rapid mixing through convective currents. The mesosphere is dominated by molecular oxygen (O_2) and carbon dioxide (CO_2). The radiative heating of molecular oxygen and radiative cooling by infrared emission of carbon dioxide determine the heat balance in this region. The temperature decreases rapidly from stratopause to altitude ~80-90 km. Compared to lower regions, the concentrations of ozone and water vapor in the mesosphere are negligible, hence the lower temperatures. Its chemical composition is fairly uniform. Pressures are very low. The mesopause, which separates the thermosphere and mesosphere, is coldest region in the Earth's atmosphere whose temperature is ~ 180 K at altitude ~ 80 km -100 km. Extreme low mesopause temperature occur during Northern Hemispheric Summer. At the end of above these altitudes, the atmosphere becomes ionized (the ionosphere), causing reflection of radio waves, a property of the upper atmosphere which is of great practical importance. **The Thermosphere** is the region of high temperatures above the mesosphere. It includes the ionosphere and extends out to several hundred kilometers. It is here that very short wavelength UV is absorbed by oxygen thus heating the region. Molecules (including O_2) are dissociated (photolysed) by high-energy UV. Because of the scarcity of polyatomic molecules, Infra Red (IR) loss of energy is weak, so the temperature of the region gets very high in the order of 500 K –2,000 K and the densities become very low. The thermosphere is that part of the heterosphere which does not have a constant chemical composition with increasing altitude. The thermopause is the level at which the temperature stops rising with height. Its height depends on the solar activity and is located between 250 and 500 km. **The Exosphere** is the most distant atmospheric region from Earth's surface. The upper boundary of the layer extends to heights of perhaps 960–1,000 km. The exosphere is a transitional zone between Earth's atmosphere and interplanetary space.

1.2. The Upper Troposphere and Lower Stratosphere (UTLS)

The UTLS region, or equivalently, the tropopause region, has been identified as being of key importance for chemistry and climate. The tropical tropopause is situated at around altitude 18 km, typically characterized as the 380 K isentropic (line of constant potential temperature (θ)) surface. Because the tropopause slopes downward as one moves away from the equator, reaching an altitude of roughly 8 km, at polar latitudes, there is a significant part of the stratosphere with 380 K isentropic surface –dubbed the "lowermost stratosphere" by *Holton et al.*, [1995]. In this region, isentropic surface passes through the tropopause, potentially allowing for rapid stratosphere- troposphere exchange. The lower part of the tropical tropopause is likewise a distinct region, as the top of the region of moist convective adjustment , at about 12 km altitude, lies well below the tropical tropopause, and a layer in between is in many ways more characteristics of the stratosphere than troposphere [*Thuburn and Craig,* 2002]. Together these two regions are now generally referred as the UTLS. The UTLS is deserving of special treatment because its properties are in many ways quite distinct from those of the main body of the stratosphere, yet are also distinct from lower stratosphere [*Haynes and Shepherd,* 2001]. The tropical part of the UTLS is known as the tropical tropopause layer (TTL), although there is no consensus on its definition [*Haynes and Shepherd*, 2001]. The Tropical Tropopause Layer (TTL), sets the chemical boundary conditions for the stratosphere. The radiative balance of the TTL, including clouds, is important for the global energy balance.

The extra-tropical tropopause layer (ExTL) or extra-tropical UTLS, regulates its ozone budget with important impacts on chemistry. Dynamical coupling between the troposphere and stratosphere may be modulated by the tropopause region, and this will affect stratospheric dynamics and polar ozone chemistry, as well as surface climate, particularly at high latitudes where dynamical forcing is strong.

1.3. The Tropical Tropopause

The tropopause is defined as region rather than a fixed boundary, means that it has some vertical structure. Tropopause altitude shows temporal as well as special variation. The temporal variation of tropopause in times scales such as from sub-daily to solar cycle. The spatial variation tropopause shows both latitudinal as well longitudinal variations. The temporal variation of the tropopause will be discussed in forthcoming sections. The latitudinal variation of the tropopause altitude is from 7-10 km in polar regions to 16–18 km in the tropics. Tropical tropopause is higher and colder, whereas polar tropopause is lower and warmer. The tropopause altitude also varies from troughs to ridges, with low tropopause altitude in cold troughs and high in warm ridges. Since these troughs and ridges propagate, the tropopause height exhibits frequent fluctuations at a particular location during midlatitude winters [*Mohanakumar*, 2008].

Severe thunderstorms in the intertropical convergence zone (ITCZ) and over midlatitude continents in summer continuously push the tropopause upwards and as such deepen the troposphere. A pushing up of tropopause by 1 km reduces the tropopause temperature by about 10 K. Thus in areas and also in times when the tropopause is exceptionally high, the tropopause temperature becomes very low, sometimes below 190 K. The highest tropopause is seen over south Asia during the summer monsoon season, where the tropopause occasionally peaks above 18 km. The oceanic warm pool of the western equatorial Pacific also exhibits higher tropopause height of 17.5 km. On the other hand, cold conditions lead to lower tropopause, evidently due to weak convection [*Mohanakumar*, 2008].

There are various tropical tropopause definitions which has some advantages and disadvantages. These definitions are based on the thermal properties of the tropical atmosphere.

Lapse rate tropopause (LRT): The following lapse rate definition has been used most often [e.g., *Reid and Gage,* 1985; *Gage and Reid,* 1987]: It is defined by the World Meteorological Organization (WMO) as the lowest level at which the lapse rate decreases to 2 K/km or less, provided that the average lapse rate between this level and all higher levels within 2 km does not exceed 2K/km [*WMO*, 1957]. However, these authors suggest, this level is arbitrarily defined for operational use and has limited physical significance. Generally there seems to be little direct connection between any convective processes and in the lapse rate definition.

The temperature minimum or cold point tropopause (CPT): The temperature minimum or cold point was deemed important for stratosphere- troposphere exchange (STE) by *Selkirk* [1993], found that the cold point may coincide with lapse rate tropopause, but commonly lies above it. It is also observed that LRT and CPT often lay within stable transition layer of varying depth, overlaying much deeper, marginally stable layer in the upper troposphere. The CPT is only reliable tropopause definition when lower stratosphere is not close to being isothermal i.e., within deep tropics.

The top of convective outflow/Convective tropopause (COT): The level of the top of nearly all the convection is arguably physically more meaningful. Thus, the tropopause is considered at the levels of main convective outflow (top of the convection), i.e., at ~150 hPa (θ =355 K, 14 km) where θ is potential temperature. Below, air is radiatively cooling (subsiding), and ascent occurs predominantly in moist convection. Above that level, air is radiatively heated under all sky conditions and the lapse rate departs from the moist adiabat. In general, tropical deep convection reaches altitudes of 10 km –15 km. However, some convection may reach higher, and very rarely, convection may even penetrate into the lower stratosphere. There is some debate about the highest altitudes reached by convection, with evidence that it may go as high as 19 km (θ = 420 K), well above the CPT (θ = 380 K) [*Sherwood*, 2000]. However, such events are very infrequent and the frequency of convection drops rapidly with altitude above the COT [*Holton*, 1995]. Tropical rainfall measuring mission (TRMM) measurements suggest that only about 0.1% of the tropics have convection reaching the CPT at any given time.

Clear-sky radiative tropopause (CSRT): The level of zero radiative heating under clear-sky conditions is called the clear sky radiative tropopause. The CSRT is typically at 14-16 km. The level of zero radiative heating under clear-sky conditions is slightly higher than COT. This level is another candidate tropopause, from a radiative-dynamical perspective.

***The 100 hPa level*:** The 100 hPa level surface has been used as a proxy for the tropical tropopause, for example by *Mote et al*, [1996], because of its direct availability from models. The 100 hPa level is sometimes used as a surrogate for the tropical tropopause [*Frederick and Douglass*, 1983].

***Tropical tropopause layer (TTL)*:** TTL is the region between the COT and the CPT. The notion of a 'tropical tropopause layer' between the CPT and the COT was revived by *Atticks and Robinson* [1983] and, more recently by *Highwood and Hoskins* [1998]. Based on the overall radiative-convective balance, one might regard the TTL as being more stratospheric than tropospheric in character.

The factors that determine the altitude and physical properties of the tropical tropopause is not fully understood, although twin fact is that the troposphere is heated from below by the surface and that the stratosphere is heated internally by direct absorption of solar radiation, guarantee that a temperature minimum must exist.

1.4. Annual Variation of the Tropical Tropopause

Several studies of the relative contribution of the radiative effect and dynamical heat transfer to the formation of the tropopause [*Staley*, 1957] have been carried out. The ultimate driving force for the radiative and dynamical effects in the atmosphere is the intensity of the solar radiation. *Gage and Reid* [1981] argued that the tropopause properties are related to small changes in the sea surface temperature (SST) and consequent change in the intensity of cumulus convection and hence upward branch of the tropical Hedley cell. Hadley cell is meridional circulation pattern between 30°N and 30°S latitude. The meridional circulation contains three distinct cells namely Hadley cell, Ferrel cell (between latitude 30^o N-60^o N and 30^o S-60^o S) and Polar cell (between latitude 60^o N-90^o N and 60^o S-90^o S) as shown in Figure 1.2. In the Hadley cell energy transport is accomplished by a relatively simple overturning circulation, with rising motion near the equator, poleward motion (~10 km-15 km above the surface) near the tropical tropopause, sinking motion in the subtropics, and an equator ward return flow near the surface.The annual variation in average potential temperature of tropopause at fixed altitude (18 km) was discussed by *Newell et al* [1969] and *Reed and Vlcek,* [1969] as evidenced for annual modulation of the Hadley cell link to the tropopause altitude.

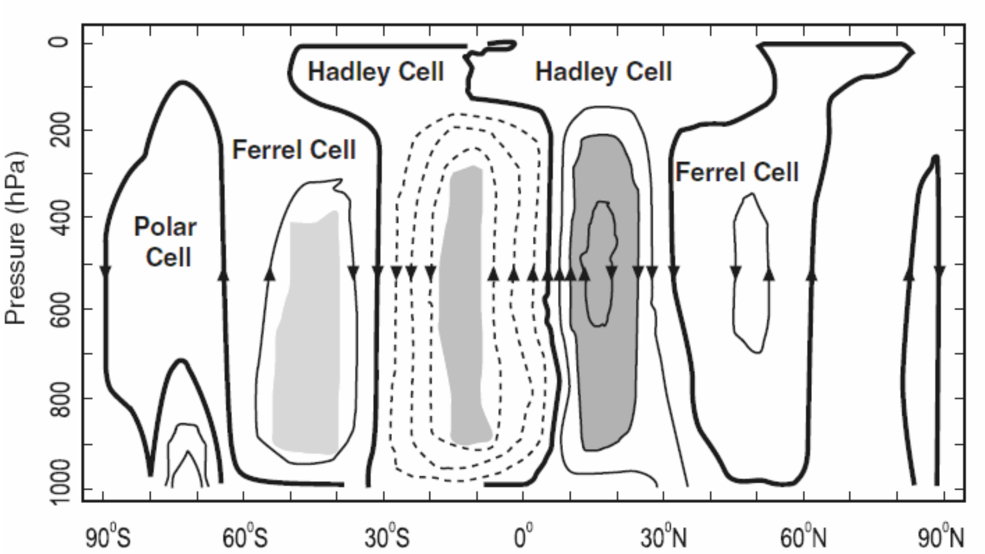

Figure 1.2: *The zonally averaged mass circulation. The arrows depict the direction of air movement in the meridional plane. [Courtesy, Mohanakumar, 2008]*

The equilibrium level of an ascending air parcel is reached when it encounters stratospheric air of the same potential temperature, this is the level at which the tropopause should form. While estimating the variation in altitude, the potential temperature variation in the troposphere and in lower stratosphere both needs to be taken into account.

Ga*ge and Reid*, [1981] observed that when upper tropospheric potential temperature reaches its maximum, tending to produce a high tropopause, even if the stratospheric potential temperature were constant. In fact, associated increase in the adiabatic cooling (possibly combined with variation in stratospheric ozone concentration) causes minimum in the lower stratospheric temperature also causing an increase in the tropopause altitude. These two effects usually reinforce each other, amplifying in the change in the tropopause altitude. Further *Reid and Gage* [1981] observed that the annual variation in the thermal field in the lower stratosphere is found to out of phase with tropospheric variation. The annual variation in the tropopause altitude is thus attributed to (1) the annual variation in the tropical surface insolation that causes (2) the annual variation in the sea surface temperature, which in turn causes (3) a variation in the absolute humidity of surface air that (4) give rise to annual variation in potential temperature at tropopause and lower stratosphere. This is summarized in Figure 1.8.

The annual cycle of tropical has been linked to seasonal variations in solar radiation and its impact on tropical convection [*Reid and Gage*, 1981; *Shimizu and Tsuda*, 2000] and to remote forcing during boreal winter associated with the intensification of the Brewer-Dobson circulation (discussed in section 1.11) [*Yulaeva et al*., 1994, *Reid and Gage*, 1996]. The upwelling Brewer-Dobson circulation in the tropical stratosphere is driven by a combination of effects including wave drag, transient radiative driving, and the stratospheric (i.e. non-convective) Hadley circulation. The annual variation of the CPT is important for understanding water vapour transport in and through the TTL. The CPT temperature not only affected by large scale process but also by small scale forcing by convective clouds and waves resulting from clouds, to the ultimate drivers such as sea surface temperatures. Tropopause temperature changes may occur through direct radiative effects, radiative-convective effects or indirect dynamical effects (through changes to the Brewer Dobson circulation).

1.5. The Interannual Variation

Gage and Reid, [1982] observed that Interannual and annual variation in the thermal field of lower stratosphere and upper troposphere are out of phase. The interannual and annual variations are explained as response of the variations of incoming solar radiation. These responses include direct radiative effects (diabatic heating) and indirect dynamical effects similar interpretations were made by *Reid and Gage*, [1981] and *Gage and Reid,* [1981]. Based on their approach, *Gage and Reid,* [1982] proposed that the convective activity is modulated by changes in solar radiation and that the temperature field in the troposphere responds positively to increase in convective activity. This positive response is due to a combination of the release of latent heat within convective cells and adiabatic heating due to subsidence in the environment of thunderstorms. In the lower stratosphere the collective effect of changing thunderstorm activity is to modulate the intensity of the ascending branch of the Hadley circulation. When thunderstorm activity is at a maximum, strong ascent in the Hadley cell cools the lower stratosphere adiabatically as suggested by *Newell et al.* [1969] and *Reed and Vlcek,* [1969]. Conversely, when the thunderstorm activity is at a minimum and the troposphere is relatively cold, the lower stratosphere is relatively warm.

Following *Reid and Gage,* [1981] the annual forcing is attributed to annual variation in solar radiation received at tropical latitudes. The response of the lower stratosphere is out of phase with the tropospheric variations due to the response of the varying Hadley circulation. *Gage and Reid,* [1981] have suggested that inter-annual variations represent the atmospheric response to a small variation of the insolation that was positively correlated with solar-activity cycle. Interannual variations in the tropical tropopause have been linked to the quasi-biennial oscillation of the equatorial stratosphere, the El Nin˜o-Southern Oscillation and episodic volcanic eruptions.

Tropopause Variation with Solar Cycle: The variation of the tropopause altitude is found increased with increased sunspot number (*Stranz*, [1959]; *Rasool*, [1961]). Based on the model as discussed earlier the potential temperature at the tropopause is calculated which was consistent with the observation with some deviation which were attributed due to solar activity. The observed variation in the altitude of the tropical tropopause can thus be explained if the solar constant varies by less than 1% during course of the 11-year cycle of solar activity [*Gage and Reid*, 1981]. *Wilson et al*,[1980] repotted that an increase of 0.4% solar luminosity between rocket-born radiometer flight during June 1976 and November 1978, an interval in which monthly mean sunspot number increased from 12 to 97. Based on the observation, it is further indicated that tropical ocean acts as a vast water bath that responds to small changes in the sun’s radiative output, and that the resulting small changes in the average sea surface temperature are magnified at the tropopause through medium of the latent heat release in deep cumulus convection in the tropics.

The increase in UV radiation will increase the potential temperature in the lower stratosphere that lead to lowering the tropopause. However, tropopause may lower due to dynamics which is not clear at present. The connection between the solar output and tropopause has implications in the global climate [*Gage and Reid*, 1981].The temperature in the tropical lower stratosphere is determined by the competition among three deriving forces, to which fourth has to be added if perturbation in the atmospheric constituents, especially volcanic aerosols are taken into account. The three forcings fluctuations are (1) the normal seasonal cycle, (2) the quasi biennial oscillation in zonal winds, and (3) the ENSO related effects.

1.6. The Quasi-Biennial Oscillation

The quasi-biennial oscillation (QBO) in stratospheric winds and temperatures is discovered by *Reed et al.*, [1961] and *Veryard and Ebdon* [1961] and has been investigated from several decades (e.g. *Plumb and Bell,* [1982]; *Naujoket*, [1986]) .The mean-flow interaction involving upward propagating wave from troposphere has been generally accepted as a explanation for the QBO [*Holton and Lindzen*, 1972; *Plumb*, 1977]. This oscillation has the following observed features: (i) zonally symmetric easterly and westerly wind regimes alternate regularly with periods varying from about 24 to 30 months, (ii) successive regimes first appear above 30 km, but propagate downward at a rate of 1 km month^{-1}, (iii) the downward propagation occurs without loss of amplitude between 30 and 23 km, but there is rapid attenuation below 23 km, and (iv) the oscillation is symmetric about the equator with maximum amplitude of about 20 m s^{-1}, and an approximately Gaussian distribution in latitude with a half-width of about 12^{o} [*Andrews et al.*, 1987].

Departures from the regular seasonal cycle are dominated by the QBO in the middle stratosphere, and the QBO continues to exert an important influence in the lower stratosphere, where it interacts with the annual cycle. The net result of this interaction is to modulate the amplitude of the annual cycle, producing a weak cycle when the QBO effect opposes the normal cycle and a strong cycle when it reinforces it. The interaction appears to take place mainly in northern winter months, however, when the annual cycle is in its cool phase, while variations in northern summer months are significantly smaller. Since the QBO itself is nearly biennial, the modulation that it produces in the annual cycle has a strong biennial component, i.e., weak and strong cycles tend to alternate. The quasi biennial forcings at higher altitudes is thus turned into a biennial variation in the lower stratosphere that is phase locked to the annual cycle.

The detailed relationship between the QBOs in wind and temperature has been discussed by several authors [e.g., *Reed,* 1964; *Dunkerton and Delisi,* 1985]. The essential points, however, are clear from the thermal wind equation, which can be written approximately as:

$$\frac{\partial T}{\partial y} = -\frac{2\Omega T}{gR} y \frac{\partial u}{\partial z} \tag{1.1}$$

in the vicinity of the equator, where u , T and y are the zonal wind speed (m/s), temperature and distance (meter) from the equator, respectively, Ω , g and R are the Earth’s rotational angular velocity, gravitational acceleration, and radius. Inserting numerical values this equation becomes

$$\frac{\partial T}{\partial y} = -2.3\times 10^{-12} Ty \frac{\partial u}{\partial z} \tag{1.2}$$

A typical value for the vertical shear in the QBO wind at the equator is about 30 m/s in 6 km or about 0.005 s^{-1}. Taking a typical undisturbed temperature of ~ 210 K, a variation of the order of 2 to 4 K occurs within 10^{o} of the equator, which was found comparable with annual cycle [*Reid*, 1994].

The period is found close to well known QBO in tropical stratospheric zonal winds [e.g., *Wallace,* 1974] and a similar QBO in global tropopause pressure has identified by *Angell and Korshover* [1964, 1974]. *Reid and Gage*, [1985] found the difference between high and low ~ 0.3 km in the tropopause QBO. The interpretation of the tropopause QBO is not clear, however, they link its maxima and minima occurring during easterly phase and westerly phase of the QBO. *Reed*, [1962] shown that the QBO component of the zonal wind was in geostrophic balance even at that near-equatorial latitude. Since warm stratosphere implies a low tropopause (assuming that upper troposphere is not equally warmed) the minimum in tropopause altitude should occur close to westerly wind maxima at the base of the stratosphere. The swing in temperature just above the tropopause that accompanies the swing in the tropopause altitude can be estimated by assuming that the tropopause follows as isentropic surface as temperature changes. Using the standard definition of the potential temperature $\theta = T(1000/p)^{0.288}$, tropopause altitude (pressure) can be related through (taking log and differentiating);

$$dT/T = 0.288dP/P \tag{1.3}$$

For the peak to peak QBO swing in the tropopause altitude of about 300 m corresponds of about 5.4 hPa. Therefore substituting in equation (1.3) together with average tropopause pressure and temperature of values of 100 hPa and 192 K, respectively, the temperature swings ~ 3 K were observed in the lower stratosphere just above the tropopause. The QBO in tropopause altitude can thus be tentatively attributed to the corresponding QBO in lower stratospheric temperature, which is itself probably consequence of the weak vertical motion needed to maintain geostrophic balance in the zonal wind field. However, later *Zhou et al.*, [2001] reported that the QBO signature in the tropical CPT is probably caused by the downward-propagating QBO meridional circulation (computed by *Plumb and Bell*, [1982]) in the equatorial stratosphere. *Zhou et al.,* [2001] observed that that the westerly shears at 50 hPa, which are accompanied by warm temperature anomalies [*Plumb and Bell* 1982], lead the tropical CPT temperatures by about 6 months and are positively correlated with the tropical CPT temperatures. The westerly shear at 50 hPa takes about 3–4 months to reach 100 hPa while easterly shear 5-6 months to propagate from 50 hPa to 100 hPa [*Naujoket* 1986]. The stratospheric QBO signatures in the tropical CPT are mainly zonally symmetric.

1.7. El Niño—Southern Oscillation (ENSO)

The east–west pressure gradient associated with the Walker circulation undergoes an irregular interannual variation. This global scale “see-saw” in pressure, and its associated changes in patterns of wind, temperature, and precipitation, was named the *southern oscillation* by Walker as shown in Figure 1.3. The surface pressure anomalies at Darwin Australia and Tahiti are negatively correlated and have strong variations in the period range of 2–5 years. During normal condition the high pressure with cold water at

Peru and low pressure and warm water at Darwin exists which drive the trade wind from west to east, while abnormally the pressure reverse between the Peru and Darwin which cause El Niño. These patterns of reversal occur in the period range of 2–5 years known as the E1 Nino/Southern Oscillation.

ENSO events clearly cause an additional variation in the tropical lower stratospheric temperature, again with main effect occurring in northern winter months. The simplest explanation is based on the thermodynamics is that the warming takes place in the tropical troposphere during ENSO warm events, presumably caused by increase in latent heat release, is compensated by cooling in higher regions, where there is no internal heat source. Assuming there is some upper level above which ENSO effect vanish, the average temperature below this level, as reflected by it geopotential height, must be unchanged. Since the troposphere warms, the overlaying upper troposphere and stratosphere must cool. That is, the thermal expansion of the troposphere implies a contraction of the lower stratosphere, since geopotential heights are unchanged above the "capping" level, and a contraction at constant pressure must be accompanied by a decrease in temperature.

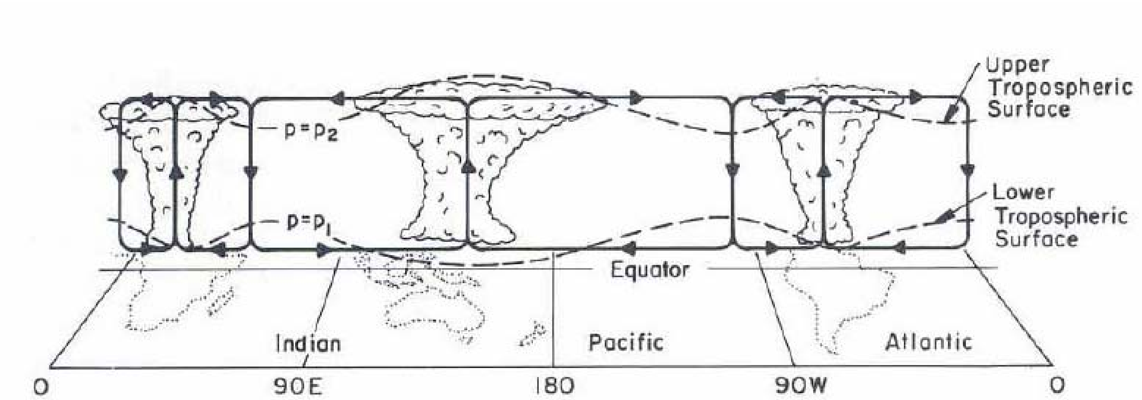

Figure 1.3: *Schematic diagram of the equatorial Walker Circulation* [Courtesy : *Webster*, 1983]

There is general agreement that the principal dynamical deriving force for the tropical atmosphere is provided by the release of the latent heat accompanying deep cumulus convection [e.g., *Holton*, 1979]. A saturated air parcel that is carried up in the core of deep convective cloud has its potential temperature increased to high values by latent heat release, and buoyancy forces prevent it from sinking again once it reaches the vicinity of the tropopause. Since net radiative heating rates near the tropical tropopause are small [*Manabe and Hunt*, 1968], the air that leaves the core of one of these clouds is likely to remain for some time at tropopause levels, spreading laterally outward to merge with the (potentially) warm air from other clouds. This horizontal spreading can be directly seen in the rapid dispersion of volcanic dust clouds around the tropics [e.g., *Barth* et al., 1983] and is probably the agent responsible for the spatial averaging of tropopause properties that is seen in the similarity of the annual variation in altitude all over the tropics [*Reid and Gage,* 1981]. The tropopause peak may be amplified through a coincidental combination of a cool stratosphere caused by the QBO and a warm troposphere caused by the high SST. In previous section it is motioned that the annual cycle of the zonal mean tropical tropopause is driven by extratropical stratospheric wave forcing [*Yulaeva et al*. 1994], but the zonal asymmetrics in the tropical tropopause can be attributed to the direct response of the atmosphere to a large-scale region of tropospheric diabatic heating [*Highwood and Hoskins* 1998]. Using ECMWF data [*Zhou et al* , 2001b] characterized the ENSO signatures in the CPT which shows distinct East–West dipole and North–South dumbbell features.

1.8. Equatorial Intraseasonal Oscillation

In addition to the interannual variability associated with El Niño, the equatorial circulation has an important intraseasonal oscillation, which occurs on a timescale of 30–60 days and is often referred to as the Madden–Julian oscillation (MJO) in honor of the meteorologists who first described it. The structure of the equatorial intraseasonal oscillation is shown schematically in Figure 1.4, which shows the time development of the oscillation in the form of longitude–height sections along the equator, with time increasing at an interval of about 10 days for each panel from top to bottom. The circulations in Figure1.4 are intended to represent anomalies from the time-mean equatorial circulation. The oscillation originates with development of a surface low-pressure anomaly over the Indian Ocean, accompanied by enhanced boundary layer moisture convergence, increased convection, warming of the troposphere, and raising of the tropopause height. The anomaly pattern gradually moves eastward at about 5ms^{-1} and reaches maximum intensity over the western Pacific.

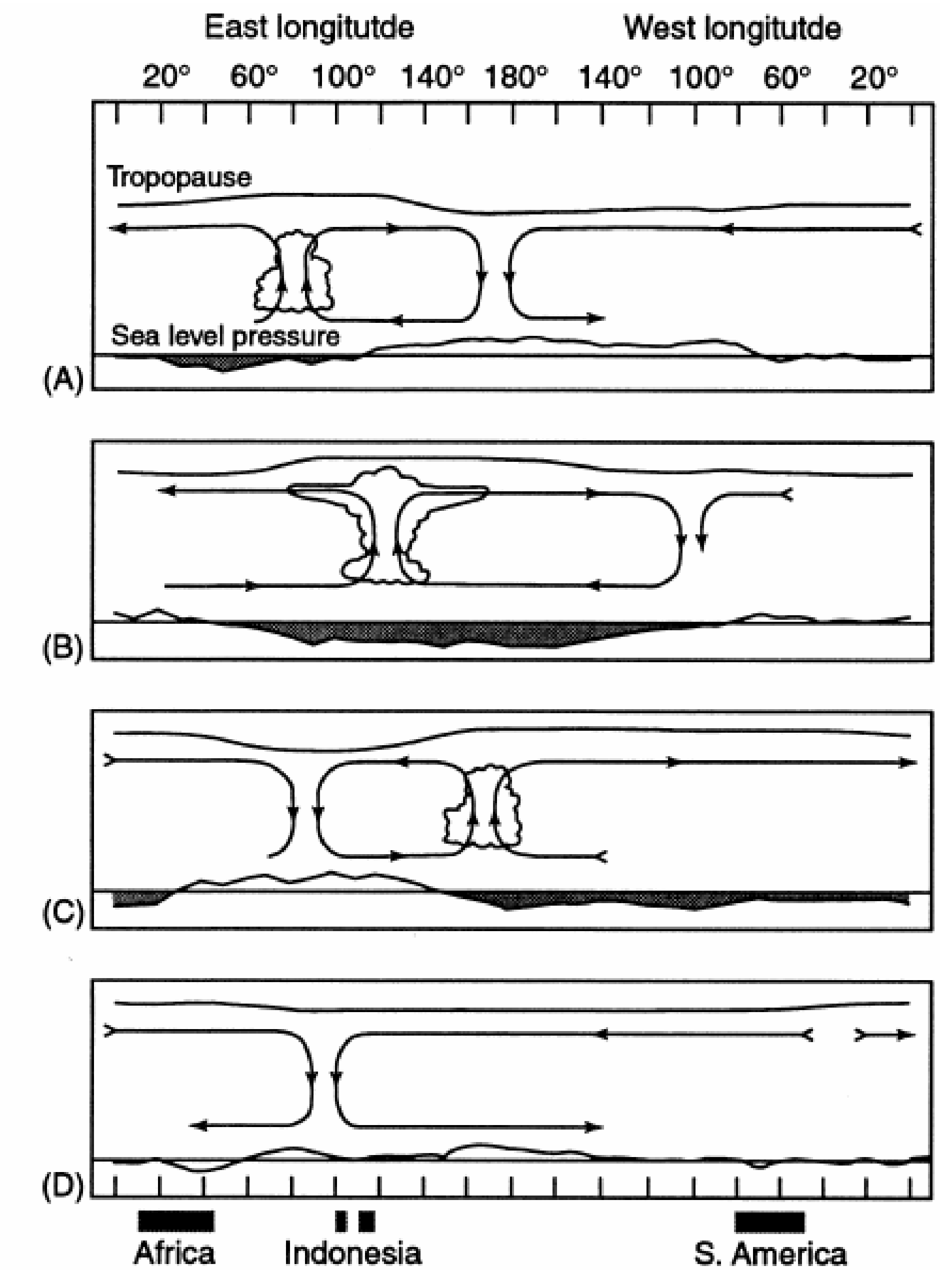

Figure 1.4: *Longitude-height section of the anomaly pattern associated with the tropical intraseasonal oscillation (MJO). Reading downward the panels represent a time sequence with intervals of about 10 days. Streamlines show the west–east circulation, wavy top line represents the tropopause height, and bottom line represents surface pressure (with shading showing below normal surface pressure).* [*After Madden, 2003; adapted from Madden and Julian, 1972.*]

As the anomaly moves over the cooler waters of the central Pacific, the anomalous convection gradually weakens, although a circulation disturbance continues eastward and can sometimes be traced completely around the globe. The observed interaseasonal oscillation is known to be associated with equatorial Rossby and Kelvin waves.

1.9. Vertically Propagating Equatorial Waves

Vertically propagating gravity waves in the presence of rotation for a simple situation in which the Coriolis parameter was assumed to be constant and the waves were assumed to be sinusoidal in both zonal and meridional direction. Such inertia–gravity waves can propagate vertically only when the wave frequency satisfies the inequality $f < \nu < N$. Thus, at middle latitudes, waves with periods in the range of several days are generally vertically trapped (i.e., they are not able to propagate significantly into the stratosphere). As the equator is approached, however, the decreasing Coriolis frequency should allow vertical propagation to occur for lower frequency waves. Thus, in the equatorial region there is the possibility for existence of long-period vertically propagating internal gravity waves. Both Kelvin and Rossby–gravity modes have been identified in observational data from the equatorial stratosphere. The observed stratospheric Kelvin waves are primarily of zonal wave number s = 1 and have periods in the range of 12–20 days. An example of zonal wind and temperature oscillations caused by the passage of Kelvin waves at a station Singapore near the equator is shown in the form of a time–height section in Figure1.5 (a) and (b) during the descending westerly phase of the QBO. However, from Figure 1.5 it is clear that the downward propagation of the perturbation with period between speed maxima of about 12 days and a vertical wavelength (computed from the tilt of the oscillations with height) of about 6–7 km. As shown in Figure 1.5 (c) of the temperature field for the same period reveal that the temperature oscillation leads the zonal wind oscillation by 1/4 cycle (i.e., maximum temperature occurs prior to maximum westerlies), which is just the phase relationship required for upward propagating Kelvin waves. Additional observations from other stations indicate that these oscillations do propagate eastward at the theoretically predicted speed. Therefore, there can be little doubt that the observed oscillations are Kelvin waves.

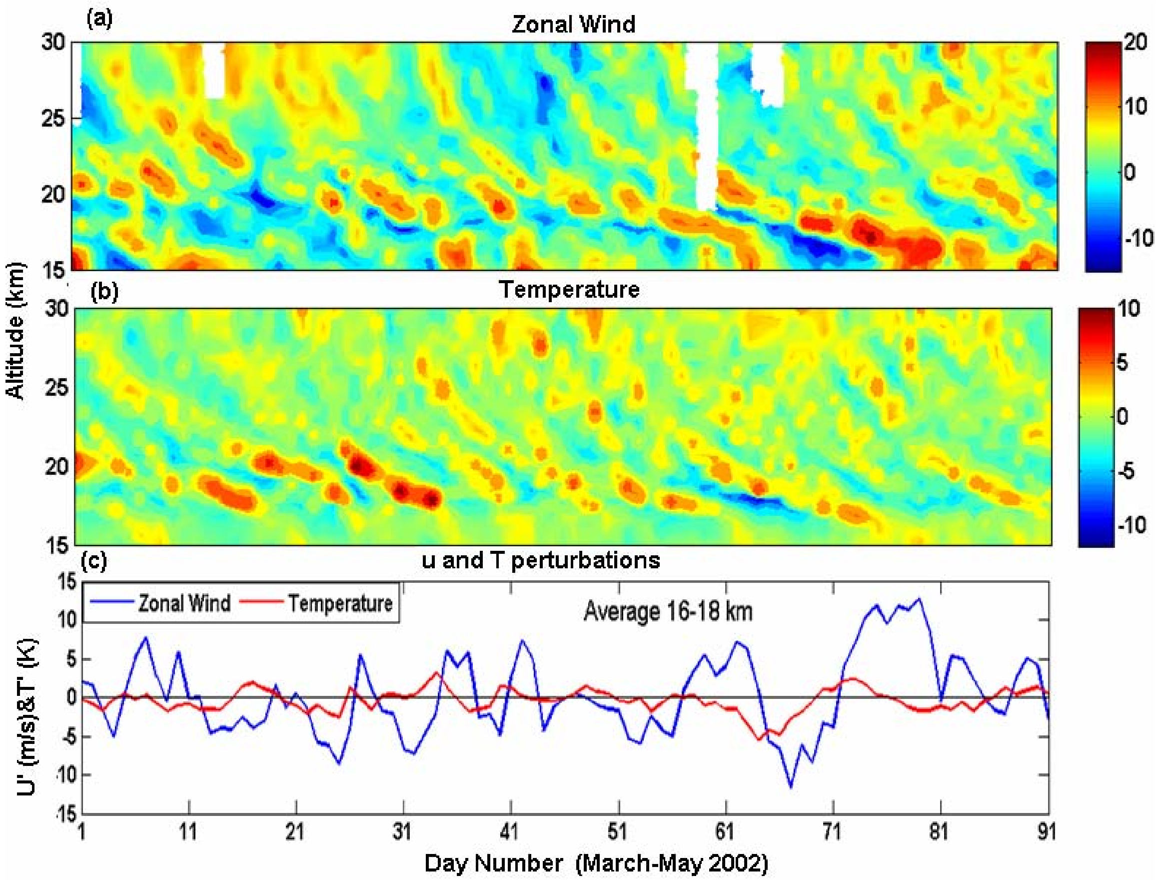

Figure1.5: *(a) Zonal wind perturbation (b) Temperature perturbation and (c) perturbation average for altitude 16-18 km observed over Singapore during March-May 2002.*

The existence of the Rossby–gravity mode has been confirmed in observational data from the stratosphere in the equatorial Pacific. This mode is identified most easily in the meridional wind component, as v is a maximum at the equator for the Rossby–gravity mode. The observed Rossby–gravity waves have s = 4, vertical wavelengths in the range of 6–12 km, and a period range of 4–5 days. Kelvin and Rossby–gravity waves each have significant amplitude only within about 20◦ latitude of the equator. A more complete comparison of observed and theoretical properties of the Kelvin and Rossby–gravity modes is presented in Table 1.1. In comparing theory and observation, it must be recalled that it is the frequency relative to the mean flow, not relative to the ground, that is dynamically relevant. It appears that Kelvin and Rossby–gravity waves are excited by oscillations in the large-scale convective heating pattern in the equatorial troposphere. Although these waves do not contain much energy compared to typical tropospheric weather disturbances, they are the predominant disturbances of the equatorial stratosphere, and through their vertical energy and momentum transport play a crucial role in the general circulation of the stratosphere. In addition to the stratospheric modes considered here, there are higher speed Kelvin and Rossby–gravity modes, which are important in the upper stratosphere and mesosphere. There is also a broad spectrum of equatorial gravity waves, which appears to be important for the momentum balance of the equatorial middle atmosphere.

Table1.1: *Characteristics of the Dominant Observed Planetary-Scale Waves in the Equatorial Lower Stratosphere* [*After Andrews et al., 1987*].

Theoretical description	Kelvin wave	Rossby–gravity wave
Discovered by	Wallace and Kousky (1968)	Yanai and Maruyama (1966)
Period (ground-based) $2\pi/\omega$	15 days	4–5 day
Zonal wave number $s = ka \cos \varphi$	1–2	4
Vertical wavelength $2\pi/m$	6–10 km	4–8 km
Average phase speed relative to ground	+25 m s^{-1}	–23 m s^{-1}
Observed when mean zonal flow is	Easterly (maximum≈−25m s^{-1})	Westerly (maximum≈ +7 m s^{-1})
Average phase speed relative to maximum zonal flow	+50 m s^{-1}	–30 m s^{-1}
Approximate observed amplitudes		
u'	8 m s^{-1}	2–3 m s^{-1}
v'	0	2–3 m s^{-1}
T'	2–3 K	1 K

1.10. Stratosphere-Troposphere Exchange

In the tropics, it has been suggested that a tropical tropopause layer (TTL) spans the transition region from the convectively dominated overturning circulation of the

Hadley cell to the region of slow upwelling (primarily wave-driven) of the lower stratospheric Brewer-Dobson circulation. In general, the transport between stratosphere and troposphere takes place in two ways (i) along the isentropic surfaces which may occur adiabatically (wavy arrows in Figure 1.6) and (ii) across the isentropic surfaces, which may require diabatic processes, including three-dimensional turbulent process.

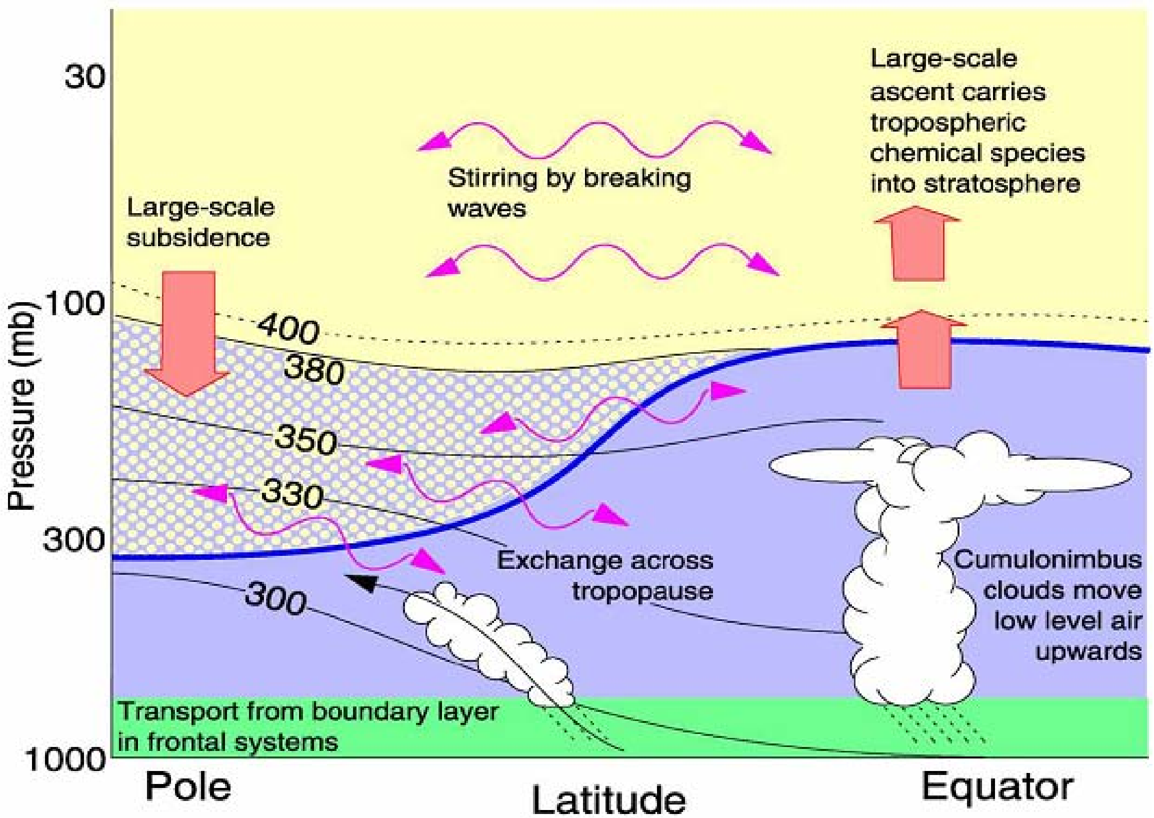

Figure 1.6: *Dynamical aspects of the stratosphere-troposphere exchange. The tropopause is shown by thick line (blue). Thin lines are isentropic or constant potential surface temperature labeled in kelvins. The wavy double headed arrows denote meridional transport by eddy motions* [*After Holton et al, 1995*].

Since, the tropopause intersects the isentropes, transport can occur in either way and likely to occur in both ways. In the UTLS region consisting of the isentropic surfaces that intersect the tropopause, air and chemical constituent can be irreversibly transported as adiabatic motions lead to large latitudinal displacements of the tropopause followed by irreversible mixing on small scales. From the knowledge of the eddy effects, the extra-tropical stratosphere and mesosphere act non-locally on the tropics as global scale fluid dynamical suction pump. The pumping action is slow but inexorable and causes large-scale upward transfer of mass from the tropical troposphere into the tropical stratosphere, at rate that is largely independent of local condition near the tropical tropopause. Indeed, on contrary, as pointed out by *Yulaeva* et al. [1994] and *Rosenlof* [1995], the local condition must respond to the pumping rate, insofar as stronger extra-tropical pumping must tend to pull tropical UTLS temperature below radiative equilibrium, encouraging deep cumulonimbus and producing higher and colder tropopauses.

Also well known are the fact that water vapor shows similar upward extending plume, but that in contrast with aforementioned tracers, very low values of the water vapor mixing ratio extends upward from a minimum within a few kilometers of the tropical tropopause. The minimum mixing ratio is only a few parts per million by volume (ppmv) and far lower than the tropospheric values. It is generally accepted, with good reason, that the basic mechanism responsible for the low values is freeze drying [*Brewer*, 1949] a process in which air passing through the tropical tropopause has its water vapor mixing ratio reduced to ice saturation value at or near the tropopause. Recently *Sathiyamurthy and Mohanakumar*, [2000] and *Mohanakumar and Pillai* [2008] observed the relation between tropospheric biennial oscillation (TBO) and QBO which indicates troposphere-stratosphere interaction over Indian monsoon region.

1.11. Brewer-Dobson circulation

The Brewer-Dobson circulation is a slow circulation pattern, first proposed by Brewer to explain the lack of water in the stratosphere. The Brewer-Dobson Circulation is an equator-to-pole circulation pattern that features slow lifting motion in the tropics and sinking motion in the polar latitudes. This tropical lifting circulation out of the lower stratosphere is quite slow, of the order of 20-30 m per day. Lifting by the Brewer-Dobson Circulation carries ozone out of its tropical lower and middle stratosphere, which is the photochemical source region**,** into the lower polar stratosphere, where it accumulates due to sinking motion. He presumed that water vapor is freeze-dried as it moves vertically through the cold equatorial tropopause. Dehydration can occur in this region by condensation and precipitation as a result of cooling to temperatures below 193 K. The lowest values of water are found just near the tropical tropopause. Later Dobson suggested that this type of circulation could also explain the observed high ozone concentrations in the lower stratosphere polar regions which are situated far from the photochemical source region in the tropical middle stratosphere. The Brewer-Dobson circulation additionally explains the observed latitudinal distributions of long-lived constituents like nitrous oxide and methane. That Brewer-Dobson circulation is controlled by stratospheric wave drag, quantified by the Eliassen-Palm flux divergence, sometimes lays claim to the extratropical pump, with the circulation at any level being controlled by the wave drag above that level. However, the wave drag can be difficult to compute accurately and it is common to diagnose the mean circulation from the diabatic heating. It is possible to estimate the net mass flux across a given isentropic surface from the diabatic heating. Figure 1.7 shows the average annual flow of the Brewer Dobson Circulation.

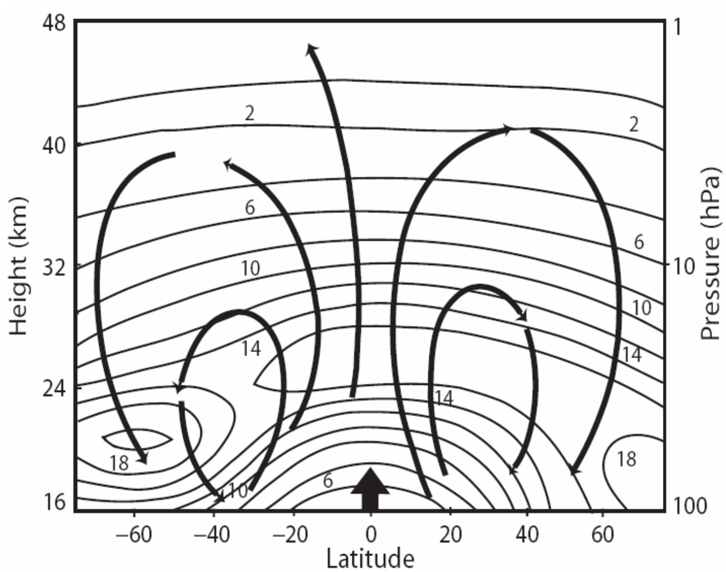

Figure: 1.7 *Zonal mean middle atmospheric circulation and annual average ozone density (DU/km), from Nimbus-7 SBUV Observations during the period 1982–89* [*Courtesy: NASA*]

1.12. The Stratospheric Fountain

Kley et al. [1979] reported measurements over Brazil of stratospheric water vapor mixing ratios of just 3 ppmv at an altitude of about 21 km. This value corresponds to a frost point of about -89^{o}C at that altitude or about -84^{o}C at 16 km which is approximately the altitude of tropical tropopause. The local temperature of the tropical tropopause was only about -80^{o}C and therefore passage of air through this region could not have been responsible for drying the air. *Kley et al.* [1979] suggest that the stratospheric air must have entered from troposphere in another geographical region where tropopause is close to frost point necessary to remove the moisture (i.e., ~ -84^{o}C) assume that the largest vertical motion into stratosphere occurs where the temperature are lowest. If lower limit of the stratospheric water vapor contains is ~ 3.5 ppmv that corresponds to a mass mixing ratio of 2.2 μg g^{-1} which is close to the minimum values reported by *Mastenbrook*. The corresponding frost points are -84^{o}C at 80 hPa and -82.4^{o}C at 100 hPa. *Newell and Stewart*, [1981], selected critical temperature at 100mb and assumes that air which has reached this low temperature by 100m can pass into the stratosphere without altering the stratospheric humidity. Therefore the area outlined by the -82.4^{o}C isotherm at 100 hPa represents the region where air may enter the stratosphere. Areas where air enters the stratosphere from the troposphere are west pacific in the December-February; northern South America in January-March and in May-September, Bay of Bengal, India and Malaysia. In general, the fountains are most active in October-March and moves to the monsoon region for the Northern Hemisphere summer.

1.13. The Extratropical Pump

To understand the STE, the existence of nonlocal dynamical effects in the atmosphere is to be taken into account. Reorganization of the nonlocal effects is crucial for understanding any fluid-dynamical system that supports fast waves whose travel times are short in comparison with other time scale of interest. For example to understand why air moves towards the inlet of any suction pump, one needs to recognize that the travel times of the acoustic waves are short in the sense and that there is corresponding nonlocal effect. Mass conservation has a key role and for practical purposes, acts instantaneously, as a nonlocal constraint. The time delay between turning on the pump and establishment the flow towards suction tube is order of an acoustic propagation time, usually negligible of all the time scale of interest. This non local picture is to be contrasted with statements like “air moves toward the suction tube because the pressure-gradient force pushes it," which miss the point that the pressure gradient adjusts nonlocally, to fit in with mass mass-conservation constraint.

There is a fundamentally similar nonlocal effects having direct relevance to the STE problem, namely the effect extratropical stratosphere and mesosphere on the tropical stratosphere. This depends on the fact that the global-scale travel times of acoustic waves and large scale gravity waves are short in comparison with other time scale of interest. The effect has been demonstrated, indeed has been intensively studied, in the dynamical literature beginning with pioneering work of *Eliassen* [1951] and *Dickson* [1968]. These and many other studies have shown that the extratropical stratosphere and mesosphere as a kind of global scale fluid dynamical suction pump, driven by certain eddy motions. The distinction between tropics and extratropics arises from the Earth's rotation, on which extratropical pumping action depends. The word "suction" is that statistically speaking, the most important of the eddy motions, so called "breaking Rossby waves" and related potential vorticity transporting motions, have ratchet like character related to the sense of Earth's rotation.

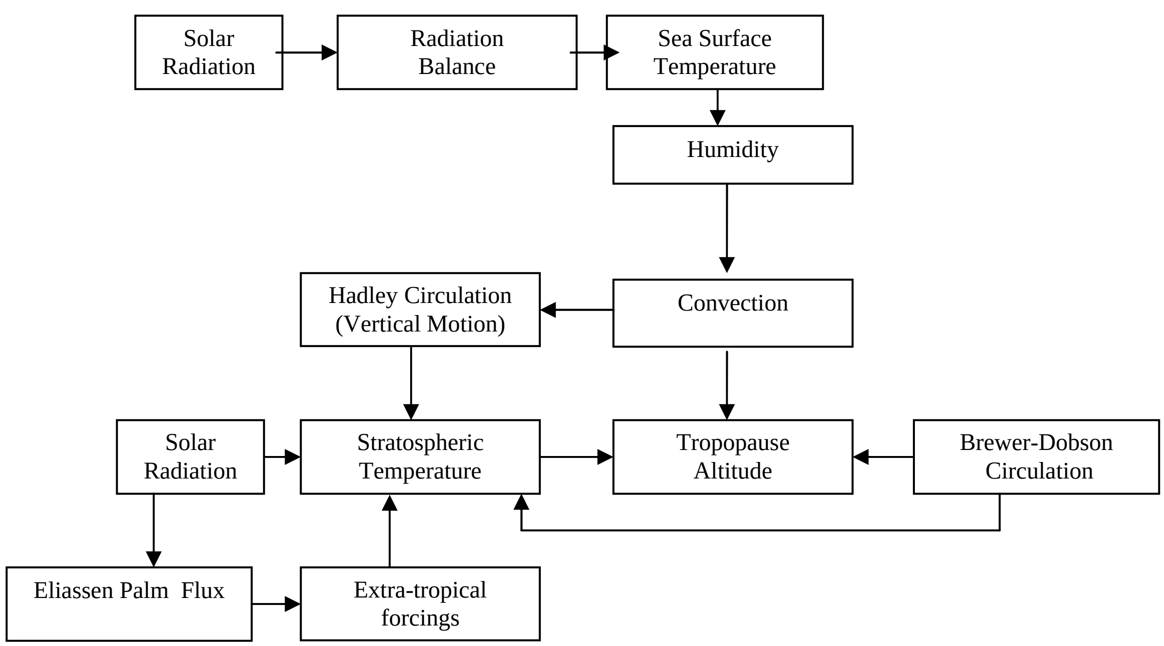

Figure1.8: *Schematic diagram of the factors that determine the altitude of the tropical tropopause* (*modified after Reid and Gage,* [1981])

These eddy effects has a strong tendency to add up and give persistently one-way pumping action, whose strength varies seasonally and interannually and air gradually withdrawn from tropical stratosphere and pushed poleward and ultimately downward. Where air parcel are being pulled upward (as in tropical stratosphere), adiabatic cooling pulls temperature below their radiative values and where air parcels are being downward (as happens most strongly in high latitudes in winter and spring), adiabatic warming pushes temperatures above their radiative values. This mechanically pumped global-scale circulation is often referred as the “wave driven circulation”.

1.14. Thesis Layout

All previous sections dealt with the factors affecting the tropical tropopause right from the seasonal to solar cycle variations. In general, understandings of the tropopause behavior on these time scale are well established. However, in short scales, particularly day-to-day and sub-daily scales, characteristics of the tropopause, which are equally important is least explored due to limitations in the existing techniques. In addition, large scale features affecting the tropopause are dealt by assuming zonal mean variation. However, there are large longitudinal behavior exist which was paid less attention until now. The tropical tropopause has been studied in past but they are meager because of the limited data sets. In addition, the existing tropical tropopause studies are mainly focused on the western pacific region and the studies over monsoon region which is expected to behave differently is yet to be done. By using the daily radiosonde launching and simultaneous MST radar observations along with GPS RO data an attempt has been made to study the tropical tropopause behavior with special emphasis on the Indian monsoon region. The tropopause over the Indian monsoon region is found to be highest during winter season when convection is week. What causes the winter high tropopause, whether the extra-tropical wave forcing is the only answer? There are many such issues remain unexplained. This thesis is intended to find the reasons for few such questions. Thus, keeping in mind of these limitations in previous works the present thesis attempts to overcome some of these limitations by utilizing the measurement from the state of art techniques like MST Radar and GPS Radiosonde observation together with high vertical resolution and high accuracy GPS RO measurements.

The following are the objectives attempted in the present thesis.

1) How the tropospheric convective outflow level is compared with altitude of minimum potential temperature gradient and what is its relation to brightness temperature? What is the nature of the tropical tropopause layer over Indian monsoon region?
2) How tropical tropopause parameters vary in various scales (ranging from seasonal to sub daily scale) especially over Indian monsoon region? Does a sub-daily variation show any diurnal or semidiurnal component? How tropical tropopause parameters are associated with convection, especially on short term?
3) Whether the tropical tropopause shows longitudinal behavior, if it is so, why? At which region it has the pronounced longitudinal characteristics? Does tropical tropopause show different characteristics in convectively active (west pacific and Indian monsoon) and non –active region?
4) How the multiple tropopauses which commonly appear in the tropical region can be interpreted? Are the existing (WMO) definitions are adequate to quantify the multiple structure of the tropical tropopause or new definition is needed?
5) How the tropical tropopause is modulated by equatorial Kelvin wave during different seasons and different phases of the quasi-biennial oscillation (QBO)?

The complete work is distributed in eight chapters and content of each chapter is briefly summarized below

A brief introduction about the tropical tropopause properties based on present understanding is presented in Chapter1.

As mentioned earlier, to attempt these issues, the MST radar, GPS Radiosonde observation at Gadanki (13.5^{o} N, 79.2^{o} E), and Global positioning system (GPS) Radio occultation (RO) observations in the tropical belt (±30^{o}) are used. Descriptions of each system are provided in Chapter 2.

Chapter 3 establishes the concept of the convective tropopause using MST radar vertical velocity observations at Gadanki, a tropical station. This is compared with the altitude of local minimum of potential temperature lapse rate obtained from simultaneous radiosonde observations. The convective tropopauses altitudes are also compared with the cloud top altitudes obtained using satellite brightness temperature.

Chapter 4 presents detail features of the tropical tropopause characteristics and its variability over the Indian monsoon region with special emphasis on the variation of tropical tropopause on shorter time (sub-daily) scales. The shorter-term (sub-daily) variability of the cold point tropopause is also examined in relation to convection and tidal modulation.

Chapter 5 characterizes the longitudinal variability of the tropical tropopause, tropical convective tropopause and TTL using radiosonde and GPS RO data. In this study the behavior of the tropopause in pacific (convective region), non-pacific and Indian monsoon region is emphasized. There are several studies (eg. *Geller et al*, 2002) has been carried for the longitudinal characteristics of the tropical tropopause. However present study of tropical tropopause over Gadanki reveals some new longitudinal characteristics when compare to pacific and non pacific region, which are not reported earlier.

Chapter 6 deals with characteristics of the multiple tropopauses (MTs) in the tropics using Radiosonde and GPS RO data. The multiple tropopauses are mainly focused on the mid-latitude regions which are found associated with subtropical jet streams. These reports show that the MTs in the tropical region are less explored since the occurrences are very few. The present study shows that less number of occurrences of MTs over tropical region is restricted due to threshold value used in WMO criteria. In this study an alternative criterion is proposed which is based on the cold point tropopause and points of inflection rather than lapse rate as in WMO criteria. Based on present method the annual variation of occurrence statistics of MTs (LT ST and TT) is studied by using several radiosonde stations data within the tropical region. Using GPS RO observations, the inter-annual variation in altitude, temperature and pressure in different longitude sector divided into 60^o grid are presented. The physical processes responsible for the formation of MT above and below the cold point are also discussed.

Chapter 7 deals with the tropical tropopause modulation by equatorial waves in different seasons. The main focus of this chapter is to quantify the seasonal behavior of the Kelvin wave/ Rossby gravity wave which play dominant role in the modulation of the tropical tropopause. The modulation of the tropical tropopause in easterly phase, westerly phase and transition zone of easterly and westerly phase of quasi biennial oscillation (QBO) is discussed briefly. The spectrum analysis has been performed to extract the dominant period.

Chapter 8 describes the summary drawn from the present study. Few suggestions and recommendations for further studies are also briefly outlined.

---END---

Chapter 2

Systems Description and Methods of Analyses

In the present thesis both ground and space borne observation along with model data whenever required is used. The ground based observation includes radiosonde and MST radar observations while space borne observation is mainly GPS Radio Occultation. These techniques provided the atmospheric parameters measurements with good time or height resolution, particularly in the study region of the present thesis. The present thesis focused on the characteristics of the Tropical Tropopause. These unique data sets in the Indian monsoon region enable to study many interesting features about the tropical tropopause. The basic information about the technique involves in these instruments and their limitation and source of error are briefly outlined.

2.1. Atmospheric Radars and Techniques

The first detection by radio techniques of presence of an aeroplane occurred accidentally in 1930 [*Skolnik*, 1962]. From the modulation of the received continuous signal as the wave reflected off the target interacted with the primary (direct) continuous wave between two stations of a bi-static system, presence of an object could be detected. *Watson-watt's* development in 1935 gave **radar** (**RA**daio **D**etection and **R**anging) in modern form. Watson-watt presented pulsed, mono-static radar, allowing the determination of both the range and the direction of the detected object. With the advent of the improved technologies in electromagnetics, electronics, and signal processing, atmospheric radars can support a wide range of applications and cover a large extent of altitudes with both finer time and height resolution. The information is derived from the echoes of hydrometeors or from variations in index of refraction of the clear air atmosphere. Hence, it is customary to differentiate between weather and clear-air atmospheric radars.

Weather radars are used to investigate particular weather phenomena such as thunderstorms, squall lines, tornadoes, cyclones, and precipitation. Typically, they operate at centimeter wavelengths, deriving information from the echoes backscattered from aerosols, water droplets, and ice particles.

Atmospheric radars are designed to probe the optically clear atmosphere, from troposphere to mesosphere (thus generic name of **MST** (**m**esosphere-**s**tratosphere-**t**roposphere) radars) [*Balsley and Gage*, 1978]. Therefore, clear air atmospheric radars offer many possible applications, besides measuring the background mean wind, for the study of the small scales atmospheric phenomena, such as turbulence and scattering processes, as well as large scale phenomena, such as gravity waves, atmospheric constituent and energy transport and coupling of the different atmospheric regions. Also, operational atmospheric radars provide continuous measurements of synoptic data which are crucial to weather forecasting and meteorological analysis.

2.1.1. General principles of the atmospheric radar

Figure 2.1 shows a simplified block diagram of an MST radar system up to the detection of the received signal. A stable oscillator (OSC) generates the electromagnetic (EM) wave at the desired frequency, in the range from medium frequency (MF) to ultra-high frequency (UHF) depending on the system requirements and the applications. The waveform is modulated (MOD) with rectangular pulses and later amplified in the transmitter (TX) in order to provide the necessary power output for emission at antenna (ANT). The transmitted radio wave pulses propagate through the atmosphere but are also partially backscattered towards the radar. The received signals from the antenna are directed to the receiving part of the radar through transmitter receiver (TR) switch which protects the receiver from high power signal of the transmitter when radio wave pulses are emitted. The radio-frequency signal (RF-SIG) received are first pre-amplified (RF-AMP) before they are mixed (MIX) with coherent local frequency (LO) to down convert them the system intermediate-frequency signal (IF-SIG). It is at this stage the received signal is amplified and filtered to provide maximum peak signal-to-noise power ratio (SNRp). Thus, the IF amplifier (IF-AMP) can be seen as an approximate matched filter with gain. The filtered and amplified IF signal is then transferred to a quadrature (complex) detector (QUAD-DET) which remove the IF frequency reference carrier (REF) and yields the time series of the cosine (cos) and sine (sin) component of the backscattered signal. The detected complex signal (DET-SIG) is later digitized (DIGITAL SIG) through an analog digital converter (ADC) to allow digital computer processing of the detected echoes in order to derive the desired atmospheric parameters.

It is usual to first perform some coherent integration before any analysis is done. That is, successive points in the digitized time series are added together to generate one data value. The time separation between resulting data points will be increased but the useful signal will be greatly improved. Indeed, the characteristics of the useful signal (the signature of the atmospheric motion) vary somewhat slowly compared to noise component which is randomly distributed. Hence, coherent integration will increase the resulting signal-to-noise ratio (SNR) as long as the useful signal characteristics do not significantly change over the integration time. Coherent averaging will also decrease the bandwidth of the signal that can be detected and thus act as a low pass filter. Sometimes, to enhance the delectability of the signal after some pre-processing (like spectrum analysis, etc.), incoherent integration is performed which corresponds to averaging successive sets preprocessed data. Figure 2.2 illustrate the processes of coherent and incoherent integration.

.

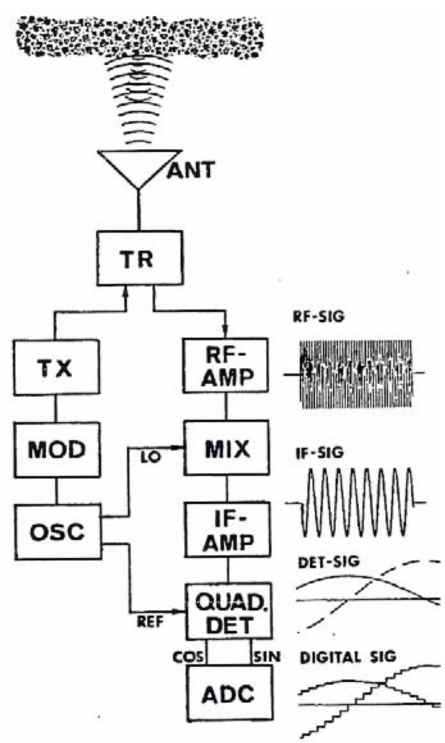

Figure 2.1: *Block diagram of an MST radar system: transmission, reception and signal detection, together with the corresponding signal waveforms [After Tsuda, 1988].*

The altitude or range resolution of MST radar is determined by the pulse width (τ) and is usually defined by $c\tau/2$,where c is the speed of light while corresponding sampling altitude Z is given by $c\Delta t/2$ as shown in Figure 2.3. Hence, shorter pulse will provide a better altitude resolution. However, shorter pulses require a wider system bandwidth, defined by $1/\tau$ in the ideal case. The bandwidth is a particularly important factor for the IF filters amplifier stage design. The integrated noise power is proportional to the receiver bandwidth while integrated signal power increases rapidly for small bandwidth but then asymptotically tends to be a constant value for larger bandwidth. Therefore an optimum bandwidth which maximizes the SNR can be defined, depending on the signal spectrum.

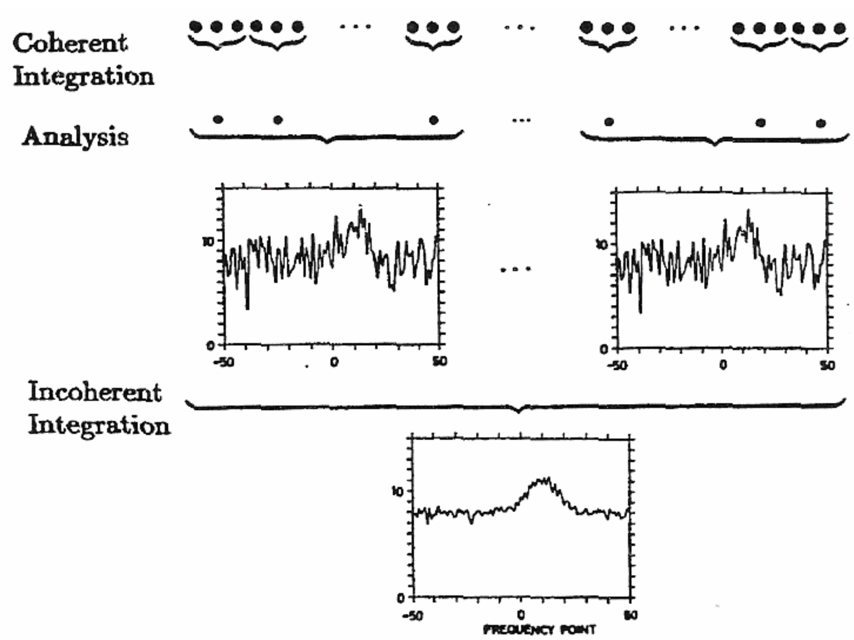

Figure 2.2: *The concept of coherent and incoherent integration in the signal processing flow.*

For practical reason it is customary to approximate the optimum matched filter by a rectangular band pass filter (BPF). It can be shown that the IF bandwidth of BPF corresponding to an emitted rectangular pulse of width τ, should be $1.4/\tau$ [*Skolnik*, 1962]. To improve the SNR and preserve the high resolution achieved, it is customary to use longer coded pulses with short sub pulses. The minimum altitude that can be probed by the radar is determined by the emitted pulse duration plus the receiver recovery when the TR switch activates the receiving system. Theoretically, there is no maximum altitude but fading of the emitted EM wave and the minimum sensitivity threshold of the radar system combine to restrict the maximum range that can be probed. Accordingly, the later will vary with the atmospheric conditions. Usually, the time separation between the successive emitted pulses or pulse-repetition period (PRP, or inter-pulse-period IPP) will define maximum unambiguous altitude that can be probed. Nonetheless spurious echoes can arise from the return due to previous pulses backscattered at higher altitudes and create ambiguities.

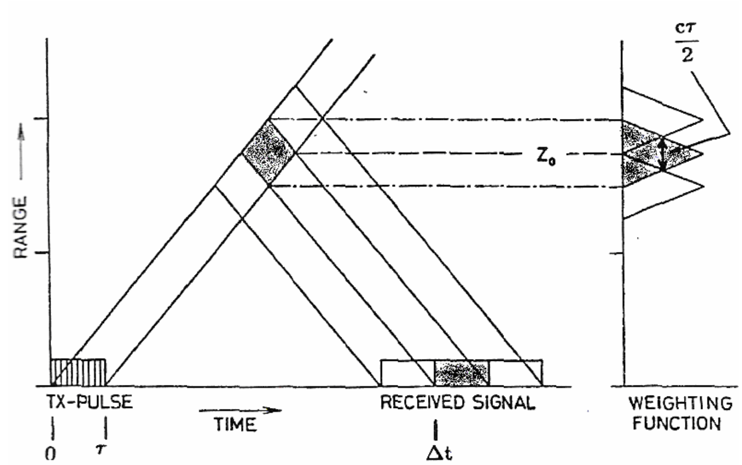

Figure 2.3*: Time height chart and sampling weight diagram for a transmitted rectangular pulse. [After Tsuda, 1988].*

The Doppler technique makes one or more narrow beams pointed in different directions. For the practical reasons such as antenna size, the radar is usually operated at very high or ultra high frequencies (VHF, 30-300 MHz; UHF, 300MHz-3GHz). The Doppler shift measured in each beam direction corresponds to radial velocity, a projection of the background wind vector along the antenna –beam line of sight. It is current practice to use a vertical beam and /or two or more orthogonal oblique beam directions in order to resolve the there- dimensional wind vector. Doppler radar which sequentially switch one beam from one position to another position are often called Doppler Beam Swinging (DBS) systems.

2.1.2. The atmosphere as an echoing medium

The optically clear atmosphere is source of the significant echoes received by the atmospheric radars considered in the present study. These echoes arise from scattering and reflection from inhomogeneities in the atmospheric dielectric constant ε or index of refraction n [*Friend*, 1949; *Booker and Gordon*, 1950; *Woodman and Guillen*, 1974], caused by turbulence or layered structures of different index of refraction.

In general, the radio index of refraction is in the MF to UHF frequency range is appropriately given by the approximation [*Gage and Balsley*, 1980]

$$n-1=\frac{3.73\times10^{-1}e}{T^{2}}+\frac{77.6\times10^{-6}P}{T}-\frac{N_e}{2N_C} \tag{2.1}$$

Where P the atmospheric pressure in (millibars) is, e is the partial pressure of the water vapor (millibars), T is the absolute temperature (Kelvin), N_e is the number of the density of the electron (m^{-3}), and N_C is the critical plasma density (m^{-3}) [*Yeh and Liu*, 1972]. The first term in the right hand side of the equation is called water vapor term and is dominant contribution to the refractive of index in the lower troposphere due to the high humidity content. The second term or dry air term, is the most important contribution from the mid-troposphere up to the stratosphere. The third term expresses the contribution due to presence of the free electrons in the neutral atmosphere. The ratio N_e/N_C is negligible below 50 km, but becomes the major contributor to the refractive index above that level, where the electron density increases rapidly with altitude. Figure 2.4 schematically shows the regions of the relative influence of the different terms in (2.1).

2.1.3. Turbulent (Bragg) Scattering

Booker and Gordon, [1950] pioneered the analysis of the EM wave scattering by a turbulent atmosphere. Noting that, although the mean wind speed and direction can be fairly constant over extended period of time, instantaneous measurements can reveal wide variations from those of mean values, they deduced that the turbulent behavior of the atmosphere will create fluctuations in the index of refraction which, in turn, support the scattering of EM waves. Their basic assumption are that turbulence is isotropic in nature and departure from mean index of refraction at different points in space exhibit a degree of correlations which decreases with distance and become negligible beyond the scale of the turbulence. However, their approach can be criticized as they used an arbitrary equation for algebraic simplicity. The other approach to the problem is based on the well-recognized initial range theory of the atmospheric turbulence pioneered by *Kolmogorov*

[1941] and further developed by *Batchelor* [1955], *Silverman* [1956], and *Tatarskii,* [1971]

$$\eta_{turb} = \frac{\pi^2}{2} k^4 \Phi_n(k) \tag{2.2}$$

Where $k = (4\pi/\lambda).\sin(\Theta/2)$ is the Bragg wave number which expresses that the scattering process is sensitive to the vertical structures of size $\lambda/2\sin\Theta$, λ is the radar wavelength, Θ is the scattering angle (i.e. angle between direction of propagation of the incident electromagnetic wave and the direction of propagation of the scattered electromagnetic wave).

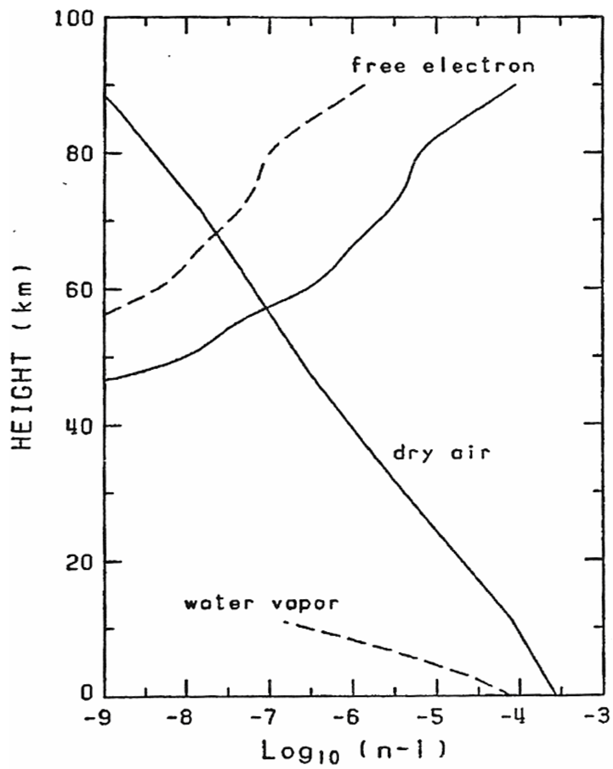

Figure 2.4: *Typical altitude profiles of the water vapor, dry-air, and free electron contribution to the radio index of refraction of the atmospheric medium. [After: Gage and Balsley, 1980]*

In back scattering situation, $\Theta = \pi$ (the backscattered signal wavelength is equal to one half of the radar wavelength) $\Phi_n(k)$ is the three dimensional wave number spectral densities for the index of refraction fluctuations. The three dimensional spectral density is normalized, (*Gage and Balsley*, [1980]) so that

$$\overline{(\Delta n)^2} = \iint\int_0^\infty \Phi_n(k) d^3k \tag{2.3}$$

with
$$\Phi_n(k) = 0.033 C_n^2 k^{-11/3} \tag{2.4}$$

valid over the inertial sub-range and where C_n^2 is the refractivity turbulence structure constant. For locally homogeneous and isotropic inertial sub-range turbulence, C_n^2 is defined as [*Silverman,* 1956].

$$C_n^2 = 5.45\overline{(\Delta n)^2} L_0^{-2/3} \tag{2.5}$$

Where, L_0 is the outer scale of the turbulence. The initial sub-range extends from L_0, where the atmospheric flow energy is transferred from small to large wave numbers through eddy fragmentation [*Tatarskii, 1971*], to l_0 , the inner scale of turbulence where all the energy is dissipated in the viscous range of wave numbers [*Kolmogorov*, *1941*]. The height distribution of l_0 determines the maximum altitude from which radar echoes at a given wavelength can be detected. The inner scale of turbulence characterizes the smallest in-homogeneities in the turbulent flow.

Combining equation (2.2) and (2.4), leads to:

$$\eta_{turb} = 0.38 C_n^2 \lambda^{-1/3} \tag{2.6}$$

However, *Gage and Balsley*, [1980] showed that these approaches will lead to estimated return signal strengths that agree within an order of magnitude, in the VHF frequency range.

2.1.4. Fresnel (partial) reflection/scattering

Fresnel reflection (also called partial or specular reflection) arises when coherent structure, usually stable horizontal layers, exhibiting sharp gradients of the index of refraction are present in the atmosphere. Fresnel reflection/scattering occurs from horizontally stratified refractive index gradients in the neutral atmosphere of troposphere and stratosphere [*Gage and Green* 1978; *Röttger and Liu* 1978] and electron density stratification in the mesosphere [*Fukao et al*. 1980]. At any particular height, the horizontal layer structure determines whether the radar return is due to reflection or scattering. “Fresnel reflection” [*Röttger and Larsen,* 1990] is observed if a signal arises from prominent discontinuity of the refractive index in vertical direction whereas

"Fresnel scattering" [*Gage et al.* 1981; *Hocking and Röttger* 1983] occurs from randomly distributed refractive index discontinuities in the vertical direction, which exist in a range gate. It means that Fresnel reflection is a single layer concept whereas Fresnel scattering is a multi layer concept and it is a kind of volume scattering that leads to specular echoes. Fresnel reflection process is also sometimes referred as "partial reflection" because only a very small fraction of the incident power gets reflected. Occurrence of Fresnel reflection/scattering is more likely for longer radar wavelengths, i.e., in the lower VHF range. The concepts of Fresnel reflection and scattering have been introduced to indicate that the horizontal correlation distance of the discontinuities is of the order of the first Fresnel zone dimension $\sqrt{r\lambda/2}$. The spectral width is narrow due to sharp vertical gradient in the radio refractive index. This particular feature can be utilized to distinguish these echoes from those arising due to the refractive index irregularities associated with turbulence.

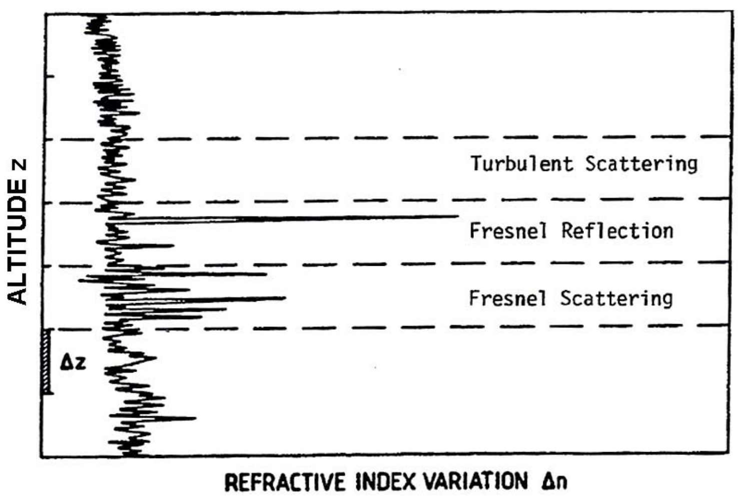

Figure 2.5: *Schematic representation of the index of refraction variation (Δn) for different backscattering mediums. [After Röttger and Larsen, 1989].*

2.1.5. Radar Equation

Let us assume that a transmitter with emitted (transmitted) power P_t and antenna of gain G. The power which illuminates a target of effective cross-section σ located on the main beam axis at a distance r from the emitter is given by:

$$P_i = \frac{P_t.G}{4\pi r^2}\sigma \tag{2.7}$$

Where it is assumed that there is no propagation loss through the atmosphere and plane-wave propagation in the antenna far-field ($r \geq 2D^2/\lambda$, where D is the antenna diameter and λ is the radar wavelength).

The reflected power intercepted by the receiving antenna, assuming isotropic radiation from the target is in mono-static case,

$$P_s = \frac{P_t.A_e}{4\pi r^2}\sigma = \frac{P_{t.}G.A_e}{(4\pi)^2 r^4}\sigma \tag{2.8}$$

Where A_e is the effective area of the antenna. For large array A_e is almost equal to the physical area of the array [*Avery*, 1985].

Thus the power available at the receiver is given by

$$P_r = \frac{P_{t.}G.A_e.v}{(4\pi)^2 r^4}\sigma \tag{2.9}$$

Where, v is the efficiency factor (<1) which accounts for the losses and attenuations due to the various radar system components. The gain (G) and effective are (A_e) of the radar antenna are selected by universal relation [*Stutzman and Thiele*, 1981]

$$G = \frac{4\pi}{\lambda^2}.A_e \tag{2.10}$$

Where $\lambda = c/f$ is the radar wavelength and f the radar frequency. Therefore (2.9) can be expressed as

$$P_r = \frac{P_{t.}G.A_e.v}{4\pi\lambda^2 r^4}\sigma \tag{2.11}$$

The above equation is valid for a localized target, or “hard target”. It is important to note that the received power is proportional to $1/r^4$ and to $(A_e/\lambda)^2$. If there are several targets in radar volume and they are randomly and independently distributed throughout the volume, i.e., they exhibit no correlation between them, the scattering cross section σ of equation (2.11) can simply be replaced by the sum of individual target cross sections: $\sum_i \sigma_i$ [*Battan*, 1973].

In case of very large number of scatterers uniformly in space, it is useful to define the "volume refractivity" (η), as σ increases linearly with the radar volume:

$$\sigma = V.\eta \tag{2.1.2}$$

with
$$\eta = \frac{d\sigma}{dV} \tag{2.13}$$

and
$$V \cong \pi \left(\frac{r\vartheta_{1/2}}{2} \right)^2 \Delta r \tag{2.14}$$

where $\vartheta_{1/2}$ represents the half-power beam-width of the antenna (assuming a circular aperture), and Δr is the length of radar range resolution cell. It is also important to account for a more realistic power distribution across the beam. Indeed, to derive (2.11), it is assumed that the factor G is constant and equal to the on-axis gain within the entire volume determined by half-power beam width. A Gaussian distribution is more satisfactory representation.

Introducing (2.12) into (2.11), and with usage of (2.10), (2.13), and (2.14), on can derive

$$P_r = \frac{P_{t.}A_e.v.\pi.\Delta r}{64r^4}\eta \tag{2.15}$$

in the event of uniformly distributed volume scatters. Equation (2.15) is often referred to as the "soft target" radar equation. It is proportional to $1/r^2$.

Another type of backscattering or reflection mechanism may arise from well-formed horizontal layers which have a slightly different index of refraction compared to the surrounding atmosphere and extended over a sufficiently large region. This mechanism is called Fresnel reflection. This layer can be treated as a planar mirror with small refractivity (ρ) for incident electromagnetic waves. The equivalent received power can be derived as in the case of a one way transmission to the mirror image of the receiving antenna.

$$P_r = \frac{P_{t.}G.A_e.v}{4\pi(2r)^2}|\rho|^2 \tag{2.16}$$

Using (2.10), equation (2.16) can be written as

$$P_r = \frac{P_{t.}G.A_e}{4\lambda^2 r^2}|\rho|^2 \tag{2.17}$$

which reveals dependency in $1/r^2$ as distributed scatters and proportionality to $(A_e/\lambda)^2$ as in the hard target case. An important aspect of Fresnel reflection is its secularity, or aspect sensitivity [*Rottger*, 1980]. As beam gets more oblique with regard to the layer, the reflected power rapidly falls off. Equation (2.17) corresponds to the beam perpendicular to the layer.

2.1.6. The Gadanki MST Radar

The Gadanki MST radar (Figure 2.6) is located at Gadanki (13.5°N, 79.2°E) which is 120 km towards NW from Chennai. The Gadanki radar is a highly sensitive, pulse coded (modulated) and phased coherent monostatic radar operating at fixed VHF frequency of 53 MHz [*Rao et al*, 1995]. Variable pulse lengths can be selected between 1 μs and 64 μs .The corresponding maximum height resolution is, thus, 150 m. The pulse repletion period (PRP) of inter-pulse period (IPP) is variable and can be specified in the range of 1000 μs -4000 μs . To improve the SNR characteristics of the measured echoes and preserve the higher resolution capabilities, binary phase coding is available with 1 μs and 32 μs (32 bits).

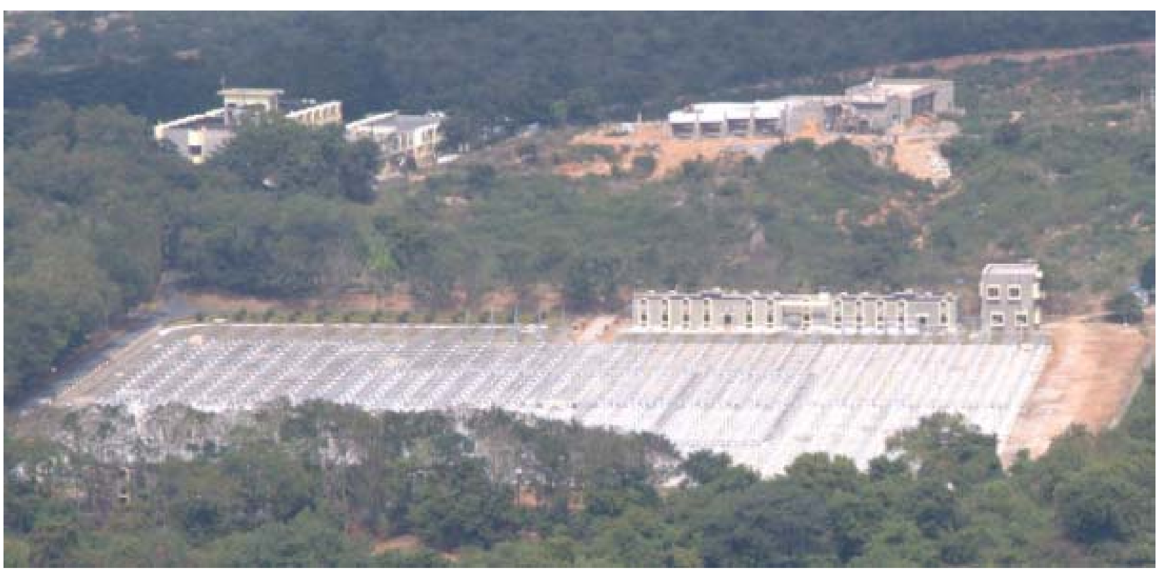

Figure 2.6: *Hill top view of the Gadanki MST radar site*

Barker and complementary codes can be used. A 16 bit (16 μs) complementary coded pulse, routinely used for tropospheric and stratospheric observations, allows a minimum observation altitude of 3.6 km (16 μs impulse + 8 μs for system recovery time).The rectangular antenna array (Figure 2.7) is composed of 1024 three element crossed Yagi-Uda antenna arranged into 32×32 matrix and has an overall physical area of $130m \times 130m$.The phased antenna elements are positioned into orthogonal direction, for E-W and N-S polarizations with a separation of 0.7λ between elements, which allows grating lobe free beam upto 20^{o} steering from zenith (vertical). The radar beam can, in principle be positioned at any look angle over a range of ±20 degrees from zenith in the EW and NS planes with a resolution of 1 degree by using the 8-bit phase shifters. The antenna pattern has been characterized in the receive mode by recording the radio source Virgo-A (3C 274) using the phase switching interferometer technique of *Ryle* [1952]. Based on the measurements, it has been found that the beam pointing accuracy is better than 0.2° and 3 dB beam width is in the range of 2.8° to 3° [*Rao et al*., 1995].

Figure 2.7: *View of the individual three-element crossed Yagis from antenna array floor.*

Each sub array (32 antenna element) is activated by solid state power amplifier whose output power ranges from 15 kW to 120 kW (for a total peak power of 2.5 MW). The transmitters can operate upto a duty cycle of 2.5%, limiting the total average power to about 60 kW. Thus, there are 32 separate transmitter-receiver (TR) modules which contains transmitter power amplifier and receiver preamplifier placed in four Huts (each contains 8 TR modules). The power distribution along the sub array follows a modified Taylor distribution to achieve desired first side lobe level of –20 dB. The conversion of between the 53 MHz radar frequency and the 5 MHz intermediate frequency (IF), for transmission and reception, is also performed in the TR modules. Therefore, only IF low power signals are transferred between the TR and radar controller which is computer driven for electronically controlled beam steering operations. The signal then goes through an IF amplifier chain with a gain of 73 dB and a bandwidth of 1.7 MHz. The IF is then split into two and applied to a pair of quadrature mixers which mix them with 5 MHz LO signals having quadrature phases of 0^0 and 90^0. The quadrature signals (In phase (I) and Quadrature (Q)) from the mixers are fed to two identical channels of low pass filter (LPF) and video amplifier to obtain the two bipolar video signals of $ACos\phi$ and $ASin\phi$ at the output. The receiver has an overall gain of about 120 dB and a dynamic range of 70 dB.

Table2.1: *Main Specification of the Gadanki MST Radar*

Antenna array	130 m x 130 m
Frequency	53 MHz
Wave length	5.66 m
Transmitted peak power	$2.5x10^6$ Watts
Beam width	3°
Receiver band width	1.7 MHz
Inter Pulse Period (IPP)	User defined
Maximum duty ratio	2.5%
Transmitting Pulse Width	1,2,4,8,16,32 or 64 μs
Starting Height	3.6 km
Max. No. Coherent integrations	512
Max. No. Incoherent integrations	User defined
FFT points	64-1024

The quadrature (I and Q) outputs of the receiver are limited to ±5 volts, which are given to a preprocessor unit consisting of two identical channels of A/D converter (ADC), decoder, and coherent integrator. A 16 bit parallel interface multiplexes the integrated outputs from I and Q channels and transfers the data to the host computer for further processing. The input to the data processing system is the decoded and coherently integrated complex time series data. The complex time series data are subjected to fast Fourier transform to compute Doppler power spectrum for each range bin of the selected range window. To improve delectability, sometimes spectral averaging is done. The specifications of the Gadanki MST radar are given in table 2.1. The spectral data with averaging or without averaging is stored for off line processing.

2.1.7. Moment Computation

The three lower order spectral moments (0^{th}, 1^{st} and 2^{nd}), providing total power, mean Doppler, and variance are then computed through numerical integration using the expressions given by *Woodman* [1985].

The 0^{th} moment representing the total signal power

$$M_0 = \sum_{i=m}^{n} P_i \tag{2.18}$$

The 1^{st} moment representing the weighted mean Doppler shift

$$M_1 = (1/M_0)\sum_{i=m}^{n} P_i f_i \tag{2.19}$$

The 2^{nd} moment represents the variance, a measure of dispersion from the mean frequency.

$$M_2 = (1/M_0)\sum_{i=m}^{n} P_i (f_i - M_i)^2 \tag{2.20}$$

where m and n are the lower and upper limit of the Doppler bin of the spectral window. P_i and f_i are the powers and frequencies corresponding to the Doppler bins within the spectral window.

Signal-to-noise ratio (SNR) in dB is calculated as

$$SNR = 10\log(M_0 / N.L) \tag{2.21}$$

where, N and L are the total number of Doppler bins and mean noise level, respectively, which on multiplication gives the total noise over the whole bandwidth.

Doppler width, which is taken to be the full width of the Doppler spectrum, for the present study is calculated as

$$\text{Doppler width} = 2(M_2)^{1/2} \tag{2.22}$$

2.1.8. Doppler Beam Swinging (DBS) Technique

Gadanki MST radar use Doppler Beam Swinging (DBS) method for the determination of the component of the wind. DBS technique utilizes large antenna array with correspondingly narrow radiation patterns, and with a minimum of three beams pointed in different non-coplanar directions to measure the wind velocities. These three directions generally include one at zenith and other two at off zenith angle in two orthogonal planes (i.e. E-W and N-S planes). The velocity vectors are computed from the line-of-sight (radial) velocities from these directions. This technique assumes that vector wind field is steady in time and uniform in space over the volume containing the range cells used. In the DBS method, for the determination of the component of the wind ,off-zenith angle need to be chosen carefully. The smaller zenith angle of the oblique beam leads to a better utilization of antenna aperture but it leads to the error in determination of the horizontal wind, as the contribution of horizontal wind along the radar beam would be small. On the other hand, large zenith angle would result in partial utilization of the effective aperture of the array. For these reasons an oblique beam zenith angle of 15º is considered to be optimum. For Gadanki MST radar oblique beams with zenith angle of 10° is utilized for wind estimation in place of 15º, to avoid 15 º N beams, which is almost orthogonal to the earth's geomagnetic field at Gadanki.

2.1.9. Calculation of radial velocity and height

For presenting the observation results in physical parameters, the Doppler frequency and range bin have to be expressed in terms of corresponding radial velocity and vertical height.

$$V = \frac{c \times f_d}{2 \times f_c} \tag{2.23}$$

where, f_d is Doppler shift as determined from the first moment of the spectrum given in equation (2.19)

$$Z = \frac{c \times t_r \times \cos\theta}{2} \tag{2.24}$$

where, c is velocity of light in free space, f_d is Doppler frequency, f_c is carrier frequency, θ is beam tilt angle and t_r is Range time delay.

2.1.10. Computation of absolute wind velocity vector (UVW)

After computing the radial velocity for different beam positions, the absolute velocity (UVW) can be calculated. To compute UVW, at least three non-coplanar beam radial velocity data are required. If higher numbers of independent beam data are available, then the equations have to be solved in the least square sense to obtain the optimum result. The line-of-sight component, V_d , of the velocity vector $\vec{V} = (\vec{V}_x, \vec{V}_{y,} \vec{V}_z)$ at a given height is expressed as

$$V_d = \vec{V}.\vec{i} = V_x \cos\theta_x + V_y \cos\theta_y + V_z \cos\theta_z \tag{2.25}$$

where $.\vec{i}$ is the unit vector along the radar beam and X, Y and Z directions are aligned to east-west, north-south and zenith(vertical), respectively. θ_x, θ_y and θ_z are the angles that the radar beam makes with the X, Y and Z axes, respectively. Using least square method [*Sato,* 1989]

$$\varepsilon = (V_x \cos\theta_x + V_y \cos\theta_y + V_z \cos\theta_z - V_{Di})^2 \tag{2.26}$$

Where, $V_{Di} = f_{D\,i} \times \lambda / 2$ and i represents the beam number.

To satisfy the minimum residual, $\partial\varepsilon^2 / \partial V_k = 0$, K corresponds to X, Y and Z.

$\vec{V}_d = \vec{V}.\vec{i} = V_x \cos\theta_x + V_y \cos\theta_y + V_z \cos\theta_z$

$$\begin{bmatrix} V_x \\ V_y \\ V_z \end{bmatrix} = \begin{bmatrix} \cos\theta_{x1} \cos\theta_{y1} \cos\theta_{z1} \\ \cos\theta_{x2} \cos\theta_{y2} \cos\theta_{z2} \\ \cos\theta_{x3} \cos\theta_{y3} \cos\theta_{z3} \end{bmatrix}^{-1} \times \begin{bmatrix} V_{d1} \\ V_{d2} \\ V_{d3} \end{bmatrix} \tag{2.27}$$

Where, $V_d = -f_d \lambda_R / 2$.

Thus, solving equation (2.27), we can derive V_x, V_y and V_z , which corresponds to U(zonal), V(meridional),and W(vertical)components of wind velocity.

In the present thesis, the specification used to collect the vertical wind is listed in table 2.2. The MST radar experiment carried out for three 3 days continuously with interval of 8 hours. From the collected power spectrum data the 1st moment is computed using equation (2.19) by utilizing the software Atmospheric data processor developed by *Anandan* [2005].

The first moment gives Doppler shift, thus the vertical velocity is calculated as multiplying with half of radar wavelength. From the vertical wind observation temperature profile are derived following *Revathy et al.,* [1996]. From use of vertical wind and temperature data the horizontal divergence profile is calculate following method perposed by *Satheesan and Krishna Murthy* [2005].

Table2.2: *Experiment specification file (ESF) used for present study of the MST Radar Observation.*

Parameter	Specification
Pulse width	16 μs
Inter-pulse period	1000 μs
Code flag	Coded
No. of beam	1(Zenith)
No. of FFT points	512
No. of coherent integrations	64
No. of incoherent integration	1
Nyquist frequency	± 3.9 Hz
Doppler resolution	0.03Hz
No. of range gates	150
Data type	Doppler power spectrum

2.1.11. Retrieval of the Temperature from MST radar vertical wind

From the vertical wind spectra the altitude profile of the Brunt Väisälä (BV) frequency can be identified. The BV frequency is found ~ 0.01 rad/s in troposphere and ~ 0.022 rad/s in the lower stratosphere indicating demarcation between troposphere and stratosphere. From BV frequency, atmospheric temperature can be derived from the relation

$$N^2 = \frac{g}{T}\left[\frac{dT}{dz} + \Gamma\right] \tag{2.28}$$

Where N is BV frequency in rad/s. T is temperature, g is acceleration due to gravity, z is altitude and Γ is adiabatic lapse rate.

Equation (2.28) can be solved for T as:

$$T(z^*) = \frac{1}{I(z^*)}\left[I(z_0)T_0 - \Gamma\int_{z_0}^{z^*} I(z_0)dz\right] \tag{2.29}$$

Where, $I(z) = \exp\left[-\int \frac{N^2}{g}dz\right]$, $T(z^*)$ is the temperature at altitude z^* and T_0 is reference temperature at altitude z_0.

In order to obtain the temperature profile the temperature measurement at reference altitude (surface temperature) is required. From the surface temperature the temperature at altitude 3.75 km is calculated taking environmental lapse rate 6.5 K/km. From temperature at 3.75 km, the temperature profile is obtained using equation (2.29). This iteration process is continued till the lapse between 3.75 km and 5 km is conversed.

2.1.12. Derivation of the horizontal divergence

Neglecting the local rate of change of density and horizontal advection (of density) term, the equation of continuity can be written as

$$\frac{\partial u}{\partial x}+\frac{\partial v}{\partial y}+\frac{\partial w}{\partial z}+w\left(\frac{d\ln\rho_0}{dz}\right)=0 \qquad (2.30)$$

where x, y and z represent east, north and vertical coordinates, respectively. u, v and w represent velocity components in east-west, north-south and vertical respectively, and ρ_o represents basic state density.

From equation (2.30), the horizontal divergence D can be expressed as

$$D=\frac{\partial u}{\partial x}+\frac{\partial v}{\partial y}=-\frac{\partial w}{\partial z}-\frac{w}{\rho_0}\left(\frac{d\,\rho_0}{dz}\right)=0$$

$$D=\frac{w}{H}-\frac{\partial w}{\partial z} \qquad (2.31)$$

$$\text{and } \frac{1}{H}=\frac{1}{\rho_0}\frac{d}{dz}=\frac{mg}{kT}-\frac{1}{T}\frac{dT}{dz} \qquad (2.32)$$

Here H is the density scale height. The first term in the right hand side (r.h.s) of equation (2.32) is the pressure scale height. The second term in the r.h.s is generally much smaller than first one. In *Satheesan and Krishna Murthy* [2005] the second term is omitted. However neglect of the second term does not affect D significantly and has little effect on the vertical structure of the D profile.

2.2. Radiosonde

Originally named a radio-meteor graph, the instrument is now referred to as a radiosonde, a name apparently derived by *H. Hergesell* from a combination of the words "radio" for the onboard radio transmitter and "sonde", which is messenger from old English. Operational weather observations often serve as primary observational data in atmospheric research. The high vertical resolution of radiosonde data offers a distinct advantage over some satellite data and reanalysis products. The earliest radio soundings were made in the late 1920's and 1930's by V. Väisälä. However, archived data generally begin in the 1940's, with significant expansion of the network at the time of the International Geophysical Year (1957-58). Currently, the radiosonde network includes about 900 upper-air stations, and about two-thirds make observations twice daily (at 0000 and 1200 UTC). The network is predominantly land-based and favors the Northern Hemisphere.

Instrument intended to be carried by a balloon through the atmosphere, is equipped with devices to measure one or several meteorological variables (pressure, temperature, humidity, etc.), and is provided with a radio transmitter for sending this information to the observing station. At most operational sites, the radiosonde system is also used for upper-wind determination. In addition, some radiosondes are flown with sensing systems for atmospheric constituents, such as ozone concentration or radioactivity. The wide range of meteorological conditions are: 1050 to 5 hPa for pressure, 50 to –90°C for temperature and 100 to 1 per cent for relative humidity, with the systems being able to sustain continuous reliable operation when operating in heavy rain, in the vicinity of thunderstorms, and in severe icing conditions. Radiosonde observations are used regularly for measurements up to heights of about 35 km. However, many observations worldwide will not be made to heights greater than about 25 km, because of the higher cost of the balloons and gas necessary to lift the equipment to the lowest pressures.

The radio frequency spectrum bands currently used for most radiosonde transmissions allocations specified by the International Telecommunication Union (ITU) Radio communication Sector radio regulations. The radio frequency actually chosen for radiosonde operations in a given location will depend on various factors. At sites where strong upper winds are common, slant ranges to the radiosonde are usually large and balloon elevations are often very low. Under these circumstances, the 400-MHz band will normally be chosen for use since a good communication link. When upper winds are not so strong, the choice of frequency will, on average, be usually determined by the method of upper-wind measurement used.

A basic radiosonde design usually comprises three main parts as follows: (a) The sensors plus references; (b) An electronic transducer, converting the output of the sensors and references into electrical signals; (c) The radio transmitter. Radiosondes are usually required to measure more than one meteorological variable. Reference signals are used to compensate for instability in the conversion between sensor output and transmitted telemetry. Thus, a method of switching between various sensors and references in a predetermined cycle is required. Most modern radiosondes use electronic switches operating at high speed with one measurement cycle lasting typically between 1 and 2 s. This rate of sampling allows the meteorological variables to be sampled at height intervals of between 5 and 10 m at normal rates of ascent. A wide variety of transmitter designs are in use. Solid-state circuitry is mainly used up to 400 MHz. Modern transmitter designs are usually crystal-controlled to ensure a good frequency stability during the sounding. Good frequency stability during handling on the ground prior to launch and during flight are important. At 400 MHz, widely used radiosonde types are expected to have a transmitter power output lower than 250 mW. The modulation of the transmitter varies with radiosonde type.

2.3. Radiosonde Sensors

The radiosonde sensors used to measure the temperature, pressure and relative humidity of the atmosphere are described below.

2.3.1. Temperature

Most modern radiosonde systems measure temperature in the troposphere with a standard error of between 0.1 and 0.5 K. Unfortunately, standard errors larger than 1 K are still found in some radiosonde networks in tropical regions. The rapid escalation in radiosonde temperature measurement errors at very low pressure results from an increase in temperature errors associated with infrared and solar radiation coupled with a rapid increase in errors in the heights assigned to the temperatures. At very low pressures, even relatively small errors in the radiosonde pressure measurements will produce large errors in height and, hence, reported temperature.

Large height errors in the stratosphere resulting from pressure sensor errors of 2 or 3 hPa are likely to be of greatest significance in routine measurements in the tropics, where there are always significant temperature gradients in the vertical throughout the stratosphere. In most modern radiosonde, coatings are applied to the temperature sensor to minimize solar heating. Software corrections for the residual solar heating are then applied during data processing. A radiosonde should be capable of transmitting an intelligible signal to the ground receiver over a slant range of at least 200 km.

The best modern temperature sensors have a speed of response to changes of temperature which is fast enough to ensure that systematic bias from thermal lag during an ascent remains less than 0.1 K through any layer of depth of 1 km. At typical radiosonde rates of ascent, this is achieved in most locations with a sensor time-constant with a response faster than 1 s in the early part of the ascent. The main types of temperature sensors in routine use are *thermistors* (ceramic resistive semiconductors), *capacitive sensors, bimetallic sensors* and *thermocouples*.

2.3.2. Pressure

Radiosonde pressure sensors must sustain accuracy over a very large dynamic range from 3 to 1 000 hPa, with a resolution of 0.1 hPa over most of the range and a resolution of 0.01 hPa for pressures less than 100 hPa. The main pressure sensor is *aneroid capsule*. Changes in pressure are usually identified by a small electrical or mechanical change. For instance, the typical maximum deflection of an aneroid capsule is about 5 mm, so that the transducer used with the sensor has to resolve a displacement of about 0.5 μm. Changes in calibration caused by sensor temperature changes during the ascent must also be compensated. These temperature changes may be as large as several tens of degrees, unless the pressure sensor is mounted in a stabilized environment. Thus, pressure sensors are usually mounted internally within the radiosonde body to minimize the temperature changes that occur. The pressure sensor and its transducer are usually designed so that sensitivity increases as pressure decreases. The time-constant of response of radiosonde pressure sensors is generally very small, and errors from sensor lag are not significant.

2.3.3. Relative Humidity

The successful operation of a radiosonde relative humidity sensor relies on a rapid exchange of water molecules between the sensor and the atmosphere. If a relative humidity sensor is to provide reliable measurements throughout the troposphere it must be able to resolve to 1 per cent of saturated water vapor pressures from 46 hPa at 30°C down to at least 0.06 hPa at –50°C. At temperatures below 0°C, relative humidity sensors should be calibrated to report relative humidity with respect to a water surface. Newly developed relative humidity sensors agree fairly closely at temperatures higher than about–70°C and show a similar relative humidity structure in the vertical. Satisfactory relative humidity sensor operation is often extremely difficult to obtain at very low temperatures and pressures. If the free exchange of water molecules between the sensor and the atmosphere is hampered as the temperature falls during an ascent, contamination of the sensor from high water vapor concentrations earlier in the ascent may cause substantial systematic bias in sensor measurements at the lowest temperatures. The main relative humidity sensor is *aneroid Carbon hygristor* and *thin-film sensors.* Carbon hygristor sensors are usually mounted in a protective duct in the radiosonde, and thin-film sensors are usually mounted on an outrigger from the radiosonde and protected with a cover against precipitation. The calibration of most relative humidity sensors is temperature dependent. The relative humidity measurements increase as temperature decreases. Most relative humidity sensors require protection from contamination by precipitation early in the ascent. The evaporation of contamination from protective covers, internal duct surfaces or sensor supports early in flight may also cause errors in the reported relative humidity. None of the operational radiosonde relative humidity sensors are reliable enough for good-quality relative humidity measurements at low temperatures and low pressures in the stratosphere.

In the present thesis, data collected from the launching of three GPS radiosondes are used viz. Väisälä RS-80, Väisälä RS-92(EN-SCI Corporation, Colorado, Boulder) and MEISEI (MEISEI electric co. Ltd, Japan), depending upon the availability of radiosonde systems over the observational site. The system setup of the MEISEI GPS radiosonde is shown in Figure 2.8. Its main specifications are listed in table 2.3.

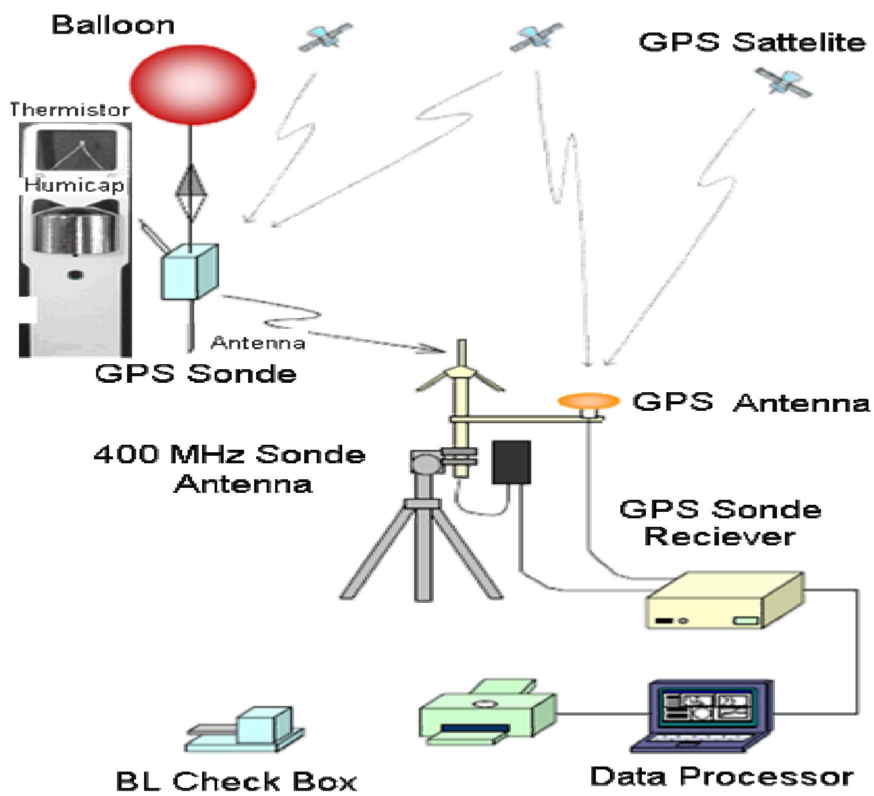

Figure 2.8: *The system setup of the MEISEI GPS radiosonde (RD-06G).*[*Courtesy: MEISEI electric co. Ltd*].

Table 2.3: *Main Specifications of Meisei Radiosonde (RD-06G)*

Parameter	Specification		
	Range	Resolution	Accuracy
Frequency			
GPS Antenna	403.7-405.2 MHz +/- 2 MHz		
Radiosonde Antenna	400-406 MHz		
Temperature (*Thermistors*)	-90^{o} C to 60^{o}C	-0.2^{o}C -0.5^{o}C	0.1^{o}C
Relative Humidity (*Thin film capacitor*)	0 % to100%	2%	1%
Pressure (*Derived from GPS height*)	3 to1080 hPa,	1 hPa,	0.1 hPa
Telemetry (*from GPS*)			
Wind Speed	0-60 m/s	0.15 m/s	0.1 m/s
Wind Direction	0 to 360 degree	2 degree	
Height		10 meter	

2.4. The Global Positioning System (GPS)

The Global Positioning System (GPS) is a satellite-based navigation system that was developed by the U.S. Department of Defense (DoD) in the early 1970s. GPS provides continuous positioning and timing information, anywhere in the world under any weather conditions. Because it serves an unlimited number of users as well as being used for security reasons, GPS is a one-way-ranging (passive) system. GPS consists, nominally, of a constellation of 24 operational satellites but now it consists of 29 satellites (Figure 2.9). To ensure continuous worldwide coverage, GPS satellites are arranged so that four satellites are placed in each of six orbital planes. GPS satellite orbits are nearly circular (an elliptical shape with a maximum eccentricity is about 0.01), with an inclination of about 55° to the equator. The semi-major axis of a GPS orbit is about 26,560 km (i.e., the satellite altitude of about 20,200 km above the Earth's surface). The corresponding GPS orbital period is about 12 sidereal hours (~11 hours, 58 minutes).

The GPS consists of three components: a space segment, a control segment and a user segment. The control segment of the GPS system consists of a worldwide network of tracking stations, with a master control station located in the United States at Colorado Springs, Colorado. The idea behind GPS is rather simple. If the distances from a point on the Earth (a GPS receiver) to three GPS satellites are known along with the satellite locations, then the location of the point (or receiver) can be determined by simply applying the well-known concept of resection. Each GPS satellite transmits a microwave radio signal composed of two carrier frequencies (or sine waves) modulated by two digital codes and a navigation message. Every GPS satellite has a high stable atomic oscillator whose frequency (f_0) is 10.23 MHZ and it can produce two carrier frequencies referred as the L1 ($f_1 = 154 \times f_0$ =1,575.42 MHz or λ ~19 cm) and L2 ($f_2 = 120 \times f_0$ =1,227.60 MHz, or λ ~24.4 cm). The availability of the two carrier frequencies allows for correcting a major GPS error, known as the ionospheric delay. The choice of L-band frequencies allows GPS to work well under all weather conditions, i.e. there is little attenuation. But the signal is delayed and bent when it goes through the atmosphere. Ionospheric delay; The ionosphere is a dispersive medium, which means it bends the GPS radio signal and changes its speed as it passes through the various ionospheric layers to reach a GPS receiver. As the ionosphere is a dispersive medium, it causes a delay that is frequency dependent. The lower the frequency, the greater the delay; that is, the L2 ionospheric delay is greater than that of L1. The combination of L1 and L2 carrier-phase measurement is used to remove the ionospheric delay. Unlike the ionospheric delay, the tropospheric delay cannot be removed by combining the L1 and the L2 observations. This is mainly because the tropospheric delay is frequency independent.

2.4.1. GPS Radio Occultation Technique

Radio Occultation is a remote sensing technique to explore the atmosphere, was first used in NASA's planetary missions to probe the planetary atmosphere [*Fjeldbo* and *Esleman*, 1969]. This technique has been applied for the limb-sounding of the Earth's atmosphere from Low Earth Orbiters (LEOs, 400-1300 km altitude). The GPS receivers carried by the LEO acquire signals from constellation of GPS satellite. The GPS radio Occultation technique concept has been successfully demonstrated for the first time by the GPS/MET (MicroLab-1) experiment in 1995 [*Ware et al*., 1996].

Figure 2.9: *Schematic diagram of GPS constellation* [Courtesy: NASA]

The fundamental principal is that transmitted GPS signals are delayed when LEO is setting into or rising above Earth's atmosphere. This delay could measure in the form of radar Doppler shift and a bending angle of Radar path. Finally, the atmospheric refractivity, temperature, pressure, air density as well as water vapor can be retrieved by assuming knowledge of appropriate boundary conditions.

After the success of the GPS/MET proof-of-concept mission, the current German CHAllenging Minisatellite Payload (CHAMP, launched in July 2000) [*Reigber et al.*, 2002] and Argentina's SAC-C (Launched in July 2000) carrying a new generation of GPS flight receiver ("Blackjack") provide quasi-contineous GPS occultation measurements. In addition, The U.S. – German Gravity Recovery and Climate Experiment (GRACE, launched in March 2002) mission [*Tapley et al.,* 2004a, b], and The Taiwan-U.S. multi-satellite Constellation observing System for Meteorology, Ionosphere and Climate (COSMIC, launched in April 2006) mission is providing unprecedented opportunities to continuously observe the Earth's atmosphere by GPS radio occultation technique.

2.4.2. GPS Radio Occultation Profile retrieval using Geometric Optics

In geometric optics [*Born and Wolf,* 1993], the propagation path of electromagnetic (EM) waves can be assumed as a dimensionless rays connecting the transmitter and the receiver. The solution is based on the assumption of spherically symmetric distributed atmosphere described by *Snell's law*. The change of the Doppler frequency along the orbit of the Low earth Orbiter (LEO) satellite is used to derive incident ray direction (or phase front slope) at each point on the orbit. The bending of the ray is geometrically obtained thereafter. This method is valid when no more than one ray arrives at every observation point on the LEO trajectory. The vertical profile of the atmospheric refractivity is related to the bending angle through the Abel Transformations [*Fjeldbo et al.,* 1971]. Afterward, the atmospheric pressure temperature, and humidity can be inverted from the refractivity through well established formulas. This method is relatively simple and straight forward. Usually, this method is applied in regions with no multi-path effect such as upper troposphere and stratosphere.

2.4.3. The ray trajectory and refractivity

The trajectory of the ray connecting two points when passing through a region with varying refractive index obeys Fermat's principle of least time:

$$\int_{1}^{2} n(\vec{r})ds = \text{minimum} \tag{2.33}$$

Where n is refractive index of the atmosphere. It is usually impossible to retrieve the three-dimensional distribution of the refractivity in the vicinity of the ray perigee (defined in Figure 2.10) from the one dimensional measurements along the trajectory of the receiving satellite. The problem can be simplified by considering the fact that the characteristic horizontal scale of meteorological fields is much bigger than the horizontal displacement of the ray perigee that crosses the atmospheric layers [*Gorbunov and Sokolovsky*, 1993]. This implies that the bending of the ray is generated dominantly by the vertical gradient of the refractive index in the occultation plane (the plane is formed by connecting two satellite points and the refraction center). The gradient of the refractive index normal to the occultation plane has negligible effect on the Doppler measurements. Thus, we assume the ray path resides only in the vertical occultation plane. The gradient of n is in the radial direction by assuming that the local refractivity distribution spherically symmetric in the vicinity of the ray perigee, such that

$$n(\vec{r}) = n(r) \tag{2.34}$$

.

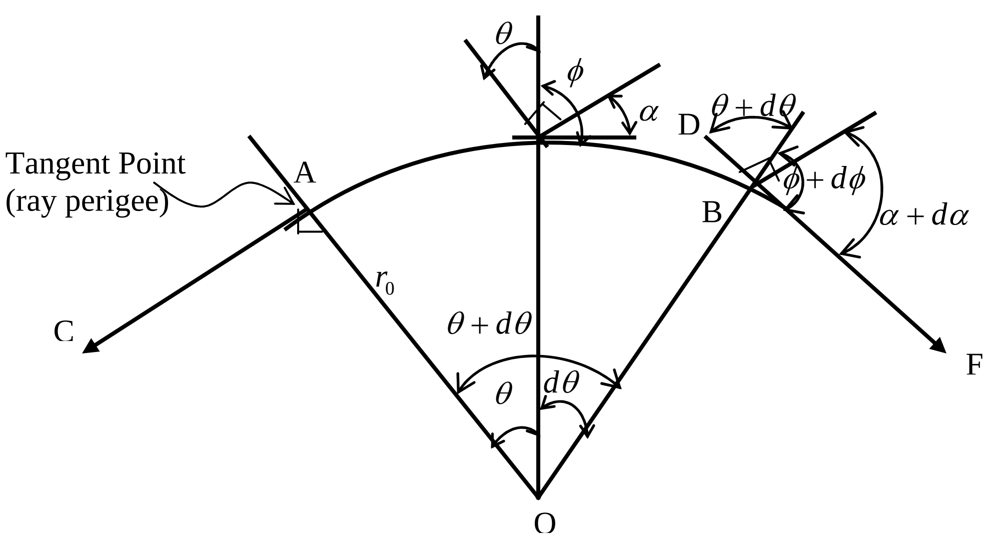

Figure 2.10: *The geometry of the refraction of the ray.*

Substitute the above equation in to equation (2.33), the ray path is described as Snell's law:

$$rn(\vec{r})\sin(\phi) = p \tag{2.35}$$

Where, ϕ is the angle between the ray path and the refractivity gradient vector and p is a constant for a given ray trajectory. It is usually called impact factor or impact parameter If the ray passes through a spherical symmetric refractive field and lies within the occultation plane, the change of the ray direction can be described by a polar coordinate system in such a plane with the origin at the center of the refractive field. The refractive index is only a function of the radius r, since the atmospheric density is distributed symmetrically in layers (like an onion) and its value increases as r decreases.

The geometry of the total bending of a ray is shown in Figure 2.10. ϕ is the angle between the ray path and the local radial direction, which can be expressed using the polar coordinates

$$\tan(\phi) = \frac{rd\theta}{dr} \tag{2.36}$$

From figure 2.10, the total bending angle α of the ray is

$$\alpha = \theta + \phi - \frac{\pi}{2} \tag{2.37}$$

Differentiating equation (2.37) and combining with equation (2.36), we obtain

$$d\alpha = d\theta + d\phi \tag{2.38}$$

The expressions $d\theta$ for and $d\phi$ are needed to compute the change of the bending angle $d\alpha$.

From Snell's law, $\tan\phi$ can be derived in another form from equation (2.35) as:

$$\tan(\phi) = \frac{p}{\sqrt{(nr)^2 - p^2}} \tag{2.39}$$

Combining the above two equations (2.36) and (2.39), $d\theta$ is written as

$$d\theta = \frac{pdr}{r\sqrt{(nr)^2 - p^2}} \tag{2.40}$$

For the expression of $d\phi$, we can differentiate equation (2.35),

$$r\sin\phi dn + n\sin\phi dr + nr\cos\phi d\phi = 0 \tag{2.41}$$

Rewrite above as:

$$d\phi = -\frac{\tan\phi(rdn + ndr)}{nr} \tag{2.42}$$

Substituting equation (2.39) into the above equation for $\tan\phi$, yields

$$d\phi = -\frac{p(rdn + ndr)}{nr\sqrt{(nr)^2 - p^2}} \tag{2.43}$$

From equations (2.40) and (2.43), $d\alpha$ in equation (2.38) can be written as:

$$d\alpha = \frac{pdr}{r\sqrt{(nr)^2 - p^2}} - \frac{p(rdn + ndr)}{nr\sqrt{(nr)^2 - p^2}} = -\frac{p}{\sqrt{(nr)^2 - p^2}}\frac{d\ln(n)}{dr}dr \tag{2.44}$$

Integrating equation (2.44) along the entire ray path, the total bending angle obtained as:

$$\alpha = \int_0^{\alpha'} d\alpha = -2p\int_{r0}^{\infty}\frac{1}{\sqrt{(nr)^2 - p^2}}\frac{d\ln(n)}{dr}dr\ ) \tag{2.45}$$

The "2" in the above equation is introduced due to the assumption of the spherical symmetry of the atmosphere, i.e., the ray is symmetric about the tangent point.

Equation (2.45) gives us a forward relationship to compute the bending angle profiles when we have *n* (*r*) along the ray path. It reflects that the bending angle is caused by the radial variations of the refractivity. This equation is usually called the *Abelian integral equation*.

2.4.4. The Abelian Inversion:

The Abelian integral equation (2.45) can be inverted to express the refractive index as a function of the bending angle and the impact factor. To facilitate the derivation of the formula, an auxiliary variable is defined as:

$$x = nr \tag{2.46}$$

Equation (2.45) can be rewritten as

$$\alpha(p) = -2p\int_{x=p}^{x=\alpha}\frac{1}{\sqrt{x^2 - p^2}}\frac{d\ln(n)}{dx}dx \tag{2.47}$$

Dividing both sides of the equation (2.47) by the factor $\sqrt{p^2 - p_0{}^2}$ and integrating with respect to p and p_0 to ∞, we obtained the following relation.

Where, p_0 is the impact factor corresponding to the radius r_0 at the tangent point:

$$\int_{p=p0}^{p=\infty} \frac{\alpha(p)}{\sqrt{p^2 - p_0^2}} dp = -\int_{p=p0}^{p=\infty} \frac{2p}{\sqrt{p^2 - p_0{}^2}} \left[\int_{x=p}^{x=\infty} \frac{2p}{\sqrt{x^2 - p^2}} \frac{d\ln(n)}{dx} dx \right] dp \qquad (2.48)$$

Changing the order of the integration and choosing the proper limits corresponding to the same integral region on the right side of the equation, yields:

$$\int_{p=p0}^{p=\infty} \frac{\alpha(p)}{\sqrt{p^2 - p_0^2}} dp = -\int_{x=p0}^{x=\infty} \frac{d\ln(n)}{dx} \left[\int_{p=p0}^{p=x} \frac{2p}{\sqrt{(x^2 - p^2)(p^2 - p_0{}^2)}} dp \right] dx \qquad (2.49)$$

Let us introduce another auxiliary variable u as a function of p ,

$$u(p) = \frac{p^2 - p_0{}^2}{x^2 - p_0{}^2} \text{ and } du = \frac{2pdp}{x^2 - p_0{}^2} \qquad (2.50)$$

By substituting (2.50) into the inner integral expression in equation (2.43), it becomes:

$$\int_{p=p0}^{p=x} \frac{2p}{\sqrt{(x^2 - p^2)(p^2 - p_0{}^2)}} dp = \int_{u=0}^{u=1} \frac{du}{\sqrt{u - u^2}} = \arcsin(2u-1)\Big|_{u=0}^{u=1} = \pi \qquad (2.51)$$

Then, equation (2.49) is simplified as:

$$\int_{p=p0}^{p=\infty} \frac{\alpha(p)}{\sqrt{p^2 - p_0^2}} dp = -\pi \int_{x=p0}^{x=\infty} \frac{d\ln(n)}{dx} dx = \pi \ln n(r_0) \qquad (2.52)$$

Rearranging equation (2.52), yields:

$$n(r_0) = \frac{1}{\pi} \left[\int_{p=p0}^{p=\infty} \frac{\alpha(p)}{\sqrt{p^2 - p_0^2}} dp \right] \qquad (2.53)$$

This is the classical *inverse Abel transformation.* The refractivity can be derived from the bending angles and the impact factors in the occultation plane.

2.4.5. The relationship between refractivity and atmospheric properties

The gas contents and properties contribute to refractive index n in the neutral atmosphere as discussed previously in section 2.1.2 for VHF radar. Since the value of the refractive index is very close to 1, it is usually more convenient use the refractivity N , which is defined as: $N = (n-1)\times 10^6$

Omitting the contribution from ionosphere, the equation (2.1) for the refractivity can be rewritten as:

$$N = c_1 \frac{P}{T} + c_2 \frac{p_w}{T^2} \tag{2.54}$$

The values for the constant coefficients are: $c_1 = 77.60$, $c_2 = 3.73 \times 10^5$. These constant are usually valid for radio frequencies less than 20 GHz.

2.4.6. Derivation of the Atmospheric Properties

In the neutral atmosphere, both the dry air and moist air contribute to the total refractivity. In lower part of the atmosphere, especially in tropical regions, the rapidly changing moisture content is big contributor to the refractivity, and needs special considerations. For the regions where, there's no moist air or the moist air has negligible effect on the refractivity, the atmospheric parameters can be easily derived using a combination of the equation (2.54) and ideal gas law (or Equation of State):

$$P = \frac{\rho RT}{m} = \rho R_m T \text{ with } R_m = \frac{R}{m} \tag{2.55}$$

Here, ρ is the air density, R is the universal gas constant (R =8.3144 J mol^{-1}K^{-1}), m is the mean molecular mass of the gas and R_m is specific gas constant, which depends on molecular weight of the air.

$$P = \rho R_d T(1+0.608q) = \rho R_d T_v \quad \text{with} \quad T_v = T(1+0.608q) \tag{2.56}$$

Where, $q = M_w / M_d$ and $\varepsilon = m_w / m_d$, M_d and M_w are the mass of the dry and moist air, respectively and m_d and m_w molecular mass of dry air and moist air, respectively.

This is another form of the Equation *of State*. T_v is called virtual temperature. With this virtual temperature correction, presence of water vapor is compensated.

Dry air density: If only the dry part of the air is considered, equation (2.54) becomes:

$$N = c_1 \frac{P}{T} \tag{2.57}$$

Combining with equation (2.55), the dry air density profile is given as:

$$\rho_d(z) = \frac{m_d}{Rc_1} N(z) \tag{2.58}$$

Where, z is the altitude, or height above the reference surface (ellipsoidal height or mean sea level height).

Dry air pressure: Usually, for a large volume of air, in the vertical direction, the gravity and the pressure gradient force are in balance. It is called the hydrostatic equilibrium. The expression is:

$$\frac{\partial p}{\partial z} = -\rho(z)g(z) \tag{2.59}$$

Where, $g(z)$ is the acceleration due to gravity at altitude z. Substuting equation (2.51) into the above equation and integrating it, the pressure is represented as a function of height:

$$P(z) = \int_z^\infty g(z')\rho_d(z')dz' = \frac{m_d}{Rc_1}\int_z^\infty g(z')N(z')dz' \tag{2.60}$$

Dry air temperature: Using either equation (2.59) or equation (2.58) again, the temperature profile is given as:

$$T(z) = \frac{1}{R_d N(z)}\int_z^\infty g(z')N(z')dz' \tag{2.61}$$

The temperature profile can be derived directly from refractivity profile under the assumption of non-existence of the moist air.

Air Humidity: In the GPS occultation, the retrieval of the pressure and temperature from the refractivity also requires the knowledge of water vapor pressure P_w. In the upper troposphere and stratosphere, atmosphere can be assumed to be dry with negligible error. However, in the lower troposphere and warmer tropical regions, when the condition of the wet component to the refractivity (sometimes ~ 30%) is significant, the water vapor can't be easily separated from the dry component. Neglecting the moist component will cause a big error. The extra moisture term in the equations makes the calculation of the air temperature, density and pressure difficult. This ambiguity is difficult to distinguish between the contribution of the dry and moist terms in the total refractivity unless independent or *priori* information is provided. Another important reason is that the hydrostatic equation only works with total pressure. In order to compute the water vapor pressure an accurate and independent estimate of temperature must be known. This may come from the NCEP or ECMWF meteorological analyses or forecast models. By substituting ρ in equation (2.56) to equation (2.59), it becomes:

$$\frac{dP}{P} = -\frac{g}{R_d T_v} \tag{2.62}$$

Integrating the above equation from z to z^*, yields:

$$P(z) = P(z^*)\exp\left(\int_z^{z^*} \frac{g(z')}{R_d T_v(z')} dz'\right) \tag{2.63}$$

If $P(z)$ is known, $P_w(z)$ can be derived from equation (2.54) as:

$$P_w(z) = T^2(z)\frac{N(z) - c_1 P(z)/T(z)}{c_2} \tag{2.64}$$

The specific humidity is defined as:

$$q(z) = \frac{\varepsilon P_w(z)}{P(z) - (1-\varepsilon)P_w(z)} \tag{2.65}$$

Where ε =0.622 is usually given.

The data collected using above instruments, techniques and methods is used to study the characteristics of the tropical tropopause which are divided into following Chapters

-----END-----

Chapter 3

Identification of Convective Tropopause and its Association with Cold Point Tropopause

3.1. Introduction

The tropical troposphere is characterized by low static stability and short vertical mixing time scale in contrast to the stratosphere. It marks the transition between convective-radiative equilibrium and radiative equilibrium. As discussed by *Attics and Robinson* [1983] and more recently by *Highwood and Hoskins* [1998], the tropopause in the tropics is not a material surface but a transition region between the troposphere and the stratosphere. The region between the main convective outflow (~12 km or 200 hPa) and cold point of the temperature profile (~17 km) is taken as the tropical tropopause layer (TTL) and is considered important as the source region for much of the air entering the stratosphere [e.g., *Holton et al*. 1995]. The upper boundary of the TTL determined by the cold point is better established than its lower boundary.

There are various methods adopted to determine the convective outflow level. *Gettelman et al.* [2002] used the altitude of minimum lapse rate of potential temperature as a good marker for the influence of convection on the temperature profile and hence the lower boundary of the TTL. The altitude of minimum lapse rate of potential temperature is taken as the level of maximum impact of convection on the thermal structure of the upper troposphere [*Gettelman and Briner,* 2007]. This level marks the level where radiation begins to influence the temperature lapse rate as it deviates from a saturated moist adiabat. However, some convection can occur above this level as well [*Gettelman and Foster*, 2002]. *Vomel et. al*., [2002] pointed out that the altitude of the local minimum of the relative humidity can be considered as lower boundary of the TTL. *Gettelman and Forster* [2002] further reported that the altitude of potential temperature lapse rate minimum matches with that of minimum in Ozone mixing ratio. The Outgoing Long wave Radiation (OLR) which gives a measure of the cloud top altitude can also serve as an indicator for the level of convection [*Highwood and Hoskins,* 1998] especially in the case of deep convection. The radiative cooling in clear skies is balanced by adiabatic heating through subsidence. The strong decline of the radiative cooling with altitude must be accompanied by strong divergence of mass from convective region. This divergence of mass is associated with frequent occurrence of the convective anvil cloud at this level [*Hartman and Larson*, 2002]. The mean heat balance of the troposphere is considered to be between convective heating (through the sensible heat flux from the surface and latent heat released during precipitation/by convective clouds) and cooling by radiation from water vapor. Thus, radiative cooling is an important constraint on convection [*Hartman and Larson*, 2002]. This implies that the most active convection will be limited to the altitude range where radiative cooling is efficient. The peak in detrainment of convection occurs at the level of peak mass divergence. This detrainment and divergence occur well below the cold point tropopause and do not appear to be caused in any direct way by lapse rate changes [*Hartman and Larson*, 2002]. In fact the cold point is essentially a stratospheric feature depending more on photochemistry of Ozone than on convection [*Kirk-Davidoff et al*. 1999; *Thuburn and Craig*, 2002]. The structure of the tropopause layer should be sensitive to large-scale vertical motion [*Reid and Gage, 1996*].

Recently *Satheesan and Krishna Murthy* [2005] devised a method to find the level of peak divergence using vertical wind data obtained from MST radar. In this method, the altitude of major peak of divergence closest to and below the cold point tropopause is identified from the horizontal divergence profile obtained using vertical wind data of MST radar and is taken as the major convective outflow level. This chapter presents the results of a detailed study of the altitude of major convective outflow at the tropical location, Gadanki (13.5^{0}N, 79.2^{0}E) obtained from vertical wind data of MST radar determined by the method of *Satheesan and Krishna Murthy* [2005]. This is compared with the altitude of minimum potential temperature lapse rate obtained using GPS radiosonde data and the results of this comparison are also presented in this chapter.

3.2. Data Base

The MST radar experiment with vertical antenna beam and GPS radiosonde experiment have been conducted near simultaneously at Gadanki on 43 occasions during May 2006 to April 2007. A detailed description of the MST radar at Gadanki is presented in Chapter 2 and brief details can be found in *Rao et al.*, [1995]. Vertical wind data was collected from the radar at ~35 s intervals for a duration of two hours around 1730 hours (all the times mentioned in the thesis are in Indian Standard Time, IST, corresponding to 82.5^{0}E longitude) in a day. The altitude resolution of these measurements is 150 m. The start times of the radar and radiosonde experiments are nearly the same (1730 hours). The

43 near simultaneous data sets of MST radar and GPS radiosonde (Väisälä RS-80 and RS-92) constitute the basic data for the present study. Radiosonde data was collected at 2 second intervals corresponding to an altitude spacing of ~10m. Later it is suitably averaged to bring the altitude resolution to 150 m, on par with MST radar altitude resolution. On a few days in October and November, 2006, the two hour vertical wind data collection was repeated 3 or 4 times in a day. Simultaneous hourly cloud top equivalent blackbody temperature, called Brightness Temperature (TBB) from GOES (Geostationary Operational Environmental Satellite) -9 IR (Infrared) recorded in longitude/latitude 0.05^{o} grids [*Miyakawa and Satomura*, 2006] from latitude 11^{o}N-15^{o}N and longitude 77^{o}E-81^{o}E covering the location of Gadanki are also used in this study.

3.3. Identification of altitude of major convective outflow

The vertical wind data of 2 hours on each day are averaged and these averaged profiles (*w*) are used to obtain the horizontal divergence profiles following the method adopted by *Satheesan and Krishna Murthy*, [2005]. This method uses the continuity equation in which the local rate of change of density and the horizontal advection terms are considered negligible. The divergence *D* is given by:

$$D = \frac{w}{H} - \frac{dw}{dz} \qquad \dots (3.1)$$

where positive (negative) value of *D* represents horizontal divergence (convergence) and z is the altitude (see Chapter 2 for details). The scale height H is obtained using the temperature profile derived from vertical wind data of MST radar for the corresponding 2 hours period following the method of *Revathy et al*., [1996; 1998] taking the mean molecular mass as 29. This method involves identification of the Brunt-Väisälä frequency (N) from the temporal spectrum of the vertical wind. From the altitude profile of N, the altitude profile of temperature is obtained by integration using the surface temperature as the boundary value [*Revathy et al*. 1996]. The profiles of N^2 i.e.$\left(\frac{g}{} \frac{d \ln \theta}{dz} \right)$ where g is acceleration due to gravity in ms^{-2}, θ is potential temperature in Kelvin, from the radiosonde observation for all the 43 cases are also calculated. The mean of the 43 profiles of N^2 along with standard deviation is shown in Figure 3.1(a). It is seen N^2>0 thus indicating that the conditions are statically stable. Identification of N from the temporal spectra of vertical wind may become difficult due to Doppler broadening which may happen when the back ground wind speed is greater than ~40m/s [*Revathy et al*. 1996; 1998].

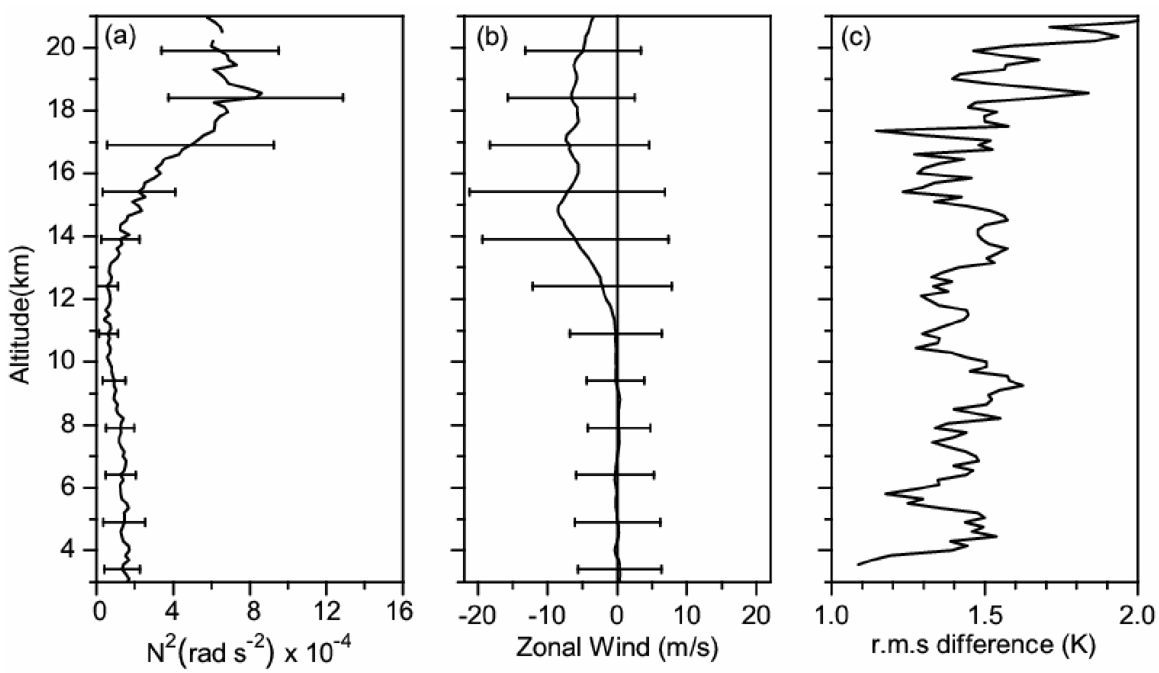

Figure 3.1: *Profile of mean (a) Brunt Väisälä frequency square (N^2), and (b) zonal wind. Horizontal bars show standard deviations obtained while considering all the 43 cases observed during Apr. 2006 to Mar. 2007 from radiosonde measurement over Gadanki. (c) Profile of r.m.s. difference of the temperature measured from radiosonde observation and that derived from MST radar observation obtained while considering all the 43 cases.*

The mean profile of zonal wind along with standard deviation observed by radiosonde for all the cases corresponding to the vertical wind profiles collected by MST radar is shown in Figure 3.1(b). Although mean zonal wind and standard deviation do not exceed more than 10 ms^{-1} and 25 ms^{-1}, respectively, note that individual profiles reached up to 35 ms^{-1} particularly during Indian summer monsoon season (June-September). However, except in three cases none of the profiles of the zonal wind reached values more than 35 ms^{-1}. This shows that conditions were favorable for identification of N from vertical wind temporal spectra and hence determination of temperature profile. In fact, no difficulty has been encountered, in general, in identifying N from the vertical wind temporal spectra. Further, the temperature profile obtained from the MST radar vertical wind observation is compared with radiosonde measurement as shown in Figure 3.1(c). The root mean square (r.m.s) value of the difference between the two varied between 1.2 K and 1.6 K below cold point tropopause and between 1.6 K and 2.0 K above cold point tropopause. This comparison further strengthens the validity of the method of deriving temperature profile from the radar data.

Averaging of vertical wind over ~ 2 hours for obtaining the D profile effectively smoothes out any perturbations due to gravity waves of periods ≤ 2 hours. As it is known that for longer period gravity waves, the vertical wind perturbations will be very small [*Fritts and Alexander*, 2003] the effect of gravity waves on the D profiles can be considered to be negligible. The D profiles obtained represent average over 2 hours as 'w' profiles used in obtaining the D profiles are averages over 2 hours. Further, the altitude profiles of D are subjected to 9-point running mean filter to smooth out small scale fluctuations, if any. This smoothed profile is designated as $\langle D \rangle$ profile. It may be noted here that gravity waves due to non-steady heat sources [*Mapes*, 1993] may affect the vertical wind (2hour averaged) profiles and hence the divergence profiles. However, such waves can occur mainly during deep convection events [*Mapes*, 1993]. It is to be noted that only four deep convection events occurred in the data considered in the present study (see Section 3.4.2). As such wave effects would leave their signature on the zonal and meridional winds as well, these profiles together with 'w' profiles are examined and found that there were no similar vertical structures in these profiles. Further, such effects, if any, would be largely minimized, if not removed, by the 9 point running mean filtering.

The $\langle D \rangle$ profile generally exhibited more than one peak indicating convective detrainment at more than one level. From the $\langle D \rangle$ profile the altitude of major convective outflow Z_D is determined following the criteria/procedure given below.

1. The maximum in the $\langle D \rangle$ profile below the cold point tropopause is identified.
2. If there is a peak between the maximum and tropopause whose $\langle D \rangle$ value is greater than 20% of the maxima the altitude of that peak is taken as Z_D. In case there is more than one such peak then the altitude of that one that is nearest to the tropopause is taken as Z_D.
3. If there is no peak satisfying the above criterion then the maximum is taken as Z_D.

The 20% criterion followed here may appear as somewhat arbitrary. However, this criterion is established after examining a number of divergence profiles. As convection leads to mass flux divergence the altitude of major peak in the $\langle D \rangle$ profile (Z_D) can be considered to be the level up to which convection dominates. So, Z_D is designated as the altitude of convective tropopause.

Using the vertical profiles of temperature and pressure obtained from the GPS radiosonde, altitude profiles of the potential temperature θ (i.e. $T\,(1000/P)^{0.286}$), where T is the temperature in Kelvin and P is the pressure in hPa, and its vertical gradient θ' are obtained. A 9-point running mean smoothing is applied to the θ' profile also. From the smoothed θ' profile (designated as $\langle \theta' \rangle$), the altitude of trough of $\langle \theta' \rangle$ nearest to the cold point tropopause is obtained which is designated as Z_L. In identifying the trough, similar criteria as for divergence peak is followed. That is, the trough between the minimum of $\langle \theta' \rangle$ and the cold point tropopause whose value is less than 5 times the minimum value and is less than ~ 5K/km is identified and its altitude is taken as Z_L. If there is more than one such trough then one closest to the tropopause is taken. If there are no such troughs then the minimum itself is taken for obtaining Z_L. Further, this low in $\langle \theta' \rangle$ should also mark the level above which the stability (indicated by $<\theta'>$) increases drastically [*Gettelman and Foster*, 2002]. It may be noted that $\langle \theta' \rangle$ less than 5K/km amounts to a temperature lapse rate of ~7.2 K/km. On examination of a number of radiosonde temperature profiles it is found that the closest the temperature lapse rate gets to the dry adiabat is ~8K/km. The criterion of $\langle \theta' \rangle$ less than 5K/km is based on this observation. From thermal structure consideration, the cold point marks the tropopause. As main purpose in the present study is to identify the level up to which convection plays a dominant role on the thermal structure (in the troposphere), the low in $\langle \theta' \rangle$ profile (and high in $\langle D \rangle$ profile) nearest to the cold point for identifying Z_L (and Z_D) have been taken. The trough in $\langle \theta' \rangle$ profile, thus identified (following the criteria given above), can be taken as the local minimum. It is to be noted that Z_L will not necessarily be the same as that from the definition of *Gettelman and Forster* [2002] who used the minimum of θ'.

As mentioned earlier, hourly data of TBB, which is considered as the cloud top temperature, are also made use of in the present study. An altitude is assigned to the TBB using the corresponding radiosonde temperature profile.

3.4. Results

3.4.1. Comparison of Z_D and Z_L

In many of the profiles it is found that the altitudes Z_D and Z_L match very well. It is observed that sometimes there is more than one divergence peak and among these the strongest divergence peak generally occurred in the height region of 10 km to ~16 km notwithstanding a few cases in which it occurred below this region. Convergence around melting layer 4.5-5.5 km with steep gradient in lower side of the peak is also seen in many of the profiles. Similar feature has also been reported by *Mapes and Houze* [1995]. Typical examples of comparison between the altitudes Z_D and Z_L are shown in Figures 3.2 (a), (b), and (c) for three different types of divergence profiles indicating sharp, multiple and broad convective outflow levels, respectively. In the following, the altitude of cold point tropopause is referred to as Z_C. Figure 3.2(a) shows the $\langle D \rangle$ profile derived from the radar and $\langle \theta' \rangle$ profile obtained from radiosonde measurement on 29 June 2006. The Z_D and Z_L are indicated by an arrow and a dot mark, respectively, in the figure. The Z_D is at 14.35 km whereas Z_L is at 14.65 km. In the $\langle D \rangle$ profile a secondary divergence peak is also present at ~8.05 km and a trough in $\langle \theta' \rangle$ profile is also seen at about the same altitude. The secondary peak is not of importance in the present study. The TBB at 1730 hours is 246.1K corresponding to an altitude of 9.3 km. This is lower by about ~5 km than the convective outflow altitude obtained from the radar. However note that the secondary peak in the $\langle D \rangle$ profile is closer to the cloud top altitude from TBB. Similar features can also be noticed for the case of multiple convective outflows, shown in Figure 3.2(b), on 25 February 2007. The Z_D is at 15.85 km exactly matching with Z_L. Besides the major convective outflow identified there are three more convective outflows present at altitudes 12.85 km, 9.55 km, and 6.70 km in $\langle D \rangle$ profile which match fairly well with minima in the $\langle \theta' \rangle$ profile at altitudes 12.4 km, 9.70 km, and 7.15 km, respectively.

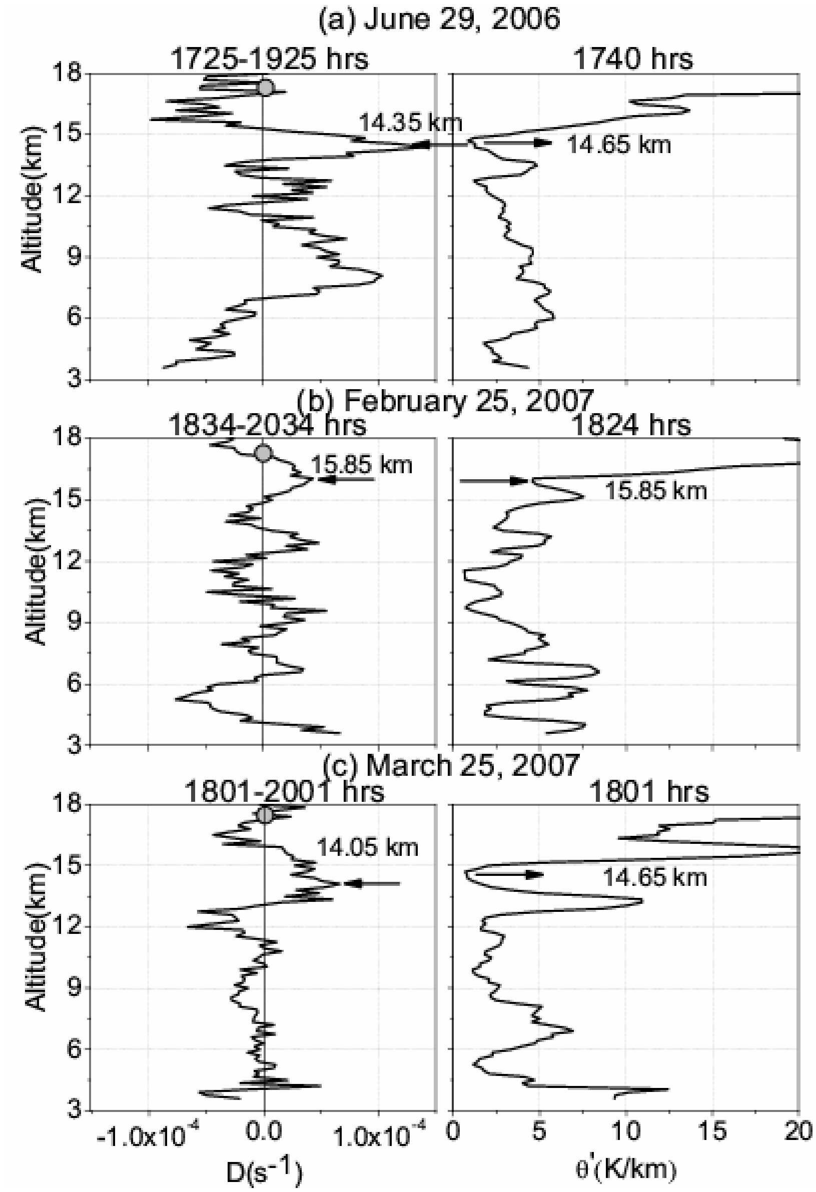

Figure 3.2: *Typical examples showing profile of (a) $\langle D \rangle$ from MST radar observation on 29 June 2006 (left panel) and the corresponding profile $\langle \theta' \rangle$ from GPS radiosonde measurement over Gadanki (right panel). (b) & (c) same as (a) but observed on 25 February 2007 and 25 March 2007 showing multiple convective outflow levels and broad convective outflow level, respectively. Filled circle denotes the altitude of the cold point tropopause. Arrows in the left and right panel indicate the major convective outflow altitude from MST radar and altitude of $\langle \theta' \rangle$ minimum from Radiosonde observation, respectively.*

An example of broad convective outflow observed on 25 March 2007 is shown in Figure 3.2 (c). The Z_D is 14.05 km whereas the Z_L is 14.55 km having difference of 0.5 km. The major convective outflow in $\langle D \rangle$ profile is broad and the corresponding minimum in $\langle \theta' \rangle$ profile is also broad. A notable feature of the above examples is that both $\langle D \rangle$ as well as $\langle \theta' \rangle$ profile show similar altitude structures. The overall comparison is summarized as scatter plot shown in Figure 3.3. In this figure, Z_D from $\langle D \rangle$ profiles are plotted against Z_L from $\langle \theta' \rangle$ profiles along with the best line. The correlation coefficient between the two is significant and is 0.62. The r.m.s difference considering the 43 cases is estimated to be 0.8 km. The Z_D from the radar is obtained using two hour average divergence profiles and hence can be taken to represent convection over scales ≥ 2 hours. So, essentially it is a non-local representation of convection (meso-scale convection). The Z_L which is obtained by using GPS radiosonde data is also essentially a non-local representation of convection and represents the level of maximum/prominent convective impact on upper tropospheric temperature [*Gettelman and Foster*, 2002]. The very good correlation between Z_D and Z_L shows that Z_D from the radar can be taken to represent the level up to which convective impact dominates. The average values of Z_D and Z_L considering all the 43 cases are found to be 14.1±1.5 km and 13.5±1.0 km, respectively, which are quite close.

The physical basis for the observed correlation between Z_D and Z_L could be discerned from an examination of the thermodynamic energy equation in a simplified way. The first law of thermodynamics in the isobaric system can be written as:

$$\left(\frac{\partial T}{\partial p} + u\frac{\partial T}{\partial x} + v\frac{\partial T}{\partial y}\right) - S_p w = \frac{J}{c_p} \qquad \text{… (3.2)}$$

Using this equation and neglecting horizontal advection of temperature and its rate of change, the vertical velocity:

$$w \cong (J/c_P S_P) \qquad \text{… (3.3)}$$

where

$$S_p \equiv -\frac{T}{\theta}\frac{\partial \theta}{\partial p} \qquad \text{…. (3.4)}$$

is the stability parameter and J is the rate of heating (e.g. due to radiation and latent heat release). It can be seen from this equation that a low in stability (S_p or θ') would tend to give rise to a high in w which in turn would lead to a high in horizontal mass divergence. It would be interesting to obtain closure on this relationship by estimating the clear sky radiative heating rate J. However, this is out of scope of the present study and will be pursued later.

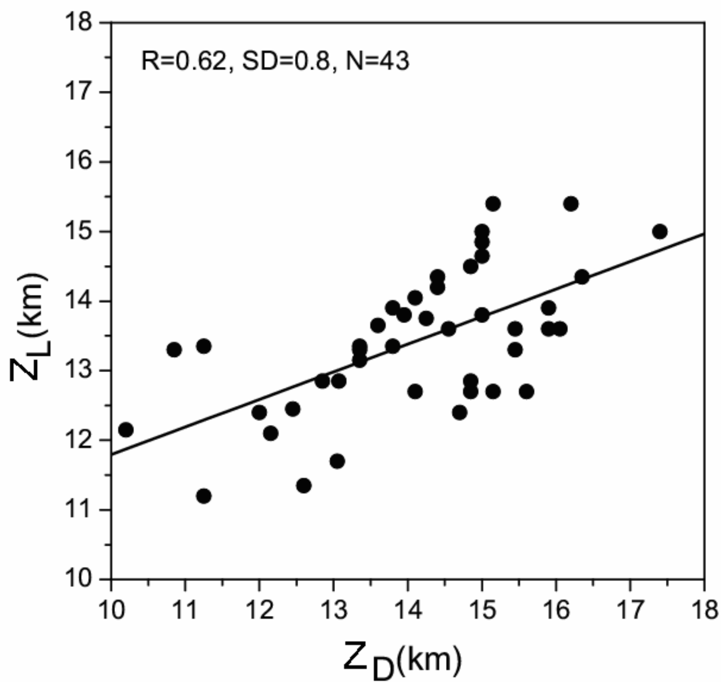

Figure 3.3: *Scatter plot between Z_D and Z_L. Correlation coefficient (R), standard deviation (SD) and number of cases (N) are given in the figure.*

3.4.2. Temporal variation of Convective Outflow Levels

Figure 3.4 shows the temporal variation of Z_D and Z_L during 1 to 4 October, 2006 (panel a) and during 2 to 6 November 2006 (panel b) when observations were available on a few times in a day. The Z_D and Z_L are indicated by square dot and diamond, respectively. The cloud top altitude and TBB represented by filled circle and cross are also shown in the figure. The scale for TBB is shown on the right hand side ordinate. The Z_D is generally in good agreement with Z_L. Except on two occasions during 1 to 4 October 2006, TBB has not revealed deep convection as can be seen from Figure 3.4 and has shown low level clouds with cloud altitudes much lower than both Z_D and Z_L. (TBB <240 K is considered as indicating deep convection.) During 1 to 4 October 2006, TBB revealed deep convection on two occasions with temperatures of 208 K and 230 K which occurred at ~0330 hours on 2 October and at ~0930 hours on 3 October 2006, respectively. On these occasions the altitudes of convective outflow are high. The altitudes corresponding to TBB (cloud top altitudes) of 208 K and 230 K are 14 km and 11.5 km, respectively, while the convective outflow altitudes are 14.8 km and 12.15 km, respectively, which are quite close to the cloud top altitudes. The corresponding Z_L values are 12.7 km and 12.15 km, respectively. The Z_C (or Z_{CPT}) values on these occasions are higher at 16.9 km and 17.05 km with temperatures of 191.1 K and 192.4 K, respectively.

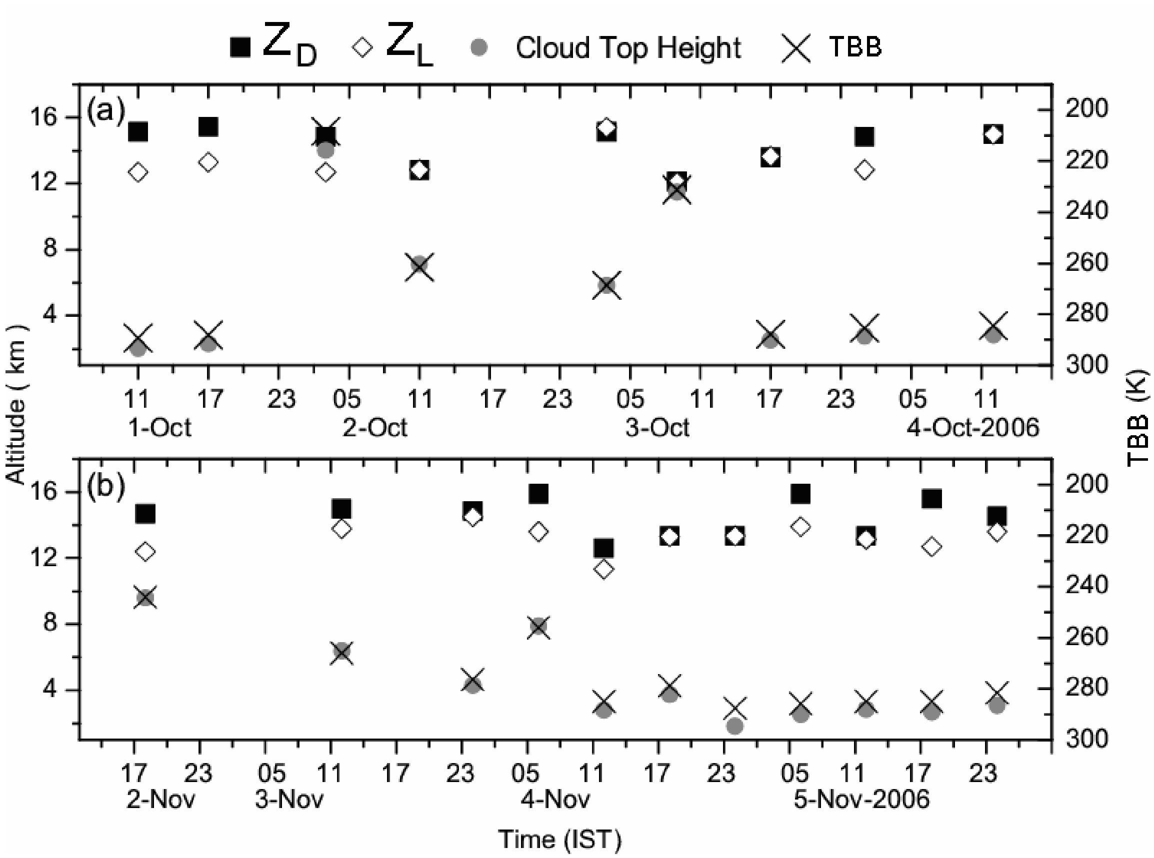

Figure 3.4: *Time series of (a) Z_D, Z_L, TBB and cloud top altitude observed during 1 to 4 October 2006. (b) same as (a) but observed during 2 to 6 November 2006. The Z_D, Z_L, TBB and cloud top altitude are indicated by filled square, diamond, filled circle, and cross, respectively.*

At ~1700 hours on 2 November and ~1000 hours on 3 November TBB are somewhat low with values of 243 K and 265 K and the respective cloud top altitudes are 9.6 km and 6.15 km while Z_D values from radar are 14.7 km and 15 km which are more than 5 km higher than the cloud top altitudes.

In addition to the two deep convection events mentioned above, two more occurred during the study period as indicated by TBB. These are at (i) ~1247 hours on 28 July 2006 and (ii) ~1100 hours on 4 September 2006 with TBB at 230 K and 220K, respectively. These temperatures correspond to altitudes of 11.4 km and 12.6 km, respectively. The corresponding Z_D values are at 15 km and 13.8 km and Z_L values at 14.7 km and 13.4 km, respectively. These are somewhat higher than the cloud top altitudes. The Z_C values corresponding to these two values are 16.35 km and 16.05 km, respectively. Interestingly on all the four deep convection events, the convective outflow altitudes Z_D and Z_L match well. An examination of $\langle D \rangle$ (and$\langle \theta' \rangle$) profiles showed no prominent differences in the general features between the profiles with and without deep convection (as indicated by TBB<240K).

It appears from the above that during deep convection Z_D values are close to the cloud top altitudes. However, at other times with no deep convection Z_D values are higher than the cloud top altitudes. Some caution needs to be exercised in comparing the cloud top altitude from TBB with Z_D and Z_L. The Z_D obtained from the radar (and the Z_L from radiosonde) is a non-local indicator of convection as pointed out earlier whereas the cloud top altitude is mainly a local parameter. Thus it is not unexpected that Z_D (and Z_L) does not follow the cloud top altitude from TBB. But, when deep convection occurred as seen from BT, the agreement between these parameters is good as can be expected. This is because during the deep convection events, as seen locally from TBB, the Z_D (and Z_L) would be influenced by the local deep convection as well. The correlation coefficient between Z_D and the cloud top altitude considering all the 43 cases is estimated to be -0.05. It may be noted here that *Gettelman and Foster* [2002] analyzing data of one year at Koror (7.3^{o}N, 134.5^{o}E) reported a low correlation of 0.3 between Z_L and cloud top altitude from satellite data of TBB.

3.4.3. Correlation analysis

In order to study the dependence of TTL on Z_D and Z_C, the thickness of TTL is obtained as (Z_C- Z_D). It may be noted here that *Gettelman and Foster* [2002] used Z_L as the base level of TTL. In view of the correlation between Z_L and Z_D, use of Z_D as base level of TTL is justified. Figure 3.5 (a) shows a scatter plot between TTL thickness and Z_C and Figure 3.5 (b) a scatter plot between TTL thickness and Z_D. There is large scatter in the plot between TTL thickness and Z_C showing poor correlation. On the other hand, there is very little scatter in the plot between TTL thickness and Z_D showing a very high correlation of - 0.94. The best fit line is also shown in the panel.

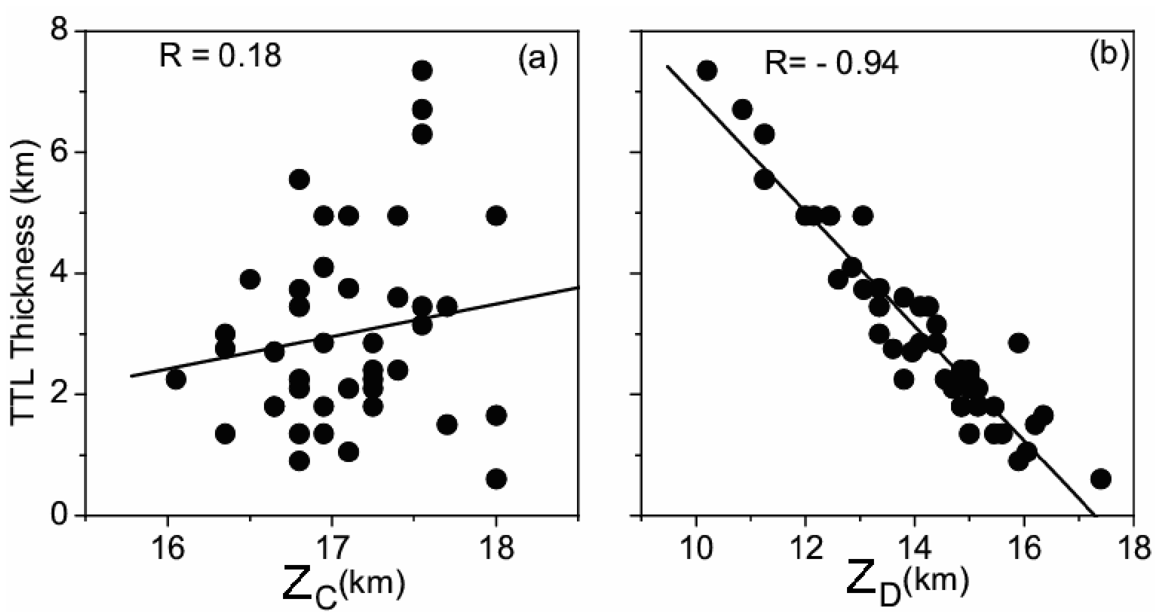

Figure 3.5: *Scatter plot between (a) Z_C and TTL thickness, and (b) Z_D and TTL thickness. Correlation coefficients (R) are given in the respective panels.*

The high correlation between TTL thickness and Z_D may seem to be an expected result as TTL thickness is obtained from Z_D. However, it shows a very interesting result that when the convective outflow reaches higher altitude, it is closer to the cold point tropopause. In other words, the TTL shrinks when convection reaches a high altitude. This is further examined by considering the monthly mean Z_D and Z_C. Figure 3.6 shows the monthly mean plot of these two. This figure clearly reveals that the difference between Z_C and Z_D i.e., thickness of TTL becomes a minimum during July, September and October approximately when monsoon prevail over India**.** It is seen that during these monsoon months Z_L is lower and Z_D is higher.

3.5. Discussion

In the present study, the altitude of major convective outflow (Z_D) obtained from the radar and that of minimum of θ' (Z_L) are found to match well with an r.m.s. difference of 0.8 km. It is to be noted that these two are obtained using two entirely independent techniques. The Z_D is obtained directly from the divergence profile and is taken to represent the convective tropopause. The altitude of minimum of potential temperature gradient though influenced largely by convection will also be influenced by other processes like horizontal advection of heat and heating due to ozone. The Z_L marks the altitude where radiation begins to influence the temperature as it departs from the moist adiabat [*Gettelman and Forster*, 2002]. Thus, Z_L can be considered as a good proxy for the altitude of convective outflow but not as a direct measure. The observed scatter in the plot between Z_D and Z_L can at least partly be due to this aspect.

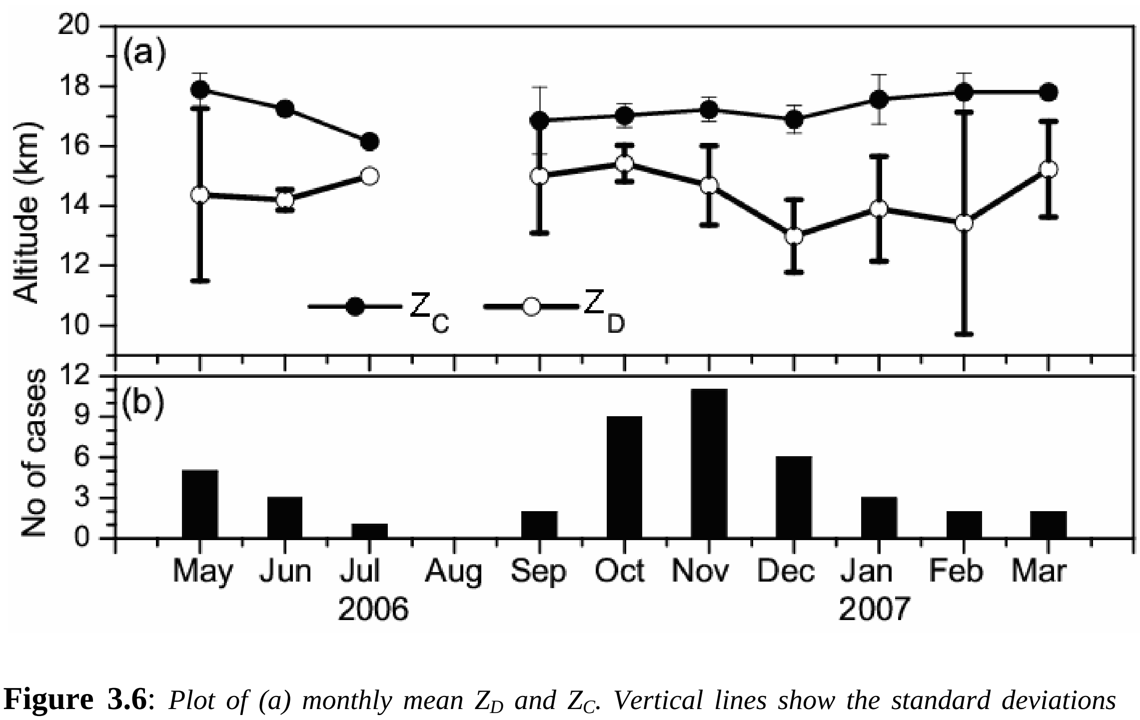

Figure 3.6: *Plot of (a) monthly mean Z_D and Z_C. Vertical lines show the standard deviations obtained while averaging the number of cases shown panel (b) in respective months*

.

Highwood and Hoskins [1998] pointed out that in simplified climate change model, it is important that the tropopause is at the top of the convective region and the region above is essentially in radiative equilibrium. This level is more meaningful physically than the traditional temperature lapse rate tropopause in this context. Thus, it is important to identify the level up to which convection plays a dominant role in influencing the temperature profile. In the present study an attempt has been made to identify this level and it is proposed that Z_D from the radar serves this purpose.

It is seen in the present study that while in deep convection events, the cloud top altitudes from TBB are somewhat close to Z_D, at other times the clod top altitudes are much lower than Z_D. This is in accordance with the earlier observation that during deep convection TBB is a good indicator of top of convection [*Highwood and Hoskins*, 1998]. As pointed out earlier, disagreement between Z_D and cloud top altitude is to be expected as Z_D is essentially a non-local indicator whereas the cloud top altitude is a local indicator during periods without deep convection. In deep convection occurring locally, Z_D would be influenced by local conditions as well.

It is found that although in deep convection events Z_C values are high; these are high at some other times as well. This implies that the cold point is influenced not only by convection but also by other factors (such as ozone heating and horizontal advection of heat), perhaps more strongly. The present study shows that when convection reaches a high altitude, the thickness of the TTL shrinks. This indicates that when convection rises to high altitude, the extent of transition region between convective and radiative equilibria becomes small. The observed lack of correlation between Z_D and Z_C lends support to the view that the cold point tropopause is not only governed by convection but also by stratospheric processes more strongly.

3.6. Summary

The present study can be summarized as the following:

1. The altitude of major convective outflow from the MST radar and that of the local minimum of potential temperature gradient match well.

2. The altitude of major convective outflow from the radar gives a good measure of the base of the tropical tropopause layer (TTL) and can be taken as the altitude of convective tropopause.
3. As the altitude of major convective outflow raises so does the cold point tropopause altitude.

In this Chapter the temporal variation of the convective tropopause and TTL is presented. The detailed analysis of the tropopause parameters are further studied using radiosonde data sets for longer duration is carried out in chapter 4.

---END---

Chapter 4

Variability of the Tropical Tropopause over Indian Monsoon Region

4.1. Introduction

The tropopause is the boundary between troposphere and stratosphere which varies in response to any changes in the physical, chemical and thermal characteristics of the two regions. It is well recognized that the troposphere and stratosphere are distinct in their characteristics namely vertical mixing time scales, static stabilities, trace constituents (mainly water vapor and Ozone) and thermal balance. The characteristics of the tropopause vary on a wide time scale starting from annual to a few hours. The variability in the tropical tropopause is considered as a sensitive indicator of climate change [*Sausen and Santer*, 2003; *Santer et al*., 2003; *Son et al*., 2009]. Thus, it is very important to study the behavior of the tropical tropopause on all the time scales.

While there are a number of studies on the long-term variation of the tropical tropopause such as annual/inter-annual, seasonal and monthly variations [e.g., *Reid and Gage*, 1985; 1996; *Krishna Murthy et al*., 1986; *Randel et al*., 2000] studies on its variability on a time scale of a day or less [*Son and Lee* 2007] are meagre [See *SPARC* newsletter 11]. This variability is likely to be the result of variations in local convective activity, while the variation on the longer seasonal time scale is more plausibly related to the effects of extra-tropical wave forcing [*Reid and Gage*, 1996]. It is however unclear how the tropopause varies on a shorter time scale and how it is related with local convection.

Studies on short-term variation on time scale of a day or less are mainly from Radiosonde and VHF Radar observations. *Yamamoto et al*. [2003] have proposed convective activity and diurnal tides as possible causes for the observed diurnal variation in the tropical tropopause altitude. *Das et al*. [2008] reported tidal modulation of the tropical tropopause altitude. Using Radiosonde data, the day-to-day variation has been linked to local convection [*Reid and Gage*, 1996] and planetary wave activity [*Tsuda et al*., 1994; *Krishna Murthy et al*., 2002]. *Johnson* [1986] studied the short term (~ 1 week) variation of the tropopause altitude using Radiosonde data from southern South China Sea during Winter MONEX and found that during deep convection the tropopause altitude descends.

In recent years, the tropical tropopause is no more considered as a material surface and the concept of the tropical tropopause layer (TTL) as a transition layer between the convectively dominated tropical troposphere and radiatively controlled stratosphere has instead been proposed [*Highwood and Hoskins*, 1998; *Gettelman and Forster*, 2002; *Mehta et al*., 2008]. The TTL is generally considered to lie between the level of top of convection and cold point tropopause [*Gettelman and Forster*, 2002]. *Fueglistaler et al*. [2009] has recently proposed that the TTL can be considered to be between 150 and 70 hPa pressure levels. The TTL is important as the source region for much of the air entering the stratosphere [*Holton et al*., 1995] and sets the upper limit for stratospheric water vapor mixing ratio [*Brewer*, 1949]. Variations in the tropopause altitude may have direct bearing on energy source for stratospheric motions [*Holton*, 1982], exchange of water vapor and ozone between troposphere and stratosphere. Concerning the latter issue, *Brewer* [1949] has argued that water vapor transport must occur in the equatorial "cold trap" where rising air can be freeze- dried to a large degree accounting for the low water vapor mixing ratio observed in the lower stratosphere. However, *Brewer* [1949] only focused on vertical motion to explain the observed aridity in the tropical lower stratosphere. Recently *Holton and Gettelman* [2001] suggested that horizontal transport though the "cold trap" causes the aridity of the lower stratosphere at other longitudes. The upward water vapor transport in the Hadley cell is accomplished by hot towers [*Robinson*, 1980] and their effect on water vapor distribution of the lower stratosphere depends on the local tropopause temperature as well as rate of injection of ice crystals into the stratosphere [*Holton*, 1984]. The STEP (Stratosphere Troposphere Exchange Processes) aircraft experiments showed the importance of deep convection over the western Pacific warm-pool region [e.g., *Russell et al*., 1993] providing evidence for exchange between troposphere and stratosphere. In addition, the UARS (Upper Atmospheric Research Satellite) water-vapor measurements showed clear evidence for slow upwelling driven by extra-tropical wave forcing [e.g., *Mote et al*., 1996]. As a result of deep convection there exists the possibility that subsidence in the environment of overshooting turrets may contribute to a downward transport of ozone rich air from the lower stratosphere, thereby leading to an enhancement of ozone heating rate and descent of the tropopause (CPT).

As pointed out earlier, while there are several studies on variations of tropical tropopause on long time scales (annual and seasonal), there are relatively few studies on day-to-day and sub-daily time scales. Moreover, many of the studies pertain to tropical stations over Pacific. There is a paucity of such studies over the Indian region which is convectively very active in the summer monsoon periods. It is to be noted that during summer season (June-August), the Indian summer monsoon prevail. Thus, June-August is considered as summer monsoon season in this study, although, it is to be noted that Indian summer monsoon extended up to September. In this Chapter, the detailed features of the tropical tropopause characteristics and its variability over the Indian monsoon region with special emphasis on the variation of tropical tropopause on shorter time (sub-daily) scales is examined.

4.2. Data Base and Analysis Procedure

High resolution radiosondes (Väisälä RS-80, Väisälä RS-92 and Meisei) were launched once daily on a regular basis from Gadanki (13.5^{o}N, 79.2^{o}E), a tropical station in the Indian monsoon region, during April 2006 to December 2008 at around 1730 IST (IST = UT+0530hrs). The details about the system Väisälä and Meisei radiosonde system are given in Chapter2. In addition, on a few occasions several launches within a day were also conducted. In total 780 profiles of temperature (T), pressure (P), relative humidity (RH) and horizontal wind are obtained. There is a major data gap during December 2006 (only six balloons were launched) and April 2007(there is no data for complete month). The data are collected with an altitude resolution of 25-30 m (sampled at 5 seconds intervals) from RS-80 type (April 2006 to March 2007) and 10 m (sampled at 2 seconds intervals) from RS-92 (from 17 July 2006 to 31 August 2006) and Meisei (May 2007 to December 2008). Quality checks were then applied to remove further, outliers arising due to various reasons following *Tsuda et al*. [2006] to ensure high quality in the data which otherwise contaminate entire results.

Simultaneous hourly cloud top equivalent blackbody temperature, called Brightness Temperature (TBB) from MTSAT-1R (Multi-functional Transport SATellite) data provided by the Japan Meteorological Agency (JMA) through Kochi University, Japan is also used. Data were recorded in longitude/latitude grids of 0.05^{o} between 11^{o}N-15^{o}N latitude and 77^{o}E-81^{o}E longitude covering the location of Gadanki. The TBB data, averaged from the pixel data, are used to examine the characteristics of meso-scale cloud systems. This data has been used as a proxy for tropical deep convection. In the satellite data retrievals for obtaining TBB, it appears variation of cloud emissivity with season is not considered.

The above data set is used to study the seasonal, day-to-day, and sub-daily variations in the tropical tropopause parameters such as temperature and altitude of cold point tropopause (CPT) and convective tropopause (COT), and tropical tropopause layer (TTL). The minimum temperature and corresponding altitude was determined from each profile and it is represented as CPT temperature (T_{CPT}) and CPT altitude (Z_{CPT}), respectively. Traditionally, the tropopause has been defined according lapse rate criteria mentioned in the Chapter1. This is called lapse rate tropopause (LRT). Both LRT altitude (Z_{LRT}) and temperature (T_{LRT}) are examined in this study. The concept of minimum theta (adiabatic temperature) lapse rate for defining TTL is proposed by *Gettelman and Forster* [2002]. In the present study the local minimum in potential temperature lapse rate just below the CPT, explained in detail in the Chapter1 and also in *Mehta et al*. [2008] is used to identify the level or altitude of the top of the convection which is named as COT. Note that the base of TTL identified from this method generally coincides with that recently proposed by *Fueglistaler et al*. [2009]. First the COT altitude (Z_{COT}) is estimated and the corresponding temperature is represented as COT temperature (T_{COT}). The thickness of the TTL (TTLt) is taken as the region between the CPT and the COT and is obtained as the difference between Z_{CPT} and Z_{COT}.

4.3. Results

4.3.1. Seasonal Variation in the Tropical Tropopause Parameters

Figures 4.1 (a)-(f) show the plots of monthly mean values of Z_{CPT}, T_{CPT}, Z_{COT}, T_{COT}, TTLt and TBB, respectively, along with respective standard deviations. Z_{LRT} and T_{LRT} are also superimposed in Figure 4.1(a) and 4.1(b), respectively. From Figure 4.1(a) it is clear that Z_{CPT} shows strong seasonal variability ranging from a minimum of 16.5 km in August to a maximum of ~17.6 km in January. Figure 4.1(b) shows that the T_{CPT} is around 192 K in August and ~190 K in January. The CPT is warmest and lowest during summer and coldest and highest during winter a feature generally consistent with the earlier reports [for example, *Reid and Gage*, 1996; *Seidel et al*., 2001]. The Z_{CPT} is almost steady during January to May and starts to decrease from May to August and then increase up to December. The decrease of the tropopause altitude from May to August is steeper than the increase from August to December.

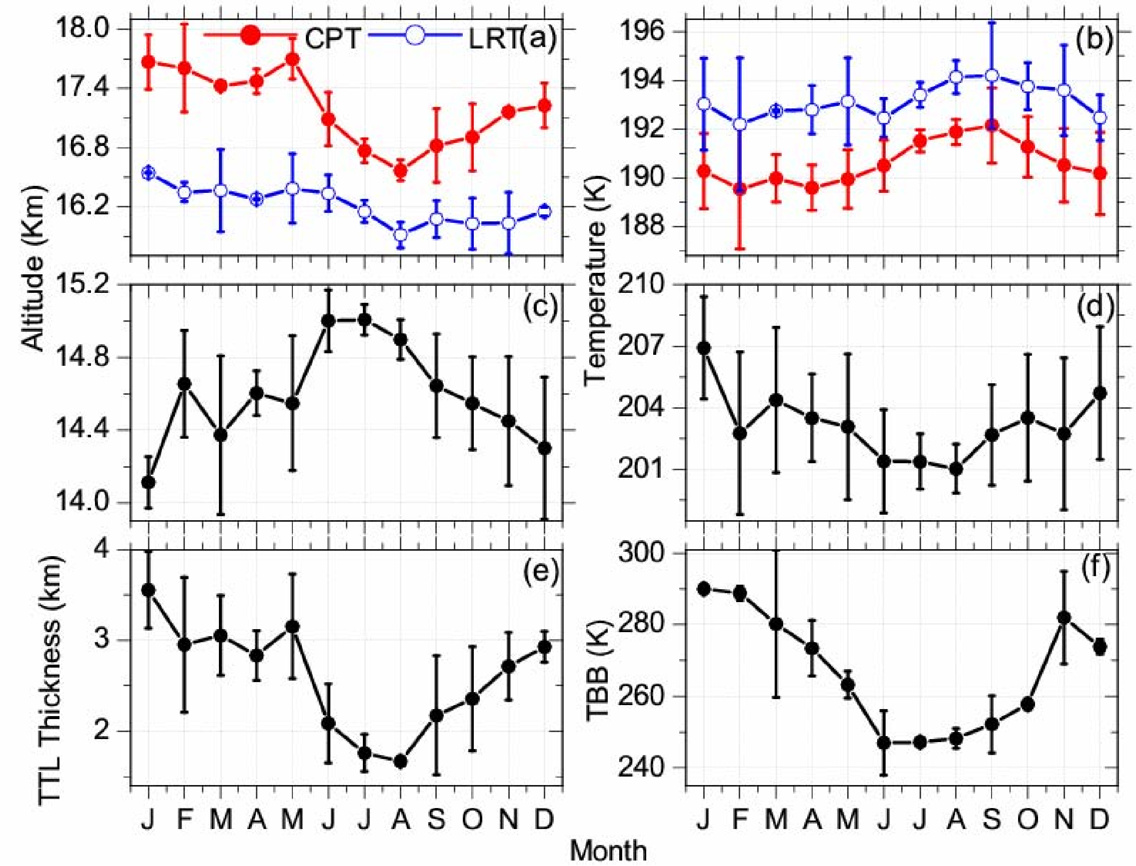

Figure 4.1. *Monthly mean variation of (a) Z_{CPT} and Z_{LRT}, (b) T_{CPT} and T_{LRT}, (c) Z_{COT} (d) T_{COT}, (e)TTLt, and (f) TBB observed during April 2006 to December 2008. Vertical bars show standard deviation.*

It is to be noted that T_{CPT} doesn't show similar behavior. The difference between Z_{CPT} and Z_{LRT} is smallest during summer season (June-July-August, JJA), in which CPT and LRT are found to be nearest and at lower altitude. The seasonal variability of the LRT is not as strong as CPT. The CPT is ~ 2-3 K cooler than LRT. Comparison between CPT and LRT shows that, in general, the CPT is ~1.2 km and ~0.6 km higher than LRT during January and August, respectively. *Reid and Gage* [1996] reported from an analysis of data of eight years over a Pacific station Truk (7.5^{o}N, 151.8^{o}E) that the CPT is higher and cooler during December-April than during July-September. It would be interesting to compare the results for Truk with those of Gadanki though the former belong to a different period (1980-1988). The nature of seasonal variation in the tropopause parameters may not undergo any major changes with time. Though the CPT seasonal variability at Gadanki is generally in good agreement with that at Truk, there are some important differences. The CPT is higher at Gadanki by about ~0.6 km than at Truk throughout the year though Truk is at lower latitude. This aspect needs to be further investigated for any longitude effect. At Gadanki the CPT is cooler (<192 K) during summer (July –September) than at Truk (~194 K). On the other hand in winter (December-February) CPT (~190 K) at Gadanki is slightly warmer compared to that at Truk (189 K). The range of seasonal variation of T_{CPT} is greater (5 K) at Truk than at Gadanki (~2 K) whereas that of altitude is nearly the same at both the stations. Since monthly means from the data set of period June 2006-December 2008 is constructed, all the short term effects on CPT can be considered to be averaged out. So, the observed difference in the seasonal variation (from summer to winter) of CPT (between Truk and Gadanki) implies that in the region immediately below tropopause, the lapse rate at Truk (5K/km) is higher and close to moist adiabat than that at Gadanki (2K/km) which probably is a result of strong influence of radiative processes (due to ozone). However, the observed difference can also be due to the influence of sea surface temperature (SST).

As noted earlier, the Z_{CPT} is higher at Gadanki than at Truk. It is to be examined whether a higher CPT implies higher ozone concentration in the upper troposphere. This aspect needs to be investigated further which is not attempted in the present study. It may be noted here that *Reid and Gage* [1985] obtained a lapse rate of 5.8 K/km for the long term changes in the monthly mean (lapse rate) tropopause altitude and temperature for two tropical stations Yap (9.5^{o}N,138.2^{o}E) and Curacao (12.2^{o}N,69^{o}W) situated in the western Pacific and Carribean, respectively. This value is nearly the same as for Truk mentioned above. The monthly mean saturation water vapor mixing ratio corresponding to T_{CPT} at Gadanki is found to vary from 3 ppmv in winter to 4 ppmv in summer season with standard deviation of 0.5-1 ppmv, indicating drier condition during winter, where the tropopause is coldest (see supplementary figure S4.1).

Figure 4.2 represents the probability distribution of the Z_{CPT} and T_{CPT} in different seasons. There is a clear peak of Z_{CPT} and T_{CPT} at ~17.5 km and ~ 190 K, respectively, which closely coincide with the mean Z_{CPT} and T_{CPT}, respectively, during the months December to May. During June to November, the Z_{CPT} and T_{CPT} show relatively broad peaks in the range 16.5-17.5 km and 190-194 K, respectively, and the mean Z_{CPT} and T_{CPT} lies between these ranges which are clearly shown in Table 4.1. The T_{CPT} goes below 191 K more frequently during December-May than during June-November. Therefore, entry of water vapor from troposphere to stratosphere with mixing ratio less than 3 ppmv is likely to occur more frequently during December to May months than during June –November. However, it may be noted that even during June-November there are considerable number of cases with T_{CPT} < 191 K.

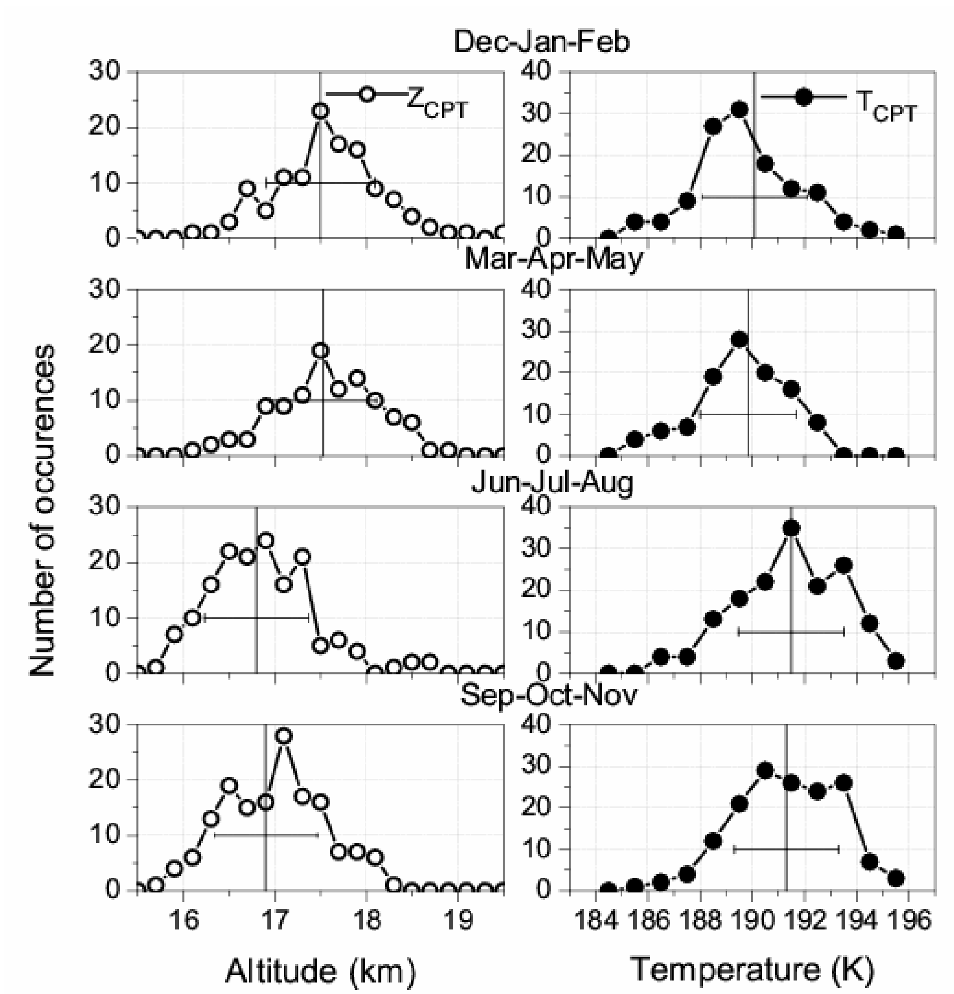

Figure 4.2: *Probability distribution of daily Z_{CPT} (left panels) with 0.2 km interval and T_{CPT} (right panels) with 1 K interval, observed in different seasons. The point at which the vertical line intersects the x-axis represents the mean Z_{CPT} (left panels) and T_{CPT} (right panels) while the length of horizontal bar represents the corresponding standard deviations associated with the respective parameters.*

The probability distribution of the Z_{LRT} and T_{LRT} in different seasons is also obtained which shows more or less similar feature as observed for Z_{CPT} and T_{CPT}, respectively (see supplementary Figure S4.2). The mean and standard deviations of Z_{LRT} and T_{LRT} is also provided in Table 4.1. The monthly mean variations of Z_{COT} and T_{COT} are shown in Figure 4.1 (c) and 4.1(d), respectively. The Z_{COT} varies from ~14.1 km to 15 km while T_{COT} varies from ~201 K to 207 K. The COT is higher and cooler in summer monsoon months than in winter months. The standard deviation in the COT variation is found to be smaller during summer monsoon months. Since the standard deviations are indicative of day-to-day variability, large standard deviations in the COT in seasons other than summer suggest that it is highly variable on a day-to-day basis in these seasons. Probability distribution of the Z_{COT} and T_{COT} are also obtained (see supplementary Figure S4.3) and the mean and standard deviations are provided in Table 4.1. Z_{COT} shows peak at 15.2 km during March to November and at ~ 14.4 km during December-February while T_{COT} shows peak at ~202.5 K during September-May and at ~ 197.5 K during June-August. It can be noticed that both Z_{COT} and T_{COT} behave differently in different seasons unlike CPT and LRT. These peaks slightly deviate from the mean as shown in Table 4.1.

Table 4.1: *Mean and standard deviations of the tropical tropopause parameters observed during different seasons.*

Season	Z_{CPT}	T_{CPT}	Z_{LRT}	T_{LRT}	Z_{COT}	T_{COT}	TTLt
DJF	17.5 ± 0.6	190.1 ± 2.0	16.6 ± 0.6	192.2 ± 2.8	14.4 ± 0.9	204.6 ± 6.8	3.12 ± 1.2
MAM	17.5 ± 0.6	189.9 ± 1.8	16.6 ± 0.5	191.7 ± 2.3	14.6 ± 0.9	203.7 ± 6.3	2.71 ± 1.2
JJA	16.8 ± 0.6	191.5 ± 2.0	16.2 ± 0.5	193.1 ± 2.7	14.9 ± 0.7	201.6 ± 4.9	1.80 ± 0.8
SON	16.9 ± 0.6	191.3 ± 2.0	16.2 ± 0.5	193.1 ± 2.8	14.6 ± 0.8	203.6 ± 6.0	2.32 ± 1.1

The TTLt (Figure 4.1e) shows strong seasonal variability with minimum and maximum thickness of ~1.5 km and 3.5 km in summer and winter, respectively. TBB (Figure 4.1f) shows a broad minimum in the months of June-August with a sharp decrease from September to June followed by a steady increase from September to November. This annual variation is more-or-less similar to that of Z_{CPT} and TTLt. It is interesting to note that TBB is minimum (indicating strong convection) in the summer monsoon season. This reveals that the strong convection leads to higher COT and lower TTLt, which is quite consistent with that, mentioned in Chapter3 and /or *Mehta et al*. [2008] using MST radar observations for this location. The standard deviations of TBB are quite small in the summer monsoon similar to the behavior of COT. The summer monsoon is known to be a synoptic scale phenomenon and as such short term changes like day-to-day changes can be expected to be small in the associated convection. It is noted earlier that during summer monsoon the Z_{CPT} (T_{CPT}) is low (high) compared to the other months when daily variations are high. Thus, it appears that CPT responds to small scale convection than large scale (synoptic). Large scale convection as in the monsoon season may not penetrate to higher altitudes in the troposphere whereas small scale convection may penetrate. From a study of horizontal divergence profiles at Gadanki, *Satheesan and Krishna Murthy* [2005] reported that in summer, convective outflow is strong and occurs in the mid troposphere whereas in winter the outflow is relatively weaker but some convection can penetrate to lower stratosphere. Basically the factors determining the altitude of tropical tropopause are tropical convection, extra tropical wave driving [*Reid and Gage*, 1996] and also lower stratospheric processes [*Thuburn and Craig*, 2002]. Wave driving allows convective overshoot raising the altitude of the tropopause. During the northern hemisphere winter months, wave driving is expected to be strong leading to a higher tropopause [*Holton et al*, 1995; *Reid and Gage*, 1996]. As pointed out by *Reid and Gage* [1996], penetration of convection into lower stratosphere leads to entrainment of stratospheric air and subsequent lateral spreading resulting in a higher and cooler tropopause as in winter. This explains qualitatively the observed feature of higher and cooler tropopause in winter compared to summer. However, stronger convection (as in summer) may lead to stronger convective outflow at a higher altitude in summer leading to a higher COT (in summer) than in winter. Further, strong (deep) convection may lead to subsidence at higher levels (above COT) resulting in downward transport of ozone-rich air and lower tropopause (CPT) altitude. Weak convection may be reaching higher altitudes (as in winter) but may not be contributing in a substantial manner to potential lapse rate minimum which is taken to represent the COT. This implies that a higher COT does not necessarily mean a higher CPT and that there are other strong processes influencing the altitude of tropopause.

4.3.2. Day-to-day Variations of the Tropical Tropopause Parameters

The day-to-day variation of the Z_{CPT} and T_{CPT} observed over Gadanki during different seasons are shown in Figure 4.3. In general, Z_{CPT} (T_{CPT}) varies in the range of 15.5 -18.5 km (184-197 K). The lowest temperatures occur generally in winter months. The Z_{CPT} (T_{CPT}) variation from one day to the next day is ~ 1 km (~3 K) except on a few occasions where it changes by as much as 2-3 km (5-7 K). From Figure 4.3, it is clear that descent in Z_{CPT} is not always associated with increase in T_{CPT} which is further discussed in section 4.4. Thus, variation of the CPT is not always governed by adiabatic processes and sometimes diabatic processes become effective.

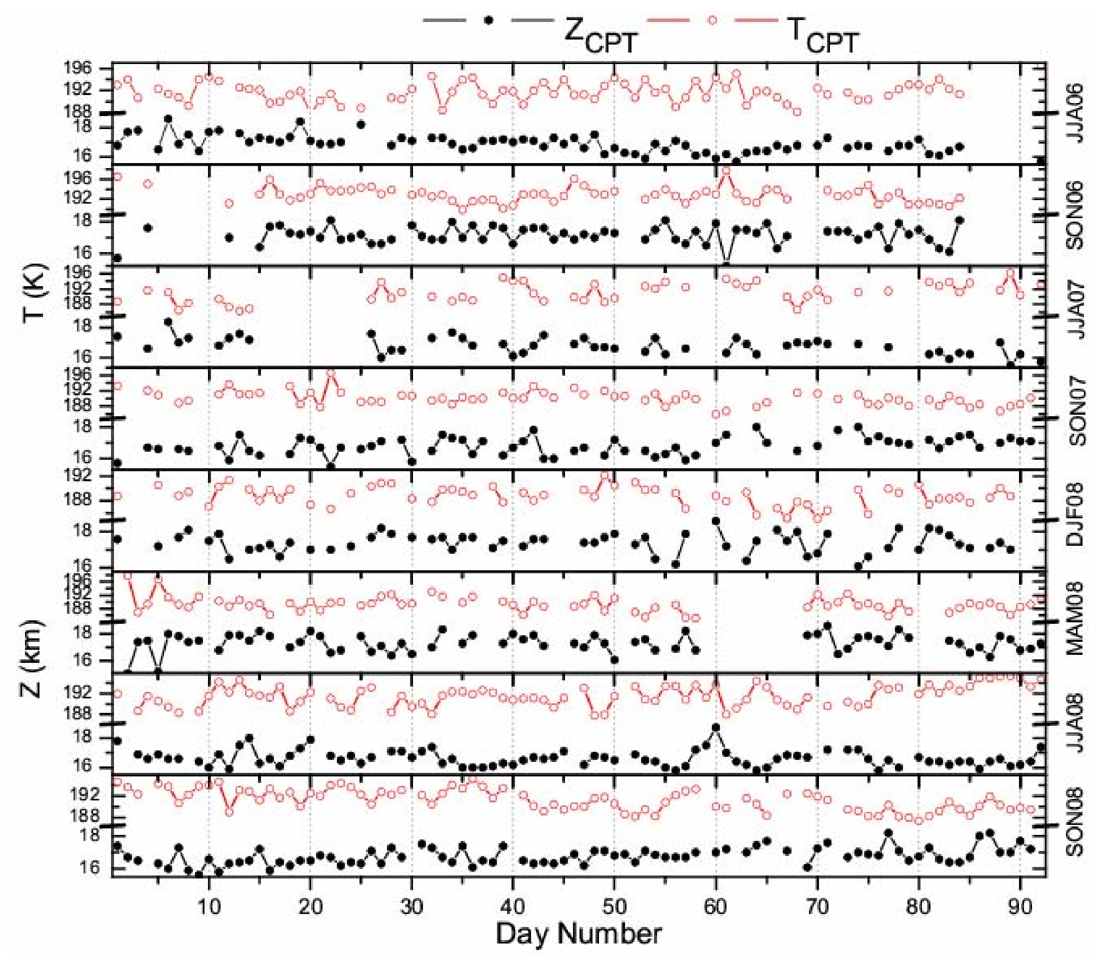

Figure 4.3: *The day-to-day variation observed in the Z_{CPT} and T_{CPT} during different seasons.*

In contrast to CPT, the Z_{LRT} and T_{LRT} mostly vary in opposite phase (see supplementary Figure S4.4). The day-to-day variation of the Z_{LRT} (T_{LRT}) ranges from 14.5-17.5 km (185-200 K). On the other hand Z_{COT} and T_{COT} are found to vary always in opposite phase (see supplementary Figure S4.5). The day-to-day variation of the Z_{COT} (T_{CPT}) ranges from 12-16 km (190-215 K). The maximum change in the Z_{COT} (T_{COT}) from one day to next day is 2-3 km (15-20 K). Figure 4.4 shows the variation of the TTLt and TBB observed during different seasons.

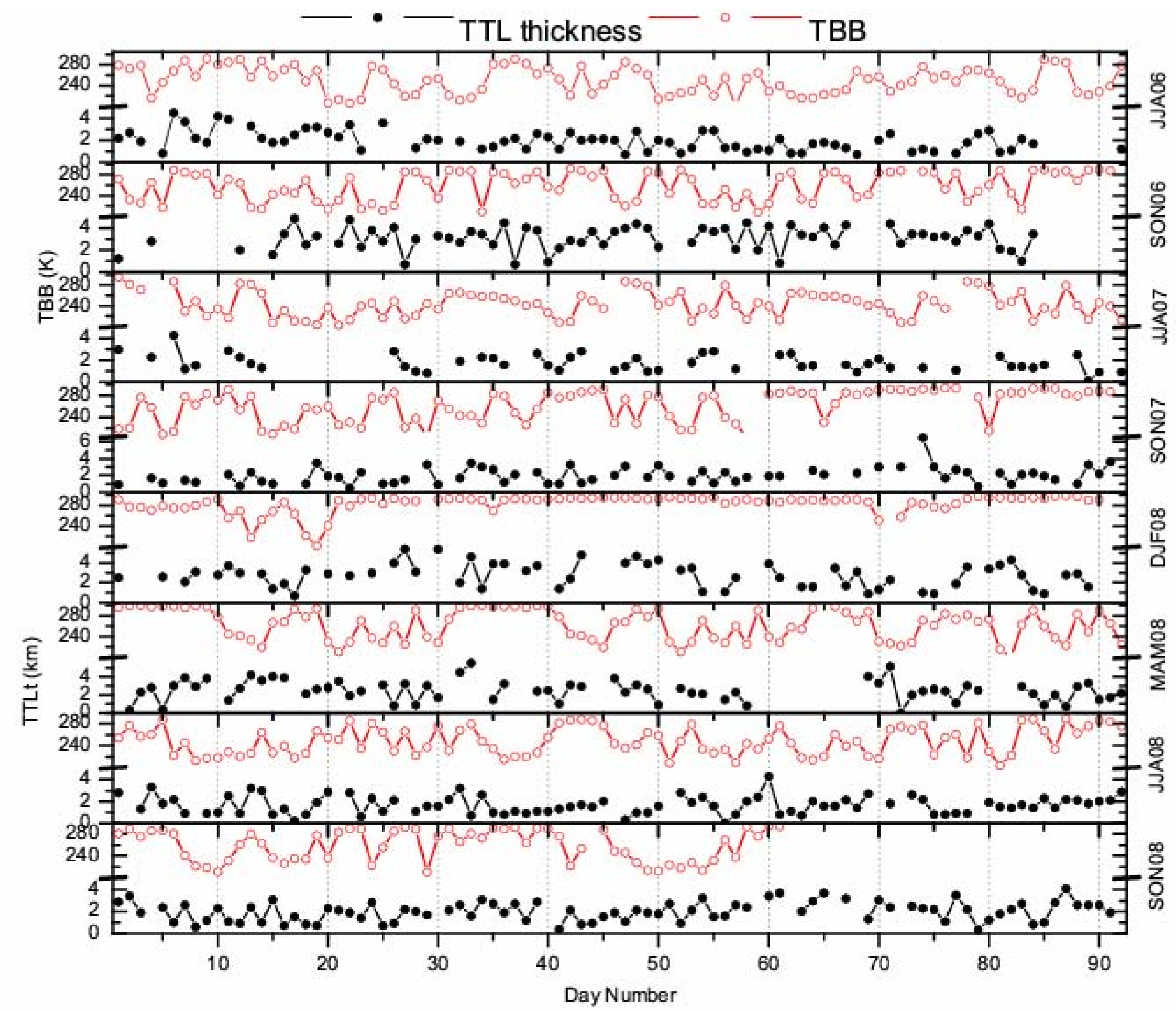

Figure 4.4: *The day-to-day variation of the TTLt and TBB observed in different seasons.*

The range of day-to-day variation of the TTLt is between 1 and 5 km. During some events, the TTLt shows minimum during deep convection, especially during monsoon season and maximum during clear sky conditions, which generally happens in winter season. While deep convection events are associated with smaller TTLt, small values of TTLt occur at other times as well. This is similar to the observation of hygropause (altitude at which minimum water vapor mixing ratio observed above the CPT) reported by *Teitelbaum et al* [2001]. This issue will be discussed with correlative analysis in section 4.3.4.

4.3.3. Sub-daily Variations in the Tropical Tropopause Parameters

In order to study the changes in tropopause characteristics on sub-daily time scales, more than two radiosonde launching were made on a few days in the period of the present study. The sub-daily variation in altitude and temperature of the CPT occurring are shown in Figure 4.5. The range of variation of Z_{CPT} and T_{CPT} is ~15.5-18.5 km and ~185-195 K, respectively, considering all the panels in the figure. Large variations in the Z_{CPT} (~1 km) and T_{CPT} (~3 K) can be noticed even within a day. However, there are cases in which altitude and temperature are more or less steady (for example in Figure 4.5(f) during 6-8 June 2008). As Z_{CPT} and T_{CPT} appear to be not dependent on the time of the day regularly, the variation in a day may not be due to tidal influence. Thus, the tidal influence if any is not pronounced. However, averaging over a number of days may bring out the tidal influence.

In order to examine the diurnal variation of tropopause characteristics the data corresponding to the intervals 03-09, 09-15, 15-21 and 21-03 hours are grouped into 06, 12, 18 and 24 hours, respectively, and are averaged. The mean and corresponding standard error bar of Z_{CPT} and T_{CPT} are shown in the Figure 4.6. Although all seven cases do not show similar behavior, the last four panels of Z_{CPT} show more less a consistent feature in Z_{CPT}, with a low value at ~12 IST and a high value at ~24 IST, indicating influence of a 24 hour component. The T_{CPT} showed similar behavior only in December and June peaking at ~12 IST and 24 IST. Z_{CPT} appears to be modulated by diurnal tide while T_{CPT} by both diurnal (for August 2007 and July 2008) and semi-diurnal (for December 2007 and June 2008) components. However, the diurnal variation in CPT could be due to diurnal variation in convection which will be taken as a separate study. The data points are not sufficient to delineate the tidal behavior except in the period 3-10 June 2005. Thus, the data observed during 3-10 June 2008 is further analyzed to bring out tidal influence, if any.

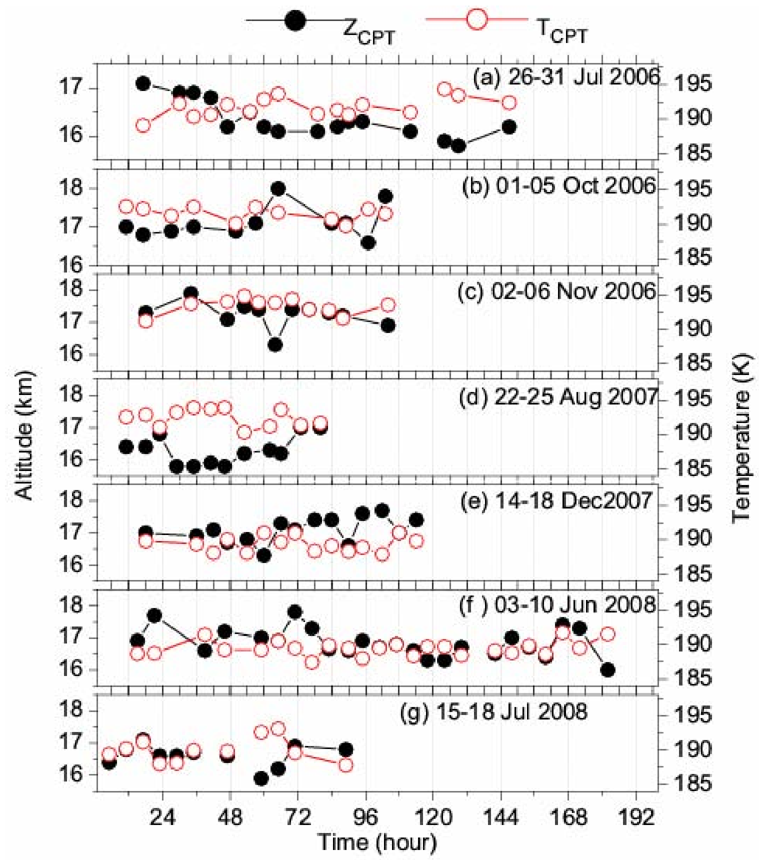

Figure 4.5: *Sub daily variation of the Z_{CPT} and T_{CPT} observed in different seasons.*

The data during 3-10 June 2008 are almost continuous with 24 observations, starting from 39 hours as shown in Figure 4.5(f). In this case, observations are available at equal intervals of ~ 6 hours, except at two timings which have 12 hours interval. The data with 12 hours interval is linearly interpolated to ~6 hours interval in order to have the complete data set in equal intervals. The zonal wind and meridional wind at 17 km, Z_{CPT} and T_{CPT} is subjected to the Fourier analysis and is shown in Figure 4.7. A broad peak at ~ 24-25 hours can be observed in zonal wind, Z_{CPT} and clear peak in meridional wind. It is well known that zonal and meridional wind in the troposphere and lower stratosphere over Gadanki show diurnal and semi-diurnal tidal oscillations [e.g., *Sasi et* *al.*, 1998; 2001]. This observation shows the role of diurnal tide in modulating the Z_{CPT}, which is consistent with earlier report by *Das et al.*, [2008]. T_{CPT} shows two peaks, one at ~16 hours and other at ~21 hours. In order to ascertain tidal influence on tropopause parameters, further study with more extensive data set is needed.

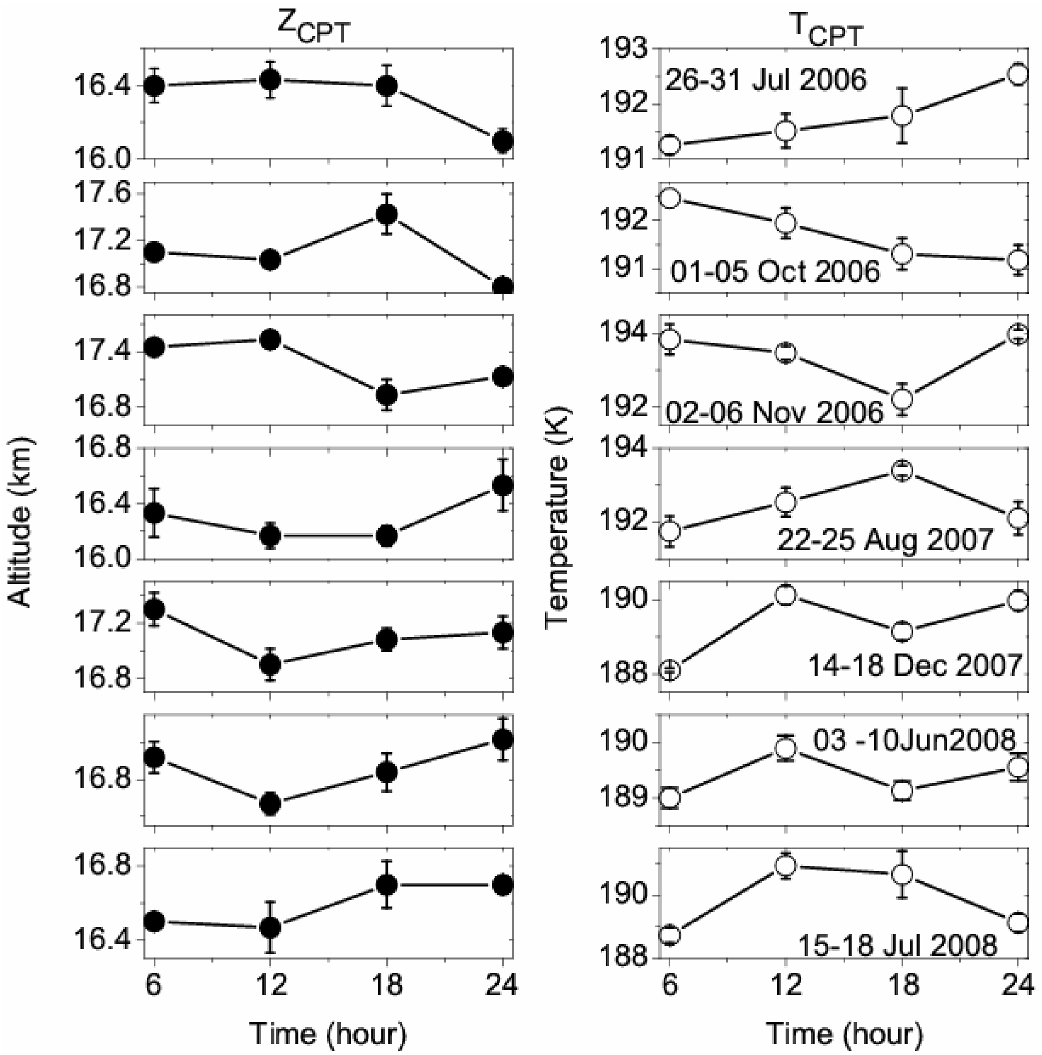

Figure 4.6: *Diurnal variation of the Z_{CPT} and T_{CPT} corresponding to the data shown in Figure 4.5.*

In general, the higher the CPT the cooler it is, with a few exceptions as for example in Figure 4.5(g), where both Z_{CPT} and T_{CPT} are increasing during clear sky conditions. While high Z_{CPT} occurs during deep convection events (TBB<240 K) they occur at other times as well. T_{CPT} remains more or less steady below 190 K during 14-18

December 2007 and 3-10 June 2008. In other cases shown in Figure 4.5, T_{CPT} goes below 190 K but occasionally. Note that 190 K corresponds to a saturation water vapor mixing ratio of 2 ppmv and thus relatively dry air can enter the stratosphere for extended durations of ~7 days.

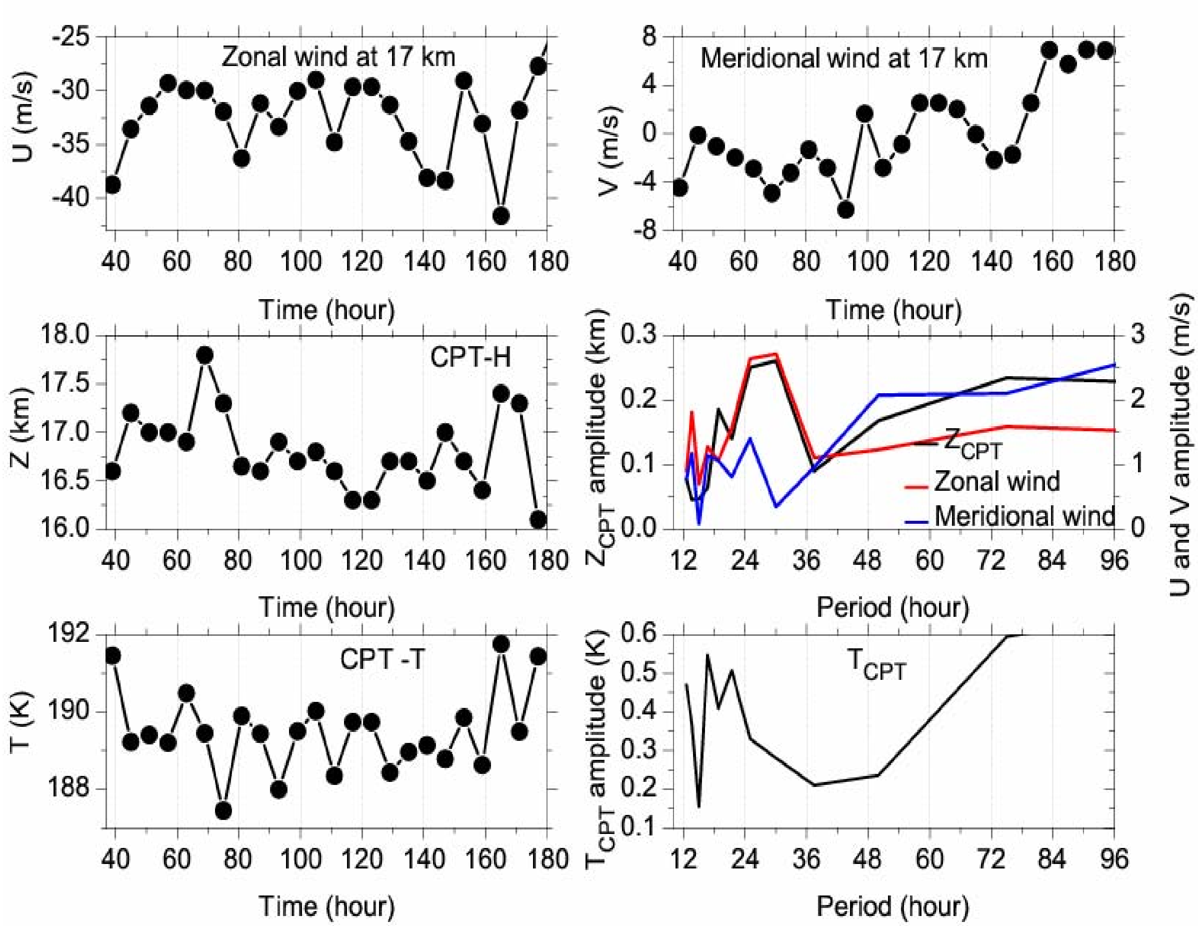

Figure 4.7: *Time series of zonal wind, meridional wind at 17 km, Z_{CPT}, T_{CPT} and corresponding periodogram observed during 03-10 June 2008.*

On sub-daily time scale Z_{LRT} and T_{LRT} vary between ~15-17 km and ~188-200 K, respectively (see supplementary Figure S4.6). The sub-daily variation in LRT is more or less similar to the day-to-day variation. The diurnal variation of Z_{LRT} and T_{LRT} does not show any regular behavior. However, interestingly they vary in opposite (see supplementary Figure S4.7). The sub-daily variation of COT is again similar to its day-to-day variation (see supplementary Figure S4.8). Though in all the cases COT doesn't show regular diurnal behavior, in general, Z_{COT} is maximum during 06 IST and 24 IST and minimum during 12 IST and 18 IST. Also, T_{COT} varies in opposite phase with Z_{COT}. On diurnal basis, variation of the Z_{COT} is more or less similar to Z_{CPT} (see supplementary Figure S4.9). However, it is interesting to note that the level of minimum potential temperature lapse rate proposed by *Gettleman and Foster* [2002] although does not show regular diurnal behavior, but, in general, varies in opposite phase with Z_{CPT}. The variation of the TTLt along with TBB observed during different seasons is shown in Figure 4.8. TTLt varies between the ranges ~ 0-5 km but the maximum sub-daily variation between two consecutive times is ~ 1-1.5 km only. As in day-to-day variations, low values of TTLt occur during deep convection events. However, they also occur at other times as well.

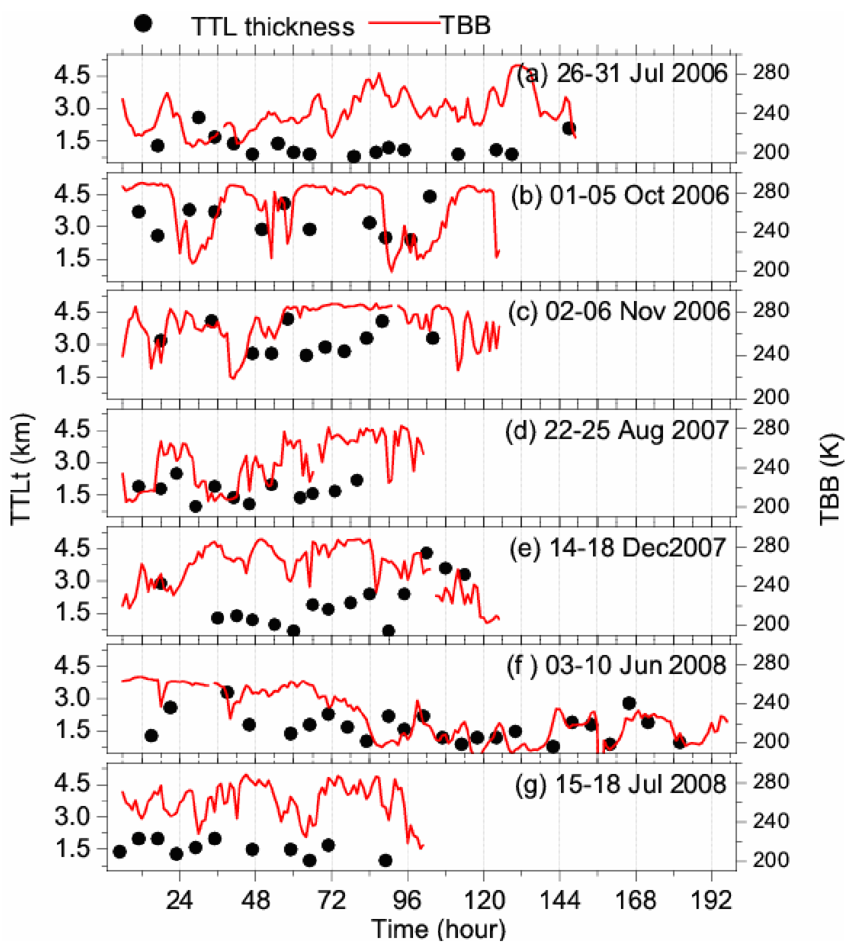

Figure 4.8: *Sub daily variation of TTLt (dot) and TBB (line) observed within a day during different seasons.*

4.3.4. Correlation Analysis

The correlation coefficients between various tropical tropopause parameters are estimated to study further the relationship between CPT, LRT, COT, TTLt and TBB at different time scales which are summarized in Table 4.2. It may be recalled that the data are available daily for about three years and on some occasions 4 to 6 times within a day. For long time scale, the correlation coefficients are obtained using monthly mean (all the data in a given month in the total period of three years are averaged yielding 12 data points), monthly (data of each month averaged separately for each year yielding 32 data points) and daily data (681 points). It is to be noted that daily data contains 681 observations. However, number of common observations with TBB is only 628. For short time scale correlation analysis for the daily data for each season is carried out.

It can be noticed that for monthly means considering the total data (seasonal), Z_{CPT} and T_{CPT} are highly anti correlated. The correlation degrades for monthly and daily data (seasonal). Further it is quite low for short time scale except in JJA 2007. Thus, the longer the time for averaging the higher is the anti correlation. This indicates that in averaging on a long term scale, effects of short lived transient are smoothed out leaving only synoptic scale effects on the parameters concerned. The good correlation between T_{CPT} and TBB for seasonal and monthly scale supports this argument. However, good correlation between the two (Z_{CPT} and T_{CPT}) is also observed for JJA 2007 which is discussed in detail in the following.

The tropopause can be affected in short time scales by processes such as horizontal advection of cold/hot air, entrainment of stratospheric air and cirrus clouds. When these processes prevail, the Z_{CPT} and T_{CPT} may not be anti-correlated. While considering the long term averages the transient processes will be averaged out leaving synoptic scale effects in which case the two may be highly anti-correlated as there is no additional heat input due to diabatic processes. The relatively good correlation between the Z_{CPT} and T_{CPT} in the monsoon months (JJA) when synoptic scale effects dominate supports this contention. However, it further depends on the strength of convection during different monsoon years (here JJA 2006, 2007 and 2008). It is seen that T_{CPT} and TTB shows good anti-correlation during the monsoon year of JJA2007 when the Z_{CPT} and T_{CPT} are also anti-correlated well. JJA2007 is exceptional monsoon year. Other years do not show strong correlation. On sub-daily time scales, the cases of deep convection events (TBB<240 K) and clear sky conditions (TBB>240 K) are dealt separately regardless of the season. During deep convection the Z_{CPT} and T_{CPT} are fairly well (anti) correlated, whereas for clear sky conditions the correlation is poor. The dependence of CPT and COT is seen on only for synoptic (seasonal and monthly) scales and the correlations are poor for short and shorter term scales. Z_{COT} and T_{COT} are highly anti-correlated for seasonal to shorter scale and hence completely governed by adiabatic processes. It is to be noted that the Z_{COT} is determined at the level where potential temperature (θ) lapse rate show a local minima. These minima ($d(\theta)/dz \sim 0$-5 K/km) correspond to near adiabatic condition.

The Z_{LRT} and T_{LRT} are highly (anti) correlated from seasonal to shorter scale in contrast to Z_{CPT} and T_{CPT}. It is to be noted that the LRT is well below the CPT. This means that LRT is more a characteristic of the troposphere than the stratosphere in contrast to CPT which behaves more like a characteristic of lower stratosphere than upper troposphere [*Thuburn and Craig,* 2002]. Though LRT and COT vary adiabatically, they may not be determined by convection alone. The tropical tropopause parameters depend more strongly on convection on seasonal and monthly scales than on shorter scales for which the correlation is poor. It is well known that the Walker circulation is forced by convection. However, its effect on day to day variation of the weather is found to be very small [*Meehl*, 1994]. Although, the dependence of tropical tropopause parameters on convection in sub-daily and day-to-day basis is poor, yet it can not be ruled out completely since convection is highly localized phenomenon and need to be investigated on event based considering deep, shallow and clear sky conditions separately. TTLt is found to depend on both COT and CPT.

4.4. Discussion

Long-term high-vertical resolution radiosonde observations over a tropical location, Gadanki, in Indian monsoon region reveal notable differences in CPT when compared to western pacific region (Truk). The T_{CPT} over Gadanki is found to be 2-3 K cooler than over western pacific region in the summer season suggesting the effect of summer monsoon over Gadanki. Further, interestingly the range of annual variation of

T_{CPT} is much smaller at Gadanki compared to Truk while the range of Z_{CPT} variation is about the same at the two stations.

Table 4.2: *The correlation analysis between height and temperature of CPT, LRT and COT observed in seasonal, short, and shorter time scales. The correlation analysis between TTLt with Z_{CPT} and Z_{COT}, and TBB with T_{CPT}, T_{COT}, T_{LRT}, and TTLt observed in seasonal, short, and shorter time scales is also shown. The correlations which are not significant at 95% level are shown with asterisk (*).*

	Z_{CPT} X T_{CPT}	Z_{LRT} X T_{LRT}	Z_{COT} X T_{COT}	Z_{CPT} X Z_{COT}	TTLt-x Z_{CPT}	TTLt-x Z_{COT}	TTLt-x TBB	T_{CPT} X TBB	T_{LRT} X TBB	T_{COT} X TBB	No. of obs.
	Seasonal										
Apr 06-Dec 08	-0.91	-0.82	-0.96	-0.53*	0.93	-0.80	0.88	-0.73	-0.65	0.66	12
	Monthly										
	-0.41	-0.63	-0.94	-0.46	0.87	-0.82	0.69	-0.30*	-0.21*	0.42	32
	Daily										
	-0.29	-0.69	-0.94	-0.23	0.70	-0.79	0.21	-0.12	-0.03*	0.12	681
	Short–term (Day-to-day)										
JJA06	-0.27	-0.63	-0.94	-0.07*	0.69	-0.72	0.19*	0.09*	0.07*	0.12*	76
SON06	0.10*	-0.74	-0.97	-0.13*	0.60	-0.82	-0.04*	-0.10*	-0.00*	-0.00*	66
JJA07	-0.63	-0.90	-0.79	0.16*	0.58	-0.59	0.19*	-0.30*	-0.20*	-0.10*	51
SON07	-0.37	-0.71	-0.93	0.04*	0.60	-0.74	0.12*	-0.20*	-0.10*	-0.10*	67
DJF08	-0.05*	-0.58	-0.97	-0.27	0.66	-0.90	0.10*	-0.00*	0.06*	0.06*	61
MAM08	-0.16*	-0.78	-0.96	-0.30	0.63	-0.78	-0.04*	0.06*	0.09*	0.09*	65
JJA08	-0.23	-0.87	-0.95	-0.02*	0.68	-0.72	0.28	-0.10*	0.17*	0.21*	83
SON08	-0.29	-0.73	-0.97	-0.06*	0.65	-0.80	0.15*	0.19*	0.18*	0.12*	83
	Shorter-term (Sub-daily)										
Total	-0.25	-0.81	-0.98	-0.15*	0.65	-0.85	0.23	0.15*	0.26	-0.09*	100
TBB>240	-0.12*	-0.85	-0.98	-0.17*	0.63	-0.87	0.23*	0.23*	0.23*	-0.12*	59
TBB<=240	-0.52	-0.78	-0.98	-0.08*	0.66	-0.81	0.12*	0.12	0.17*	0.04*	41

T_{CPT} goes below 191 K more frequently during December to May than during June to November. In addition, the entry of water vapor with mixing ratio greater than 3 ppmv from troposphere to stratosphere occurs more frequently during the later period in the Indian zone. Thus, there is a greater chance of entry of relatively dry air into lower stratosphere during winter than during the rest of the year. Although convection is weak during winter season it can extend to higher levels even penetrating sometimes to lower stratosphere [*Satheesan and Krishna Murthy*, 2005]. The variations in the Z_{CPT} and T_{CPT} can be broadly categorized into the following: 1. Changes in Z_{CPT} and T_{CPT} are out of phase indicating adiabatic processes. 2. Changes in Z_{CPT} and T_{CPT} are in phase, indicating diabatic processes. 3. Changes in Z_{CPT} occur with no changes in T_{CPT} and vice versa again indicating diabatic processes. 4. Both Z_{CPT} and T_{CPT} remain steady. The processes which involve these cases could be due to either convection or exchange processes between troposphere (mainly water vapor) and stratosphere (mainly ozone), or horizontal advection from surroundings or modulation by equatorial planetary waves or a combination of these. The occurrence of these cases in different seasons as well as in total data is also quantified. In general, monsoon months JJA show higher percentage of occurrence for case 1 than for the other cases while during DJF, MAM and SON, both cases 1 case 2 are dominant. Though the percentage of occurrence of case 3 is small, it is observed in all the seasons. Case 4 is least observed. During JJA, occurrence of case 1 is ~ 60% representing dominance of adiabatic processes in that season. For rest of the seasons both adiabatic and diabatic process are dominant. Out of a total 681 observations, the number of occurrences of case 1, case 2, case 3 and case 4 is 365, 267, 45 and 4, respectively.

The long-term variability of the CPT is similar to case 1. However, in the short-term (day-to-day) variation of CPT, all the four cases occur with no preference. Several factors may contribute to short-term variation such as variation in local convective activity [*Reid and Gage*, 1996], horizontal advection from convective regions and modulation by equatorial planetary waves of periodicity 4-20 days [*Tsuda et al*., 1994; *Ratnam et al*., 2006].

In the sub-daily variation of CPT also, all the four cases are found to occur. During deep convection it is noticed that the tropopause may descend. The possible mechanisms which act to lower the tropopause on shorter time scale may be associated with cold surges, and/or a dynamical response to the tropical depression, subsidence induced by individual cumulus towers [*Johnson* 1986]. *Johnson and Kriete*, [1982] have reported that there is slight bulging of the tropopause immediately above meso-scale convective system over southern South China Sea.

Large variation in the Z_{CPT} (~1 km) and T_{CPT} (~3 K) is noticed even on sub-daily scales. In the present study, it is observed that during a day the tropopause pushing up by ~0.6-0.8 km in some cases and down by ~ 1 km in some other cases. Interestingly, increase in both Z_{CPT} and T_{CPT} during an event of clear sky conditions is also noticed. Correlation analysis between Z_{CPT} and T_{CPT} reveals that on seasonal scales the variation in the tropical tropopause is mainly dominated by adiabatic process while for short scales both adiabatic and diabatic process may be effective.

The Z_{LRT} and T_{LRT} are highly (anti) correlated from seasonal to shorter scale in contrast to Z_{CPT} and T_{CPT}. The dependence of CPT on COT is seen on only for synoptic (seasonal and monthly) scales and the correlations between the two are poor for short and shorter term scales. Z_{COT} and T_{COT} are highly anti-correlated for seasonal to shorter scale and hence are mainly governed by adiabatic processes. While T_{COT} and TBB show good correlation in general on synoptic scale, they show poor correlation on short and shorter scales. This poor correlation on short and shorter scales is because T_{COT} may be influenced by non local phenomena and TBB by local phenomena. It is observed that TTLt depends on both CPT and COT regardless of the season. In Chapter 3, it is also seen that the TTLt becomes less during JJA mainly due to tropical deep convection prevailing during the monsoon season which may result in increasing of Z_{CPT} [*Mehta et al*., 2008].

4.5. Summary

The main findings of this study are summarized below:

1. The amplitude of the annual variation of the Z_{CPT} over Gadanki is similar to Truk but not T_{CPT}.
2. The day- today variation of the CPT is dominated by adiabatic processes during summer season while both adiabatic and diabatic processes are dominant during rest of the season.
3. The effect of both convective activity and diurnal tides observed in sub daily variation of the CPT.

4. The Z_{CPT} and T_{CPT} are well anti correlated, however, correlation between two on day to day scale is not always good during all the seasons.

From this Chapter it is observed that the characteristics of the cold point tropopause are observed over Gadanki show some distinct feature when compare to Truk, west Pacific station. Thus it suggests that longitudinal variability in tropopause characteristics exist which is investigated in detail in the Chapter 5.

---END---

Chapter 5

Longitudinal Characteristics of the Tropical Tropopause

5.1. Introduction

The simple picture of the tropical tropopause assumes that it represents the cap imposed on tropospheric deep convection by stably stratified inversion layer of the lower stratosphere. It is generally believed that the centers of active convection reside normally at the western end of the Pacific basin. These centers of active convection are clearly seen in satellite maps of outgoing long-wave radiation (OLR). Negative anomalies in OLR are associated with major centers of enhanced convection that can be observed to migrate from west to east on satellite maps [*Wickemann*, 1983; *Lau and Chan*, 1985]. While much of the observed variability is associated with the 30-60 day oscillation in the tropics, it is clear that during an ENSO (El Niño– Southern Oscillation El) event the centers of enhanced convection migrate eastward beyond the date line into the eastern Pacific. Theses dramatic shift in the location of the intense convection is accompanied by changes in the Walker circulations associated with Southern Oscillation (see, for example, *Rasmussen and Wallace* [1983]).

Gage and Reid, [1987], suggested that while tropical tropopause altitudes may well be determined globally by their formation over regions of most active convection, it is not clear that tropopause potential temperature will conserve its value away from these centers of intense convection. Clearly, if radiation plays a role, tropopause temperatures which are coldest over regions of intense convective activity will become warmer away from these regions of intense convection. Therefore significant variations in tropopause temperatures should then be evident when comparing tropopause properties close to and far from centers of active convection. These studies suggest that tropical tropopause has a strong longitudinal (zonal) structure associated with convective centers. However, studies related to longitudinal structure of the tropopause properties are very few. On the other hand, there are number of works dealing with the temporal variation of the tropical tropopause properties on various time scales [e.g., *Reid and Gage*, 1981; 1982; 1985; 1996; *Reid*, 1994, *Krishna Murthy et al*, 1985]. The temporal variations of the tropical tropopause such as seasonal and interannual and the physical processes which control such variability are relatively well documented using a series of extensive analyses of the long-term records from radiosonde stations, mainly in the western tropical Pacific region. The annual cycle has been linked to seasonal variations in solar insolation and its impact on tropical convection [*Reid and Gage*, 1981; *Shimizu and Tsuda*, 2000] and to remote forcing during boreal winter associated with the intensification of the Brewer-Dobson circulation [*Reid and Gage*, 1996].

Interannual variations in the tropical tropopause have been linked to the quasi-biennial oscillation (QBO) of the equatorial stratosphere [*Angell and Korshover*, 1964; 1974; *Reid and Gage*, 1985], the El Niño-Southern Oscillation [*Gage and Reid*, 1985, 1987], and episodic volcanic eruptions [*Reid and Gage*, 1985]. The QBO signature in the tropical tropopause is mainly zonally symmetric and has smaller amplitude than the ENSO signature. It is probably the result of the downward propagation of temperature anomalies associated with the QBO [*Zhou et al*. 2001b]. The ENSO signature shows east–west dipole and north–south dumbbell patterns. These patterns are believed to be related to the migration of the convection centers with the life cycle of the ENSO [*Randel et al*. 2000; *Zhou et al*. 2001b; *Kiladis et al*. 2001]. The variation of the tropical tropopause on seasonal time scales is related with propagation of equatorial waves. There are several evidences on the influence of the Madden Julian Oscillation (MJO) on the tropical tropopause variations (e.g., *Zhou and Holton*, 2002). Also day-to-day variations of the tropical tropopause are found to be modulated by equatorial Kelvin and Rossby-Gravity waves [*Tsuda et al*, 1994, *Krishna Murthy et al*, 2002, *Ratnam et al*, 2006]. The diurnal variation is found associated with migration of tides and locally generated convection [*Das et al*, 2008, *Mehta et al*, 2010]. The deep cumulus convection sometimes penetrates the tropopause which causes cross tropopause transport of tropospheric air into lower stratosphere. According to the stratospheric fountain hypothesis, tropical tropospheric air enters the stratosphere preferentially in areas where the tropical tropopause temperatures are below their annual and longitudinal mean values. The fountain region is mainly over the western Pacific, with some variation with season. However, recent studies indicate that the western Pacific may actually be an area with net subsidence at the tropopause [*Sherwood* 2000; *Gettelman et al*. 2000]. This paradox can be resolved by assuming that horizontal transport through the ‘‘cold-trap’’ region (i.e., the western Pacific) causes air parcels that reach the tropopause at other longitudes to be dehydrated to the very low saturation mixing ratios characteristic of the cold trap [*Holton and Gettelman*,2001]. This mechanism implies that tropopause temperature variations in areas other than the western Pacific also affect the entry value of water vapor mixing ratio from the troposphere into the stratosphere.

Gage and d Reid, [1987] made an attempt to explain the longitudinal variation of the tropical tropopause properties that accompany zonally non-uniform convection. From an intercomparison of tropopause properties over western Pacific region and Curacao (12.2^{o}N, 69.0^{o}W), it is found that Curacao is systematically warmer than over western Pacific stations and argued that potential temperature of tropopause increases away from major centers of convections. However, these studies are relatively very few and full account of longitudinal characteristics of the tropical tropopause is yet to be made. The zonal mean picture of the tropopause does not reveal its longitudinal variations. In this chapter the longitudinal variations in the tropical tropopause properties are explored.

5.2. Data and Analyses

The radiosonde data obtained at both 00 and 12 UTC for the 10 year period (1999-2008) for stations Truk, Rochambeau, Singapore, Seychelles and Darwin distributed across the globe within ±15^o latitude from equator are used in the present study. High resolution radiosondes (Väisälä RS-80, Väisälä RS-92 and Meisei) were launched once daily on a regular basis from Gadanki, a tropical station in the Indian monsoon region, during April 2006 to December 2008 at around 1730 IST. More details about the data are explained in Chapter 2, 3 and 4. The extensive details of the radiosonde data over Truk, Rochambeau and Singapore are presented in Chapter 6. The location of these stations is shown in Figure 5.1.

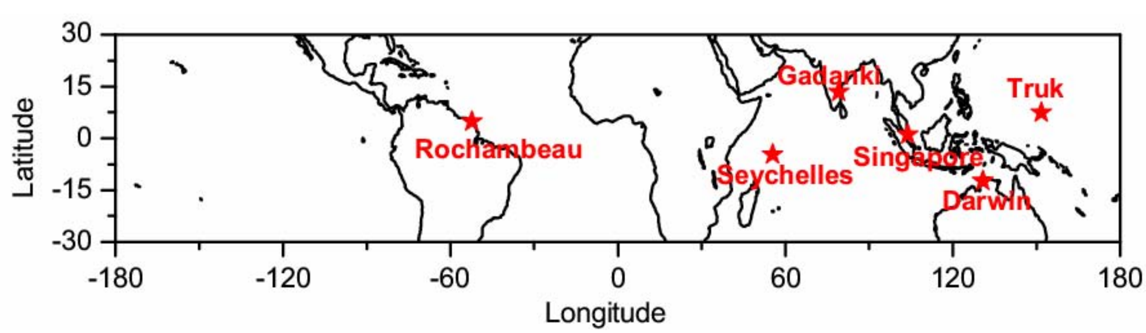

Figure 5.1*: Map of the location of the selected radiosonde stations in the tropical belt. Three years of data from April 2006-December 2008 from Gadanki and Ten years of data from 1999-2008 over rest of the stations is used in the present analysis*

In addition to these radiosonde data, COSMIC GPS-RO (Global Positioning System-Radio Occultation) data for the period of August 2006- August 2008 is also used for the global coverage of whole tropical belt. Six COSMIC GPS-RO satellites were launched in April 2006, providing about 2000 occultation events per day around the globe [*Anthes et al*., 2008]. More details about the data are provided in Chapter 2 and Chapter 6.

The daily OLR data is also used which is represented as a proxy for the convective activity during the period of the observation from 1999-2008. The OLR is derived from Infrared radiances at high space and time resolutions as described by *Salby et al*. [1991], interpolated by the National Oceanic and Atmospheric Administration (NOAA), and provided by NOAA climate Diagnostics center, Colorado (http://www.cdc.noaa.gov/).

The study of the tropical tropopause parameters over Gadanki are carried out on Chapter 4. From Chapter 4, it is observed that there are noticeable difference between tropopause over Gadanki and Truk. This suggests that pronounced longitudinal difference exist in tropopause characteristics which are investigated in this Chapter. Above mentioned data set is used to study the longitudinal variations in the tropical tropopause parameters such as T_{CPT}, $Z_{CPT,}$ $Z_{COT,}$ T_{COT} and TTLt. The potential temperature CPT and COT is denoted as θ_{CPT} and θ_{COT}, respectively, and equivalent potential temperature at 900 hPa is denoted as $\theta_{E.}$

5.3. Results

5.3.1. Seasonal Variation of the Tropical Tropopause Parameters

Before discussing the seasonal variation of the tropopause, time series of monthly mean tropopause altitudes are compared among the stations as shown in Figure 5.2 for the stations mentioned in Figure 5.1. This comparison clearly illustrates the annual variation in tropical tropopause altitude as well as year to year to variability at different stations. The 12-month running mean is also shown for individual stations. The main features of the time series are well correlated among the stations. The cross correlations among these stations are greater than 0.7 estimated at 95% significance level. The correlation coefficient between Truk (7.44^{o}N, 151.83^{o}E) and Singapore (1.03^{o}N, 103.87°E) is 0.82 and between Truk and Darwin (12.41°S, 130.88°E) is 0.91 whereas between Truk and Rochambeau (4.83°N, 52.36°W) it is 0.7. Truk and Rochambeau are widely separated in longitude by ~ 204° accounting probably for the relatively lower correlation and indicating that tropopause altitude responds to local influences as well. The twelve month running means indicate a broad peak between years 1999 and 2008/2009. It is not clear whether this is a part of a longer term variation. Analysis of a longer time series of data may unravel any such trends. From analysis of 26 years (1973 to 1998) of data, *Zhou et al* [2001a] reported cooling trend in CPT temperature.

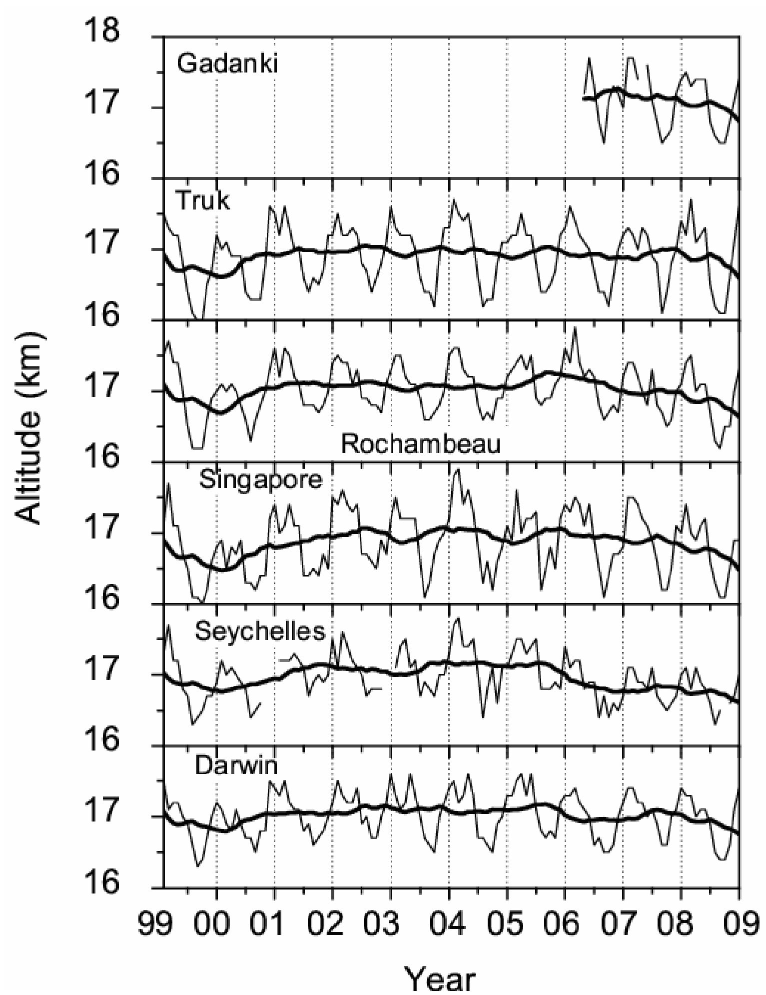

Figure 5.2: *Time series of monthly mean tropopause altitudes at Gadanki, Truk, Rochambeau, Singapore, Seychelles and Darwin. Heavy solid line is a 12- month running mean of tropopause altitude.*

The seasonal variations of the Z_{CPT} and T_{CPT} for different stations are shown in Figure 5.3. The variations of the Z_{CPT} and T_{CPT} are, in general, out of phase. During January-May, Z_{CPT} and T_{CPT} are more or les steady. It is well known that, in general, CPT is low and warm during Northern Hemisphere (NH) summer (June-August) while high and cold during NH winter season (December-February). It is evident from the figure that in general the CPT is high and cold during December-February, for all the stations. It is interesting to note that CPT at all stations does not become low and warm in the same month, during NH summer season. CPT becomes low and warm during July, August and September for the pair-stations Rochambeau and Seychelles (1.03^{o}N, 103.87^{o}E), Gadanki and Singapore, and Truk and Darwin, respectively. The amplitude of the seasonal variation of CPT temperature is minimum (~2.5K) at Gadanki in comparison with the other stations while that of CPT altitude is minimum at Seychelles. CPT over of Gadanki is highest throughout the year when compared to the other stations. Note that the Gadanki data is for ~3 years whereas for the other stations it is ~10 years. So, there may be contamination of residual inter annual variations, if any, in the seasonal variations presented for Gadanki. Although, the seasonal variations of the Z_{CPT} and T_{CPT} are, in general, out of phase, their relationship is not simple linear [*Reid and Gage*, 1996], which will be discussed in a later sections.

The seasonal variation of the convective tropopause is shown in panels of Figure 5.3(b). The COT shows different seasonal variations at different stations. The range of variation of the Z_{COT} (T_{COT}) is between ~13 km -14 km (~205K-215K) except for Gadanki. In general, all the stations except Gadanki show characteristic low values of Z_{COT} during NH summer and high during NH winter. As reported earlier in the Chapter 3 and also in [*Mehta et al*. 2010], the COT over Gadanki shows high during summer monsoon season (JJAS) and low during winter months. The range of variation of Z_{COT} at Gadanki is between ~14-15 km. Similar to the CPT, COT also is highest at Gadanki compared to the other stations. The Z_{COT} is high in summer at Gadanki in contrast to the other stations where it is generally low in (NH) summer indicating the influence of the summer monsoon over Gadanki. The seasonal variations of Z_{COT} and T_{COT} are out of phase. The seasonal variation of the TTLt along with OLR is shown in panels of Figure 5.3(c). OLR value less than 240 W/m^2 is used as proxy to indicate deep convection.

During the summer season, deep convection over Gadanki pushes up the convective tropopause thereby decreasing TTLt [*Mehta et al*, 2008; 2010].

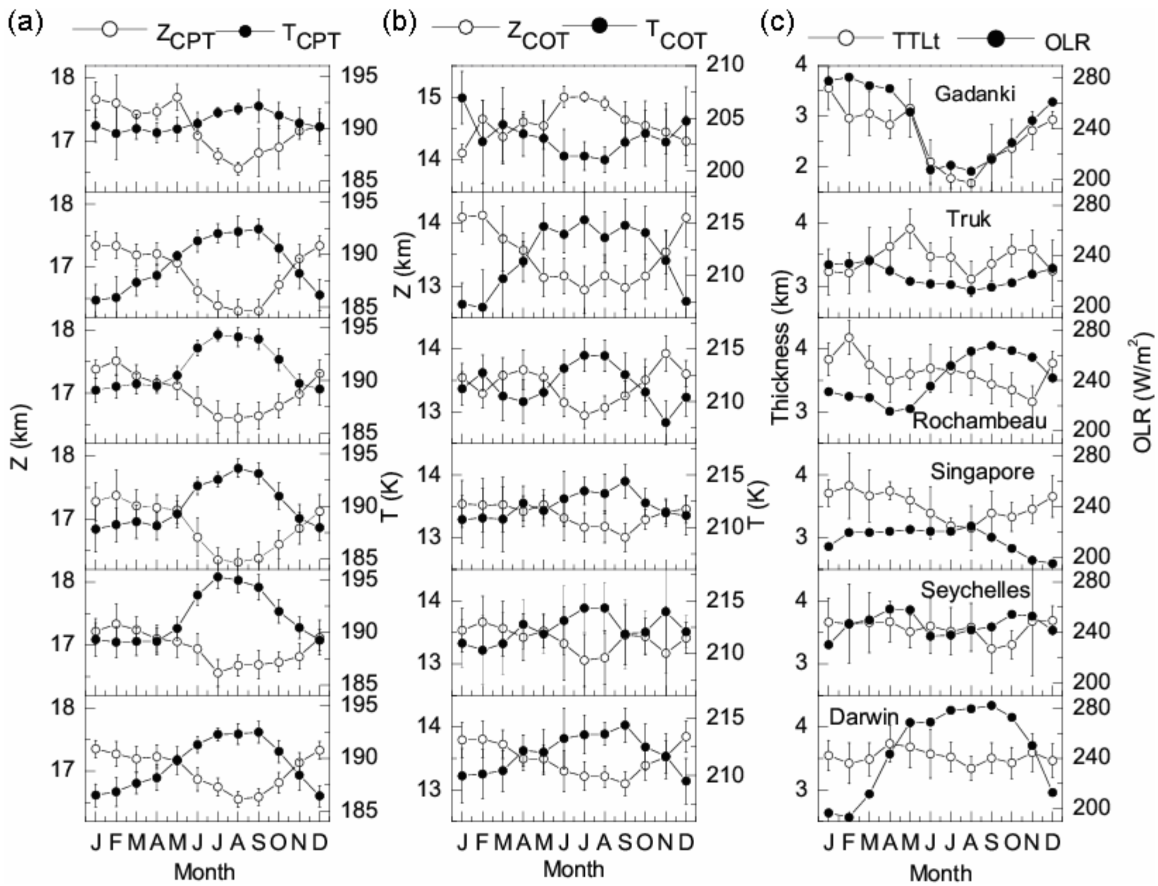

Figure 5.3: *Seasonal variation of the altitude and temperature of the cold point tropopause (Left panels), convective tropopause (middle panels) and tropical tropopause layer thickness along with outgoing long-wave radiation observed over different stations Gadanki (during April 2006-December 2008) and Truk, Rochambeau, Singapore, Seychelles and Darwin (during January 1999-December 2008).*

The range of seasonal variation of the TTLt is ~ 1 km -5 km. At Singapore and Truk, the OLR is < ~240K throughout the year indicating prevalence of deep convection. Darwin and Seychelles show the OLR <~240K in winter months. At Rochambeau, the deep convection (OLR <~240K) extends beyond winter months, till June. In contrast to these four stations, as mentioned earlier, OLR<~240K is only in the summer monsoon months at Gadanki. Further the seasonal variations of OLR and TTLt are nearly out of phase at Gadanki in contrast to the other stations.

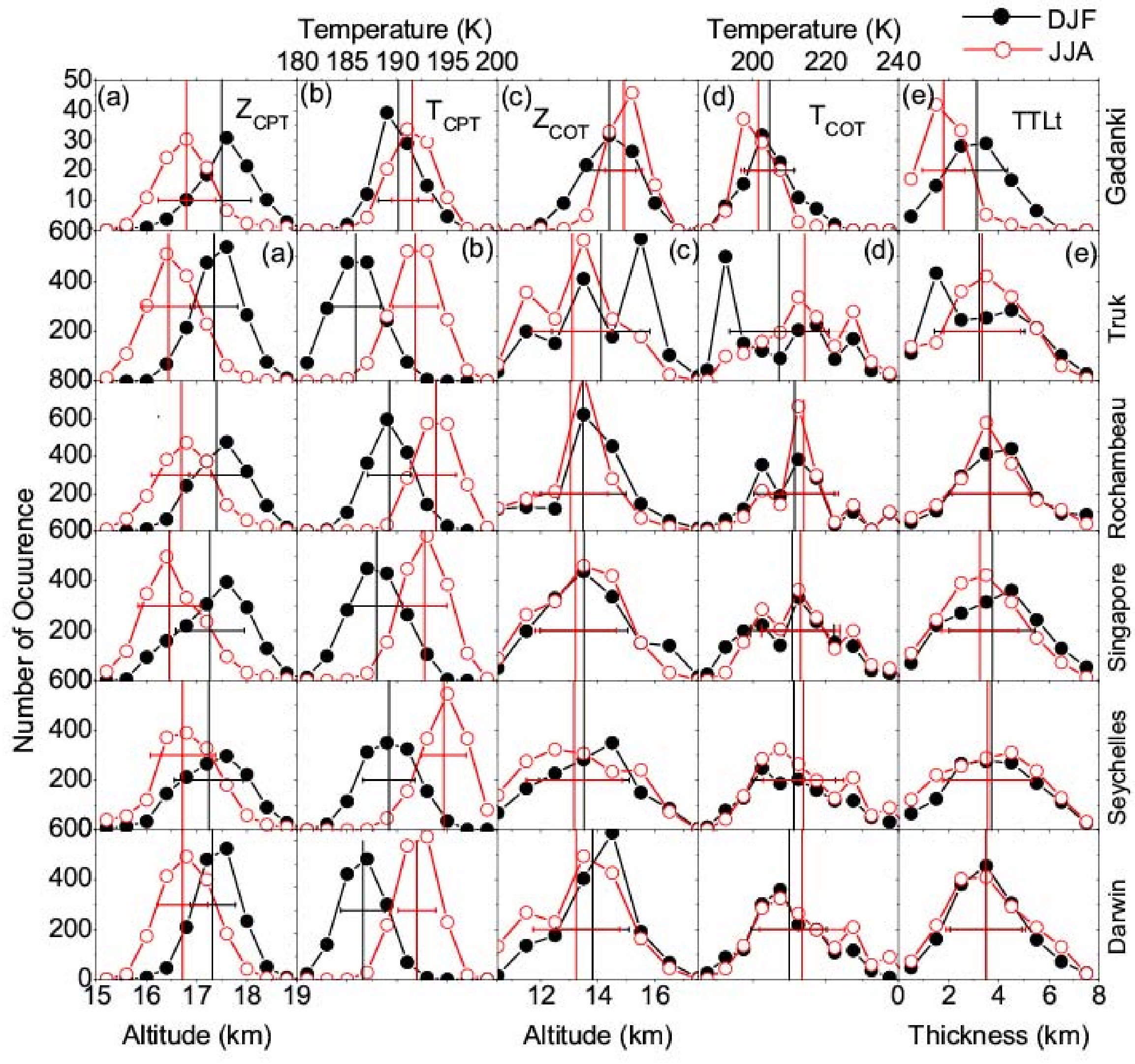

Figure 5.4: *Probability distribution of daily (a) Z_{CPT} with 0.4 km interval, (b) T_{CPT} with 2 K interval, (c) Z_{COT} with 1.0 km interval, (d) T_{COT} with 5.0 K interval and (e) TTLt with 1.0 km interval observed during DJF and JJA.*

The probability distribution of occurrence of various tropopause parameters during NH summer and NH winter season is estimated which is shown in Figure 5.4. From the figure it is clear that the day to day variation of Z_{CPT}, $T_{CPT,}$ Z_{COT}, T_{COT} and TTLt ranges from 15-19 km, 180 K- 200 K, 10.5 km- 17.5 km, 185 K – 240 K and 0-8 km, respectively. All stations show a clear peak of Z_{CPT} and T_{CPT} during both the season which nearly coincides with mean Z_{CPT} and T_{CPT}, respectively, as clearly seen from Table 5.1 in which the mean values for winter and summer are given.

Table 5.1: *Mean and standard deviation of the Z_{CPT}, T_{CPT}, Z_{COT}, T_{COT} and TTLt during Season DJF and JJA.*

	DJF	JJA
	Z_{CPT}	
Gadanki	17.50 ± 0.59	16.80 ± 0.57
Truk	17.35 ± 0.40	16.44 ± 0.52
Rochambeau	17.40 ± 0.48	16.69 ± 0.59
Singapore	17.27 ± 0.69	16.46 ± 0.62
Seychelles	17.25 ± 0.68	16.72 ± 0.65
Darwin	17.32 ± 0.45	16.72 ± 0.50
	T_{CPT}	
Gadanki	190.10 ± 1.99	191.50 ± 2.02
Truk	185.90 ± 2.46	191.80 ± 2.27
Rochambeau	189.20 ± 2.16	193.90 ± 1.99
Singapore	187.90 ± 2.61	192.70 ± 2.26
Seychelles	189.20 ± 2.57	194.70 ± 2.26
Darwin	186.60 ± 2.18	192.00 ± 1.89
	Z_{COT}	
Gadanki	14.40 ± 0.94	14.90 ± 0.66
Truk	14.11 ± 1.71	13.10 ± 1.42
Rochambeau	13.49 ± 1.49	13.05 ± 1.29
Singapore	13.52 ± 1.53	13.22 ± 1.41
Seychelles	13.52 ± 1.58	13.17 ± 1.67
Darwin	13.82 ± 1.26	13.24 ± 1.50
	T_{COT}	
Gadanki	204.60 ± 6.81	201.60 ± 4.85
Truk	207.30 ± 13.60	214.30 ± 11.3
Rochambeau	211.40 ± 11.10	214.00 ± 9.53
Singapore	210.90 ± 11.50	213.20 ± 10.8
Seychelles	211.20 ± 11.50	213.90 ± 11.1
Darwin	209.90 ± 10.40	213.50 ± 11.7
	TTLt	
Gadanki	3.12 ± 1.23	1.80 ± 0.84
Truk	3.23 ± 1.80	3.34 ± 1.54
Rochambeau	3.92 ± 1.63	3.65 ± 1.51
Singapore	3.73 ± 1.70	3.25 ± 1.53
Seychelles	3.70 ± 1.71	3.55 ± 1.77
Darwin	3.48 ± 1.43	3.48 ± 1.58

The mean Z_{CPT} ranges from 17.27 km -17.40 km during NH winter and 16.50 km -16.72 km during NH summer with lower values at stations near to equator whereas the mean T_{CPT} ranges from ~ 186 K – 189 K and ~192 K- 195 K during NH summer and winter, respectively. The tropopause at the Pacific stations (Truk, Singapore and Darwin) is comparatively cooler (by 2-4 K) than that over the Non-Pacific stations (Rochambeau and Seychelles). It can be noted that Singapore and Darwin lie near to Pacific but not within the Pacific region. As noted earlier, the tropopause at Gadanki is higher than other stations in both winter and summer seasons. The coldest tropopause in winter is at Singapore while in summer it is at Gadanki.

The probability distribution of the Z_{COT} and T_{COT} during NH winter and NH summer show similar structure with a clear peak which more or less coincides for the stations Rochambeau and Singapore, whereas slight deviations are observed for the stations Truk, Darwin and Seychelles, with their mean values ~ 13 km-14 km and 207 K-214 K, respectively as listed in Table 5.1. The convective tropopause is highest and coldest at Gadanki compared to the other stations. The probability distributions of the TTLt show similar behavior as COT with clear peak in the range ~ 3.2 km - 3.9 km.

5.3.2. Annual Cycle in the Temperature Anomalies in Upper Troposphere and Lower Stratosphere (UTLS).

Reid and Gage, [1996] attributed occurrence of high CPT during winter season to the combined effect of tropical convection and extra-tropical wave driving. The extra-tropical wave driving raises the lid at the top of troposphere, allowing deeper convective clouds to penetrate to greater altitudes, with correspondingly lower cloud top temperatures. The variation in the convective penetration lies in the annual cycle in temperature in the tropical lower stratosphere as discussed by *Gage and Reid,* [1982]. These seasonal variations of the tropopause anomalies, however, are essentially similar to those reported earlier within and outside the Pacific basin [*Reid and Gage*, 1981]. Figure 5.5 shows the monthly mean temperature departures from the annual average for the altitude region 10 km - 20 km. The annual variation is small and similarly phased in the upper troposphere as shown in Figure 5.5(a). However, the nature of this variation in temperature anomalies differs from station to station in the upper troposphere. The marked and contrasting feature is noticed for Gadanki station which is nearly out of phase from rest of the stations. Among the rest of the stations, Truk and Darwin both show one type of similar feature while the stations Rochambeau, Singapore and Seychelles show another type of similar feature. The annual cycle in temperature anomalies for the stations Gadanki, Truk and Darwin (high latitude stations within tropics) begins to change from altitudes 15 km -16 km whereas at rest of the stations it changes from altitudes 14 km -15 km as shown in Figure 5.5(b).

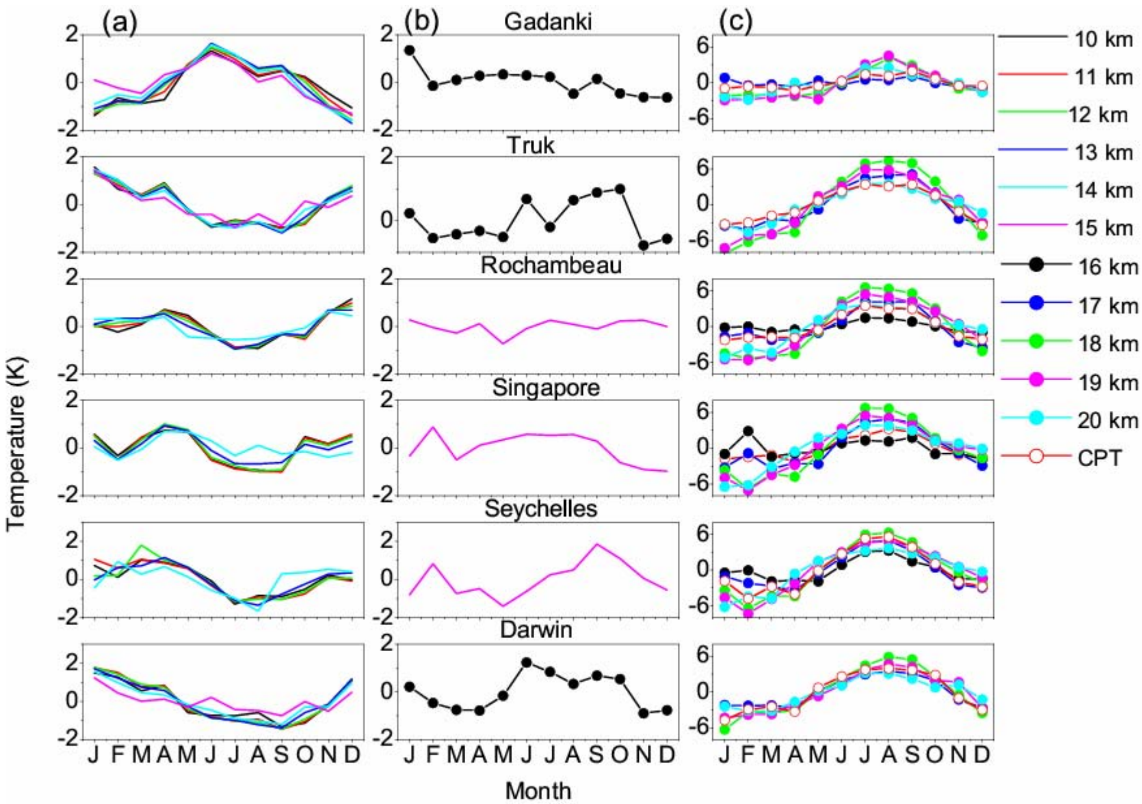

Figure 5.5: *Annual cycle in monthly mean temperature anomaly (annual average subtracted) for different height regions.*

These regions can be considered as transition regions between upper troposphere and lower stratosphere. For altitudes above the transition region to 20 km, the annual temperature anomalies are shown in Figure 5.5(c). All annual cycles in temperature anomalies in lower stratosphere are in phase having similar structure. These temperature anomalies are more or less out of phase with upper troposphere temperature anomalies except at Gadanki. The existence of the annual cycle of the temperature anomalies over Gadanki showing similar phase throughout the altitude from 10 km- 20 km is exceptional.

The annual cycle of the T_{CPT} anomaly is also shown in Figure 5.5(c). Interestingly, the variation of T_{CPT} anomaly is similar to the lower stratospheric temperature anomalies at all the stations. This suggests that T_{CPT} is influenced strongly by stratospheric processes. The T_{COT} anomaly is found to be out of phase shown in supplementary Figure S5.1 while Z_{COT} shows more or less in phase variation to the upper tropospheric temperature anomalies which is also indicated in panels of Figure 5.3(b).

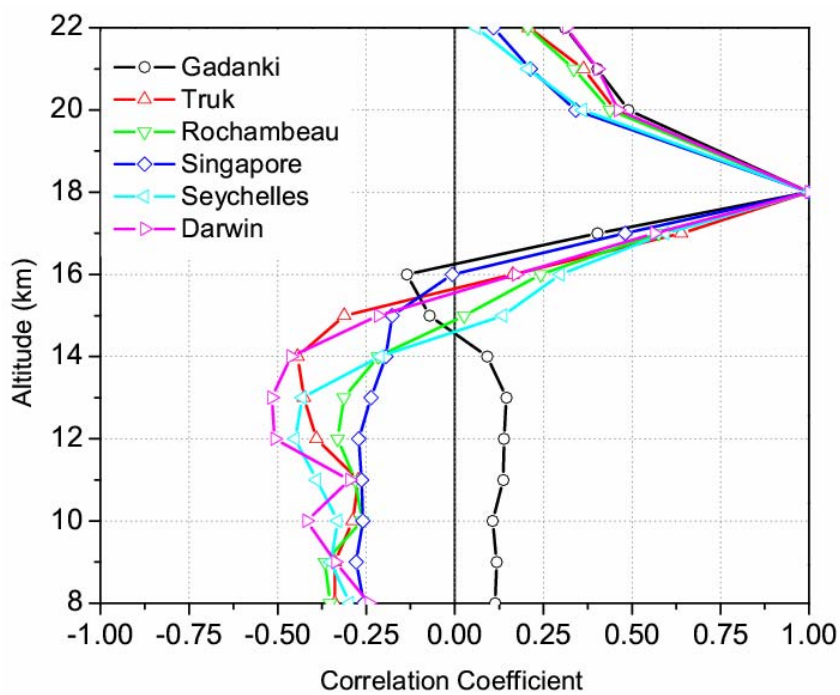

Figure 5.6: *Correlation coefficient between daily values of temperature at various altitude levels and daily values of temperature at the 18 km.*

Figure 5.6 shows correlation coefficients between daily temperatures at altitude 18 km, typical of lower stratosphere, and temperatures at other altitudes in the UTLS region considering all the data. The negative correlation (though low) in the troposphere is a well established feature of the tropical atmosphere [*Gage and Reid*, 1982; *Reid*, 1994]. This is, however, not true at Gadanki which shows positive correlation (low). As mentioned earlier the transition between upper troposphere to lower stratosphere takes place at different region at different stations which can also be seen from the correlation analysis. The transition from negative correlations to positive correlation takes place in different height regions for different stations. For Truk and Darwin transition takes place at altitude ~ 15 km -16 km while for Rochambeau and Seychelles at ~ 14 km -15 km. The correlation above 18 km decreases mainly due to increasing effect of QBO at these higher altitudes [*Reid*, 1994].

The lower stratospheric temperature cycle is governed by wave-driving mechanism [*Yulaeva et al.*, 1994] which indicates that the upward motion in the tropical lower stratosphere extends down into upper troposphere 14 km -15 km, which is found to vary from station to station. This extension into the troposphere, however, has the important consequence that lapse rates in uppermost region have pronounced annual cycle. Figure 5.7 shows average lapse rate derived from monthly mean temperatures at various altitudes. Earlier report over Truk has shown clear annual cycle that grows in amplitude as tropopause is approached and the upper most layer between 125 hPa -100 hPa shows the lapse rate varies from ~ 6 K/km in January to ~ 1 K/km in July [*Reid and Gage*, 1996]. Figure 5.7 shows the annual cycle in lapse rate that grows as tropopause approached. However, the behavior at all the stations is not exactly the same as that at Truk and differences from station to station can be marked. Within the Pacific region itself, the annual cycle of the lapse rates at Singapore and Darwin is not as pronounced as at Truk. The amplitude of the uppermost layer (15 km -CPT) is ~ 5K/km, 3.5 K/km and ~ 4 K/km at Truk, Singapore and Darwin, respectively. The stations outside the pacific basin have smaller amplitudes, ~ 3 K/km at Rochambeau and ~ 2 K/km at Seychelles throughout the layer from lowermost 13-15 km to uppermost 15 km-CPT. The amplitude of annual cycle of the lapse rate (in the layer between 15 km and CPT) over Gadanki is very less (~ 2 K/km). Further, the lapse rate is less than ~2 K/km throughout the year unlike at the other stations. *Reid and Gage* [1996] argued from the annual cycle of lapse rate at Truk that the buoyancy generated resistance to vertical motion in upper portion of the convective clouds is much less in January than in July, allowing overshooting of convective turrets to lower stratosphere to take place more easily [*Reid and Gage*, 1996]. Based on this argument the resistance to the vertical motion over Gadanki will be high throughout the year.

5.3.3. Relationship between Z_{CPT} and T_{CPT}

As reported by *Reid and Gage*, [1996] and mentioned earlier the relation between the annual cycle in Z_{CPT} and T_{CPT} is not simple linear. On the analysis of 9-years data over Truk they found that during March-May Z_{CPT} and T_{CPT} take an anomalous departure from linear relationship with greater heights than would be expected from linear relationship. This was related to increase in monthly mean potential temperature at CPT. Similar analysis at various stations in the tropical belt including Truk for the period of 10-year from 1999-2008 (for Gadanki data has been used for period April 2006-December 2008) is carried out as shown in Figure 5.8.

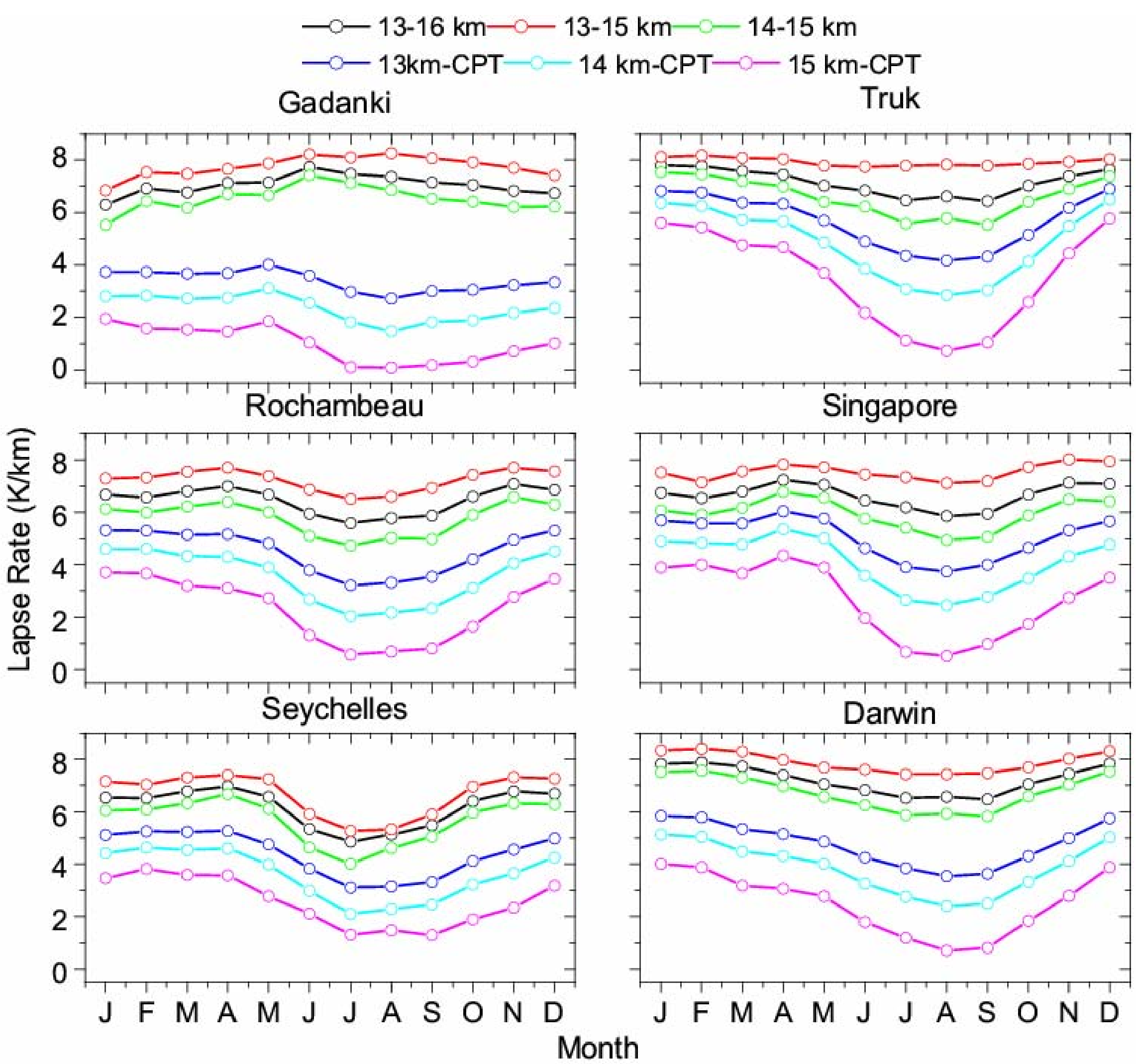

Figure 5.7: *Monthly mean temperature lapse rates between various altitude levels observed at different stations.*

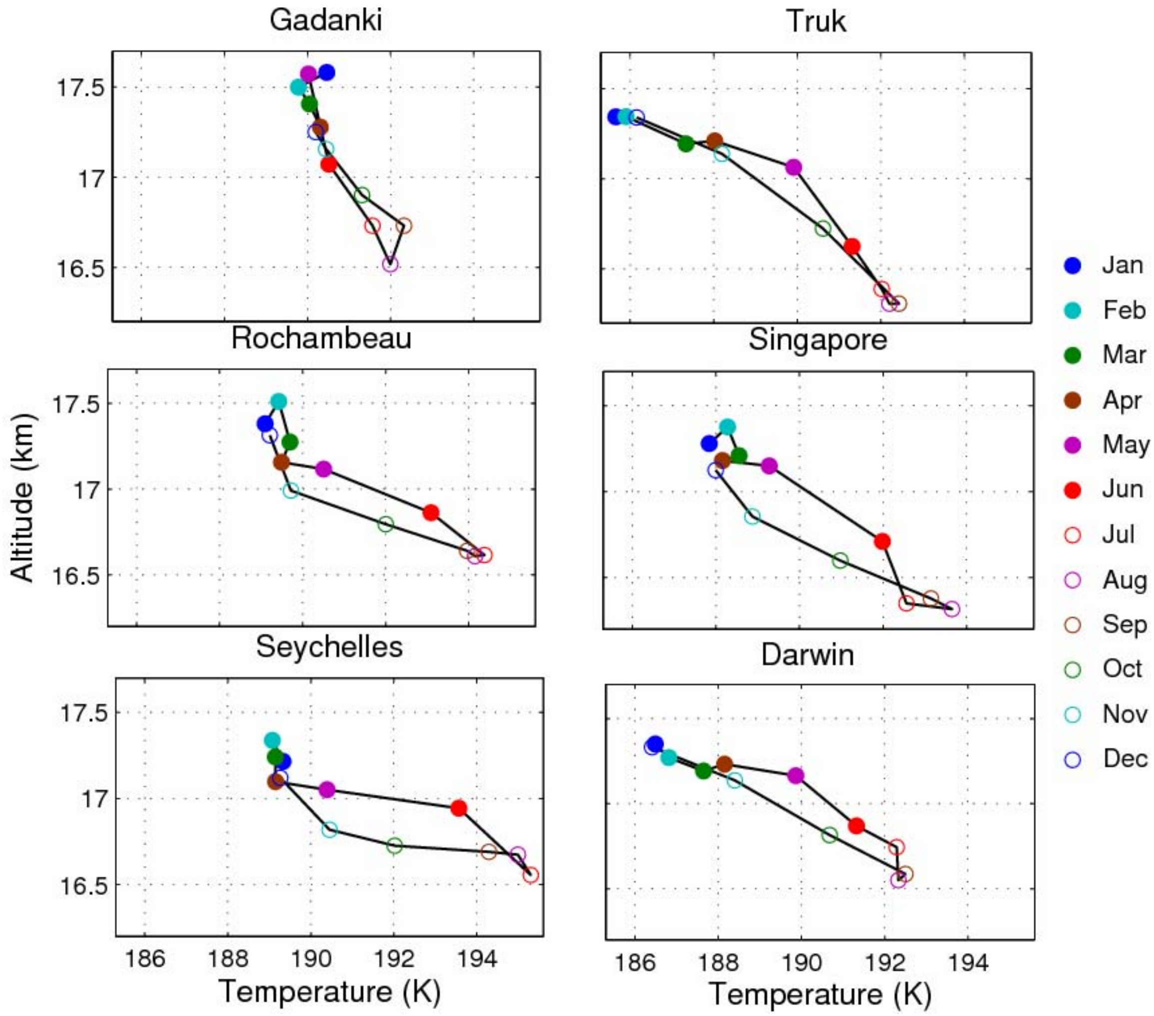

Figure 5.8: *Monthly mean tropopause altitude as a function of temperature.*

In this analysis Truk shows an anomalous departure during May month only, related to increase in θ_{CPT} as can be seen from Figure 5.9. Singapore shows anomalous departure during February, May and June from linearity (from Figure 5.8) with corresponding increase in θ_{CPT} ~ 1-3 K (from Figure 5.9). Similar to Singapore, Rochambeau and Seychelles show departure from linearity during February, May and June with ~ 1-3 K and ~4K increase in θ_{CPT}, respectively. Darwin takes departure during April- July with corresponding increasing of θ_{CPT} (~1-4 K). The linear relation over Gadanki is rather complex and different from other stations. But if data for January, May and September are excluded then temperature increases linearly from February-August as altitude decreases and followed back in same path from October to December.

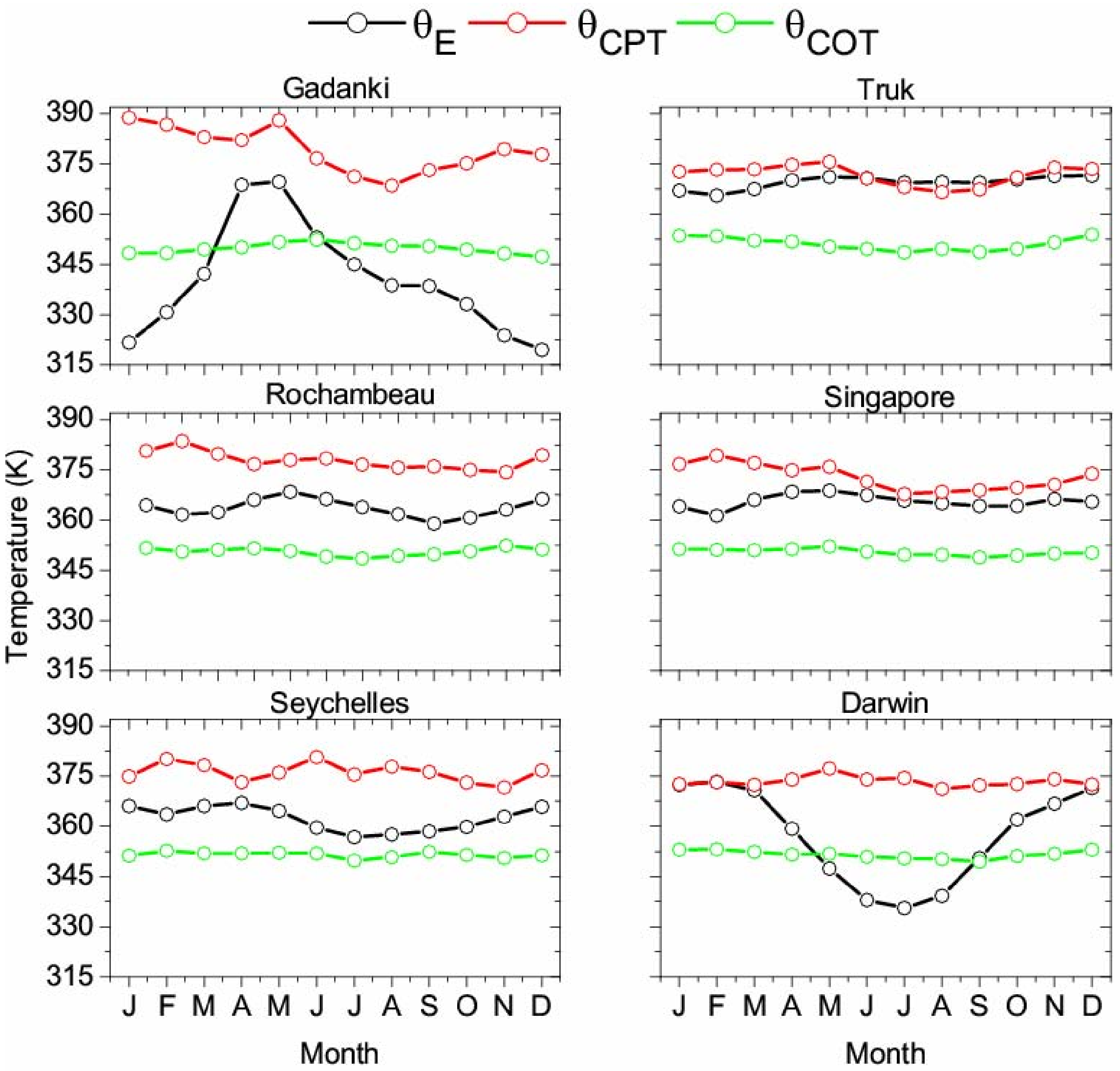

Figure 5.9: *Monthly mean of equivalent potential temperature at 900 hPa and potential temperature at CPT and COT observed at different stations.*

The Z_{CPT} over Gadanki shows sudden increase consistent with increase of θ_{CPT} ~10 K, ~6 K and ~ 5K during January, May and September, respectively. It is interesting to note that the increase in Z_{CPT} during September is followed by increase in T_{CPT} over Gadanki. Similarly, increase of Z_{CPT} during February can also be noticed as increase in T_{CPT} over Singapore and Rochambeau. This is due to diabatic heating playing dominant role in the behavior of tropopause altitude and temperatures even on monthly mean basis.

Figure 5.9 shows the monthly mean of the $\theta_{E,}$ θ_{CPT} and θ_{COT}. It has been suggested that the high potential temperatures is a consequence of overshooting convective turrets that penetrate the existing tropopause and entrain stratospheric air with high potential temperature [e.g., *Danielsen*, 1982, 1993; *Selkirk*, 1993].

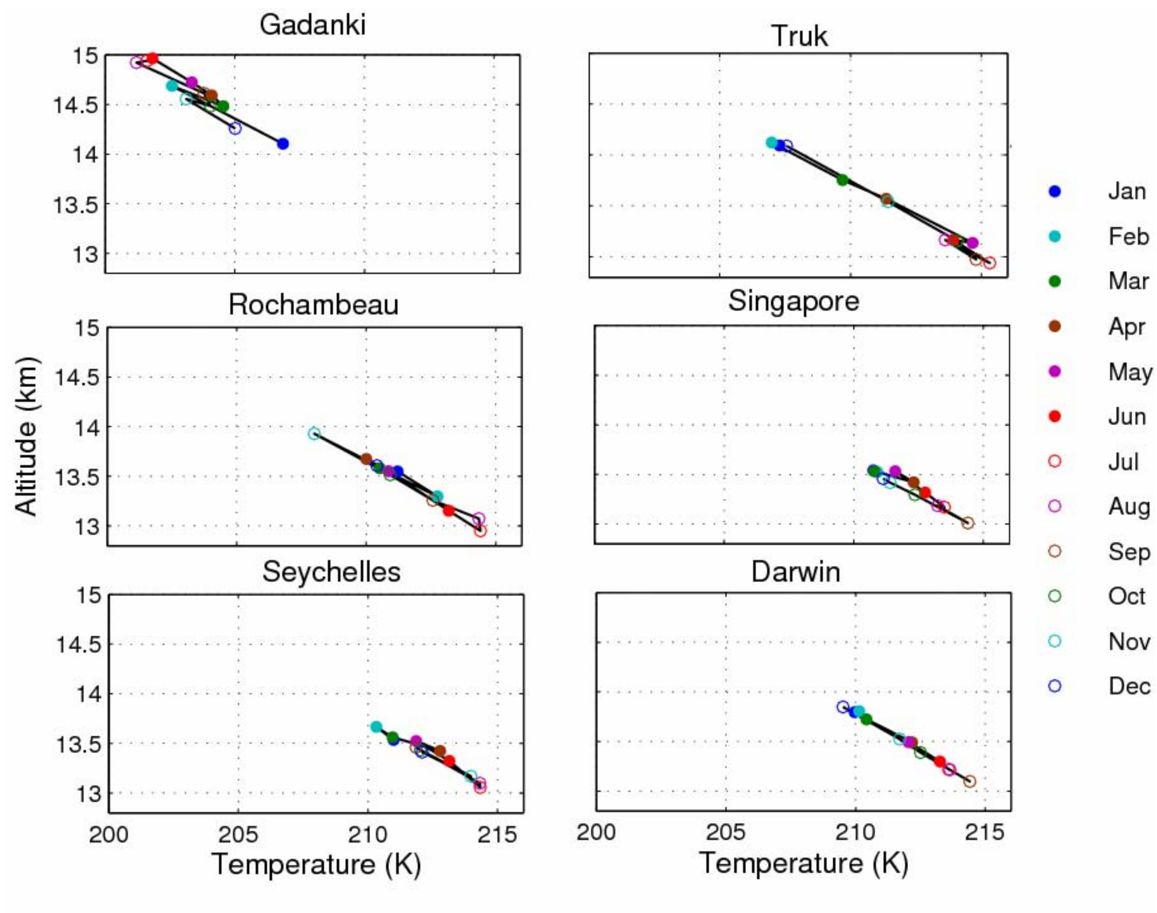

Figure 5.10: *Same as Figure 5.8 but observed for COT.*

Figure 5.9 shows that at the Pacific stations Truk and Singapore the values of θ_{CPT} in Pacific basin are quite close to $\theta_{E.}$ In particular at Truk, the two are nearly equal from June to December. At the slightly higher latitude Pacific station the two are equal during the winter. However, there is a marked difference between the two during the rest of the year. At the non-Pacific stations Seychelles and Rochambeau the difference between $\theta_{E,}$ and θ_{CPT} is in the range 6-18 K and is more than that at the Pacific stations Truk and Singapore. At Gadanki except in May and June, $\theta_{E,}$ and θ_{CPT} differ greatly. The value of

θ_{COT} is ~ 350 K (vary in the range 347 K-353 K) and is always lower than the values of θ_E and have very less seasonal amplitude for the stations Truk, Rochambeau, Singapore and Seychelles. The stations Gadanki and Darwin show large seasonal variation of θ_E in comparison to the θ_{COT}. Therefore, θ_{COT} is higher during all the months except March - June over Gadanki and during June-August over Darwin. Since θ_{COT} is more or less constant, for convective tropopause linear relationship (with more than one locus) between Z_{COT} and T_{COT} can be expected which is shown in Figure 5.10.

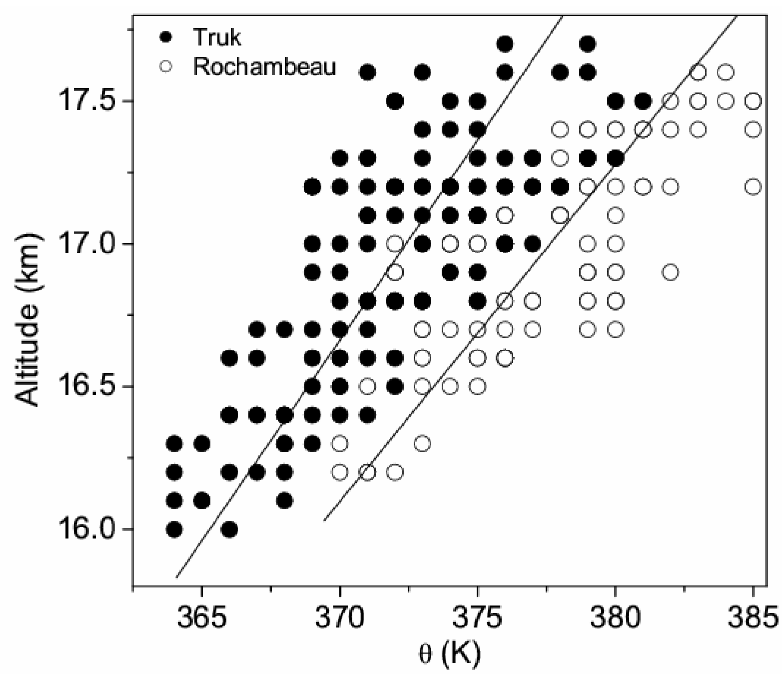

Figure 5.11: *Mass plot of monthly mean of tropopause altitudes and potential temperatures at Rochambeau and Truk. Lines represent the least square fits to the data from individual stations.*

From Figure 5.3- 5.10, it is clear that the tropopause properties are different at different stations, showing strong longitudinal differences. *Gage and Reid*, [1987] argued that tropopause temperature will be warmer close to and far from away centre of active convection. A comparison of Z_{CPT} and θ_{CPT} over Truk (in the convectively active region throughout year) with Z_{CPT} and θ_{CPT} over Rochambeau (not active throughout year) is shown in Figure 5.11. The figure contains the mass plot of the monthly mean potential temperatures and altitudes of CPT over Rochambeau and Truk. The θ_{CPT} at Rochambeau is systematically greater than that at Truk, although CPT covers roughly same range of altitudes.

5.3.4. Longitudinal Variation of the Altitudes and Temperatures of Tropical Tropopause Parameters.

Figure 5.12 shows the mean of the CPT, COT and TTLt for different seasons using COSMIC GPS RO measurements. The strong longitudinal (zonal) structure can be observed for all the parameters which are closely associated with variation of the OLR. Each parameter for different latitude bands of ±10^o, ±20^o, and ±30^o are obtained for the sake of distinguishing the longitudinal features, if any. In general, all parameters show similar behavior for all the bands. The Z_{CPT} varies between 16.6 km -17.8 km, and in general CPT is higher during December- May while lower during June-November as shown in Figure 5.12(a). Though the amplitude of the Z_{CPT} is very less ~ 0.4-0.5 km, the different longitudinal features in different season can be discerned. There are regions of maxima of Z_{CPT} in the center of longitude band ~120W-30W, ~30E-120E, ~30E-90E and 0-60E during DJF, MAM, JJA and SON, respectively, while of regions of minima of Z_{CPT} is over pacific ocean through out the season. The sharp fall of ~ 0.4 km of Z_{CPT} for the latitude band ±10^o can be noticed at ~ 60^{o}E during JJA. The T_{CPT} varies between 188 K- 198 K and shows different features during different seasons and CPT is in general warmer during June-November and Cooler during December-May, as shown in Figure 5.12 (b). There are two peaks at ~120^{o}W and ~30^{o}W clearly observed and a minimum at ~ 90^{o}W besides minima over Pacific region during DJF. During MAM, similar peaks as observed during DJF can be noticed but at ~ 150^{o}W instead of 120^{o}W and another peak ~ 60^{o}W is with decreased strength. During JJA, sudden fall of ~ 2 K in T_{CPT} is observed at ~ 60^{o}E especially for latitude band ±10^o which is associated with a fall of ~ 0.4 km in Z_{CPT}. The longitudinal structure of the T_{CPT} during SON is similar as observed during DJF. It is seen that in general the tropopause is cooler in the eastern hemisphere compared to western hemisphere except during summer at the eastern longitudes 120 ^{o}E - 180^{o}E. The Z_{COT} varies between 12.5 km-14.5 km, and in general COT is slightly higher during December- May than during June-November as shown in Figure 5.12(c).

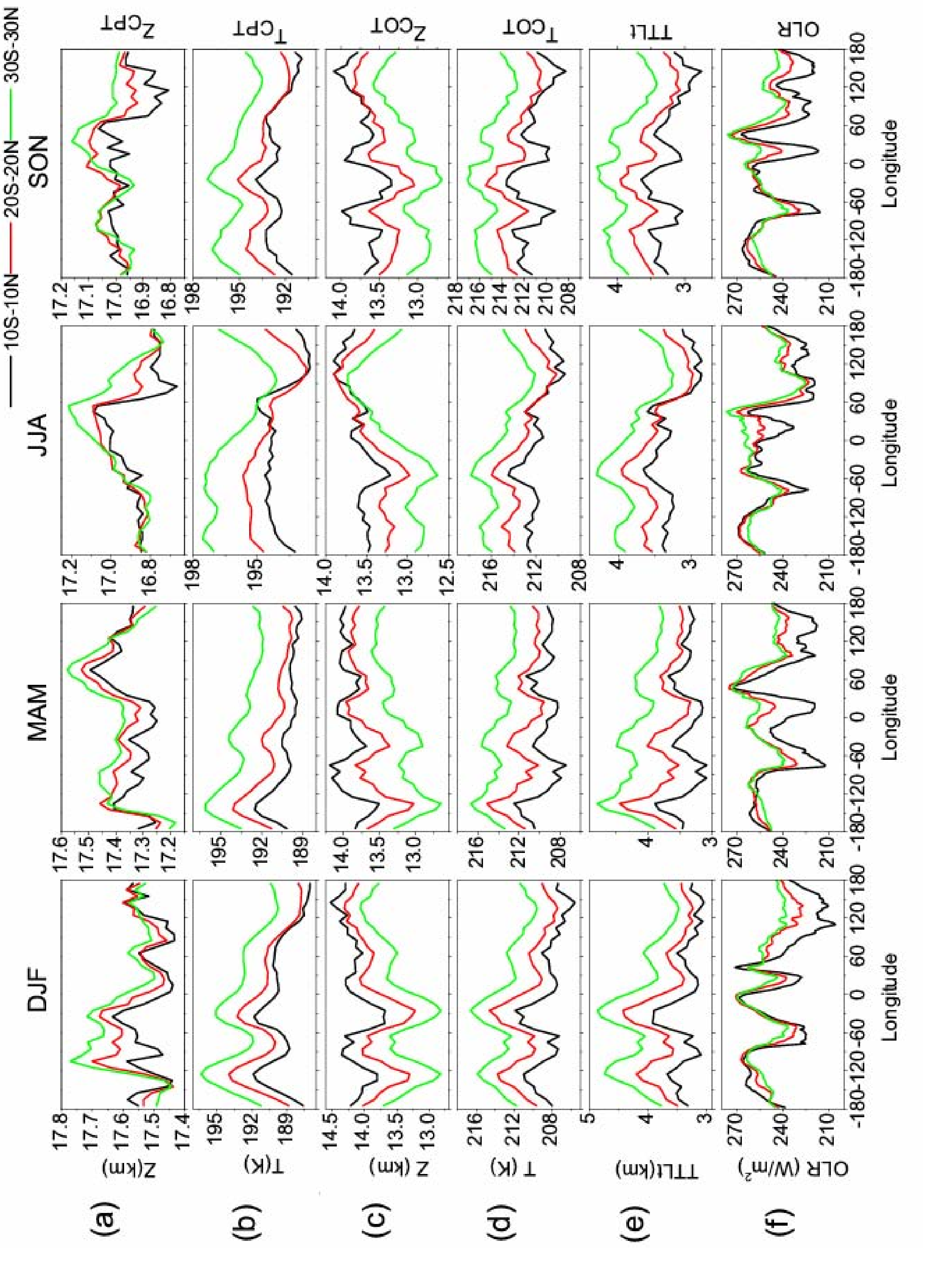

Figure 5.12: *Longitudinal variation of (a)* Z_{CPT} *(b)* T_{CPT} *(c)* Z_{COT} *(d)* T_{COT} *(e)* TTLt *and (f)* OLR *observed using COSMIC measurements during August 2006-2008.*

High values of Z_{COT} can be noticed at ~60^{o}E during JJA. The longitudinal feature of the Z_{COT} is consistently similar as T_{CPT} but in out of phase. The T_{COT} varies between 205 K- 216 K and shows different features during different seasons, and COT in general is slightly warmer during June-November than during December-May, as shown in Figure 5.12 (d). The longitudinal features of T_{COT} are consistently similar to Z_{COT} but out of phase. Figure 5.12 (e) shows the variation of TTLt between ~ 3-5 K having slightly lower value during JJA than during DJF and shows in phase variation as T_{CPT} and T_{COT}. There are three centers of convective activity, western pacific (120^{o}E-180^{o}E), South African continent (0-60^{o}E) and South American continent (60^{o}W-120^{o}W) as seen from Figure 5.12 (e) with lowest OLR values with north south migration. During JJA another centre of convection develops over Indian Ocean (60^{o}E-120^{o}E) due to the influence of the southwest monsoon. From Figure 5.12, it is clear that the distribution of the convective activity has major control on the longitudinal variability of the tropopause parameters.

5.4. Summary

This study has addressed the longitudinal characteristics of the tropical tropopause parameters over different stations Although, seasonal variability of the CPT shows coherent structure throughout the tropics, the amplitude (excursion) of T_{CPT} is less and CPT altitude is highest over Gadanki when compared to the rest of the stations. The tropopause at the Pacific stations (Truk, Singapore and Darwin) is comparatively cooler (by 2-4 K) than that over the Non-Pacific stations (Gadanki, Rochambeau and Seychelles). The seasonal differences of the COT and TTLt are not as marked as CPT. T_{CPT} goes below 191 K more frequently during DJF than during JJA suggesting entry of water vapor at less than 3 ppmv occurs more frequently during DJF all the stations. The seasonal behavior of T_{CPT} anomalies show characteristics as lower stratospheric temperature anomalies suggesting the dominance of the radiative processes than convective processes in seasonal variability of the CPT. The temperature anomalies in the upper troposphere (UT) are more or less in out of phase of temperature anomalies in lower stratosphere (LS) except at Gadanki. Between upper troposphere and lower stratosphere there is a transition region where temperature anomalies distinguish the characteristics of UT and LS. The temperature anomalies at the transition layer seem to be influenced by the characteristics of UT and LS. This transition layer indicates the region up to where the influences of stratosphere can be felt. The depth of penetration of stratospheric effect is more for the stations near the equator than the stations away. The correlation analysis of temperature at 18 km with temperatures in the different altitudes of UTLS region show unexpected positive (low) correlation for Gadanki. The lapse rate behavior between altitude (15 km) and Z_{CPT} show quit distinct characteristics among the stations. The low value of the lapse rate (~2 K/km) between 15 km and CPT over Gadanki during DJF is quite interesting. Since Z_{CPT} and T_{CPT} shows strong seasonal variation, however, the relation between Z_{CPT} and T_{CPT} is not simple linear one. The anomalous departures between Z_{CPT} and T_{CPT} show association with changes in the θ_{CPT} which indicates the influence of diabatic heating, especially, during May -June. The θ_{CPT} and θ_E for Truk and Singapore are nearly equal, which suggest boundary layer moisture flux is carried to the higher altitude near to CPT. θ_{COT} is lower than θ_E and constant throughout the year. The potential temperature of the tropopause away from the convective centers increases. The tropopause parameters are observed to be accompanied with zonally non uniform convection.

In previous Chapters, the tropical tropopause is considered as well defined. However, many times, temperature profile shows similar inflections below and above the cold point tropopause. The vertical structure of the tropopause is extensively studied in the Chapter 6.

---END--

Chapter 6

Characteristics of Multiple Tropopauses in the Tropics

6.1. Introduction

The tropopause separates troposphere and stratosphere which are very distinct in their physical, chemical and thermal properties and marks transition between contrasting characteristics such as vertical mixing time scales, static stabilities and radiative-convective equilibrium. These contrasting phenomena which vary in space and time scales make the tropopause a key feature of atmospheric structure in both the mid-latitudes [*Hoskins et al.*, 1985] and the tropics [*Reid and Gage.,* 1996]. It is extremely sensitive to changes in the thermal, dynamic, and chemical structure of troposphere and stratosphere [*Highwood and Hoskins*., 1998; *Hoinka.*, 1998; *Seidel et al.*, 2001]. Knowledge of the tropopause structure and its variability is very important to quantify the stratosphere-troposphere exchange (STE) processes [e.g. *Holton et al*., 1995; *Shepherd*, 2002; *Stohl et al.,* 2003]. Low frequency variations of the tropopause are closely coupled to stratospheric ozone changes [*WMO*, 2003]. Recently *Sausen and Santer* [2003] and *Santer et al*. [2003a, b] have suggested that changes in the altitude of the tropopause may be a sensitive indicator of anthropogenic climate change. Further, with regard to the climate change there are many interesting science questions listed by SPARC (Stratospheric Processes and their Role in Climate) community. One of these is how are double or multiple tropopauses that commonly appear in tropical radiosonde profiles, to be interpreted?

The topical tropopause structure is found to be modulated by different waves starting from short period gravity waves to planetary scale waves [*Tsuda et al.,* 1994; *Krishna Murthy et al.,* 2002; *Ratnam et al.,* 2006]. Structures in the tropopause region are sometimes recognized as stable layers and are named as multiple tropopauses. *Schmauss* [1909] was the first to note the occurrence of multiple tropopauses. Later, *Bjerknes* and *Palmen* [1937] investigated this kind of structure, which they named ‘the sub-stratosphere’.

For identifying the tropopause, different definitions and concepts exist based on the dynamic, thermal, and chemical properties of the atmosphere [e.g. *Pan et al.,* 2004; *Narayana Rao et al.,* 2007] each of it appropriate for a given band of latitude. For example, in the tropics the simple temperature minimum (or “cold point”, in the terminology of *Selkirk* [1993]) distinctly marks the tropopause where as the tropopause at mid-latitudes can be defined by more general stability criteria, quantified by potential vorticity (PV) [*Hoerling et al*., 1991]. These definitions are only to detect single tropopause but not multiple tropopauses.

World Meteorological Organization (WMO) in 1957 has provided criteria for identifying multiple tropopauses based on lapse rate and it is the only means available till now to detect multiple tropopauses. Using these criteria and realizing the importance of the tropopause structure, global occurrence of the multiple tropopauses (MTs) has been studied by many investigators using Global Positioning System (GPS) radio occultation measurements [*Schmidt et al*. 2006], Integrated Global Radiosonde Archive (IGRA) data (Añel *et al*., 2007; 2008), radiosonde and reanalysis data sets [*Randel et al*. 2007]. These studies have reported only a few occurrences of MTs over tropical latitudes. As mentioned earlier, in the tropics the cold point is well marked in the temperature profile and is more meaningful and relevant for transport of minor species especially water vapor and for STE processes [*Selkirk*, 1993] than the lapse rate tropopause which is based on stability criterion serving the purpose of operational use and has limited physical relevance [*Highwood and Hoskins*, 1998]. In view of the importance of cold point tropopause (CPT) in STE processes, in this chapter an alternate criterion to identify MTs based on cold point and other minima in the temperature profile is evolved and studied the characteristics of MTs in the tropics.

6.2. Data Base and Analysis Procedure

6.2.1 Radiosonde Data

The radiosonde data obtained at both 00 and 12 UTC for the 10 year period (1999-2008) from the website http://weather.uwyo.edu/upperair/sounding.html for five stations (Truk, Rochambeau, Singapore, Seychelles and Darwin) distributed across the globe within ±15^{o} latitude from equator are used in the present study. The detail about radiosonde is given in Chapter 2. Sometimes radiosondes are launched at slightly different times and data of the sonde launches between 09 UTC (21 UTC) to 15 UTC (03UTC) are grouped in 12 (00) UTC. Quality checks are then applied to remove outliers arising due to various reasons following *Tsuda et al*.,[2006] to ensure high quality in the data which otherwise contaminate the results.

In order to fix the altitude range to be considered for identification of MTs in the tropical region, first of all the altitude range of the variation of the cold point and lapse rate tropopause is examined. The cold point tropopause (CPT) altitude and lapse rate tropopause (as per the definition of WMO) altitude are obtained from individual temperature profiles at Singapore, a tropical station. The time series of CPT and lapse rate tropopause (LRT) altitude at Singapore are shown in Figure 6.1. From Figure 6.1 it is clear that CPT and LRT altitudes show large day-to-day variation between the altitude range 15 km and 19 km (~135-65 hPa) and 14.5 km and 18.5 km (~145-70 hPa), respectively. *Schmidt et al*. [2006] for the study of MTs determined the lapse rate tropopauses using WMO definition from CHAMP/SAC-C temperature profiles in the altitude region corresponding to pressure levels 500-70 hPa (~ 6-18 km) and used this range for identifying the MTs globally. While this range covers adequately the polar and mid-latitude tropopauses as their mean altitudes are 8 km and 12 km, respectively, it may not be adequate for the tropical location as the tropopause altitude may exceed 18 km (as seen in Figures 6.1).

If tropopause occurs above 18 km in the tropical region the occurrence estimates of MTs reported by *Schmidt et al.* [2006] could be underestimates. Another study by *Anel et al.* [2008] used the range 500-50 hPa (6-20 km) and presented the global MT occurrence using IGRA (Integrated Global Radiosonde Archive) data sets. The upper limit of 50 hPa used was based on the fact that it corresponds to typical pressure value for the triple tropopause as obtained by *Anel et al.* [2007]. However, the lower limit of 500 hPa used by *Anel et al* [2008] may contaminate the results with some unreal tropopauses. It is now widely accepted that it is physically more meaningful to consider the tropical tropopause as a layer (Tropical Tropopause Layer, TTL) than as a well defined level. *Fueglistaler et al.*, [2009] considered the region between the pressure levels 150 hPa and 70 hPa as the TTL. Taking into account all the above, the region between the pressure levels ~150 hPa and ~50 hPa (~14-20.5 km) is considered to study for the occurrence of MTs in the tropical region. The number of soundings reaching the pressure levels 500 hPa, 150 hPa, 70 hPa and 50 hPa along with those reaching the CPT levels for the five stations are calculated which is listed in Table 6.1. The total number of soundings possible in the period under consideration is 7306. The number of soundings reaching to

50 hPa is ~ 80-90 % for all the stations except for Seychelles (78%) which had major data gaps during October and November 2000, November and December 2002 and September 2008. In this study, all those soundings which reached at least up to 50 hPa level are considered for identification of MTs.

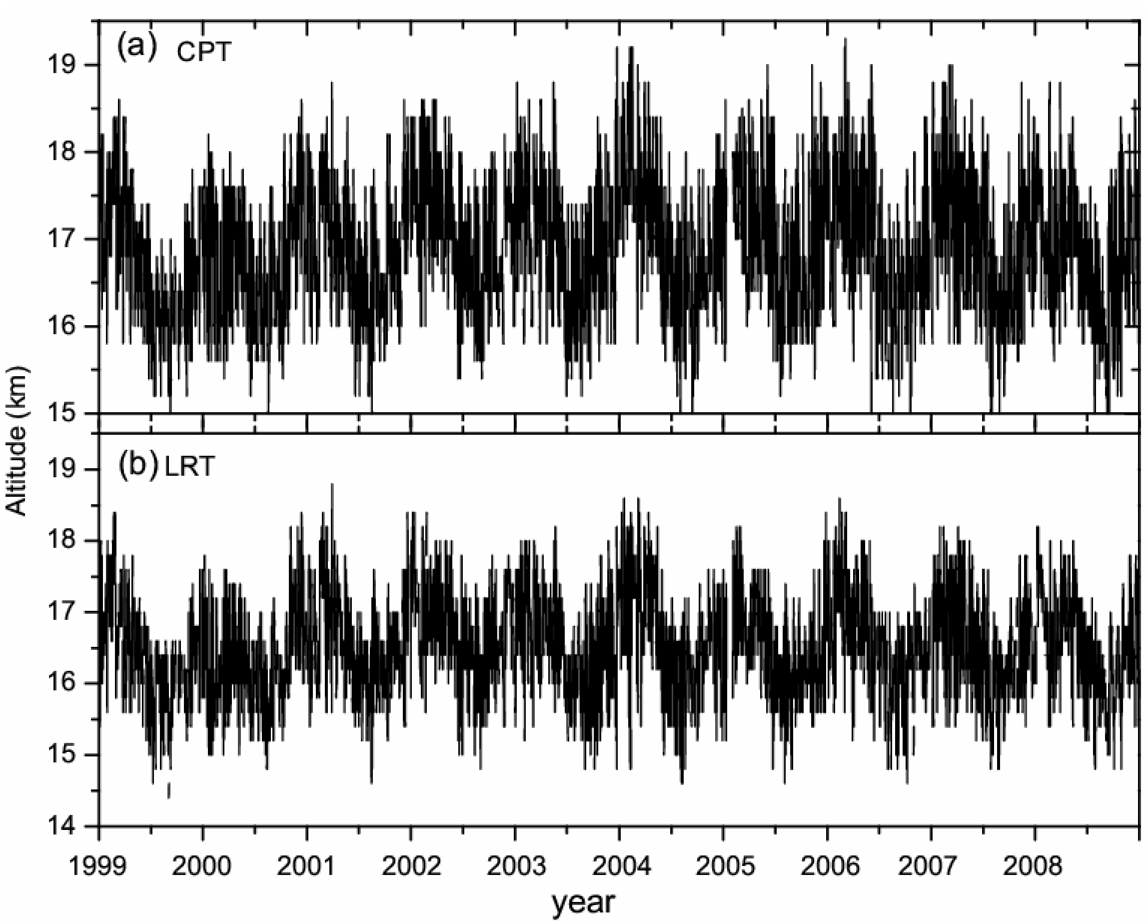

Figure 6.1. *Time series of (a) cold point tropopause (CPT) altitude and (b) lapse rate tropopause (LRT) altitude observed over Singapore during 1999 to 2008. Both the launches at 00UTC and 12UTC are considered.*

The vertical resolution of radiosonde data is not the same throughout the altitude range and varies from station to station. The number of levels reported between 150 hPa and 50 hPa for which data are available are given in supplementary Figure S6.1. The number of levels between 150 hPa and 50 hPa for which data are available ranges from ~10-20 for Truk and Rochambeau and ~10-30 for Singapore and Darwin. For Seychelles the data availability is for ~20-30 levels for years 1999-2005 and for ~10-40 levels for the years 2006-2008. Further, the statistical quantification of the number of data levels available between 150-50 hPa levels is shown in Table 6.1. It can be seen that ~95% of data have more than 10 to 30 data levels between 150 hPa and 50 hPa providing altitude resolution of ~0.6-0.2 km. Note that this is the overall altitude resolution between 150-50 hPa.

However, the data levels are more clustered near the peaks in temperature which can give finer resolution. Therefore for further analysis each individual sounding temperature profile is adjusted to 200m grid by linear fitting. The 200 m gridded and original profiles are compared as shown in supplementary Figure S6.2 (a). It is seen that both original and gridded profiles represent nearly the same vertical structure. Further, it is also checked whether gridded has modified the temperature profile, especially the peaks. The CPT temperature, pressure and altitude from original and gridded profiles for Singapore for January 1999 are also compared (shown in supplementary Figure S6.2(b)) and found that 200 m grided data does not alter in any significant manner the profile and thus can be taken as quite suitable to study the MTs. The r.m.s. (root mean square) difference between the two in pressure, temperature and altitude of CPT are 3.71 hPa, 0.46 K, and 0.21 km, respectively.

6.2.2. COSMIC Global Positioning System (GPS) Radio Occultation (RO) Data

Six COSMIC GPS-RO satellites were launched in April 2006, providing about 2000 occultation events per day around the globe [*Anthes et al.*, 2008]. The GPS RO techniques are explained in Chapter 2. The high-vertical resolution and high accuracy COSMIC dry temperature measurements available during August 2006 to August 2008 processed by Taiwan Analysis Center for COSMIC(TAAC) data center, Taiwan, are also used to study the multiple tropopause characteristics over tropical latitudes. By employing the GPS RO technique, COSMIC provides temperature and water vapor profiles (1D-var retrieval) in the troposphere and lower stratosphere. The accuracy of the COSMIC refractivity is <0.2% between 10 and 20 km, degrading to 0.7% at 30 km [*Schreiner et al*., 2007]. The accuracy of the COSMIC derived temperature is better than 0.5 K. GPS-RO errors, optimization and quality control procedures are detailed by *Kursinski et al*. [1997], *Kuo et al*. [2004] and *Lohmann* [2007]. The vertical resolutions of

GPS RO retrievals can approach to 100 m, but the data used here are sampled on a 200 m grid [*Randel et al.*, 2007]. The typical absolute difference of the latitude and longitude between pressure levels 150hPa to 50 hPa is obtained for GPS radiosonde over Gadanki and COSMIC GPS RO for the whole tropical belt ±30^o (shown in supplementary Figure S6.3). The horizontal resolution of the radiosonde temperature between pressure levels 150hPa to 50 hPa in terms of latitude and longitude is less than 0.1^o. The maximum horizontal resolution of the temperature profile in altitude range of the 14-20.5 km (150-50 hPa) is observed to be ~0.25^o-0.25^o longitude latitude.

Table 6.1. *Data availability (in percentage) at different stations at different pressure levels, 500 hPa, 150 hPa, CPT level, 70 hPa and 50 hPa normalized to total number of observations for 10 year period (1999-2008). Star indicates the major data gaps which is discussed in the text. Reported data levels available (in percentage) in the range ≥5 – 10, ≥10 – 20, ≥20 – 30 and ≥30- 40 between 150-50 hPa at the five stations are also shown.*

Stations	% of data available up to different pressure levels					% of data level between150-50 hPa					No. of observations
	500 hPa	150 hPa	CPT	70 hPa	50 hPa	≥5 - 10	≥10 - 20	≥20 - 30	≥30- 40	≥5 - 10	
Truk (7.44^{o}N,151.83^{o}E)	99	96	95	92	88	3	82	13	0	3	6985
Rochambeau (4.83^{o}N, 2.36^{o}W)	99	98	98	91	88	4	75	19	0	4	6837
Singapore (1.03^{o}N,103.87^{o}E)	100	99	99	94	91	1	9	64	23	1	6960
Seychelles (4.66^{o}S,55.53^{o}E)	99	96	96	88	78	5	24	40	20	5	5838*
Darwin (12.41^{o}S, 130.88^{o}E)	100	98	97	88	83	5	27	55	8.2	5	6964

There is a possibility that horizontal resolution may affect the multiple tropopause structure, which is checked by assuming the same temperature gradients in the horizontal as observed in the vertical (between the two tropopauses). Taking the horizontal resolution of GPS RO data into consideration, this type of temperature gradient in horizontal translates to an abnormal horizontal wind of the order of 60m/s and more for Gadanki latitude (from thermal wind considerations). So, horizontal resolution of GPS (and radiosonde data) will not be affecting the MT definition in any significant manner.

6.2.3. Methodology for Identifying the MTs

The tropical tropopause and multiple tropopauses are identified using the WMO criteria based on lapse rate [*WMO.,* 1957] i.e., "(a) The first tropopause is defined as the lowest level at which the lapse rate decreases to 2 K/km or less, provided also the average lapse rate between this level and all higher levels within 2 km does not exceed 2 K/km. (b) If above the first tropopause the average lapse rate between any level and all higher levels within 1 km exceeds 3 K/km then a second (double) tropopause is defined by the same criterion as under (a)". (c) Similar criterion applies if there is third (triple) tropopause above. Typical temperature profiles showing vertical structures observed at Singapore are shown in Figure 6.2. Using WMO criteria the first tropopause (which is refereed to as lapse rate tropopause, LRT), double tropopause and triple tropopause are identified and are shown in Figure 6.2. Note that the MTs (such as double and triple) are easily identified by WMO criteria in the profiles shown in the first column panels. In the second column panels showing the profiles as in the first column panels, WMO criteria are unable to identify the MTs even though the vertical structures are clearly observable in the respective temperature profiles. The lapse rate profiles corresponding to the temperature profiles in the first and second column panels are shown in the third and fourth panels, respectively. The first column panels cases show where all tropopauses are clearly identified by WMO criteria while in the second column panels shown the cases in which all the tropopauses could not be identified by the WMO criteria. This shows that some times the WMO criteria fail to identify all the multiple tropopauses from the temperature profile. In fact MTs identification depends on the value of the threshold lapse rate criterion chosen above LRT (3K/km in WMO definition).

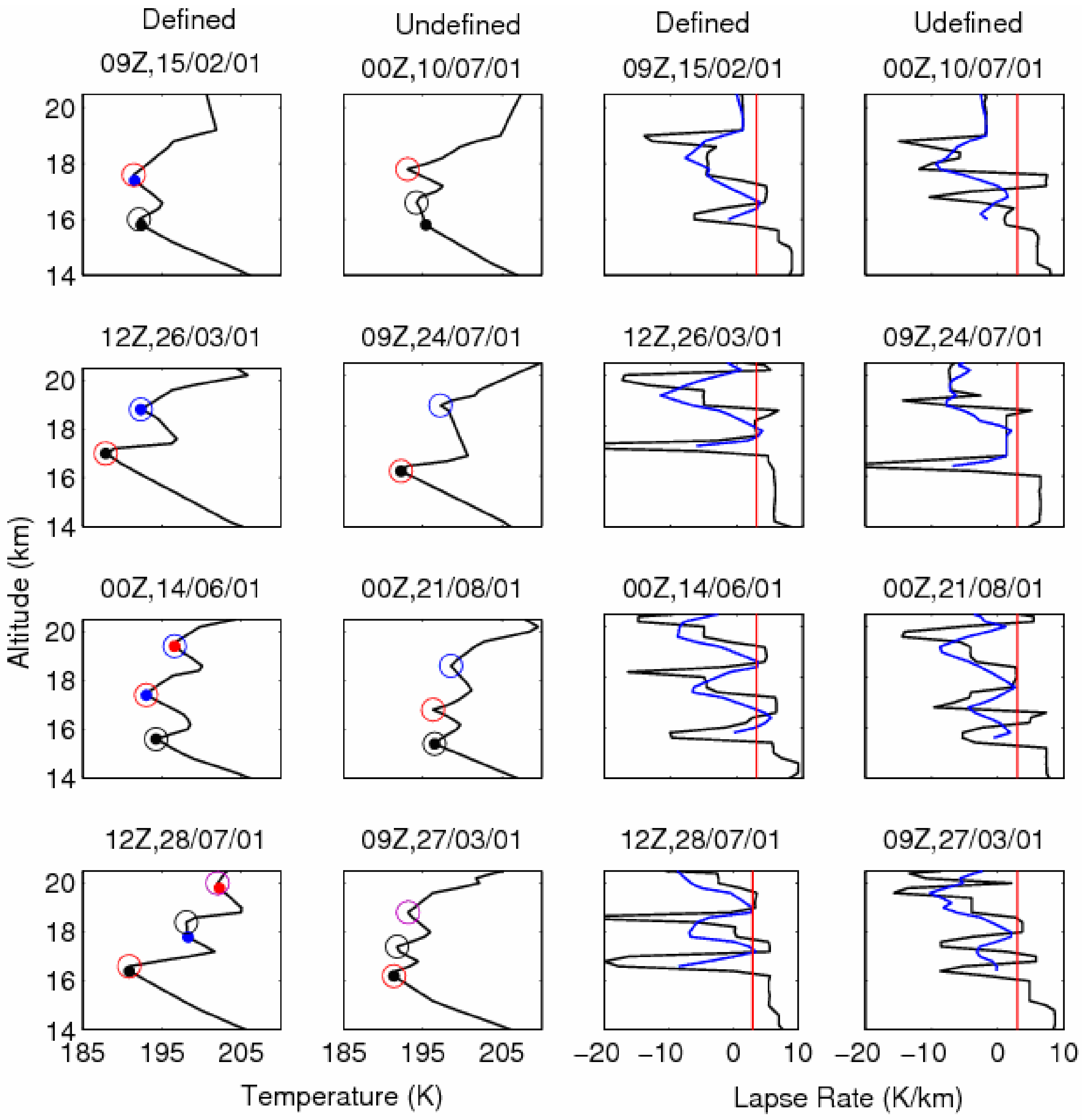

Figure 6.2: *Typical temperature profiles showing various multiple tropopause structures placed under defined (undefined) when double and triple tropopause are identified (not identified) by WMO criteria. Lapse rate tropopause (LRT), double tropopause and triple tropopause are denoted by black, blue and red dot, respectively. Circles denote tropopauses identified by the present method. Black, Red, blue and magenta circles denote the LT, CPT, ST and TT, respectively. Lapse rate profiles (black lines) corresponding to the temperature profiles in the first column panels and the second column panels are shown in third and forth column, respectively. Blue lines above the LRT altitude in the third and fourth column panels represent the five point running means of the lapse rate profiles. Red line in the third and fourth column represents lapse rate equal to 3 K/km.*

However, by changing the threshold to a lower value, more MTs can be identified. This exercise has been carried out by *Randel et al* [2007], using GPS RO data. They found that the occurrence maximum in northern hemisphere (NH) winter over North America (60%) increases to 80% if 2K/km threshold is used and decreases to ~ 30 % if a 4K/km is used. However, the spatial patterns remain unchanged. Further *Randel et al* [2007] argued that the specific percentage values for MTs will be less important than identification of some tropospheric- like stability above LRT.

In view of the above, instead of using WMO criteria an alternate criteria based on CPT is evolved. Note that the CPT is a physically meaningful and relevant parameter for transport of water vapor and STE processes [*Selkirk*, 1993]. On the other hand, the LRT serves mainly operational purposes and has limited physical significance [*Highwood and Hoskins*, 1998). Thus, MTs identified on the basis of CPT rather than the LRT would be more relevant and physically more meaningful. On examination of a number of temperature profiles at the tropical stations mentioned in Table 6.1, the following criteria/steps is evolved for identifying multiple tropopauses within the tropics where CPT is well defined, in general.

1. CPT (and corresponding altitude and temperature) is identified from the temperature profile.
2. All points of inflections are identified in the temperature profiles within 3 km of CPT with the criterion that absolute difference (ΔT) between T_{min} and T_{max} (where T_{min} and T_{max} are the temperatures at the minimum and maximum of points of inflections, respectively) is ≥ 1 K (amounting to ≥ twice the accuracy of measurements) and absolute difference in their altitudes (ΔZ) should be ≥ 0.4 km (amounting to ≥ twice the vertical resolution).

That is, all points of inflections are identified in the temperature profiles in the altitude range within 3 km of CPT subject to condition that if

$$\Delta T \geq 1\text{K, where, } \Delta T = |T_{max} - T_{min}|$$

$$\Delta Z \geq 0.4\text{ km, where, } \Delta Z = |Z_{max} - Z_{min}|.$$

Where T_{min} and T_{max} are the temperatures at the minimum and maximum of points of inflections, respectively, and Z_{min} and Z_{max} are the altitudes corresponding to the T_{min} and T_{max}, respectively.

The choice of optimum value of the ΔZ and ΔT is based on distribution of the ΔT for ΔZ =0.4 km which is shown in Figure 6.3. The ΔT distribution for ΔZ = 0.2 km – 1.6 km is calculated in the altitude range of 14 km -20.5 km which is shown in Figure 6.3(a). The maximum in ΔT for ΔZ = 0.2 km occurs in the range 0-0.5 K and for ΔZ = 0.4 km in the range 1-1.5 K. The distribution of ΔT gets broadened for ΔZ = 0.6 ,0.8, 1.0 and 1.2 km centered at ~ 2 K, 3 K, 3 K and 4 K, respectively. For ΔZ ≥1.4 km, the distribution of the ΔT is very broad with no clear peak. Since the vertical resolution of the data is 0.2 km and the temperature accuracy is ~ 0.5 K, thus, ΔZ ≥ 0.4 km and ΔT ≥ 1 K for identifying the point of inflections is only considered although the distribution for ΔZ = 0.2 km (Figure 6.3a) shows a peak at ΔT = 0.5 K. $\Delta T/\Delta Z$ is further calculated for ΔZ ≥ 0.4 and ΔT ≥ 1K whose distribution is shown in Figure 6.3(b). From the Figure it is clear that the maximum of the distribution lies between 2.5 -5.0 K/km. Most of the values of $\Delta T/\Delta Z$ are greater than 2.5 K/km. Occurrences of $\Delta T/\Delta Z < 2.5$ K/km are relatively few.

Now the rationale for choosing the region of ± 3 km of CPT for identifying the MTs is elaborated here. As mentioned above, it is now well recognized that it is physically more meaningful to consider tropical tropopause as a region/layer (TTL) rather than as a single sharp surface. *Fueglistaler et al.*, [2009] observed that this layer could lie between the pressure surfaces ~150-70 hPa which is nearly the same as the range of variability of the CPT as shown in Figure 6.1.This layer which is influenced by tropospheric processes may further extend to a few km above CPT. Thus the region between pressure levels 150 -50 hPa for identifying the MTs is considered in this study. The thickness between these two pressure surfaces translates to approximately 6 km. So, a region of CPT ± 3 km giving a width of 6 km considering the uncertainties in defining the width of TTL is considered, for identifying the MTs in the present study.

3. The minima thus identified are taken as MTs. The one occurring below CPT is designated as lower tropopause (LT) and those occurring above as second tropopause (ST) and third tropopause (TT) starting with CPT as the first tropopause.

Generally, it is found that at the most only one point of inflection occurs below CPT satisfying the above criteria.

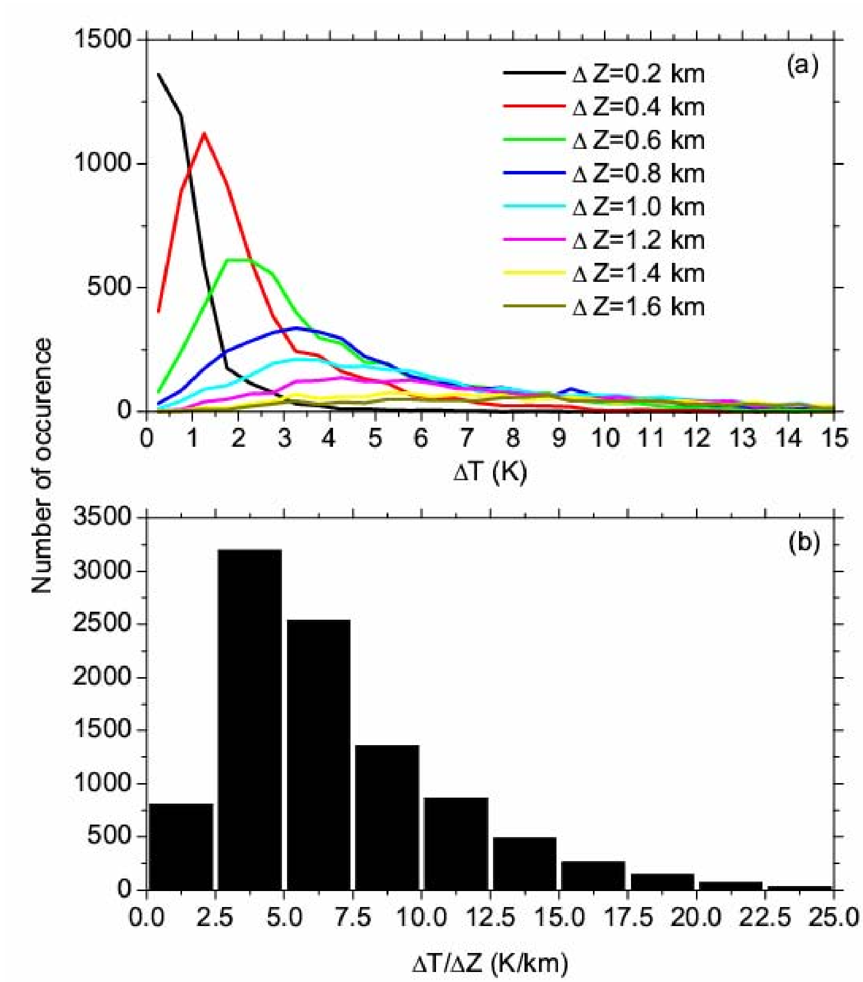

***Figure 6.3**. Distribution of (a) ΔT for different ΔZ values considering all the point of inflections, (b) $\Delta T/\Delta Z$ calculated for only those points of inflections that satisfy the criteria of $\Delta Z \geq 0.4$ and $\Delta T \geq 1K$ in the altitude interval 14 km – 20.5 km observed over Singapore.*

The altitude is restricted to 3 km above CPT for identification of the MTs. In many of the earlier studies on MTs using WMO criteria the region between 150 and 50 hPa is considered. To facilitate meaningful comparison with earlier studies, the same region is adopted for present study. However, a test has been also made to check the effect of increasing the boundary up to 30 km and the occurrence of MTs using WMO and present criteria (shown in Supplementary Figure S6.4). It is found that this increase in the upper boundary results in an increase of overall percentage of MTs by both the criteria. Nevertheless, the nature of monthly variations of MTs occurrence remains the same as per the range CPT+3 km.

As mentioned above the absolute values of the lapse rates considering the points of inflection between MTs using the present method, in general, are ≥ 2.5 K/km. Based on the above mentioned criteria MTs could be identified for all the different cases as shown in Figure 6.2. This method is adopted for identification of the MTs and to study their characteristics using the ten year period (1999-2008) radiosonde data of the five stations. Further, for covering the tropical region globally this study is extended to the whole tropical belt (± 30^{o}) using COSMIC GPS RO data for a period of two years (August 2006-August 2008).

6.3. Results

6.3.1. Occurrences of MTs in Tropics

Using the present method of MT occurrence the monthly percentage of occurrences of LT, ST and TT is obtained. The monthly percentages of occurrences are estimated by considering all the temperature profiles in the respective months. CPT could be identified in all the profiles without any exception. However, in some profiles out of the total, LRT could not be identified as shown in Figure 6.4 right hand side panel. Figure 6.4 shows monthly variation of percentage occurrence of the LT, ST and TT of the MTs obtained using the 10 year period (1999-2008) radiosonde observations at all the five stations. The total percentage occurrence of at least one additional tropopause (refereed to as total MT percentage occurrence hereafter) is also estimated and is shown in Figure 6.4. For comparison, monthly percentage of occurrences of double and triple tropopauses using WMO criteria are estimated considering only the profiles for which LRT could be identified and are shown in the figure. Note that the total percentage occurrence using WMO criteria is same as double tropopause percentage occurrence. It is clear that percentage occurrence of MTs using the present method varies from ~25 %(at the higher latitude station within tropics, Darwin) to ~60% (at the lower latitude station within tropics, Singapore). In contrast, the percentage occurrence of MTs using WMO criteria varies from 10% at Darwin to ~30% at Singapore. Note that earlier reports have shown smaller percentage (5-20%) of occurrence of MTs in the tropical latitudes using IGRA data set [*Añel et al.*, 2007] and GPS RO observations [*Schmidt et al.*, 2006] with WMO criteria. However, regardless of the values of the percentage occurrence, both present method and WMO criteria give the same type of variation for the occurrence of MTs with latitude.

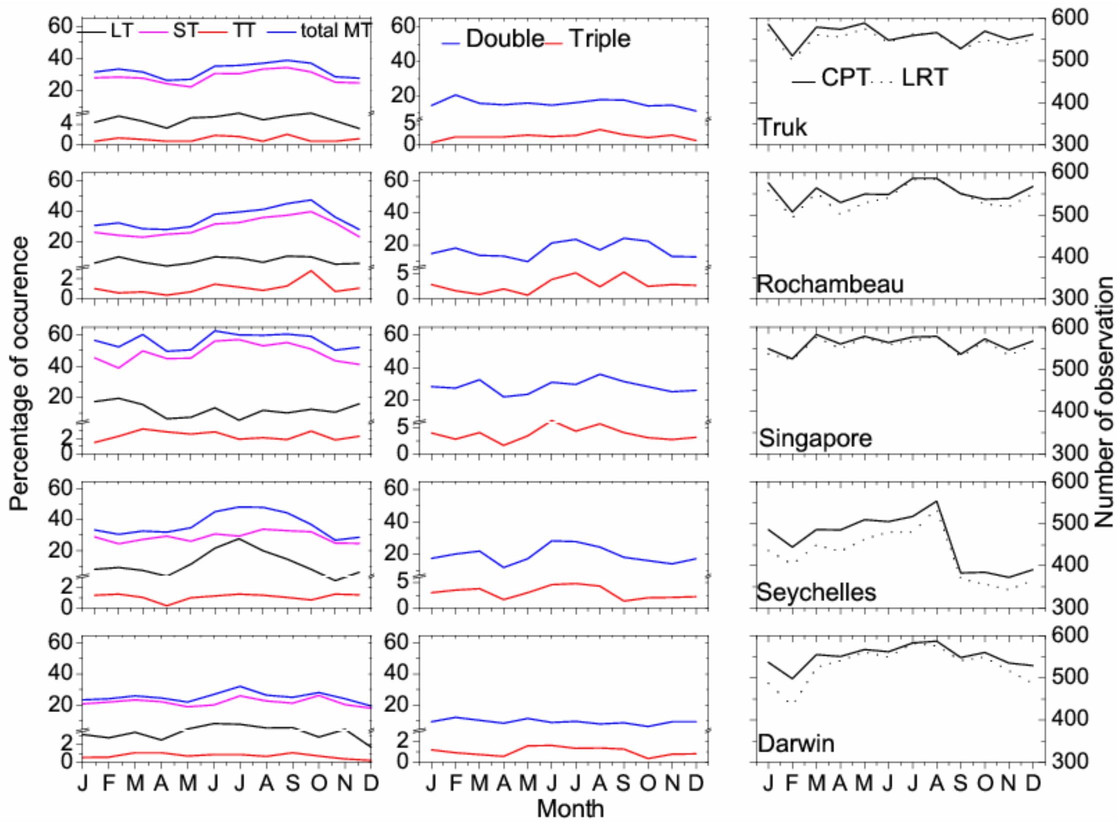

Figure 6.4. *Monthly occurrence of LT, ST, TT and MT (total) using the present method normalized to number of CPT observations (left panels) and double and triple tropopause using WMO criteria normalized to LRT observations (middle panels) constructed at different stations using data from 1999 to 2008. Number of observations considered for CPT (solid line) and LRT (dotted line) for each station is shown in right panels.*

It is seen (Figure 6.4 left panels) that the occurrence of LT is less than 10% except at Singapore and Seychelles. Percentage occurrence of LT over Seychelles is high during NH summer months (local winter) whereas over Singapore it is high during NH winter months (local). The percentage occurrence of the ST is quite significant at all the stations with Singapore showing the highest. The occurrence of the TT is quite low. There is no consistent and marked seasonal variation in MTs occurrence at all the stations. However, there is an indication of broad maximum in NH summer months. There is a clear latitudinal variation in the percentage occurrence of the MTs within the tropics, with maximum at equator. The overall percentage occurrences of LT, ST and TT along with simultaneous occurrence of LT, ST and TT estimated for the 10 year period at the five stations are presented in Table 6.2. The percentage occurrence of ST is high at all the stations followed by LT. At any time only two MTs (CPT not counted) occur and also LT and TT do not occur together.

Table 6.2: *Over all percentage of occurrence of LT, ST and TT, along with simultaneous occurrence of LT and ST, LT and TT, ST and TT and LT, ST and TT estimated for 10 year period (1999-2008) observed at the five stations.*

Station	LT	ST	TT	LT&ST	LT&TT	ST&TT	LT&ST&TT
Truk	5	29	1.1	0.9	0	1.1	0
Rochambeau	7.6	30	1.1	2.1	0	1.1	0
Singapore	12	49	2.4	4.4	0	2.4	0
Seychelles	12	29	1.1	3.6	0	1.1	0
Darwin	4.2	22	0.7	0.8	0	0.7	0

As mentioned earlier, in order to examine the spatial distribution of occurrences of MTs, COSMIC RO data is used for the tropical belt (± 30) for a period of 2 years (August 2006-August 2008). The entire data set is grided into 5×10 latitude and longitude grids. MTs occurrences are calculated using both the WMO criteria and present method from individual profiles in each grid. The percentage occurrences of double, triple tropopauses using WMO criteria and number of observations used to generate these statistics in different seasons are shown in Figure 6.5. The percentage occurrence of double tropopause is ~ 25% except at a few locations during NH summer season over Indian Ocean, which shows more occurrences (~35%).

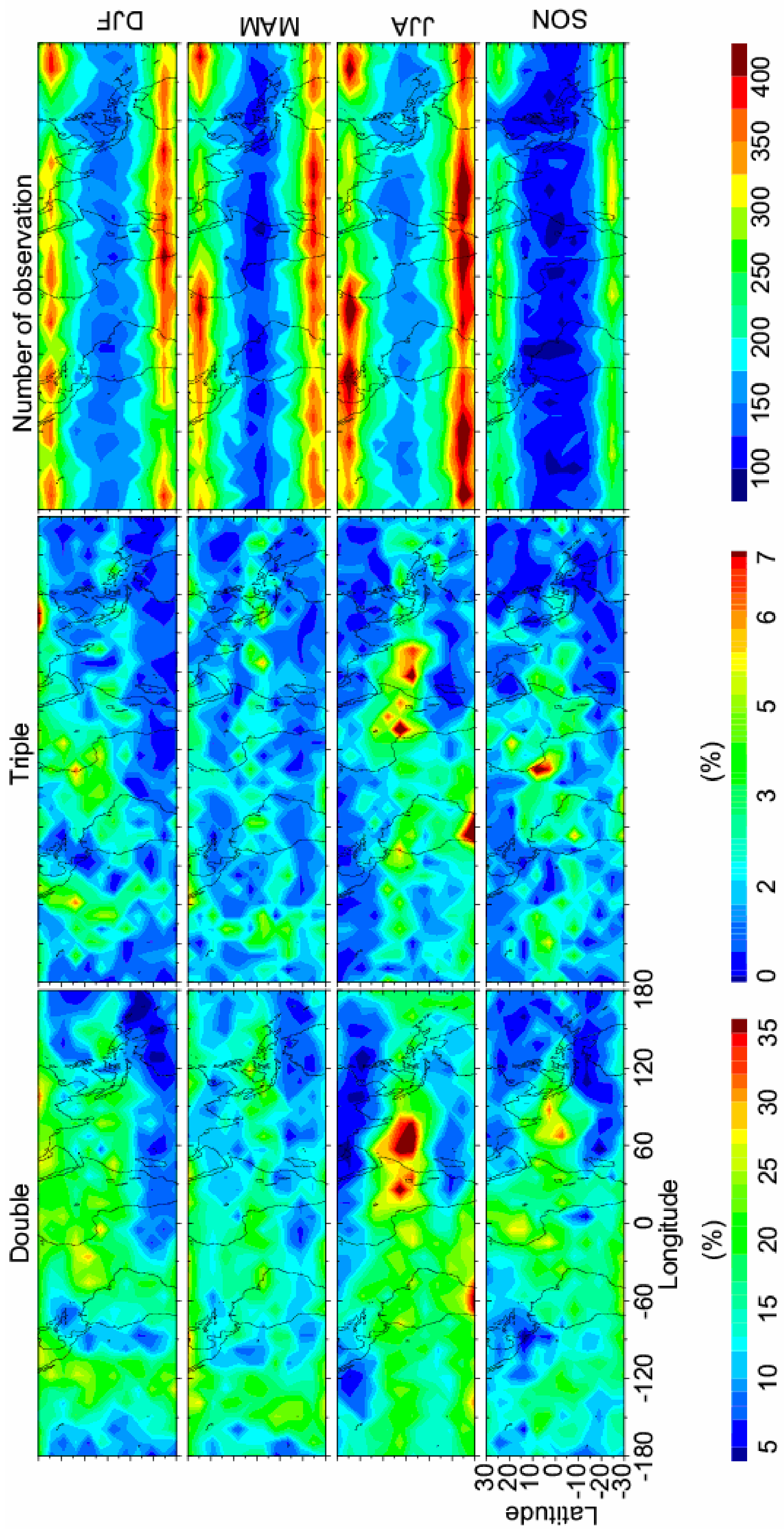

Figure 6.5: *Global distribution (in tropical latitudes) of percentage occurrence of double (left panels) and triple (middle panels) tropopause using WMO criteria observed using COSMIC RO data during different seasons for the period of August 2006-August 2008. Number of observations used in different seasons is shown in the right panels.*

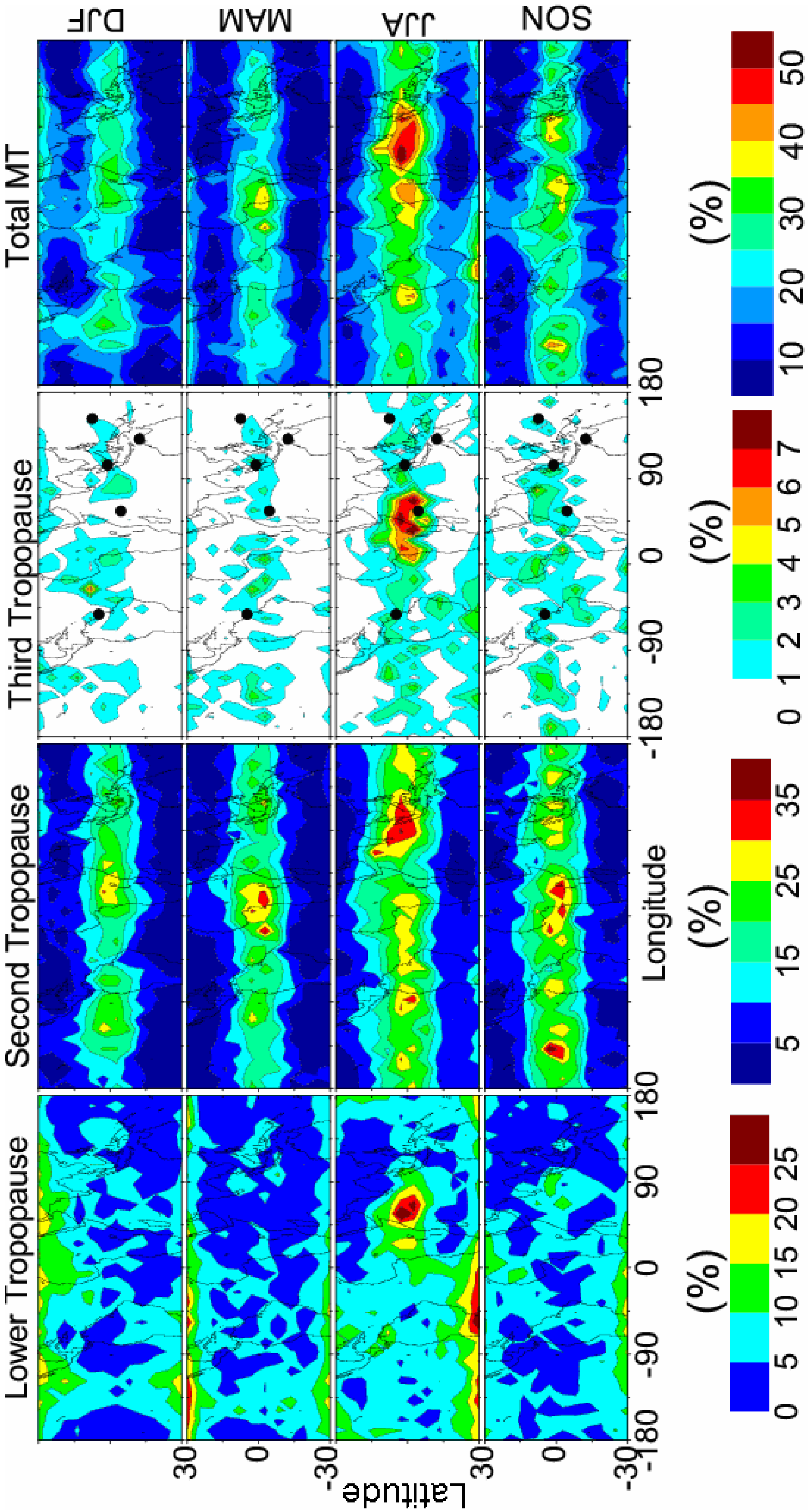

Figure 6.6:. *Global distribution (in tropical latitudes) of percentage occurrence (%) of LT, ST, MT (total) from the present method observed using COSMIC RO data during different seasons for the period of August 2006-August 2008. Black dots in third panel from left represents the location of radiosonde stations used in this chapter.*

Percentage occurrence also shows longitudinal variability. It is to be noted that the percentage occurrence enhances near the subtropics during NH winter. It is well known that the subtropical jet migrates towards equator during NH winter, leading to enhanced percentage occurrence probably related to sub-tropical jet (STJ) events [*Holton*, 2004]. During NH summer, a peak of the higher percentage occurrence in the Indian Ocean is observed consistent with the observation of *Schmidt et al.*, [2006]. The percentage occurrence of triple tropopause is generally quite small. The spatial distribution of percentage occurrence of LT, ST, TT and total MT in different seasons using the present method of identification of MTs is shown in Figure 6.5. These results suggest higher percentage of occurrence of the MTs than that obtained using WMO criteria shown in Figure 6.4. These are also higher compared to those obtained using WMO criteria by *Seidel and Randel*, [2006], *Randel et al*., [2007], *Schmidt et al*.,[2006], *Añel et al.,* [2007;2008], who reported very few (< 10%) occurrences in the tropical region. LT occurrence in general is less than 10% except at a few locations.

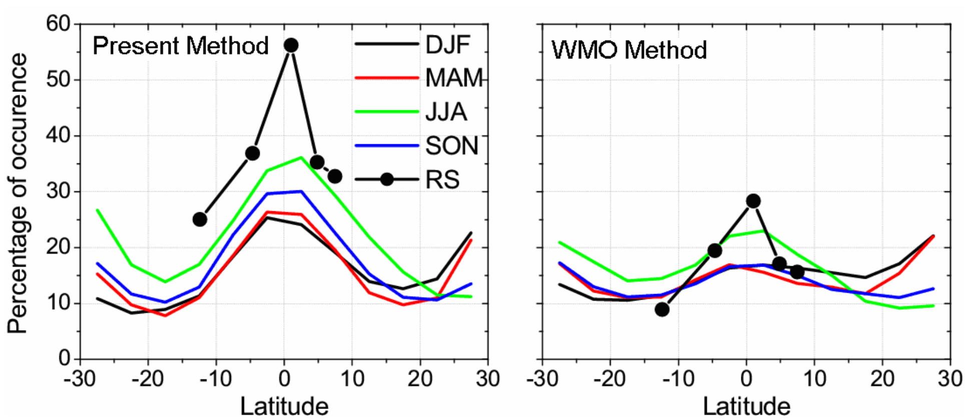

Figure 6.7: *Mean occurrence (%) of the MTs observed in different seasons using both the present method (left panel) and WMO criteria (right panel).*

There is a clear peak of percentage occurrence of more than 20% over Indian Ocean during summer season. Note that in the region of the location of Seychelles the percentage of occurrence is high during NH summer (JJA) season as can also be seen in Figure 6.4. The spatial distribution of ST, TT and total MT shows a clear maximum in the equatorial belt (±10 degree), reaching higher values during the NH summer and lower values during NH winter. The percentage occurrence of ST, TT and total MT varies between 5-35 %, 1-7% and ~10-55%, respectively. In the equatorial zone of high MT occurrence, peaks over Indian Ocean (60^oE-120^oE), African continent (0-30^oE) and west coast region of South America (~ 80^oW-120^oW) may be discerned in NH summer with typical percentage values in these zones as 35-55% for total MT, 25-35% for ST and 3-7% for TT. In NH winter, peak in percentage occurrence over Indian Ocean is not observed and occurrence peaks over other zones are smaller in extent and slightly shifted in longitude compared to that in NH summer.

The zonal mean of total MT occurrence obtained using COSMIC data and mean values of individual stations of radiosonde data using the present method and the WMO criteria are summarized in Figure 6.7. The occurrence of total MTs using the present method is more than that by the WMO criteria. The zonal mean occurrence frequency from both the methods shows similar latitudinal structure. The total MT percentage occurrence using radiosonde data, however, is quite close to zonal mean MT occurrence using COSMIC data except at Singapore (~55%). This suggests strong longitudinal dependence of occurrence of MTs in the tropics as also seen in Figure 6.6

6.3.2. Monthly Variation of Altitude and Temperature of MTs

The monthly mean altitudes of LT, CPT, ST and TT and corresponding temperatures and pressures are shown in Figures 6.8 for the five stations constructed using the ten year period (1999-2008) radiosonde observations. The mean and corresponding standard deviations are also shown in Table 6.3. Using 108 radiosonde stations located in the tropical belt (30^oN–30^oS) and considering data for 30 years, *Seidel et al.,* [2001] reported that the climatological annual mean zonal mean altitude and pressure of tropical CPT are ~16.9 km and ~ 96 hPa, respectively and exhibit very little latitudinal variability. They reported that CPT temperature values vary from 191 K-201 K. In the present study (Table 6.3), CPT altitude averaged for the five stations for the period of ten years (1999-2008) is ~17.0 ± 0.4 km; CPT temperature is ~ 190.3 ± 2.4 K; and CPT pressure is ~ 93.8 ± 6.0 hPa. These values are consistent with the earlier reports although the time period is different.

Table 6.3: *Mean and standard deviations of altitude, temperature and pressure of LT, CPT, ST and TT averaged for 10 years period (1999-2008) observed at the five stations.*

Station		Altitude	Temperature	Pressure
Truk	LT	16.08 ± 0.47	192.3 ± 2.57	109.0 ± 8.50
	CPT	16.9 ± 0.36	189.2 ± 2.26	94.7 ± 5.90
	ST	18.6 ± 0.37	195.9 ± 2.22	70.8 ± 4.38
	TT	19.2 ± 0.60	198.4 ± 3.11	64.2 ± 6.70
Rochambeau	LT	16.0 ± 0.47	194.1 ± 2.57	109.2 ± 8.50
	CPT	17.0 ± 0.36	191.2 ± 2.26	92.7 ± 5.90
	ST	18.8 ± 0.37	197.0 ± 2.22	69.1 ± 4.38
	TT	19.2 ± 0.60	199.5 ± 3.11	64.2 ± 6.70
Singapore	LT	15.7 ± 0.46	194.3 ± 2.61	115.6 ± 8.75
	CPT	16.9 ± 0.45	190.1 ± 2.46	94.9 ± 7.46
	ST	18.7 ± 0.44	196.8 ± 2.18	70.4 ± 5.14
	TT	19.1 ± 0.54	198.3 ± 2.82	65.1 ± 5.75
Seychelles	LT	15.8 ± 0.68	195.2 ± 3.98	114.7 ± 13.40
	CPT	17.0 ± 0.33	191.4 ± 2.68	93.5 ± 5.40
	ST	18.8 ± 0.44	197.3 ± 2.42	68.1 ± 5.04
	TT	19.3 ± 0.78	199.3 ± 2.97	63.9 ± 8.14
Darwin	LT	16.2 ± 0.43	192.1 ± 2.41	107.1 ± 7.74
	CPT	17.0 ± 0.32	189.4 ± 2.48	92.9 ± 5.19
	ST	18.7 ± 0.47	196.1 ± 1.84	70.5 ± 5.71
	TT	19.3 ± 0.66	199.4 ± 3.29	63.6 ± 6.90

However, note that no statistics are available on MTs (except percentage occurrences) so as to compare with our present study and the present study on this aspect is the first of its kind. The five stations mean values over 10 year period of altitude, temperature and pressure of LT (from Table 6.3) are 16.0±0.5 km, 193.6±2.8 K, 111.1±9.6 hPa, respectively: those of ST are 18.7±0.4 km, 196.6±2.2 K, 69.8±5.0 hPa, respectively; those of TT are 19.2±0.6 km, 199.0±3.1 K, 64.2±6.9 hPa, respectively. It is seen that, on the average LT is cooler and closer to CPT than ST at all the five stations. Seasonal variation shown in Figure 6.8 of the CPT altitude, temperature and pressure show quite expected variations i.e., maximum altitude and minimum temperature and pressure during NH winter while minimum altitude and maximum temperature and pressure during NH summer. The altitude, temperature and pressure of the LT, ST and TT (Figure 6.8) show similar seasonal variation as those of CPT, respectively. Note that the TT occurrence is quite low and no clear seasonal variation could be discerned. The temperature of CPT falls below 191 K at all the stations in NH winter months. LT attains temperatures of ≤191 K in a few months at some of the stations.

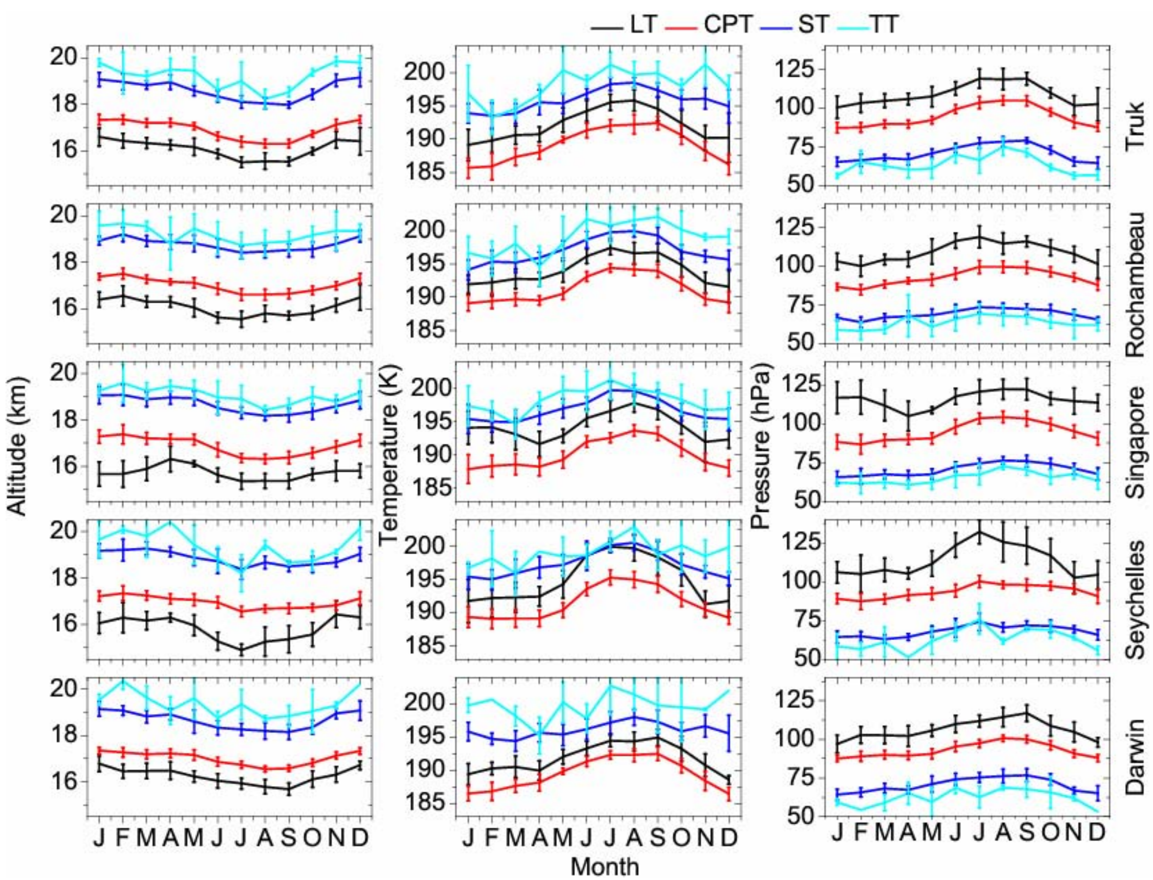

Figure 6.8: *Monthly mean variation of altitude, temperature, and pressure for LT, CPT ST and TT observed at Truk, Rochambeau, Singapore, Seychelles and Darwin for the 10 year period (1999-2008). Standard deviation (vertical bars) represents inter-annual variation.*

Mean difference in altitude, temperature and pressure between CPT and LT, CPT and ST, and CPT and TT calculated for the 10 year period (1999-2008) is shown in Figure 6.9. Considering all the five stations, the differences of altitudes, temperatures and pressures between CPT and LT vary in the range from ~0.8-1.8 km, ~2-6 K, and ~10-35 hPa, respectively. These differences are more between CPT and ST and vary in the range ~ 1.5-2 km, ~5-8 K, and ~20-28 hPa, respectively. These differences decrease away from equator (except Seychelles during NH summer). In comparison to ST, LT is around 0.7-0.8 km closer (with a few exceptions) to CPT and ~3- 4 K cooler. The difference between CPT and TT is ~ 2.3-2.8 km, ~5-12 K and ~30-40 hPa for altitude, temperature and pressure, respectively.

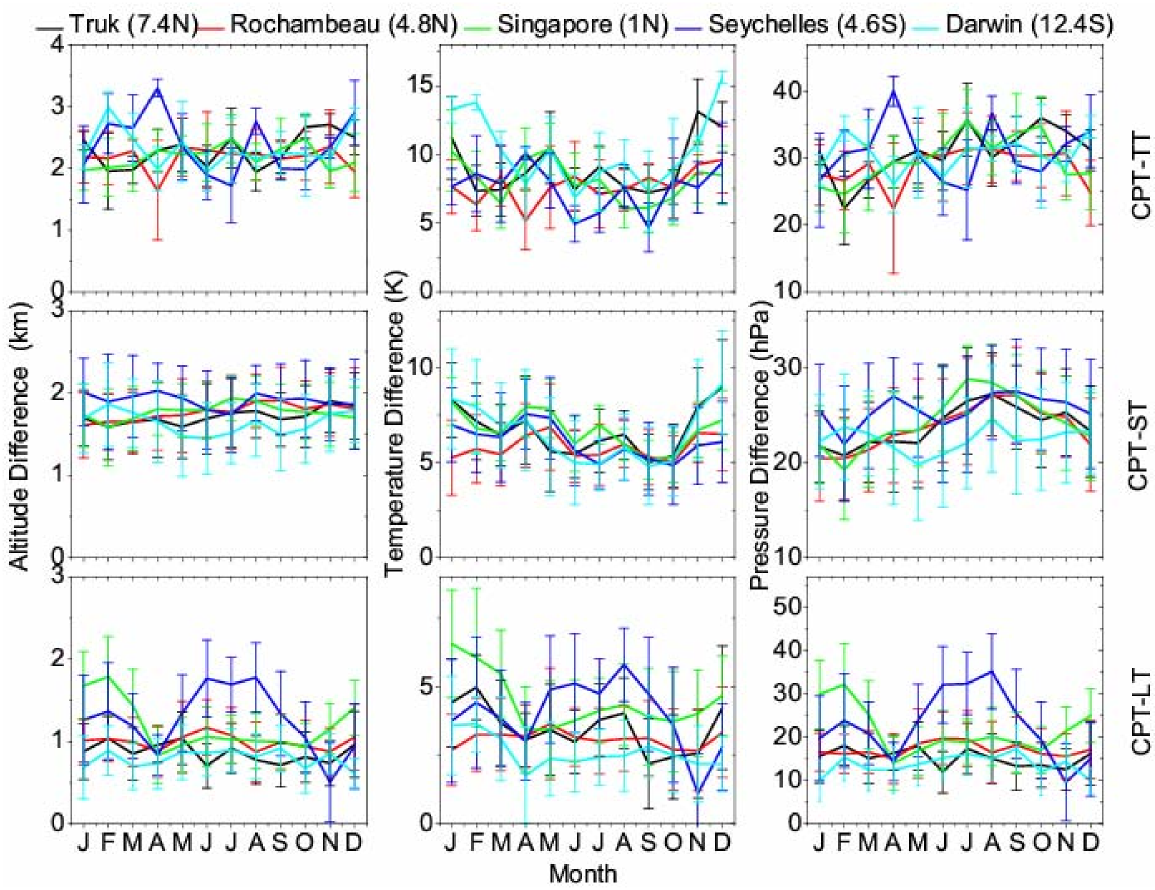

Figure 6.9. *Mean difference in altitude, temperature and pressure between CPT and LT, CPT and ST and, CPT and TT observed at different stations (Truk, Rochambeau, Singapore, Seychelles and Darwin) estimated for 10 year period (1999-2008). Vertical bar represents standard deviation.*

The differences in altitude, temperature and pressure between CPT and LT show more variability from station to station and seasonally compared to those between CPT and ST. The difference between the two is highly pronounced during NH winter at Singapore and in NH summer at Seychelles. The monthly mean saturation water vapor mixing ratios are calculated corresponding to LT and CPT and are shown in Figure 6.10. The mixing ratio corresponding to CPT is in general less than 2ppmv in the months from November- May. It is lower, in general, at the Pacific stations Truk, Singapore and Darwin compared to the non-Pacific station Rochambeau. The mixing ratio corresponding to the LT in months from November to May is in general ~3ppmv indicating dry conditions even below CPT.

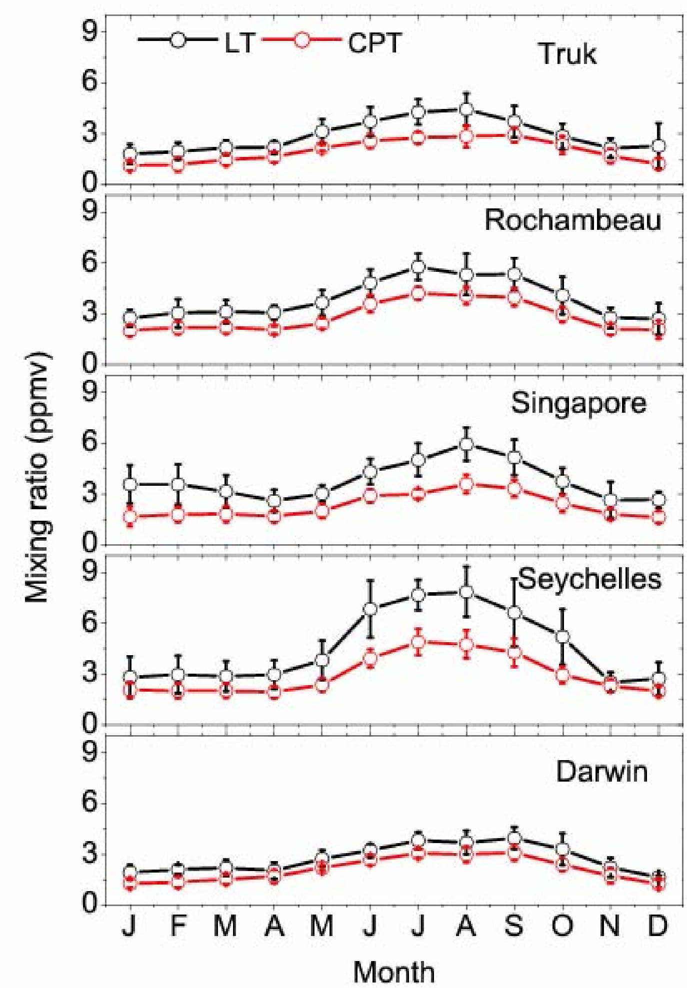

Figure 6.10: *Inter-annual variation of saturation water vapor mixing ratios at LT and CPT observed in different stations (Truk, Rochambeau, Singapore, Seychelles and Darwin) for 10 year period (1999-2008).*

6.3.3. Latitudinal Variation of Altitude and Temperature of MTs at Different Longitude Sectors

It is reported that zonal mean latitudinal structure of the CPT altitude doesn't show any variation in the tropics [*Seidel et al*, 2001]. However, the CPT altitude is found to exhibit high longitudinal variability [*Tsuda et al*, 2004; *Ratnam et al*, 2005, *Zhou et al*, 2001b]. In order to study the latitudinal variation of MTs and CPT in different longitude sectors the COSMIC GPS RO data is used as detailed earlier. The whole longitude range is divided into 60 degrees wide bins within which CPT altitude shows more or less similar latitudinal structures. The seasonal mean latitudinal variation of the altitude of LT, CPT, ST and TT observed for each sub grid of 60 degrees longitude is shown in Figure 6.11.

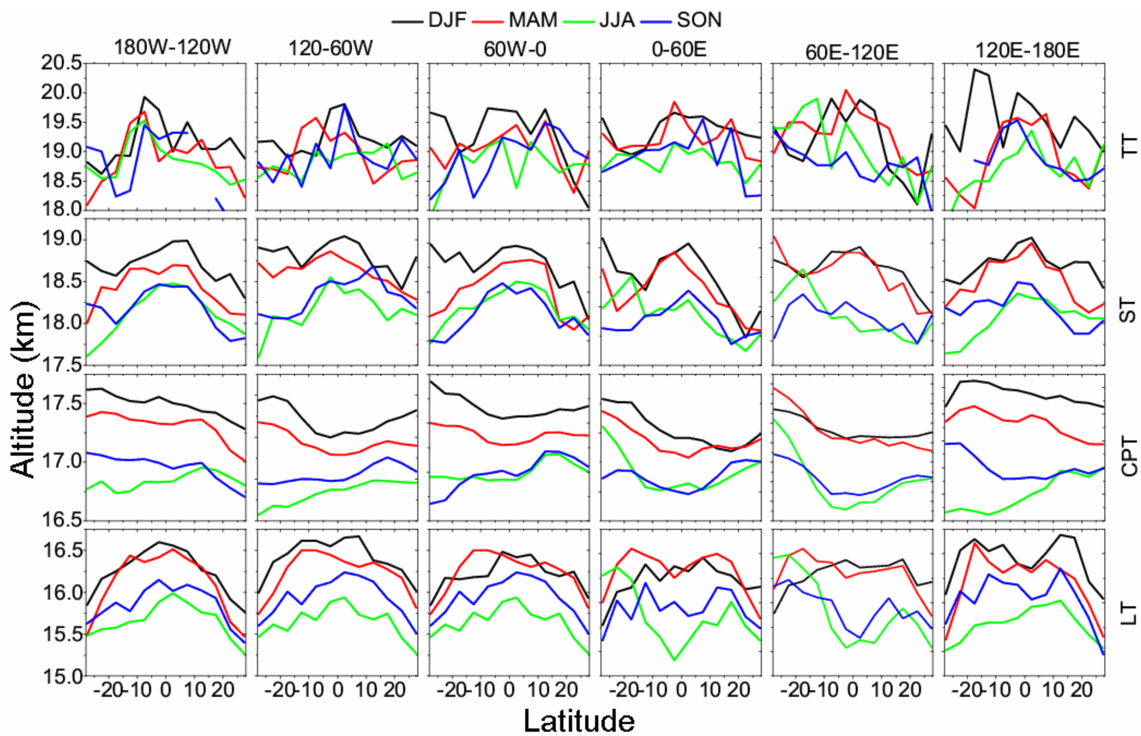

Figure 6.11: *Latitudinal distribution of the altitude of LT, CPT, ST and TT in different seasons averaged over 60 degree longitude intervals using COSMIC RO data for the period August 2006 - August 2008.*

The seasonal variation of the CPT altitude is well known with higher values during NH winter and lower values during NH summer. The LT and ST altitudes show latitudinal structure resembling inverted U shape, with high values at the equator especially in the eastern longitude sectors. The CPT altitudes, in general, do not show such structure. However, they show a U shape like structure similar to that reported by *Ratnam et al*., [2005] in some longitude sectors. These U shape structures are pronounced in the longitude sector 0-120^{o}E during June-November and in longitude sector 0-120^{o}W during months December- May. Further, within the tropics the altitude of CPT does not always peak at the equator. This is seen in at least in one season in all the longitudinal zones.

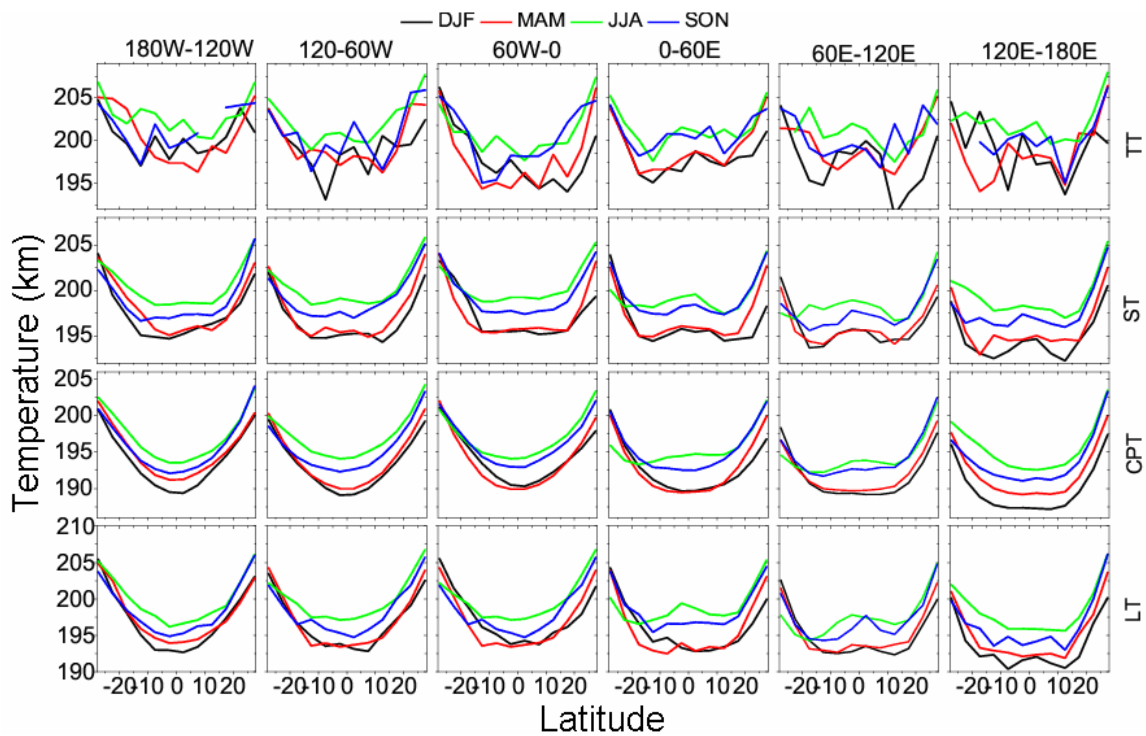

Figure 6.12: *Same as Figure 11 but for temperatures.*

The seasonal mean latitudinal distribution of MTs temperature in different longitude sectors are shown in Figure 6.12. In contrast to their altitudes, the temperatures of CPT and MTs (except TT) show quite similar behavior in general with lower temperatures at equator and higher at ±30^{o} latitudes. While at the equator, the CPT temperature is minimum, the CPT altitude is not maximum. Equatorial minimum in the temperature of CPT (and LT and ST) is relatively broad at eastern longitudinal sectors when compared to western longitudinal sectors. Further, it appears that the CPT at the equator is cooler in eastern longitudinal sectors when compared to western longitudinal sectors.

6.4. Discussion

A method of identifying MTs in the tropics is evolved based on CPT instead of lapse rate as in WMO method. Though the lapse rate method is related to the static stability of the atmosphere and hence to the thermodynamics, it serves mainly operational purpose for identifying the tropopause (LRT). Our concern in the present study is to bring out the characteristic features of MTs based on the CPT, which is more meaningful than LRT especially in the tropical region as CPT is more relevant for dehydration and STE processes. The present analysis shows that MTs can occur both below and above the CPT unlike the behavior of MTs from WMO criteria. The importance of this result is that the MTs which occur below and above the CPT have distinctly different characteristics. The MTs occurring below the CPT reveal information on warming as temperature has to increase above it instead of decreasing further and the MTs occurring above the CPT reveal information on cooling.

Interesting question is that how to interpret these MTs. Are they due to planetary scale waves or due to horizontal advection of air from surroundings or cirrus clouds formation and subsequent lowering of the temperatures or a combination of these? After examining many cases it is found that MTs can occur in groups of consecutive days or in isolated days as illustrated in Figure 6.13. Figures 6.13(a) and 6.13 (e) show the time series of LT, CPT, ST and TT altitudes observed over Singapore during June-August 2003 and December 2003 – February 2004, respectively. The corresponding number of tropopauses identified is shown in Figures 6.13 (c) and 13 (g), respectively. The MTs occurred both on isolated days and groups of days with no clear preference. Downward shift in the altitude of CPT can be clearly noticed particularly in June 2003 and January-February 2004. It is also seen that MTs occur during these two periods of downward shift. Two dimensional spectral analyses (wavelet) have been done in order to obtain the dominant wave periods and the time of their occurrences as shown in Figures 6.13 (d) and 13 (h). For this analysis the three month mean profile from individual temperature profiles is subtracted to obtain fluctuation component which is subjected to wavelet analysis and the results are shown for 16 km and 17 km in Figures 6.13 (d) and 13 (h), respectively. Although waves with periods 2-15 days dominate during the observation period, waves with periods 4-10 days are significant during 20 June to 20 July 2003 and 8-12 days during 25 January to 10 February 2004. The dominant periods only are considered above the cone of influence in order to avoid edge effects. The wave amplitudes are strong during 25 June - 10 July 2003 (Figure 6.13d) and 25 January – 10 February 2004 during which both downward phase progression of CPT and occurrence of MTs are seen as already mentioned.

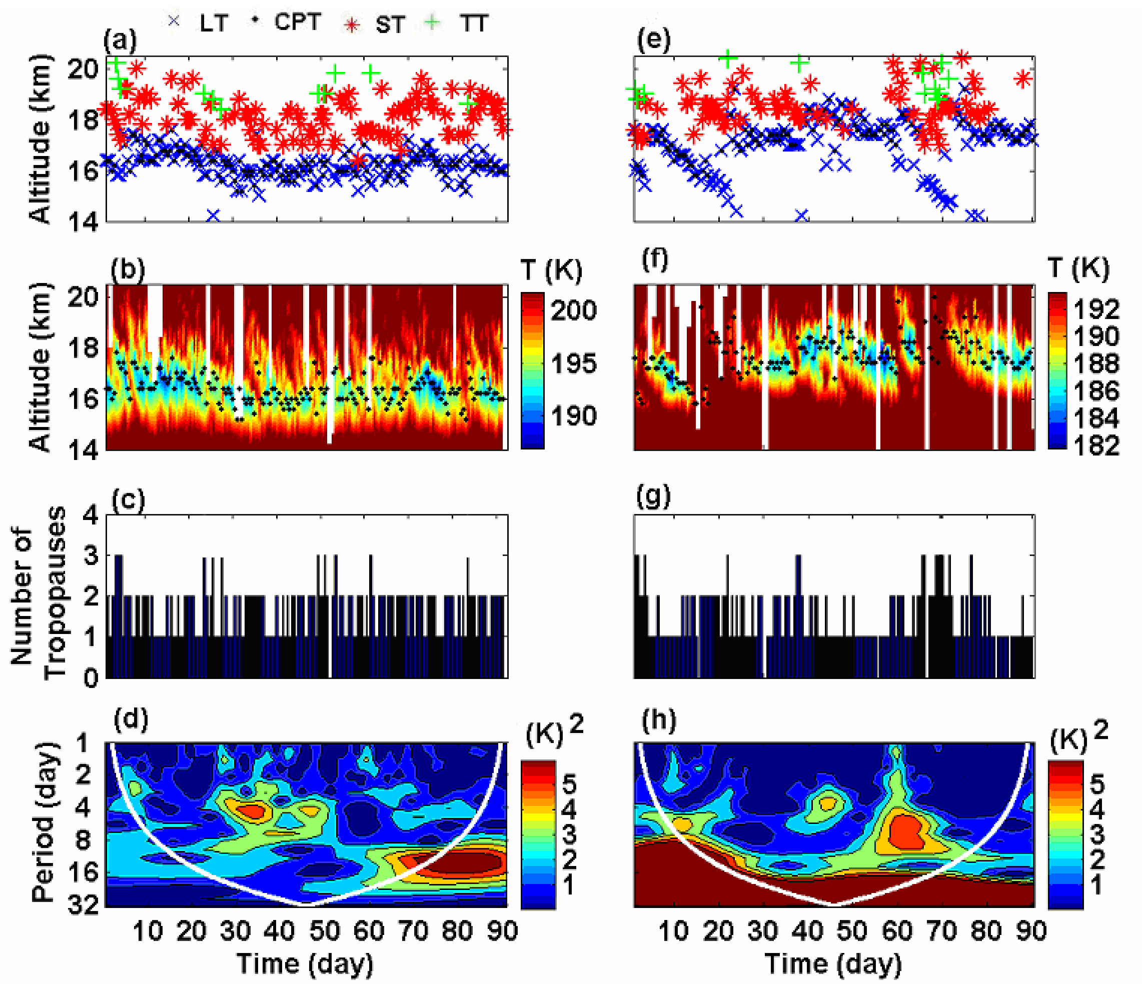

Figure 6.13: *(a) Time series of multiple tropopauses altitudes observed during June-August 2003 at Singapore. (b) Contour plot of temperature between 14 km and 20.5 km embedded with CPT altitude. (c) Number of tropopauses observed in each profile during above mentioned period. (d) Wavelet spectrum of temperature (in terms of power) at 16 km altitude. White curve represents cone of influence. (e) – (g) same as (a) – (c) but observed during December 2003-February 2004. (h) same as (d) but at 17 km altitude.*

Thus, the occurrence of MTs in groups may be due to well known planetary scale waves. But the isolated occurrence of MTs may not be due to wave effects and hence other processes could be effective. In order to ascertain the nature of these waves, the amplitude and phase of dominant wave periods in temperature and zonal wind during June-August 2003 (8 day period) and December 2003- February 2004 (12 day period) are obtained from spectral analysis and are shown in Figure 6.14. The amplitudes in temperature and zonal wind in the altitude range 15-20 km are ~1.5 K and 4-5 m/s, respectively.

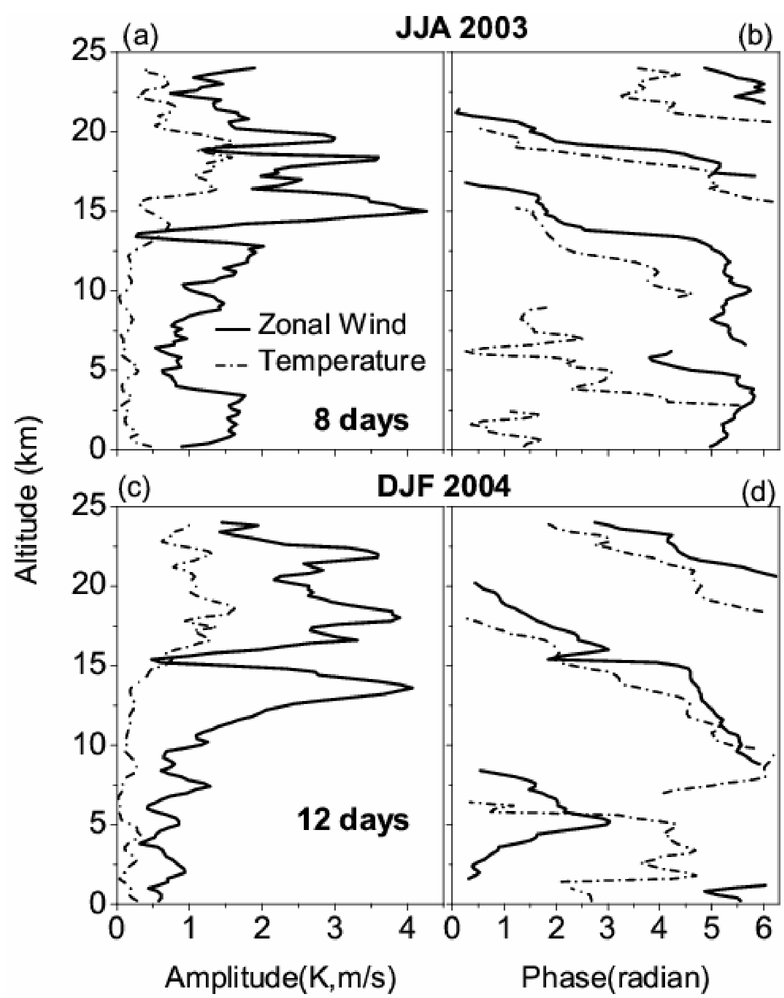

Figure 6.14: *Profiles of (a) amplitude and (b) phase fitted for 8-day period during 20 June-20 July 2003 for both zonal velocity and temperature observed at Singapore. (c) and (d) same as (a) and (b) but fitted for 12-day period during December 2003 – February 2004.*

The phase shows clear downward propagation (upward propagating wave) with dominant vertical wavelengths of 4.4 km and 6.2 km during June-August 2003 and December 2003- February 2004 cases for the wave periods 8 days and 12 days, respectively. It is worth mentioning here that these periods have not been observed in meridional winds. Moreover, the temperature phase is leading the zonal wind phase by about quarter cycle. This result suggests that these waves are mainly planetary scale eastward propagating Kelvin waves. Further, quantification of occurrence in groups and isolated MTs can reveal the dominance of the several causative effects besides waves. Note that the wavelengths and the amplitudes of the waves obtained above can lead to only small perturbations in the lapse rates (of the order of 0.25 K/km) which alone may not be adequate to produce MTs. Waves with greater amplitudes and shorter vertical wavelengths (corresponding to longer periods) would be required to cause MTs. Extensive study on the modulation of the tropical tropopause altitude and temperature by equatorial waves are dealt in chapter 7.

Below the CPT, as the temperature lapse rate is positive, LT which is a point of inflection in the temperature profile can occur if there is additional heating in a narrow altitude range to reverse the lapse rate. Similarly, above CPT, additional cooling will lead to the occurrence of ST and TT. So, advection of hot air could result in LT. This could be provided by advection of ozone-rich air from the extra tropical stratosphere [*Holton et al.*, 1995]. *Holton et al.*, [1995] elaborated on the role of extra tropical waves in the STE processes. Episodic extra tropical Rossby wave activity can inject ozone-rich extra tropical stratospheric air along the isentropic surfaces into the tropical troposphere. Strong tropical convective activity can lead to penetration of tropospheric air into stratosphere entraining ozone-rich air from above into the upper troposphere as it settles down [*Reid and Gage*, 1996]. In either case, flux of ozone-rich air can be provided to the upper troposphere which may result in additional heating. This heating, if it is strong enough, could cause reversal of lapse rate resulting in point of inflection in the temperature profile below CPT and thus, contributing to the occurrence of LT. It may be noted here that the extra tropical Rossby wave activity would be strong in the NH winter. On the other hand, deep convection can take place in different months at different stations. For example, it can be strong in the months of NH winter in the eastern Pacific sector whereas it can be strong in the NH summer months over the region under the influence of the South- East Asian summer monsoon as mentioned clearly in Chapter 3 an also in [*Mehta et al*., 2008].

Presence of (thin) cirrus clouds can cause cooling and thus could lead to reversal of the lapse rate if present above the CPT. This cooling, if strong enough, can cause a point of inflection resulting in ST and LT. Thin cirrus is found to occur above the tropical tropopause though the occurrences are relatively fewer compared to below the tropopause [*Sunil Kumar et al*., 2003]. *Wang et al*. [1996] have shown that the occurrence of thin cirrus above the tropopause is much higher in the western Pacific compared to eastern Pacific and is high in NH winter. In the present study, Singapore, a western Pacific station showed higher percentage occurrence of ST. This supports the contribution of thin cirrus to the occurrence of ST. However, the occurrence of ST has not revealed any marked seasonal variation in contrast to thin cirrus above CPT. Thus, thin cirrus alone may not account for the occurrences of ST and other processes need to be sought. MTs, particularly the ST, could also result from injection of cool air from region below CPT to lower stratosphere.

As the absolute lapse rate is greater below the CPT (upper troposphere) than above (lower stratosphere) it would require a greater perturbation (in temperature) below the CPT to cause a point of inflection (an hence a MT) in the temperature profile than above the CPT. Thus, it may be expected that MT above the CPT is more likely to occur than below as observed in the present study. In the present study, the characteristics of MTs with the method evolved based on CPT (and also with WMO criteria) using long term radiosonde data and also COSMIC GPS RO data have shown and discussed the possible mechanisms for MTs briefly. Detailed investigation on these causative mechanisms will be investigated in future work.

6.5. Summary

The main findings from the present study are listed below:

1. More occurrences (25-50%) of MTs are observed using the present method based on CPT than those from WMO criteria (10-30%).

2. In the present method, the MTs can occur both below and above the CPT unlike WMO method. It is found that MTs occur more frequently above the CPT than below.
3. At the most only two MTs (not counting the CPT) occur.
4. While there is no consistent seasonal variation in the occurrence of MTs there is an indication of broad peak in NH summer season. On the other hand, significant seasonal variation in the LT and ST altitude and temperatures is observed closely following CPT (first tropopause). LT is found to be closer to CPT and cooler in comparison to ST.
5. The occurrences of MTs are higher over equator and decrease away towards higher latitudes in the tropics. Longitudinal variation of the MTs is observed with relatively high occurrences during NH summer season over Indian Ocean.
6. While the CPT temperature is lowest at the equator the CPT altitude is not always highest at the equator. The equatorial minimum in the CPT temperature is broader and lower in the eastern hemisphere than the western hemisphere.
7. The saturation water vapor mixing ratio can attain values as low as 3 ppmv even at LT in a few months in the tropics.

From this chapter we observed that one of the factors for the generation of the multiple tropopauses is due to planetary wave activity in different seasons. It would be interesting to carry out detail analysis of the equatorial wave in modulating the tropopause. The detail investigations of the modulation of the tropopause due to equatorial wave are discussed in the Chapter 7.

---END--

Chapter 7

Modulation of the Tropical Tropopause due to Equatorial Waves: Seasonal Variability

7.1. Introduction

Equatorial waves are an important class of eastward (Kelvin waves) and westward (Rossby-gravity) propagating disturbances in the ocean and in the atmosphere that are trapped about the equator (i.e., they decay away from the equatorial region). The phenomenon of the Kelvin waves in the Ocean is well known for a long time. In the stratosphere first evidence for Kelvin waves was found by *Wallace and Kousky* [1968] and Rossby gravity waves were first detected by Y*anai and Maruyama* [1966] (therefore Rossby-gravity waves sometimes are called Yanai-waves). Diabatic heating by organized convection can excite atmospheric equatorial waves. Their propagation can cause the effect of convective storms to be communicated over large longitudinal distances, thus producing remote response to localized heat sources. As a consequence in the troposphere there are significant contributions of convectively coupled equatorial waves, directly linked to the convective systems acting as wave sources [e.g., *Wheeler and Kiladis*, 1999; *Straub and Kiladis*, 2003; *Cho et al*., 2004]. For the convectively coupled equatorial waves which are mainly observed in the troposphere (e.g., *Wheeler and Kiladis* [1999]) the nature of convective coupling determines the phase speed and therefore the vertical scale of the waves. These convectively coupled waves have typical periods of 5-10 days, wave number k = 2-3, and a phase speed of 15 ms^{-1}.

Equatorial waves also propagate vertically into the stratosphere. Equatorial waves observed in the stratosphere are dominated by "free mode" wave, which are excited by deep convection in the troposphere but no longer linked with the space-time patterns of the convective forcing [*Randel and Wu*, 2005]. In the stratosphere, different from the troposphere, in particular the Kelvin waves observed (but also other equatorial wave types) cover a larger range of periods. Therefore, for example, the stratospheric Kelvin waves can be classified as ultra-slow (periods 25–30 days, *Canziani*, [1999]), slow (periods 10–20 days, *Shiotani et al*., [1997]), fast (periods 6–10 days, *Hitchman and Leovy*, [1988]), and ultra-fast waves (periods 3 to 4 days, *Salby et al.*, [1984]; *Lieberman and Riggin*, [1997]; *Garcia et al*., [2005]). The free mode waves are mainly observed in the stratosphere. The tropospheric vertical wavelength values can be attributed to the vertical scale of the convective systems acting as source (e.g., *Chang*, [1976]; *Fulton and Schubert*, [1985]; *Salby and Garcia*, [1987]) which is in good agreement with the vertical scale of the heating. Typical vertical profiles of thermal forcing in convective systems have a broad maximum over about 2–8 km in the troposphere (e.g., *Chang*, [1976]; *Fulton and Schubert*, [1985]; *Johnson and Ciesielski*, [2000]). Both convectively coupled and free mode Kelvin waves can affect the behavior of tropical tropopause and influence the dehydration and cirrus formation [*Fujiwara et al*., 1998] and occurrence of turbulence [*Fujiwara et al*., 2003]. The equatorial planetary scales wave modes [*Hitchman and Leovy*, 1988; *Dunkerton*, 1997; *Baldwin et al*., 2001] and small-scale waves play dominant role in deriving the QBO in the stratosphere. As a result of the interaction with the QBO winds tropical wave activity itself shows modulations due to the QBO.

Since the discovery of equatorial waves, numerous studies have been carried out based on radiosonde data [e.g., *Angell et al.*, 1973; *Sato et al.*, 1994], MST Radar and Lidar data [e.g., *Krishna Murthy et al*, 2002] as well as satellite data providing a global view of the atmosphere. To mention a few studies dealing with stratospheric satellite data are *Salby et al.* [1984]; *Randel et al*. [1990]; *Randel and Gille* [1991]; *Bergman and Salby* [1994]; *Canziani et al*. [1994]; *Srikanth and Ortland* [1998]; *Tsai et al*. [2004]; *Randel and Wu* [2005]; and *Ratnam et al*. [2006]. Due to limitations in the data sets, most of these studies are confined to study of only Kelvin waves without considering much Rossby gravity waves. In addition, many analyses focus on zonal wave numbers 1–2, neglecting the higher wave numbers, which are also important for the modulation of tropical tropopause. Further, using ERA-15 temperature and wind data, *Tindall et al.* [2006a, b] proved that higher zonal wave number from 4-7 also contribute significantly to the momentum flux of waves around tropopause region. The nature of equatorial waves modulating the tropical tropopause in different seasons and in different regions is yet to be studied. Since COSMIC GPS RO consisting of six satellites, is providing relatively dense number of observations even in the equatorial region, an attempt has been made to investigate the modulation of tropical tropopause by both Kelvin and Rossby waves and extended the analysis to see the waves with wave number up to 9 although most of the effects are seen up to wave number 4.

7.2. Data and Analyses

7.2.1. COSMIC Data

COSMIC GPS-RO (Global Positioning System-Radio Occultation) data for the period of August 2006- August 2008 is used to investigate the equatorial waves and its effect on modulation of tropopause. The details about COSMIC data and GPS RO technique are provided in Chapter 2 and Chapter 6.

7.2.2. Longitudinal Grid

The locations of the occultations observed during August 2008 within ±10^o from the equator are shown in Figure 7.1 (top panel). The occultations are approximately evenly spaced with latitude with fewer near the equator. Note that the amplitude of the equatorial waves is centered over the equator with a symmetric Gaussian latitudinal structure, with typical meridional e-folding scales of ~ 15^o- 20^o latitude [*Andrews et al*, 1987; *Mote et al.,* 2002]. Bottom panel of Figure 7.1 shows the monthly number of occultations available during the observation period. The monthly numbers of measurements are in the range of 2300 - 4700. Therefore, the 10^o S-10^o N sampling provides ~ 75-150 measurements per day, approximately evenly spaced in longitude. The data over 10^{o}S-10^{o}N is averaged in 20^o longitudinal grids. There are some data gaps especially during months when occultation is less. However, 1-2 data gaps are filled by linear interpolation. The data are prescreened to remove outliers (data outside 3 sigma variance at any level over 10-30 km). Here main interest is to study the seasonal characteristics of the equatorial waves up to the zonal wave number 1 to 4 within different phases of the QBO. The 20^o grid averaging will provide 18 points in every altitude and according to Nyquist criteria one can extract the zonal wave number up to 9. The zonal mean temperature anomalies in the temperature in the grid 10^{o}S-10^{o}N latitude and 20^o degree longitude are estimated. The temperature anomalies at each altitude are subjected to Fourier analysis amplitude and frequency by applying least square method for each day during August 2006-August 2008. This observation period has been divided into eight seasons, namely, September-November 2006, December 2006-Februray 2007, March-May 2007, June-August 2007, September-November 2006, December 2007-Februray 2008 March-May 2008 and -August 2008 represented as SON06, DJF07, MAM07, JJA07, SON07, DJF08, MAM08 and JJA08, respectively. These notation will be used throughout this Chapter wherever is required.

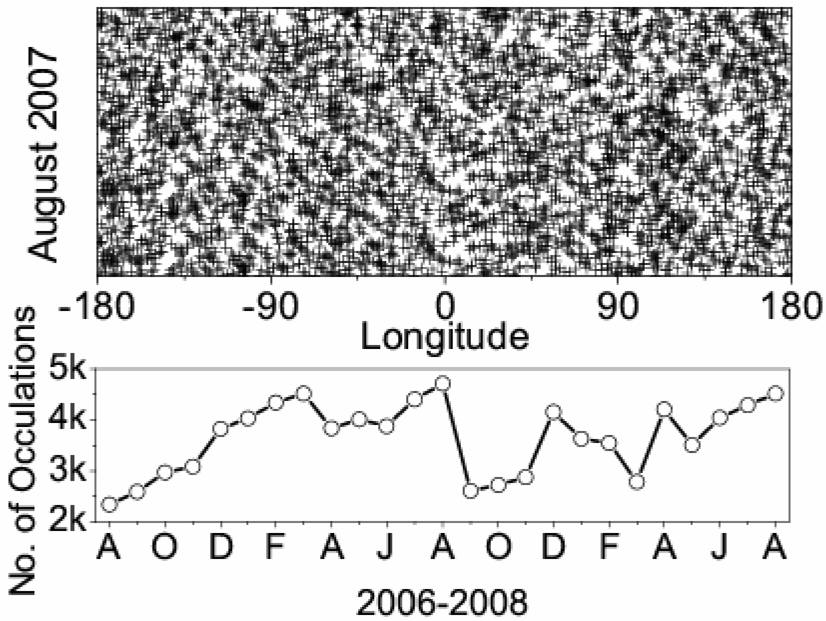

Figure7.1: *Locations of the radio occultations occurred during August 2007 within ±10^o . Bottom panel shows the monthly number of occultations available during August 2006 – August 2008.*

7.3. Results

7.3.1. Background wind conditions

The background wind conditions play crucial role in the wave characteristics. Thus, stratospheric QBO plays an important role in delineating the wave characteristics. To know exact nature of the waves, the easterly, westerly and transition phase of the QBO need to be taken into account. In this study, the planetary waves in relation to thermal variability in the equatorial tropopause are characterized in different seasons which are in different phases of QBO. Figure 7.2 shows the altitude-time sections of the zonal mean temperature anomalies (deviations from annual mean cycle) and zonal winds for the period August 2006 to August 2008. The equatorial temperature anomalies derived from COSMIC measurements and zonal wind from the NCEP data are shown in Figure 7.2 (a) and 7.2(b), respectively.

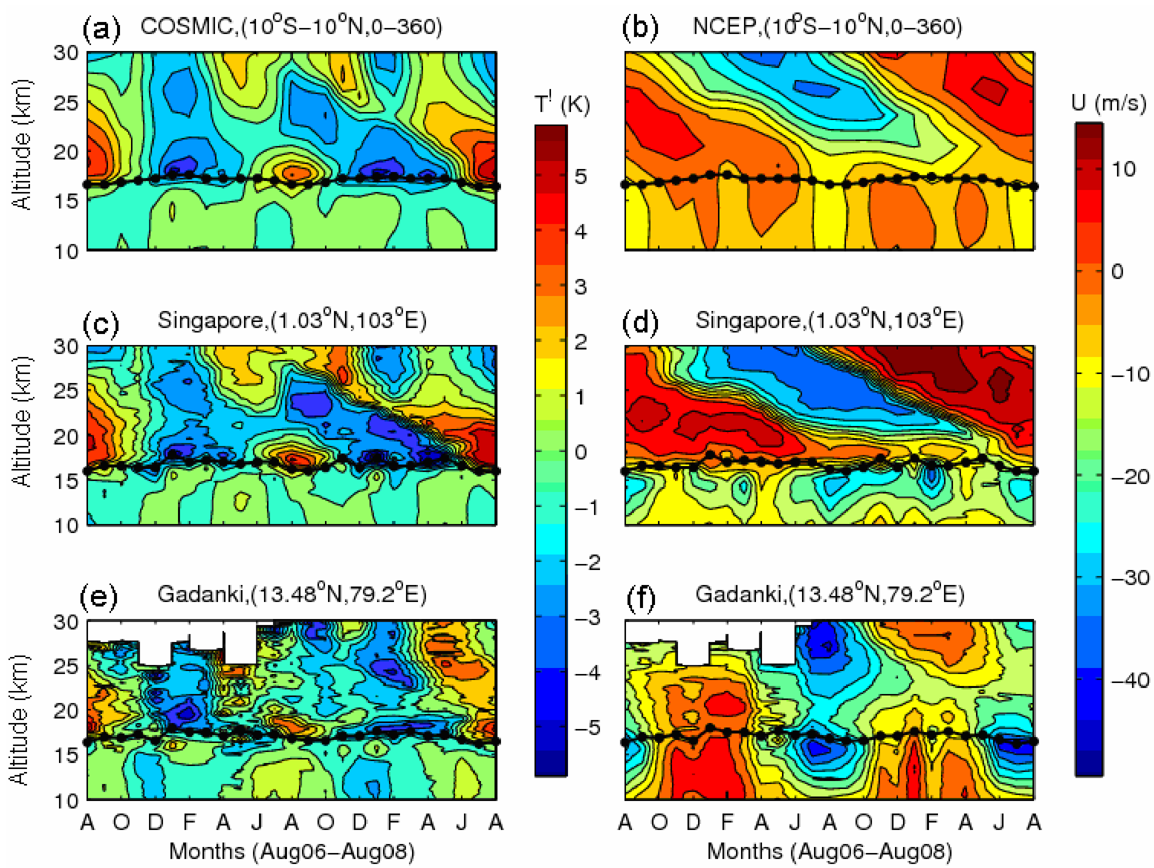

Figure 7.2: *Altitude-time variation of temperature anomalies and zonal wind (top) constructed form equatorial zonal mean using COSMIC data and NCEP Reanalysis data, respectively, during August 2006 to August 2008, (middle) using Radiosonde data over Singapore (bottom) using Väisälä and Meisei Radiosonde data over Gadanki. Dotted line shows the cold point tropopause altitude.*

The temperature anomalies and zonal wind over Singapore and Gadanki are also shown in Figure 7.2 (c) and 7.2 (d) and Figure 7.2 (e) and 7.2 (f), respectively. The temperature anomalies shows consistently similar feature in all the three data sets. The temperature anomalies near cold point tropopause altitude show clear annual oscillation with alternate warm anomalies during June-August and cold anomalies during December-February. The zonal wind shows strong variability associated with stratospheric QBO in the equatorial zonal mean NCEP data and over Singapore with descending cold anomalies associated to easterly shear zone during October 2006-April 2008. However, zonal wind over Gadanki is weakly associated with QBO and its effect can be seen above altitude region of ~20 km. The zonal wind at Gadanki shows strong variability associated with monsoonal tropical easterly jet streams (TEJ) during June-September and westerly during October –April in upper troposphere (~10 km) to lower stratosphere (~ 20 km). There is alternate reversal of zonal wind between easterly to westerly during summer and winter. Here, the characteristic of the equatorial waves and its association with tropical tropopause in different seasons with respect to QBO changes is analyzed.

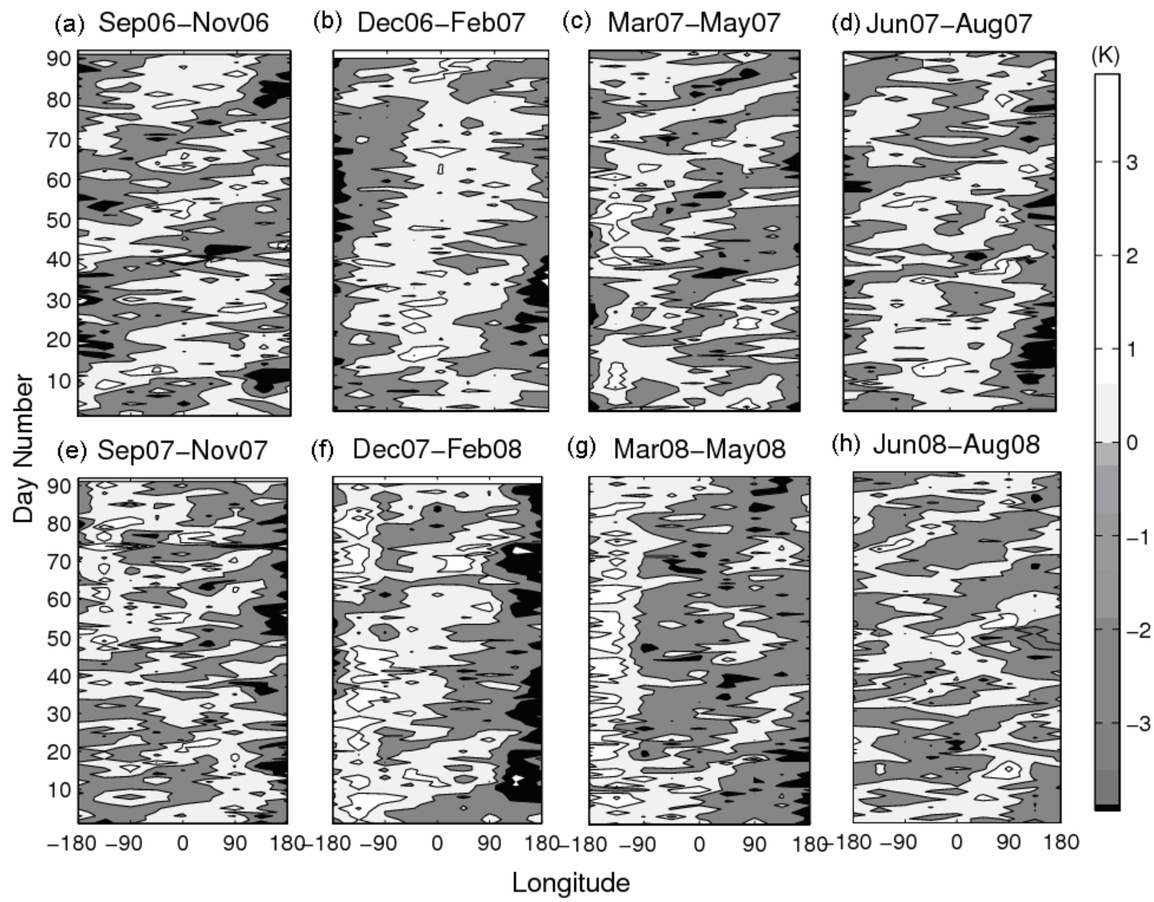

Figure 7.3: *Longitude-time diagram of the grided temperature variations over 10°N-10°S observed during different seasons during September 2006-August 2008 at 17 km.*

The grided temperature profiles from the COSMIC RO in the altitude range of 10-30 km mentioned above are the basic data for the present study. The temperature anomalies are obtained by subtracting the zonal mean temperature profiles from gridded temperature profiles each day. Figure 7.3 shows the longitude-time diagrams of temperature variations at 17 km observed in different seasons during August 2006-August 2008, constructed from grided temperature anomalies. The 17 km level is near the tropical cold point tropopause and temperature patterns are quasi-stationary, which is the known climatological structure of cold temperatures over longitudes ~90–180°E associated with maximum convection over Indonesia [e.g., *Highwood and Hoskins*, 1998; *Seidel et al.*, 2001; *Randel et al.*, 2003].

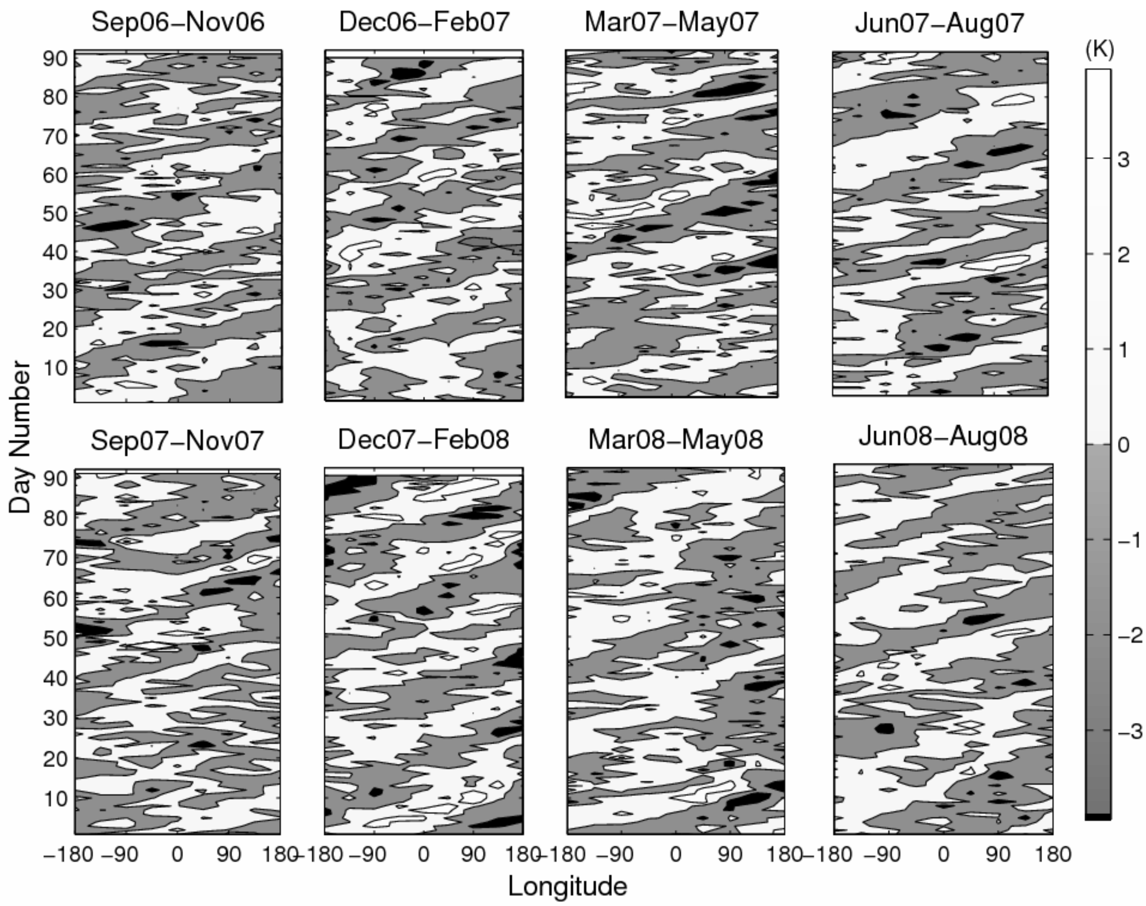

Figure 7.4: *Same as Figure 7.3 but observed at 19 km.*

However, in addition to quasi-stationary wave structure, there are the periods where eastward propagating anomalies are evident, particularly during October 2006, May 2007 and June-August 2008. The fluctuations during these months show periods of ~ 18 days (October 2006), ~ 22 days (May 2007), and ~ 12 days (August 2008). In contrast, the temperature anomalies at 19 km depicted in Figure 7.4 show a zonal wave number 1 structure with regular eastward propagation with a period of ~ 20 days. The zonal phase speed (from dispersion relation of Kelvin wave, $c^2 \equiv (\nu/\kappa)^{2,}$ ν= angular frequency and k = zonal wave number) for period 20 days and zonal wave number 1 is found to be ~ 20 m/s.

7.3.2. Dominant Periodicity for Wave 1-4 Component

Besides the zonal wave number 1, wave number 2, 3and 4 are also embedded in the anomalies which can be seen clearly from Figure 7.5. Figure 7.5 shows that the anomalies at the cold point tropopause altitude during 18- 28 December 2006 (day number 230-240, whish starting with day number 1 from 1 August 2006) fitted with 1, 2, 3 and 4 components of the wave, respectively. In order to bring out the characteristics of the eastward propagating temperature anomalies for different zonal wave numbers, amplitude (A_k) and phase (ϕ_k) of the gridded zonal temperature anomalies for each day are calculated by least square method. Later, the time series of isolated dominant wave numbers (k = 2π/λ_x) are constructed using a sinusoidal fitting function,

$$f(x) = \sum_{k=1}^{4} A_k \sin k(x - \phi_k) \qquad (7.1)$$

where, x represents the longitude in [-π: π] in 20^o interval.

The sinusoidal fitted time series profiles for each wave numbers at each altitude (in the range 10 to 30 km) for each season are subjected to Fourier analysis which provides the amplitude spectrum in the frequency domain. The Fourier transform г(ω)of temperature T(t) is given by

$$\tau(\omega) = \int_0^{t_0} T(t)\exp(-iwt)dt \qquad (7.2)$$

Where t_0 is the time (in days), ω =2πf, f (=1/Period of oscillations) is the temporal frequency and t_0 is the data length in days.

The amplitude and phase of the fitted temperature anomalies for the wave number 1 to 4 are calculated using equation 7.2. The amplitude spectra for each longitudinal grid for a season is obtained, which shows more or less coherent structures. These coherent spectra are planetary in nature. These amplitude spectrums for each longitudinal grid are averaged. The averaged spectra for wave numbers 1-4 represent the dominant periodicity throughout the equatorial belt. The amplitude spectra for the wave number 1-4 in different seasons are shown in Figures 7.6 to 7.9, respectively. Figure 7.6 shows temporal frequency (period) - amplitude spectra obtained for the zonal wave number k = 1 during different seasons. The spectra during different seasons in Figure 7.6 shows strong peaks at period from 18 to 23d (T1) which have maximum amplitude over the altitude region above tropopause to 30 km (Z1) as listed in Table 7.1.

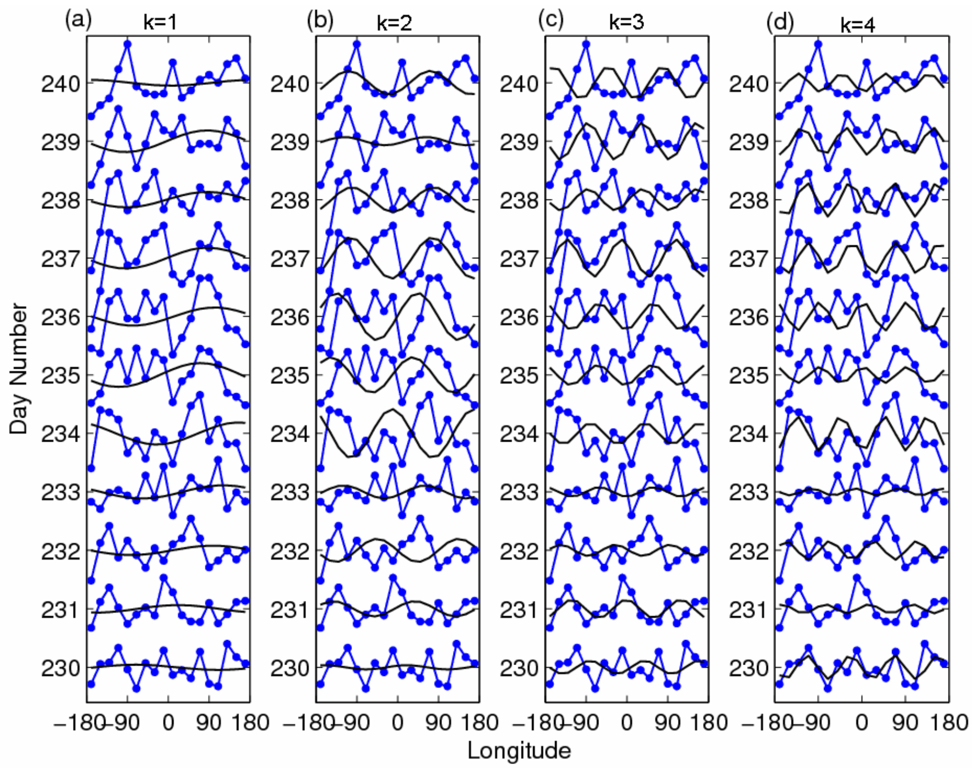

Figure 7.5: *Typical examples of the cold point tropopause altitudes anomalies (deviation from equatorial zonal mean) (blue curve) fitted for wave number 1, 2, 3 and 4 (black curve) respectively, for day number 230-240 (18- 28 December 2006, starting with day number1 as 1 August 2006). Each curve is separated by 5 scale factor.*

Two maxima of the amplitude can be seen from Figure 7.6 during JJA07, SON07, DJF08 and MAM08. The maximum at the higher altitude is most prominent during season DJF08. Weak westerly exists in lower stratosphere during September 2006- May 2007 and June2008-August 2008 while easterly appears during June 2007 –May 2008 (Figure 7.10). Although wave period is same ~ 18-23d in both these phases phases, the wave amplitude is confined to a narrower altitude region during westerly phase when compared to easterly phase of the QBO which is clear from Figure 7.10 (a). It is interesting to note that the transient wave doesn't, in general, strongly extend down to tropopause altitudes (shown as horizontal lines in figure and values are listed in Table 7.1) or below. However, there are the seasons such as SON06 and MAM07 during which the waves extend down to tropopause altitude, consistent with Figure 7.3(a) and Figure 7.3 (c), respectively.

Table 7.1: *The dominant periods (T1 and T2) and their altitude of occurrence (Z1 and Z2), the corresponding wavelength for T1 and altitude of cold point tropopause for the wave number1 are listed for different seasons.*

For wave number (k) =1						
Season	T1	Z1	T2	Z2	λ_z	Z_{CPT}
SON06	~18d	~16-23 km	~12d	~23 km	~5-6 km	16.9 km
DJF07	~18d	~18-20 km	~10d	~22 km	~4-5 km	17.5 km
MAM07	~23d	~16-19 km	~9- 12d	~21 km ~27 km	~3-5 km	17.4 km
JJA07	~18-23d & ~23d	~17-20 km & ~21-26 km	~12d	~17-30 km	~6-7 km	17.0km
SON07	~23d	~17-20 km	~10d	~19 km ~28 km	~6-7 km	17.0 km
DJF08	~18d	~17-20 km ~22-26 km	-	-	~6-7 km	17.5 km
MAM08	~23d	~17-19 km ~21-25 km	-	-	~6 km	17.4 km
JJA08	18-23d	~17-19 km	-	-	~3-4 km	16.7 km

Another interesting observation is that the wave periodicity less than 10 days does not exist in the wave number 1 spectrum. There are another class of spectral peaks with shorter period ~9-12 days (T2) in the altitude region Z2 listed in Table 7.1. Note that the wave number 1 is hardly dominant below the tropopause region. In contrast, wave numbers 2, 3 and 4 exists only in and around the tropopause region. From Figures 7.7 to7. 9, it is clear that wave number 2, 3, and 4 spectra with period ~ 5-20 days (the periodicity less than 5 days is not considered in the present analysis) are confined to the region ~ 15-20 km. Interestingly, these frequency-amplitude spectrums are observed to be located in the region of westerly shear zones [Figure 7.10 (b)].

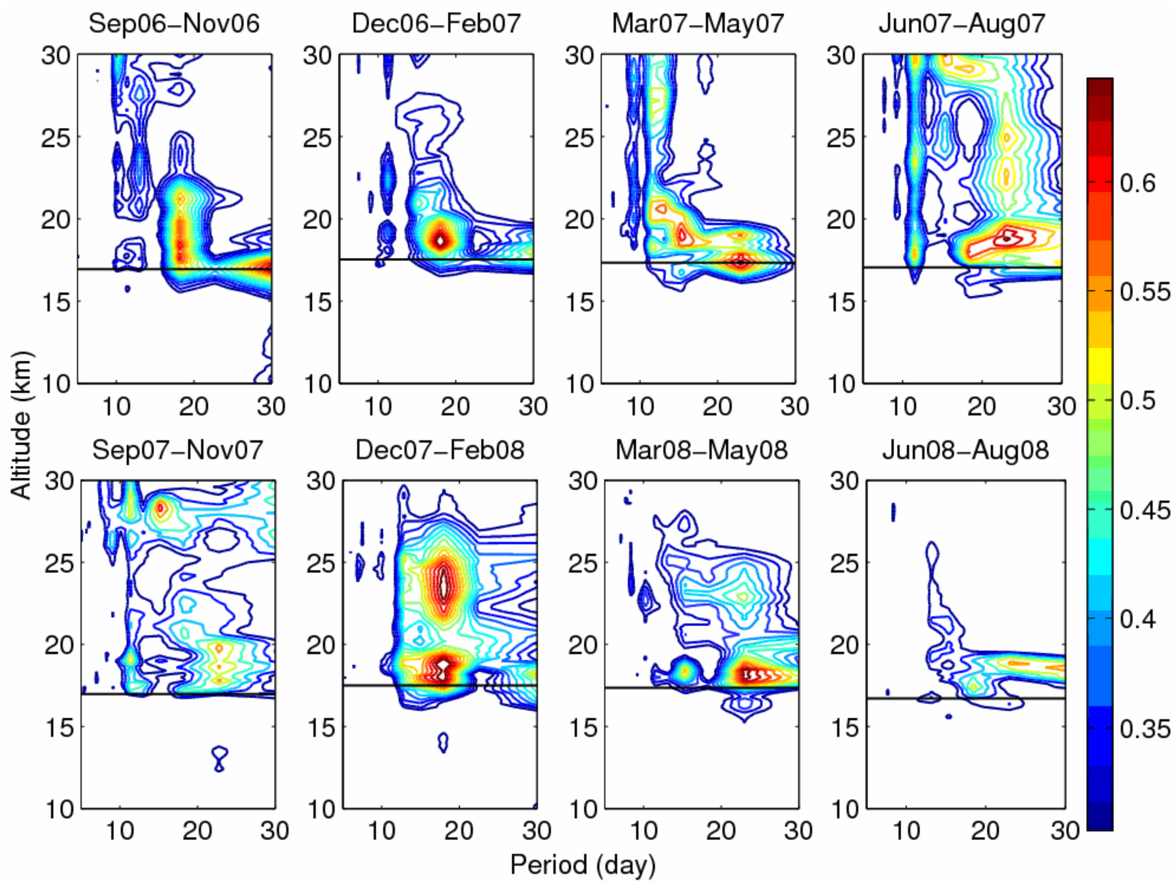

Figure 7.6: *Altitude profiles of zonal wave number 1 space time spectra calculated from gridded COSMIC data for different seasons during August 2006-August 2008. Black line represents altitude of cold point tropopause.*

7.3.3 Amplitude and Phase Characteristics of Wave numbers 1 to 4

The vertical structures of the amplitude of the waves for wave number 1of the periods T1 (~ 18-23d) (underlined values in case of range) listed in Table 7.1 during different seasons are shown in Figure 7.11. These features show the characteristics of the Kelvin wave (eastward phase tilt with height) with coherent vertical structures and large amplitude near and above the tropopause (indicated by dot in each panel). However, the amplitude decreases sharply by a factor of ~3-4 away from the altitude range of these maximum amplitude zones. It is worth to mention that there is significant depression of the tropopause altitude (~ 600 m) near ~ 60^{o}E associated with the Kelvin wave during JJA07 and JJA08. As mentioned earlier, the maximum wave amplitude is confined to narrower regions for the seasons during the westerly phase of the QBO when compared to the season falling in the easterly phase of the QBO.

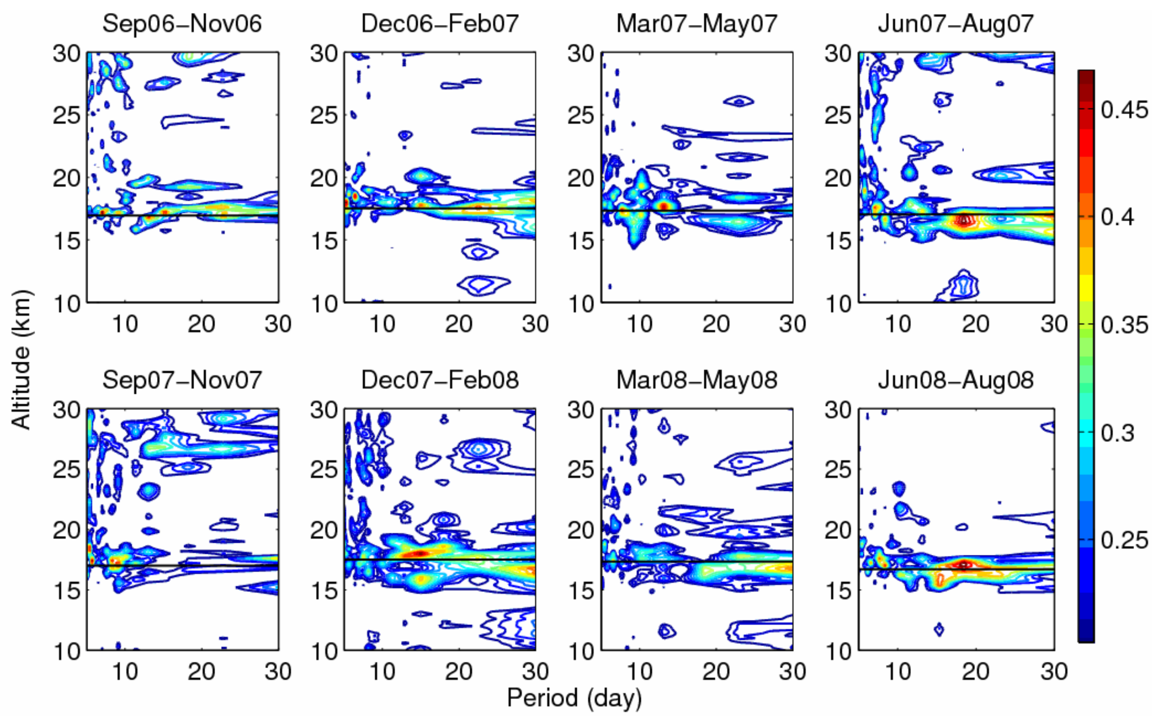

Figure7.7: *Same as Figure7. 6 but observed for zonal wave number 2.*

The coherent zonal structure of the amplitude shows two symmetric shapes. These symmetric shapes of the amplitude maxima are most evident near and above the tropopause altitudes and show different structures during different seasons which are pronounced during easterly phase of the QBO in comparison to westerly phase of the QBO. The centers of these symmetric shapes are separated by 180^{o}. Figure 7.12 shows the eastward phase propagation of the Kelvin wave corresponding to the amplitude shown in Figure 7.11. The height- longitude variations in the phase for the wave number 1 and period T1 shows the characteristics of tilted constant phase. This phase systematically progresses (grows) as one move from west longitude to east longitude at given altitude in the lower stratosphere.

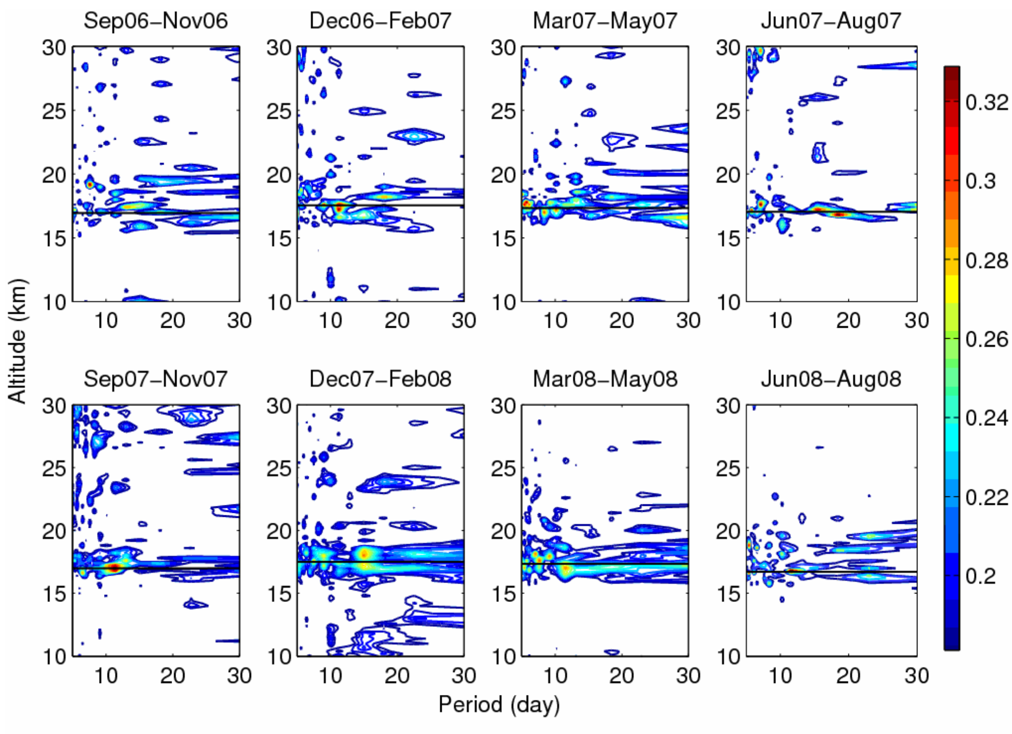

Figure7.8: *Same as Figure7. 6 but observed for zonal wave number 3.*

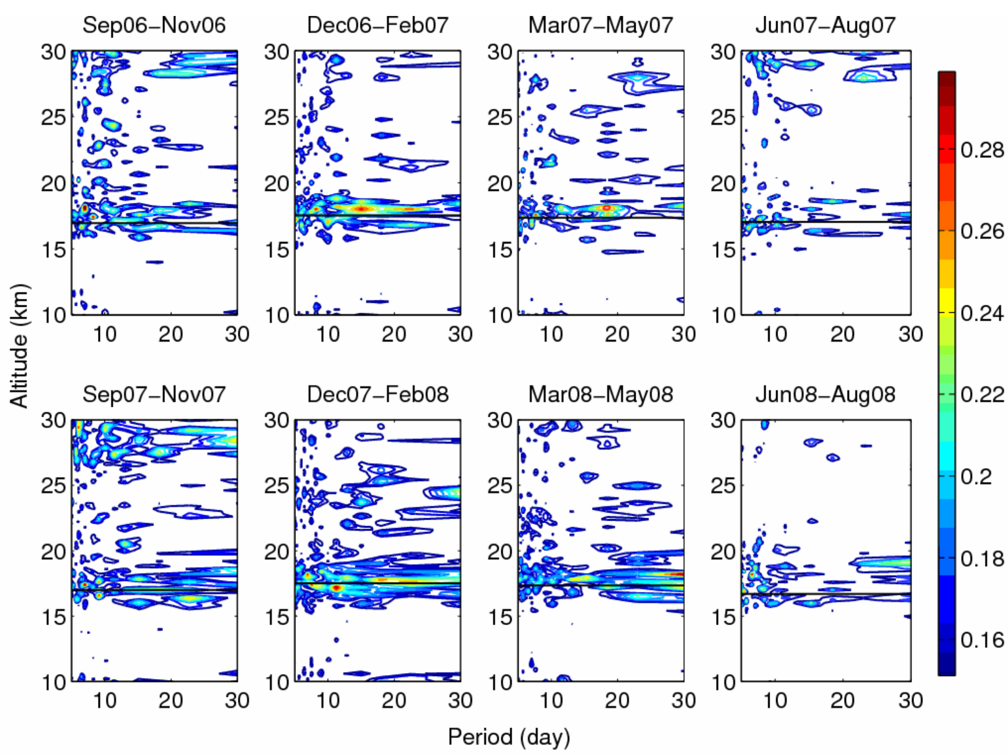

Figure7.9: *Same as Figure7. 6 but observed for zonal wave number 4.*

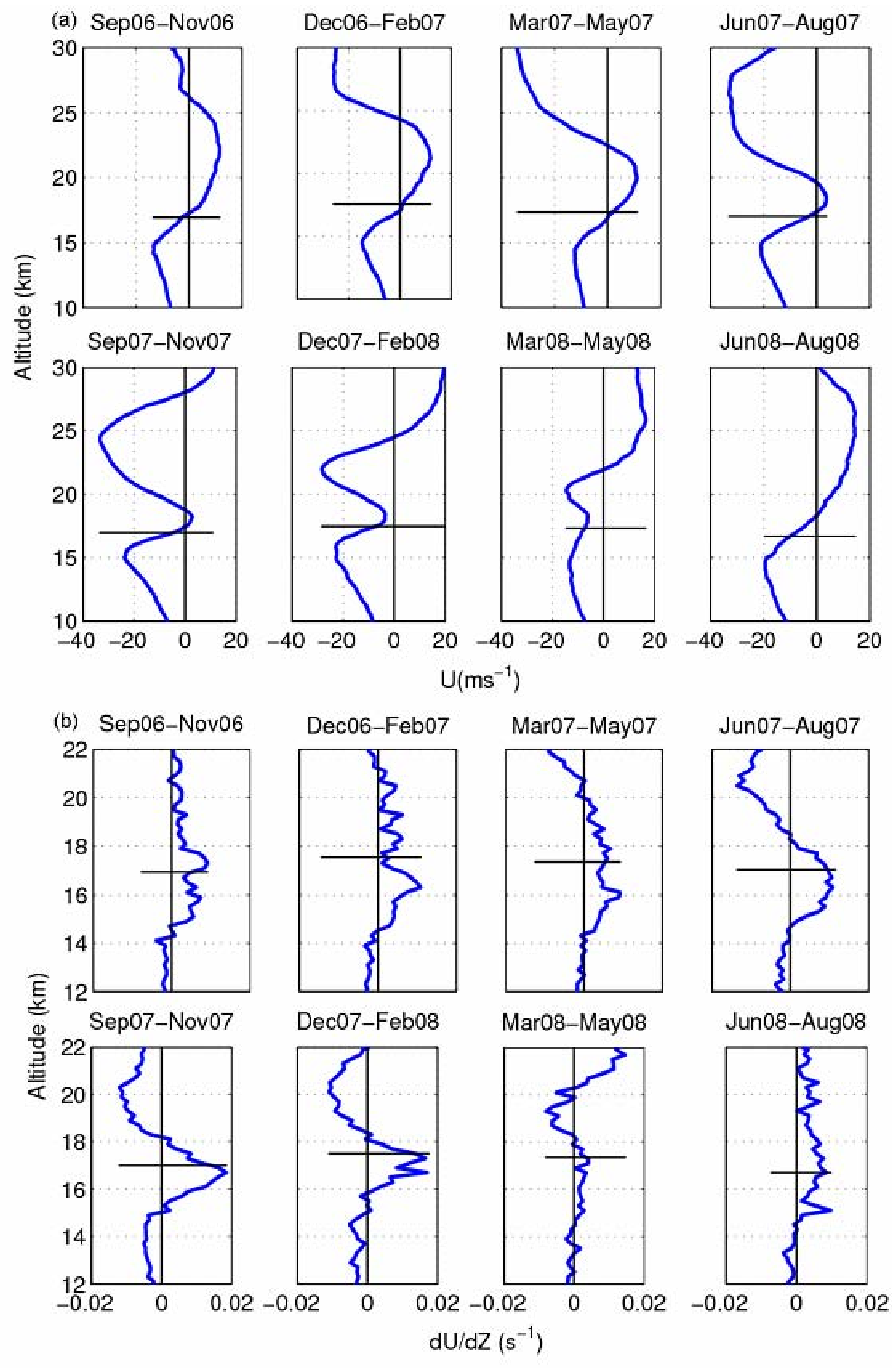

Figure 7.10: *(a) The seasonal mean zonal wind and (b) the vertical shear of horizontal wind observed over Singapore during different seasons.*

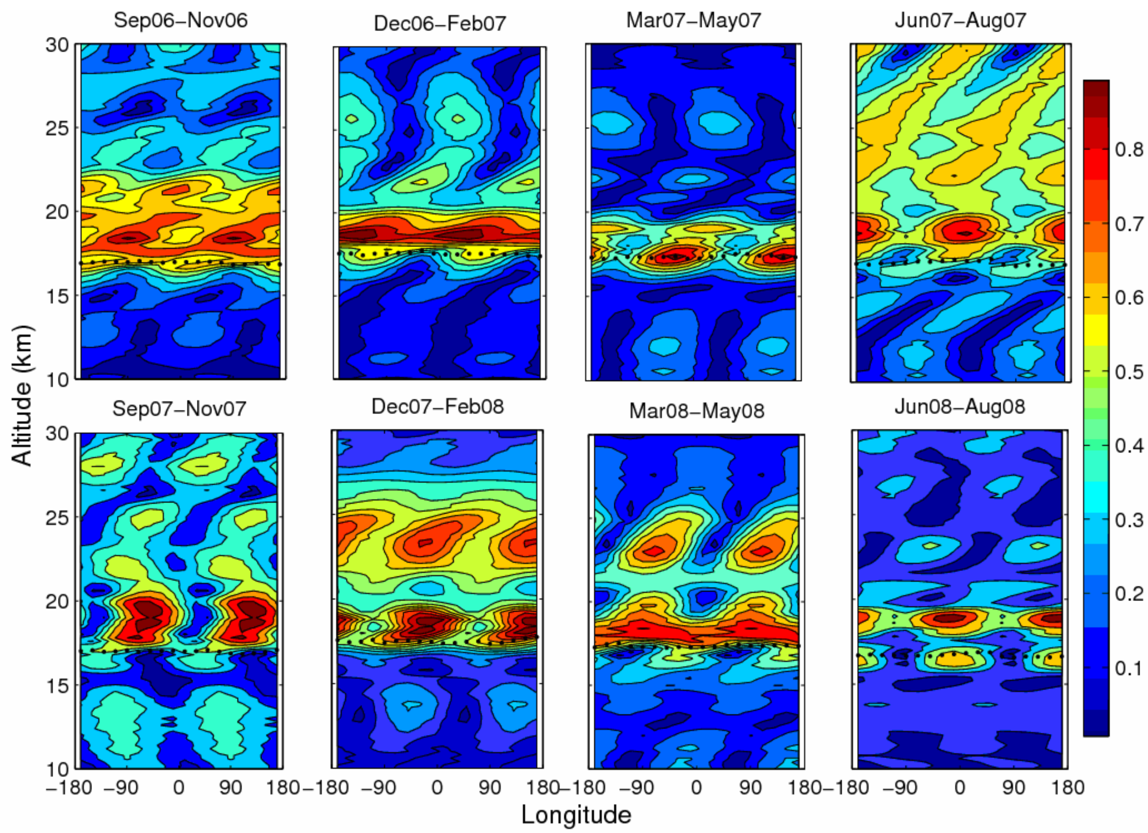

Figure7. 11: *Altitude - longitude section of the amplitude for wave number 1 and period 18-23 days (listed in Table1) during different seasons over 10^{o}S -10^{o}N.*

Therefore, constant phase tilt can be described as; the constant phase starts at lower altitude at west longitude (180^{o}W) and end at higher altitude at east longitude (180^{o}E). The vertical wavelength can be obtained as altitude difference between any two consecutive constant phase lines. The measured vertical wavelength (λ_z) is also listed in Table 7.1. It is seen that the vertical wavelength is shorter during westerly phase of the QBO (~3-6 km) in comparison to easterly phase of the QBO (~ 5-7 km). During June 2008-August 2008, the phase lines with altitude in the upper troposphere are almost steady (constant) indicating the source in this region. However, the phase lines are found to extending even below the tropopause to the upper troposphere during December 2007-May 2008 which may indicate that source lie few kilometers below the tropopause. Note that there are some discontinuities in the phase lines at ~20 km during MAM07, at ~ 17 km during SON07, at ~ 25 km during DJF08 and JJA08. At and above these discontinuities the phase lines appear as standing or tilted westward. From Figure 7.12 it is quite interesting to see that the phase lines are connected as continuous propagation from one season to other season.

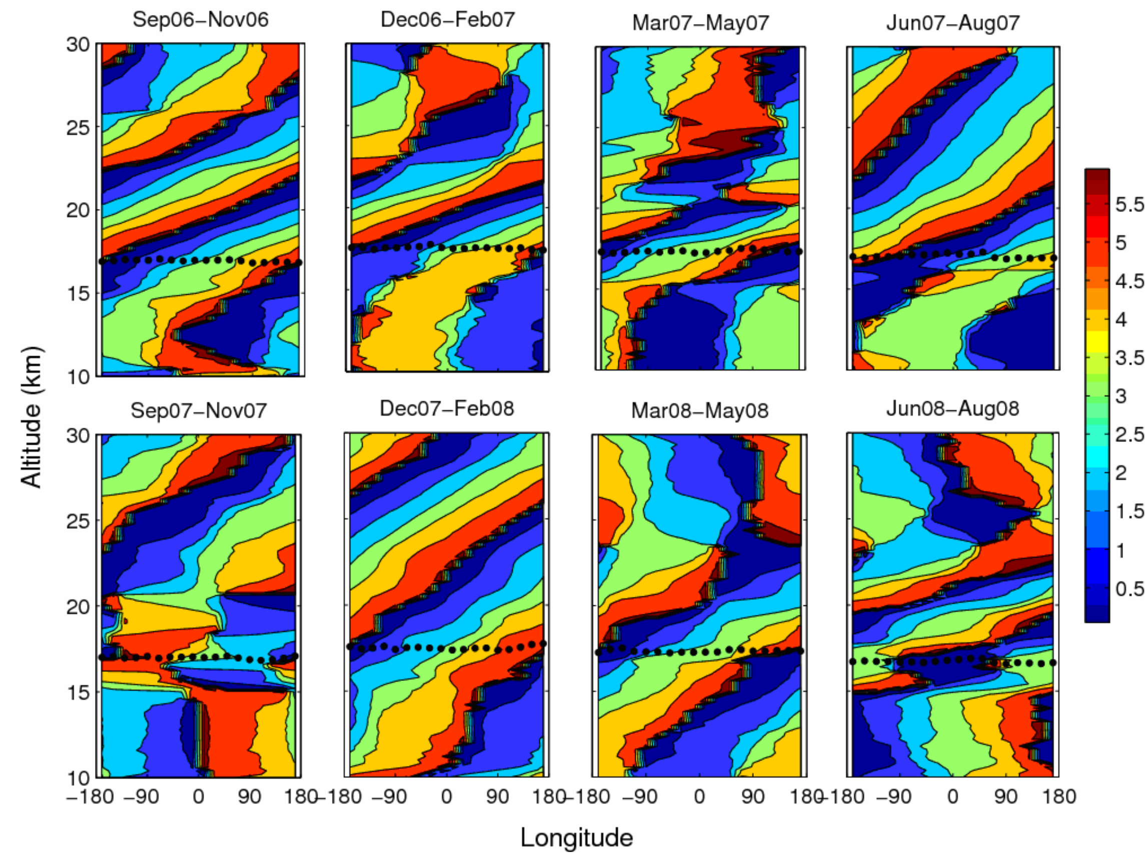

Figure 7.12: *Same as Figure7. 11 but show Phase section.*

The amplitude and phase propagation of the short period Kelvin wave (T2~ 10-12 day) of wave number 1 are shown in Figure 7.13. The amplitude shows similar structure as observed in Figure 7.11. The phase lines of the faster Kelvin waves are extended to higher altitudes above tropopause with longer vertical wavelengths in comparison to the higher period Kelvin waves. The tilting angle of the phase lines with altitude is less for short period Kelvin wave compared to higher period Kelvin waves. The amplitude and phase propagation of the wave number 2 for the period of 15 days during DJF07 and DJF08 and for period 18 days during JJA07 and JJA08 are shown in Figure 7.14. As mentioned earlier the wave number 2 is confined to the altitude region ~ 15-20 km, near the tropical tropopause. From Figure 7.14 (a) it is clear that the amplitude structures show eastward tilt with altitude.

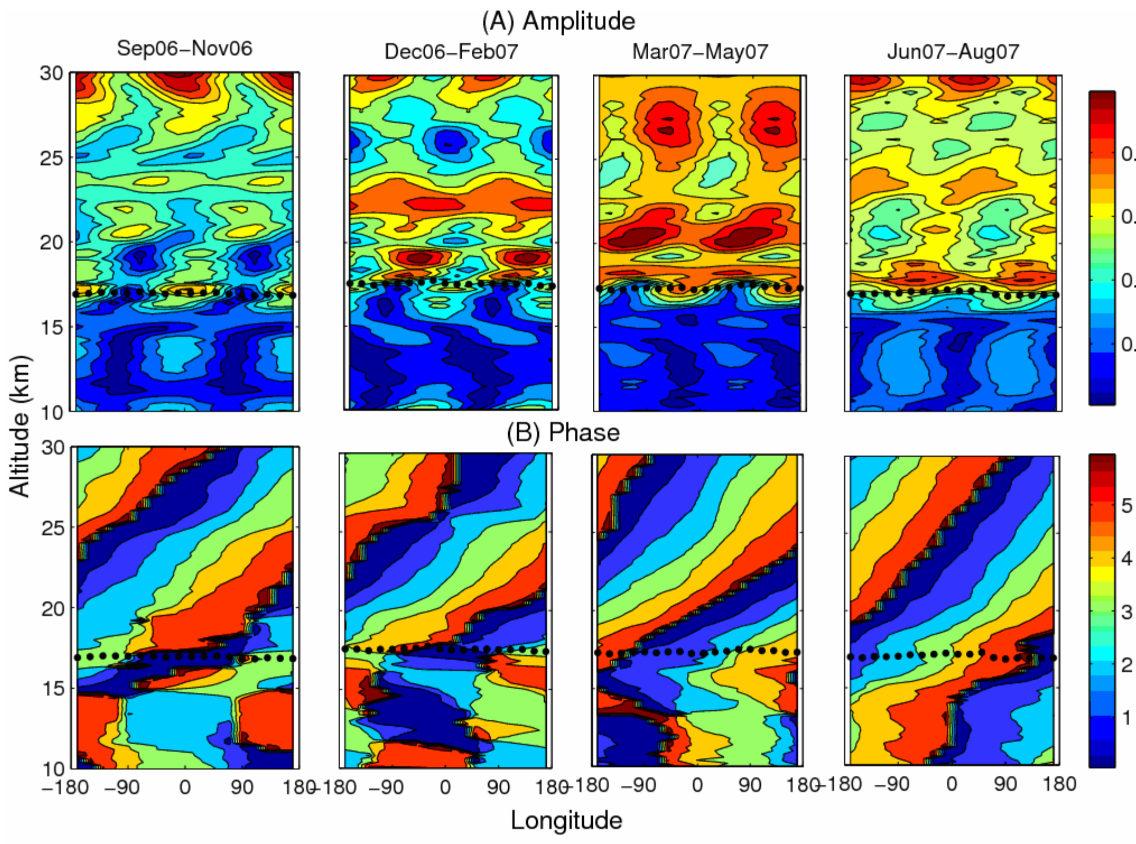

Figure 7.13: *Altitude - longitude section of the (a) amplitude and (b) phase for wave number 1 and period 10-12 days during different seasons.*

There are centers of four symmetric maxima observed near the tropical tropopause. However, there is another symmetric maximum at ~ 20 km and at ~ 16 km also seen during DJF07 and DLF08, respectively. The phase line shows eastward tilt with altitude confirming that these are of Kevin waves. The vertical wavelength is ~ 2-4 km. Similar feature can be observed for the wave number 3 for the periods 12d, 18d, 15d and 12d during DJF07, JJA07, DJF08 and DJF08, respectively, as shown in Figure 7.15. There are six centers of maxima can be observed. The vertical wavelength of wave number 3 is ~ 1-3 km.

7.3.4. Modulation of the Tropical Tropopause

The tropopause is warmer and lower during NH summer while colder and higher and NH winter, respectively. However, the day to day grided tropopause altitude and temperature in different seasons show that their variability is not always in out of phase.

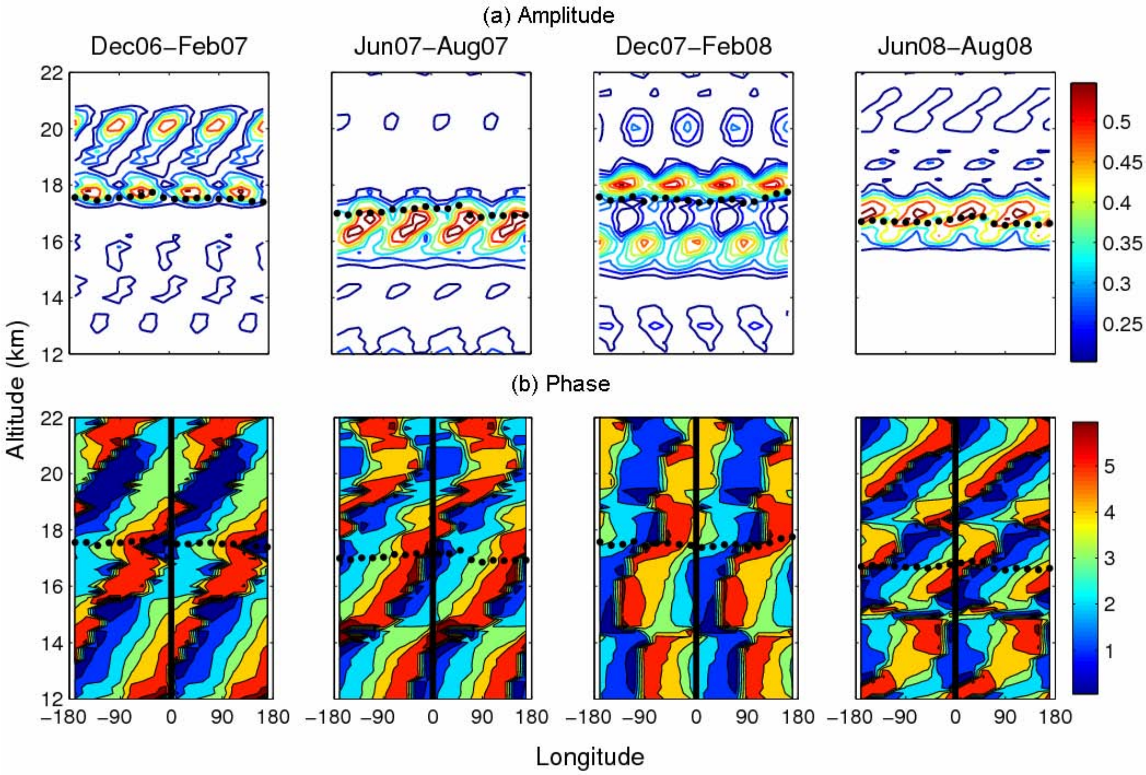

Figure 7.14: *Height - longitude section of the (a) amplitude and (b) phase for wave number 2 and period 15-18 days during different seasons.*

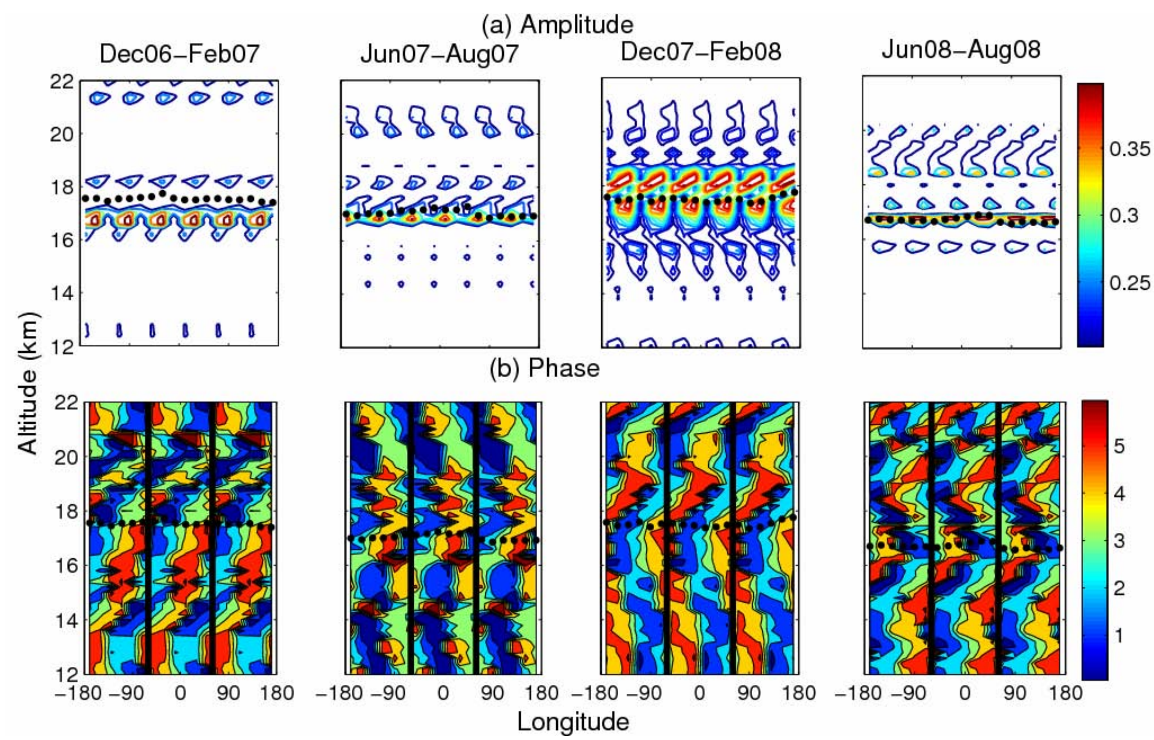

Figure 7.15: *Same as Figure 7.14 but for wave number 3.*

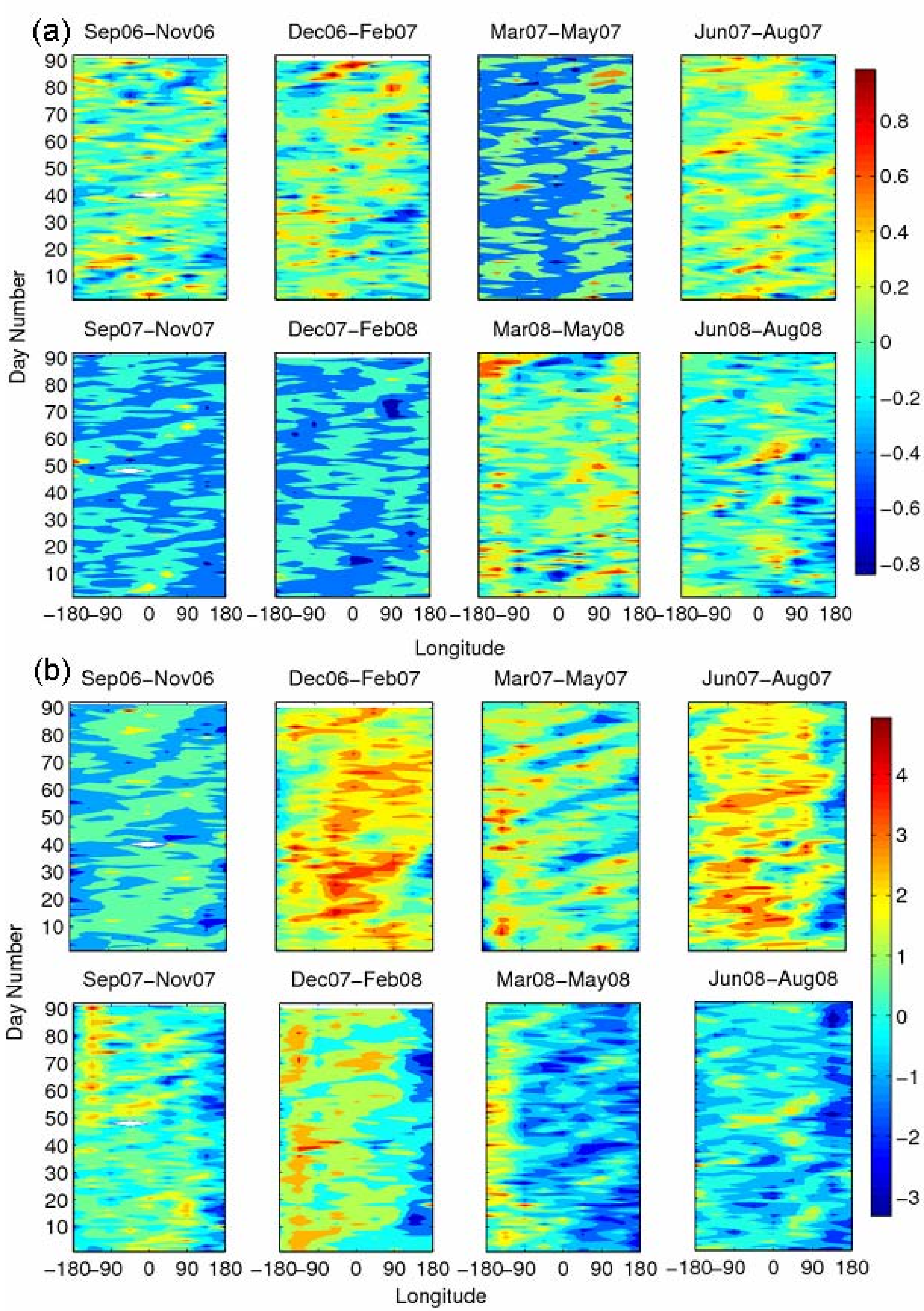

Figure7.16: *The tropopause (a) altitude, and (b) temperature anomalies observed during different seasons.*

The correlation between the grided cold point tropopause altitude and temperature in different seasons is calculated. The correlation coefficient for different seasons namely SON06, DJF07, MAM07, JJA07, SON07, DJF08, MAM08 and JJA08 are (-0.25), (-0.26), -0.06, (-0.22), (-0.48), -0.12, -0.10, and (-0.46), respectively. The correlations estimated at 95% confidence level are shown in the brackets.

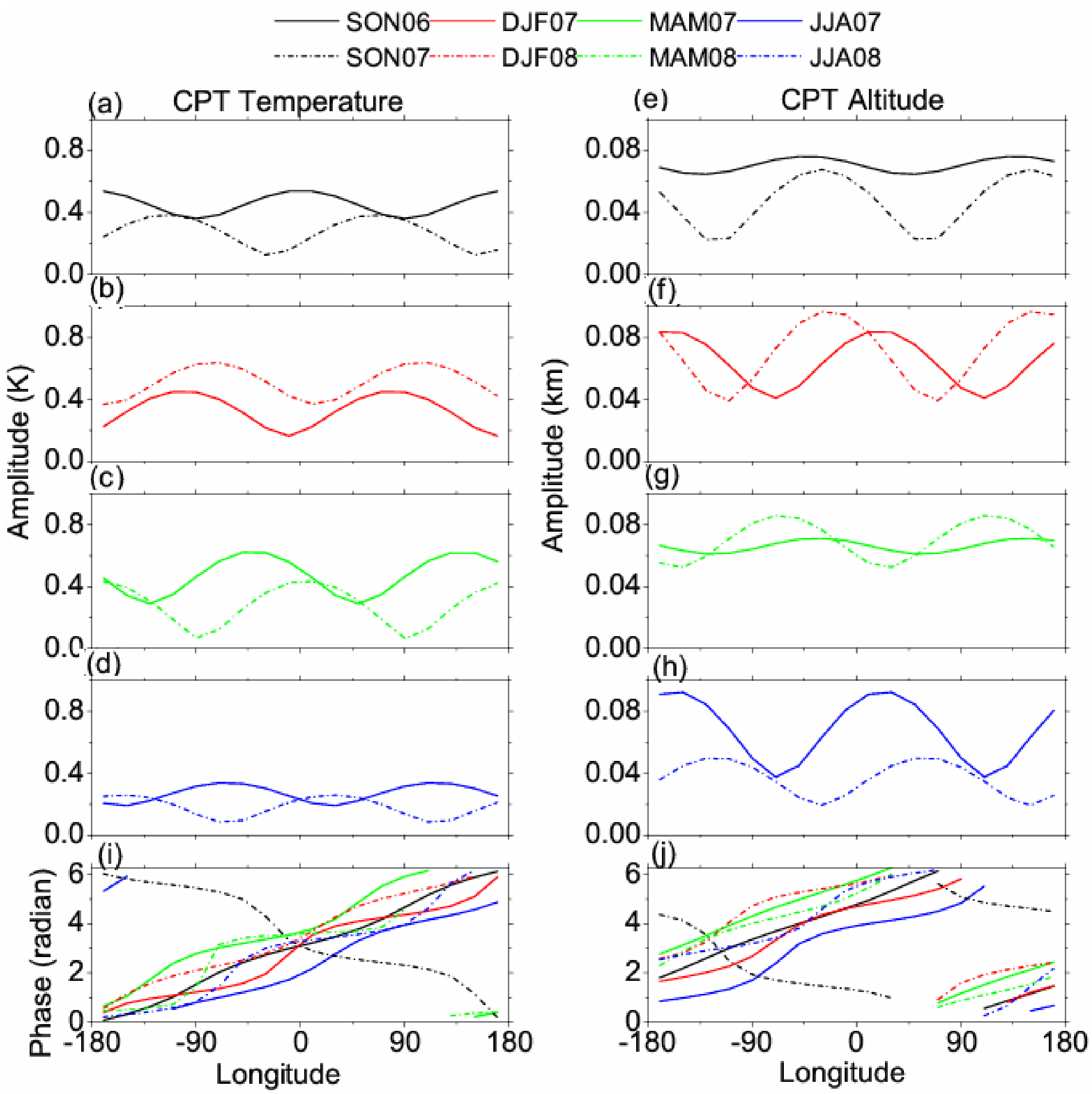

Figure 7.17: *(a) - (d) is the amplitude of CPT temperature and (e)- (h) amplitude of CPT altitude. (i) and (j) are the corresponding phases of CPT temperature and altitude, respectively, of wave number 1 observed during different seasons for the periods 18-23 days (listed in Table1).*

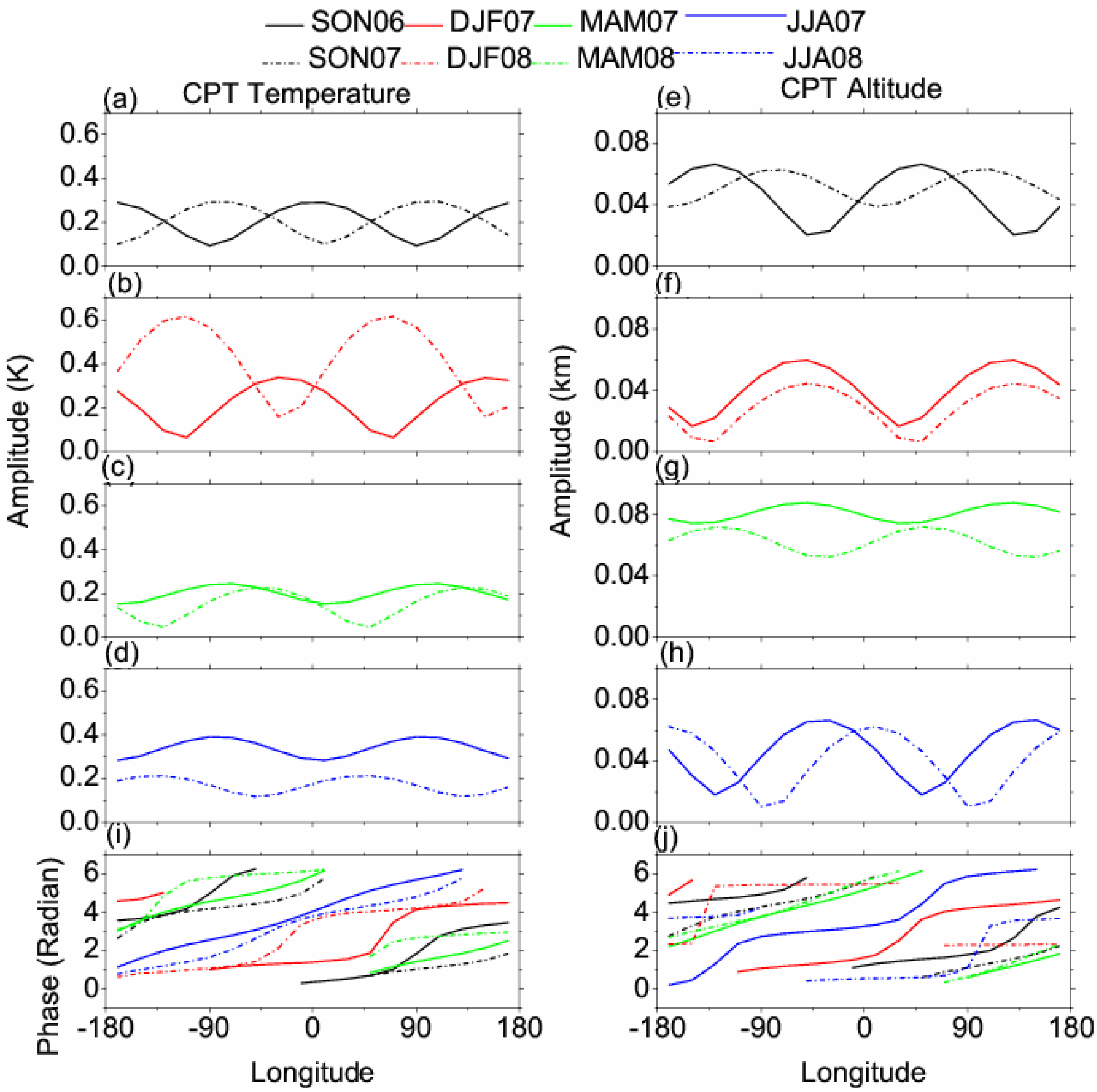

Figure 7.18: *Same as Figure 7.17 but for the period 9-15 day (listed in Table1).*

The cold point tropopause altitudes and temperatures are well negatively correlated for the seasons SON06, DJF07, JJA07 SON07 and JJA08. Poor or no correlation is found during seasons MAM07, DJF08 and MAM08. The correlation between OLR and tropopause temperature is also estimated. It is interesting to see the positive correlation between OLR and tropopause temperature only during DJF08 (0.34) and MAM08 (0.33) for which the correlation between tropopause altitude and temperature was poor. Note that the tropopause altitude and OLR are not found to be correlated. The tropopause temperature and altitude anomalies are shown in Figure 7.16.

The dominance of the waves with various scales can be clearly seen from the Figure 7.16. As mentioned earlier, note that the tropopause altitudes show the fluctuations in wave number 1 to 4 (see Figure 7.5). Spectral analysis for the tropopause altitude and temperature is carried out during different seasons.

The dominant wave periods during different seasons are listed in the Table 7.2. Figure 7.17 (a)-(h) shows the amplitude and Figure 7.17 (i)-(j) shows phase plots of the wave number 1 component for cold point tropopause temperature and altitude for the periods (18-23 days) listed (in bold) in Table 7.2. The amplitudes of the tropopause temperature and altitude show two maxima separated by 180^{o} in longitude. The tropopause altitude and temperature are modulated with same wave period in the range of 18-23 days. The phase diagram of tropopause altitude and temperature clearly show eastward traveling Kelvin waves during all the seasons except SON07. The phase of both tropopause altitude and tropopause temperature show westward propagation (Rossby waves) during SON07. Similarly, the phase of tropopause altitude and temperature for the period 9-15 days of wave number 1 shows eastward propagation which is clear from Figure 7.18.

Table 7.2:*The dominant periodicity of the cold point tropopause temperature and altitude for wave numbers 1 to4 during different seasons.*

	k=1		k=2		k=3		k=4	
Season	CPT-T	CPT-H	CPT-T	CPT-H	CPT-T	CPT-H	CPT-T	CPT-H
SON06	10,**18**	12,**18**	6.5,9	7.5,10	6.5,11	6,8	6.5,9	7.5,13
DJF07	10,**18**	12,**18**	7, 9	7.5,13	6,11	6.5,8	7,11	7,11
MAM07	9,**23**	15,**23**	6.5, 10	7.,13	7,11	6.5,8	7,10	7,13
JJA07	12,**23**	15,**23**	6.5,10	6,9	7,11	6,9	6.5,9	6.5,11.5
SON07	13,**23**	12,**23**	7.5,10	6.5,10	6.5,11	7,10	6.5,13	7,10
DJF08	15,**18**	9,**18**	7.5,10	7,9	7.5,11	6.5,9	7.5,11	7,10
MAM08	10,**23**	15,**23**	6.5,10	7,13	7,11	7,13	7.5,11	8,11
JJA08	13,**18**	12,**18**	7.5,11	7.5,	6.5,9	6,9	6.5,9	7.5,10

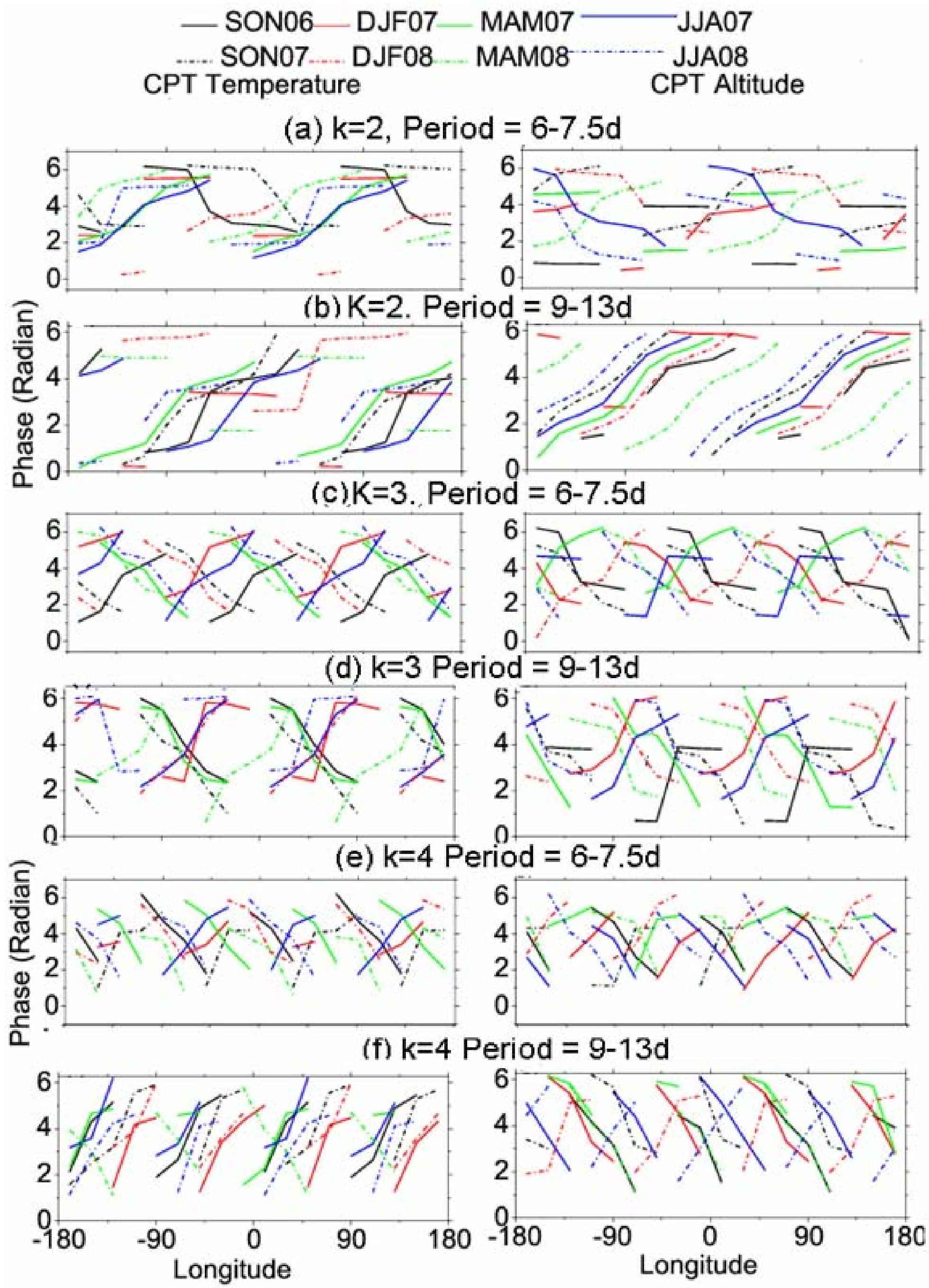

Figure 7.19: *The phase diagrams of tropopause temperature (left panels) and altitude (right panels) for period 6-7.5d and 9-13d for wave number 2-4 during different seasons.*

Note that the amplitudes of different periodicities of the wave number 1 are in the range of 0.1 to 0.7 K for CPT temperature and 0.02 to 0.08 km for CPT altitude. Similar spectral analysis is carried out for wave number 2, 3 and 4. The dominant periods are listed in Table 7.2. The phase diagrams for tropopause temperature and tropopause altitude for period 6-7.5d and 9-13d of wave number 2-4 during different seasons are shown in Figure 7.19. The evidence of modulation the tropical tropopause by both Kelvin wave and Rossby waves can be noticed. For wave number 2 and period 6-7.5d, tropopause temperature is modulated by Kelvin wave during all the seasons except during SON06 and SON07 which is seen modulated by Rossby waves as can be inferred from the phase propagation (Figures 7.7 and 7.18).

The tropopause altitude is modulated by Kelvin waves during SON06, DJF07, MAM07, SON07 and MAM08 while during JJA07 and JJA08 Rossby wave dominates. For wave number 2 and periods 9-13d, both tropopause altitude and temperature are found modulated by Kelvin waves. For wave number 3 and period 6-7.5d, tropopause temperature is modulated by Kelvin wave during SON06, DJF07 and JJA07 while the rest of the seasons show dominance of Rossby wave. The tropopause altitude is found modulated by Kelvin wave during MAM07, JJA07 and DJF08 and rest of the seasons by Rossby wave. During DJF07, DJF08 and JAJ07, JJA08, the period 9-13d is manifestation of Kevin wave and during rest of the seasons by Rossby wave.

For wave number 4 and period 6d -7.5d, tropopause temperature is modulated by Kelvin wave during DJF06 and JJA07 while rest of the seasons show dominance of Rossby wave. The tropopause altitude is modulated by Kelvin wave during MAM07, JJA07 and DJF08 and rest of the seasons by Rossby wave. During DJF07, MAM07 and DJF08, the period 9-13d are modulated by Kevin wave and rest of the seasons by Rossby wave. For period 9-13 day, only MAM08 shows Rossby waves and rest by Kelvin wave while tropopause altitude is modulated by Kelvin wave during DJF08 and JJA08 and rest show dominance of Kelvin wave.

7.4. Summary

By taking advantage of dense number of occultations from six satellite COSMIC GPS RO measurements, the modulation of tropical tropopause by the equatorial Kelvin and Rossby waves has been investigated. The main findings are summarized below:

1) Both ground based observations from Singapore and Gadanki show similar temperature anomalies as that observed by COSMIC GPS RO measurements providing strong support to use GPS RO data for studying the equatorial waves.
2) Modulation of tropical tropopause by the equatorial Kelvin wave and Rossby waves is clearly noticed. The waves with zonal wave number up to 4 are found significant in modulating the tropopause.
3) Although period remains same, it is seen that the vertical wavelength is shorter during westerly phase of the QBO (~3-6 km) in comparison to easterly phase of the QBO (~ 5-7 km).
4) Kelvin waves with periodicity less than 9 days do not exist in the wave number 1 spectrum.
5) The waves with period ~ 5-20 days are confined to the region ~ 15-20 km with dominant wave numbers 2-4.
6) The cold point tropopause altitudes and temperatures are well negatively correlated but not in all the seasons.
7) No correlation is found between the tropopause altitude and OLR. Interestingly, the positive correlation between OLR and tropopause temperatures are noticed for which the correlation between tropopause altitude and temperature was poor.

Thus detailed investigation of the tropical tropopause is carried out with possible source of data and techniques whose results are summarized in next Chapter 8.

---END---

Chapter 8

Summary

In this final Chapter, the contribution of the research which presented in Chapters 3-7 is briefly summarized. An attempt has been made to understand the characteristic of the tropical tropopause by using high resolution MST radar, Radiosonde and COSMIC GPS RO data, in particular over Indian monsoon region. Although, several studies have been carried out, but still the basic question such as how tropopause form is not fully understood. It is highly difficult to answer if someone asks that how variable the tropopause on short term scale, however, several possibilities can be listed but exact answer is still missing. There are many such question are remain to answers. In the beginning of the thesis, a few questions were arises and attempt has been made to answer those questions are briefly described in chapter 3-7 and which are summarized below. These answers are summarized under the heading of the question’s main theme.

8.1. Tropical Convective Tropopause

The base of TTL, convective outflow level, is defined by several methods. Using radiosonde observations, the convective outflow level i.e. the altitude (Z_L) of the local minimum of potential temperature is obtained. The convective out flow level can also be determined directly from vertical wind observations. Using horizontal divergence method, the altitude (Z_D) of major convective outflow level is determined. The altitudes Z_L and Z_D from theses two independent techniques are found to compare well. Further, the correlation analysis between the two, in general, reveals a good comparison with some scatter which can be explained as due to potential temperature is mainly driven by local effect while vertical wind is by non-local effect. However, these two techniques represent same altitude especially during the deep convection. The physical basis for the observed relation between the low in the potential temperature lapse rate and high in the vertical velocity i.e. maximum horizontal divergence are inversely related in the thermodynamic energy equation, in the absence of local rate of temperature and horizontal advection. Thus, the major convective outflow level gives good measure of the base of the TTL and can be taken as altitude of the convective tropopause. During deep convection, Z_D is found at higher altitude, thereby decreases the thickness of the TTL.

8.2. Variability of the Tropical Tropopause

The characteristics of tropical tropopause parameters such as CPT, LRT, COT and TTL on seasonal to sub-daily scale over Indian monsoon region is studied. The seasonal variation of the CPT and LRT are well known. However, the difference can be notice especially in temperature of CPT (T_{CPT}) over Indian monsoon region when compared to west pacific station (Truk). The amplitude of the seasonal variation of the attitude of the CPT ($Z_{CPT)}$ is more than attitude of the LRT (Z_{LRT}) with minimum separation between two during summer season. The seasonal variation of the CPT and COT is in out of phase. The COT reaches higher altitude during summer season i.e. during season when deep convection prevails and hence TTLt decreases, which found out of phase with COT and in phase with CPT. The probability distribution of the CPT shows that their peaks are coincided with mean value during different seasons. This distribution further shows that T_{CPT}<191 K occurs frequently during December-May than rest of the months. The short term scale variation of the tropical tropopause such as on day-to-day and sub-daily scales are investigated in detail. The wide range of the day-to-day variability in CPT is observed which are quantified based on how Z_{CPT} changes with T_{CPT} during different seasons. There are several processes such as planetary wave activity, extratropical forcing, convection, in general, can cause these variability. Based on the quantification it is observed that the CPT is adiabatically driven during summer season, while both adiabatic and diabatic processes are dominant during rest of the seasons.

The day-to-day variation of the COT is driven by adiabatic processes. The day-to-day variation of the TTLt shows association with convection especially during deep convention. The large variation in the tropopause parameters can be observed on sub-daily scale. The sub-daily variation of the CPT shows the effect of both diurnal as well as semidiurnal components. From the spectral analysis of the Z_{CPT} and T_{CPT} observed on 3-10 June 2008, it is found that Z_{CPT} shows periodicity of the ~ 24 hours and while T_{CPT} shows periodicity of ~16 and ~ 21 hours. Thus both convective and diurnal tides effects are observed in sub-daily variation of the CPT. The Z_{CPT} and T_{CPT} are well anti correlated, however, correlation between two on day-to-day scale is not always good for all the seasons. The correlation of Z_{CPT} and T_{CPT} on sub-daily scales is more during convection (TBB<240) than during clear sky conditions (TBB>240).

8.3. Longitudinal Characteristics of the Tropical Tropopause

This study has addressed the longitudinal characteristics of the tropical tropopause parameters using radiosonde data from different stations and global data from COSMIC GPS RO measurements. Although, in general, seasonal variability of the CPT shows coherent structure throughout the tropics, yet the longitudinal differences can be noticed. The amplitude (excursion) of T_{CPT} is less and Z_{CPT} altitude is highest over Gadanki when compared to the rest of the stations. The tropopause at the Pacific stations (Truk, Singapore and Darwin) is comparatively cooler (by 2-4 K) than that over the Non-Pacific stations (Gadanki, Rochambeau and Seychelles). The seasonal differences of the COT and TTLt are not as marked as CPT. T_{CPT} goes below 191 K more frequently during DJF than during JJA suggesting entry of water vapor less than 3 ppmv occurs more frequently during DJF at all the stations. The seasonal behavior of T_{CPT} anomalies shows characteristics of lower stratospheric temperature anomalies suggesting the dominance of the radiative processes than convective processes. The temperature anomalies in the upper troposphere (UT) are more or less out of phase with the temperature anomalies in the lower stratosphere (LS) except for Gadanki. Between upper troposphere and lower stratosphere there is a transition region where temperature anomalies distinguish the characteristics of both UT and LS. The depth of penetration of stratospheric effect is more for the stations near the equator than the stations away. The lapse rate behavior between altitude at 15 km and Z_{CPT} show quit distinct characteristics among the stations. The low value of the lapse rate (~2 K/km) between 15 km and CPT over Gadanki during DJF is quite interesting. Though, Z_{CPT} and T_{CPT} shows strong seasonal variation, yet the relation between Z_{CPT} and T_{CPT} is not simple linear. The anomalous departures between Z_{CPT} and T_{CPT} show association with changes in the θ_{CPT} which indicates the influence of diabatic heating, especially, during May -June. The θ_{CPT} and θ_E for Truk and Singapore are nearly equal, which suggests that the boundary layer moisture flux is carried to the higher altitude near to CPT. From the global measurements of the tropopause parameters over tropical region it is found that these are accompanied with zonally non uniform convection.

8.4. Characteristics of Multiple Tropical Tropopauses

In pervious sections it is assumed that the tropopause is well defined as CPT, however, several times it is observed that temperature profile exhibits structure like CPT in the altitude regions of 150 hPa -50 hPa. The detailed analysis is carried out to identify these structures using WMO definitions. Based on WMO definitions, the tropopause other than LRT are defined as multiple tropopauses (MTs). The WMO definition which is based on the lapse rate is not able to identify all the MTs, due to its threshold value used. Thus in the present study, a new method is proposed based on the CPT and neighboring points of inflection to identify the MTs. The percentage of the occurrence of MTs (LT, ST and TT) is calculated which is ~25-50% using the present method while those from WMO definitions is ~10-30% only. In the present method, the MTs can occur both below and above the CPT unlike WMO definitions. It is found that MTs occur more frequently above the CPT than below. At the most only two MTs (not counting the CPT) occur. While there is no consistent seasonal variation in the occurrence of MTs there is an indication of broad peak in NH summer season. On the other hand, significant seasonal variation in the LT and ST altitude and temperatures is observed closely following CPT. LT is found to be closer to CPT and cooler in comparison to ST. The occurrences of MTs are higher over equator and decrease away towards higher latitudes in the tropics. Longitudinal variation of the MTs is observed with relatively high occurrences during NH summer season over Indian Ocean. While the CPT temperature is lowest at the equator the CPT altitude is not always highest at the equator. The equatorial minimum in the CPT temperature is broader and lower in the eastern hemisphere than the western hemisphere. The saturation water vapor mixing ratio can attain values as low as 3 ppmv even at LT during some moths.

The possible mechanism is proposed to interpret these MTs. These MTs may occur due to planetary scale waves or due to horizontal advection of air from surroundings or cirrus clouds formation and subsequent lowering of the temperatures or a combination of these. The occurrences of the MTs are found associated with planetary wave activities which are known for modulating the day to day variation of the CPT.

8.5. Modulation of Tropical Tropopause by Equatorial Waves

Earlier reports and previous sections suggest that the short term variation of the tropopause is modulated by the planetary wave activities. The existence of the planetary waves such as Kelvin waves (period 5 -20 days and wave number 1 and 2) and Rossby gravity waves (4-5 days, wave number 4) in modulating the CPT are well known. However, from present analysis by taking advantage of dense number of occultations from six satellite COSMIC GPS RO measurements, it is observed that Kelvin waves for the wave numbers 3 and 4 besides 1 and 2 are also found in modulating the tropopause. The strength of the planetary wave activities is, in general, different during different phases of the QBO. It is seen that the vertical wavelength is shorter during westerly phase of the QBO (~3-6 km) in comparison to easterly phase of the QBO (~ 5-7 km). Kelvin waves with periodicity less than 9 days do not exist in the wave number 1 spectrum. The waves with period ~ 5-20 days are confined to the region ~ 15-20 km with dominant wave numbers 2-4. The CPT altitudes and temperatures are well negatively correlated but not in all the seasons. No correlation is found between the tropopause altitude and OLR. Interestingly, the positive correlation between OLR and tropopause temperatures are noticed for which the correlation between tropopause altitude and temperature was poor.

8.6. Recommendations for Further Studies

One important area which needs through investigation is the relationship that exists between low in the stability and high in vertical mass flux. By taking simultaneous observations of the radiosonde and MST radar the clear sky radiative heating rate can be estimated to obtain the closure on the relationship of low in the stability and high in vertical mass flux. Further, more number of the observations from the MST radar along with radiosonde can be utilized for better understanding the short term variations of the tropopause during different phases of the convection. Another important area is that the exchange of the air between the troposphere and stratosphere. It is now known that the tropopause temperature goes below 191 K during winter season, therefore, direct exchange of the mass flux from troposphere to stratosphere using MST radar observation can be obtained specially during those occasions when tropopause temperature is <191K. The detailed investigation of the process which determines the multiple structures observed in the vertical temperature profile near the tropopause region need to be investigated. This can be achieved using the radiative transfer model. This model can be utilized to get the various scales of the fluctuations in the temperature profile near the tropopause region to ascertain the dominant process leading to the multiple structures.

---End---

References

Anandan, V. K., P. Balamuralidhar, P. B. Rao, A. R. Jain, and C. J. Pan (2005), An adaptive moments estimation technique applied to MST radar echoes, *J. Atmos. Oce.Tech., 22*, 396-408.

Andrews, D. G., J. R. Holton, and C. B. Leovy (1987), *Middle Atmosphere Dynamics. Academic Press,Orlando, FL.*

Añel J.A., J.C.Antuña, L.de la Torre, R. Nieto, L Gimeno (2007), Global statistics of multiple tropopauses from the IGRA database. Geophys. Res. Lett. 34: L06709. doi: 10.1029/2006GL029224.

Añel J.A., J.C.Antuña, L.de la Torre, R. Nieto, L Gimeno J.M. Castanheira. (2008), Climatological features of global multiple tropopause events. J. Geophys. Res. 113: D00B08. doi: 10.1029/2007JD009697.

Angell, J. K., and J. Korshover (1964), Quasi-biennial variations in temperature, total ozone, and tropopause height, *J. Atmos. Sci*., *21*, 479–492..

Angell, J. K., and J. Korshover (1974), Quasi-biennial and long-term fluctuations in tropopause pressure and temperature, and the relation to stratospheric water vapor content, *Mon. Weather Rev., 102*, 29-34.

Angell, J. K., and J. Korshover (1975), Evidence for a quasi-biennial variation in eccentricity of the North Polar vortex, *J. Atmos. Sci*., *32*, 634–635.[Reference therein Angell et al., 1973]

Anthes, et al (2008), The COSMIC/FORMSAT-3 mission early results, *Bull. Am. Meteorol. Soc. 89*, 313– 333.

Atticks, M. G., and G. D. Robinson (1983), Some features of the structure of the tropical tropopause. *Q. J. R. Meteorol. Soc*.,109(460), 295–308.

Avery, S.K (1986), Lecture notes, Radar and remote sensing, *University of Colorado, Boulde*r, 1986.

Baldwin, M.P., L.J. Gray, T.J. Dunkerton, K. Hamilton, P.H. Haynes, W.J. Randel, J.R.Holton, M.J. Alexander, I. Hirota, T. Horinouchi, D.B.A. Jones, J.S. Kinnersley, C.Marquardt, K. Sato, and M. Takahashi (2001), The Quasi-Biennial Oscillation, *Rev. Geophys*.,39, 179-229.

Balsley, B. B., and K. S. Gage (1980), The MST radar technique: potential for middle atmospheric studies, *Pure Appl. Geophys., 118*, 452-493. [Reference therein Balsley and Gage, 1978,]

Barth, C. A., R. W. Sanders, R. J. Thomas, G. E. Thomas, B. M.Jakosky, and R. A (1993), West, Formation of the E1 Chichon aerosol cloud, *Geophys. Res. Lett., 10.*

Batchlor,G. K (1995), The scattering of radio waves in the atmosphere by turbulent fluctuations in refractive index, *Res.Rep.EE262,Sch of Elec Eng., Cornell Univ., Ithaca N.Y.*

Battan, L.J (1973), Radar observation of the atmosphere, *The university of Chicago, press*.

Bergman, J. W. and Salby, M. L (1994), Equatorial wave activity derived from fluctuations in observed convection, *J. Atmos. Sci*., *51*, 3791–3806.

Bjerknes J, E. Palmen (1937),. Investigation of selected European cyclones by means of serial ascents. *A. Meteorol. Soc. 12*, 62 pp Geofis. Publ. Boston M A.

Booker,H.G. and W.E.Gordon (1950), A teory in radio scaatering in troposphere, *Proc. IRE, 38*, 401.

Born and Wolf (1993), principle of optics, *Peramon press*, Oxford, UK.

Brasseur G, S. Solomon (1984) Aeronomy of the Middle Atmosphere, D Riedel Publishing Company, Dordrecht

Brewer, A. W (1949), Evidence for a world circulation provided by the measurements of helium and water vapor distribution in the stratosphere, *Q. J. R. Meteorol. Soc., 75*, 351– 363.

Canziani, P. O (1999), Slow and ultraslow equatorial Kelvin waves: The UARS CLAES view , *Q. J. Roy. Meteor. Soc., 125*, 657–676, doi:10.1256/smsqj.55413.

Canziani, P. O., Holton, J. R., Fishbein, E., Froidevaux, L., and Waters, J. W (1994),Equatorial Kelvin waves: A UARS MLS view, *J. Atmos. Sci., 51*, 3053–3076.

Chang, C.P (1976): Vertical structures of tropical waves maintained by internally-nduced cumulus heating, *J. Atmos. Sci., 33*, 729–739.

Cho, H. K., Bowman, K. P., and North, G. R (2004), Equatorial waves including the Madden -Julian oscillation in TRMM rainfall and OLR data, J. Climate, 17, 4387–4406.

Das, S. S., A.R. Jain., K. K. Kumar, and D. N. Rao (2008), Diurnal variability of the tropical tropopause: Significance of VHF radar measurements, *Radio Sci., 43*, RS6003, doi:10.1029/2008RS003824.

Danielsen, Edwin F., (1982), A dehydration mechanism for the stratosphere, Geophys. Res.Lett., 9, 605-608.

Danielsen, Edwin F., (1993), In situ evidence of rapid, vertical, irreversible transport of lower tropospheric air into the lower stratosphere by convective cloud turrets and by larger-scale upwelling in tropical cyclones, J. Geophys. Res., 98, 8665-8681

Dickson, R.E., (1971), Analytic model for zonal winds in the tropics.II. Validation of thr tropospheric mean structure with season and defferences between hemispheres. *Mon. Wea. Rev., 99*, 511-523

Dunkerton, T. J (1997), The role of gravity waves in the quasi-biennial oscillation, *J. Geophys.Res*., 102, 26,053-26,076.

Dunkerton, T. J., and D. P. Delisi (1985), Climatology of the equatorial lower stratosphere, *J. Atmos. Sci*., *42*, 376–396.

Eliassen, A., and E. E. Palm (1961), On the transport of energy in stationary mountain waves, *Geophys. Publ*., *22*, 1–23.

Ern, M., Preusse, P., Krebsbach, M., Mlynczak, M. G., and Russell III, J. M (2008), Equatorial wave analysis from SABER and ECMWF temperatures, *Atmos. Chem. Phys*., *8*, 669 845–869.

Fjeldbo, G., A. Kliore, and V.R.Eshleman (1971), The natural atmosphrere of venus as studied with mariner 5 dual radio frequency occltation experiment, *Radio Sci. 4*, 897-897

Frederick, J. E., and A. R. Douglass,(1983): Atmospheric temperatures near the tropical tropopause: Temporal variations, zonal asymmetry and implications for stratospheric water vapor. *Mon. Wea. Rev*., *111*, 1397–1401.

Friend, A.W (1939), Continuous determination of air mass boundaries by radio, *Bull, Amer. Meteor.Soc., 20* 202.

Fritts, D.C., and M.J.Alexander (2003), Gravity wave dynamics and effects in the middle atmosphere, *Rev.Geophys., 41,* 3.1-3.64.

Fueglistaler, S., A. E. Dessler, T.J. Dunkerton, I. Folkins, Q. Fu, and P.W, Mote. (2009), *Tropical tropopause layer*, *Rev. Geophys., 47*, RG1004, doi:10.1029/2008RG000267.

Fukao, S., R. M. Harper, and S. Kato (1980), Radio wave scattering from the tropical mesosphere observed with the Jicamarca radar, *Radio Sci., 15,* 447-457.

Fulton, S. R. and W.H.Schubert (1985), Vertical normal mode transforms: Theory and application, *Mon. Weather Rev., 113,* 647–658.

Gage K.S. and G.C.Reid (1987), Longitudinal variations in tropical tropopause properties in relation to tropical convection and El Niño Southern Oscillation events, J,Geophys.Res.,92, 141,97-14,203 .

Gage, K. S., and J. L. Green, (1982), An objective method for the determination of tropopause height from VHF radar observations, *J. Appl. Met*., *21*, 1150-1154.

Gage, K.S., and J.L.Green (1978), Evidence for specular reflection from monostatic VHF radar observations of the stratosphere, Radio Sci., 13, 991-1001.

Gage, K. S., B. B. Balsley (1980), On the scattering and reflection mechanism constituting to clear air echoes from troposphere, stratosphere and mesosphere, *Radio Sci*., *15*, 293.

Gage, K. S., B. B. Balsley, and J. L. Green (1981), Fresnel scattering model for the specular echoes observed by VHF radar, *Radio Sci*., *16*, 1447-1453.

Gage, K. S., W. L. Ecklund, A. C. Riddle, and B. B. Balsely (1986), An Objective tropopause height determination using low resolution VHF radar observation, *J. Atmos. Oce. Tech*., *3*, 248-254.

Gage, K. S., W. L. Ecklund, and B. B. Balsley (1985), A modified Fresnel scattering model for the parameterization of Fresnel returns, *Radio Sci*., *20*, 1493-1501.

Gage, K.S., and J.L.Green (1978), Evidence for specular reflection from monostatic VHF radar observations of the stratosphere, *Radio Sci*., *13,* 991-1001.

Garcia, R. R., and M. L. Salby (1987), Transient response to localized episodic heating in the tropics. part II: Far-field behavior, *J. Atmos. Sci., 44*, 499– 530.

Garcia, R. R., R. Lieberman, J. M . Russell III, and M.G. Mlynczak, (2005), Large-scale waves in the mesosphere and lower thermosphere observed by SABER, *J. Atmos. Sci.*, *62*, 4384–4399.

Geller, M. A., X.-L. Zhou, and M. Zhang, 2002: Simulations of the interannual variability of stratospheric water vapor. *J. Atmos. Sci*., *59*, 1076–1085.

Gettelman, A. and T. Briner (2007), Insights into Tropical Tropopause Layer processes using global models, *J.Geophys. Res., 112*, D23104, doi:10.1029/2007JD008945.

Gettelman, A., and P. M. de F. Forster (2002), A climatology of the tropical tropopause layer, *J. Meteorol. Soc. Jpn., 80*, 911–942.

Gettelman, A., J. R. Holton, and A. R. Douglass (2000) Simulations of water vapor in the lower stratosphere and upper troposphere. *J. Geophys. Res.*, *105*, 9003–9023.

Gettelman, A., M.L.Salby, and F. Sassi (2002), The distribution and influence of convection in the tropical tropopause region, *J. Geophys. Res.*, 107:D10, doi :10.1029/2001JD001 048.

Gorbunov M.E, and S.V. Sokolovsky (1993), Remote sensing of refractivity from space for global observations of atmospheric parameters, *Report 119*, Max Plank Institute for Meteorology, Hamburg, Germany.

Hartman, D. L. and K. Larson (2002), An important constraint on tropical cloud-climate feedback, *Geophys. Res. Lett., 29*, doi: 10.1029/2002GL015 835.

Highwood E.J., B.J.Hoskins (1998), The tropical tropopause. *Quart. J. Roy. Meteor. Soc. 124*: 1579-1604.

Hitchman, M. H. and C.B.Leovy (1988), Estimation of the Kelvin wave contribution to the semiannual oscillation, *J. Atmos. Sci.*, *45*, 1462–1475.

Hocking, W. K., and J. Röttger (1983), Pulse-length dependence of radar signal strengths for Fresnel backscatter, *Radio Sci.*, *18*, 1312-1324.

Hoerling M, K.Schaak, A.Lenzen (1991), Global objective tropopause analysis. *Mon. Wea. Rev. 119*, 1816–1831.

Hoinka K.P (1998), Statistics of the Global Tropopause Pressure, *Mon. Weather Rev. 126*, 3303-3325.

Holton, J. R., and A. Gettelman (2001), Horizontal transport and the dehydration of the stratosphere. Geophys. Res. Lett., 28, 2799– 2802.

Holton J.R (2004), An Introduction to Dynamic Meteorology, *Elseveir Acadmeic Press, Burlington,* USA,ISBN. 0-12-350015-1

Holton J.R., P.H. Haynes, M.E.McIntyre, A.R.Douglass, R.B.Rood, L.Pfister (1995), Stratosphere-troposphere exchange. *Rev. Geophys. 33*, 403–439.

Holton, J. R., and R. S. Lindzen (1972), An updated theory for the quasi-biennial cycle of the tropical stratosphere, *J. Atmos. Sci*., *29*, 1076–1080.

Holton, J.R (1979)., An Introduction to Dynamic Meteorology, Academic Press, New York, 1979.

Holton, J.R (1982), Waves in the equatorial stratosphere generated by tropospheric heat sources. *J. Atmos. Sci.*,*37*,1077-1087.

Holton, J.R (1984), Troposphere-stratosphere exchange of trace constituent: The water vapor puzzle, in *Dynamic of the Middle Atmosphere*, edited by J.R. Holton and T. Matsuno, pp. 369-385, *Trra Sci. Tokyo*.

Horel, J. D., and J. M. Wallace (1981), Planetary-scale atmospheric phenomena associated with the Southern Oscillation, Mon. Weather Rev., 109, 813-829.

Hoskins B.J, M.E.McIntyre, A.W.Robertson (1985), On the use and significance of isentropic potential vorticity maps, *Quart. J. R. Met. Soc. 111*, 877- 946.

Haynes P.H.and T.G.Shepherd (2001), Report on the SPARC Tropopause Workshop. *SPARC Newsletter, 17,* 3-10

Jhonson R.H (1986), Short-term variation of the tropopause height over Winter Monex area, *J. Atmos. Sci., 343*,1152-1163.

Johnson, R. H., and P. E. Ciesielski (2000), Rainfall and radiative heating rates from TOGA COARE atmospheric budgets, *J. Atmos. Sci., 57*, 1497–1514.

Johnson, R. H., and D. C. Kriete (1982), Thermodynamic and circulation characteristics of winter monsoon tropical mesoscale convection, Mon. Weather Rev., 110, 1898–1911.

Karus, E.B (1973), Comparison between ice age and present general circulations, *Nature 245*, 129-133

Kiladis, G. N., K. H. Straub, G. C. Reid, and K. S. Gage (2001), Aspects of interannual and intraseasonal variability of the tropopause and lower stratosphere. *Quart. J. Roy. Meteor. Soc.,127*, 1961–1984.

Kley, D., A. L. Schmeltekopf, K. Kel!y, R. H. Winkler, T. L (1982). Thompson, and M. McFarland, Transport of water through the tropical tropopause, Geophys. Res. Lett., 9, 617-620.

Kirk-Davidoff, D. B., E.J.Hintsa, J.Anderson, and D.W. Keith (1999) The effect of climate change on ozone depletion through changes in stratospheric water vapour, *Nature, 402,* 399–401.

Kolmogorov, A.N (1941), Local strcture in trubulence in incompressible fluid with very high Reynolds numbers, *DAN-SSR,30*, 229.

Krishna Murthy B.V., K.Parmeshwaran, and K.O.Rose (1985), Temporal variation of the tropopause charateristics, *J. Atmos. Sci., 43*, 914-922,986.

Krishna Murthy, B.V., K. Satheesan, K. Parameswaran, M. N. Sasi, G. Ramkumar, Y. B. Kumar, K. Raghunath, M. Krishniah (2002), Equatorial waves in temperature in the altitude range 4 to 70 km. *Q. J.R. Meterol. Soc. 128,* 819–837.

Kuang , Z. and C.S.Bretherton (2004), Convective influence on the heat balance of the tropical tropopause layer: A cloud resolving model study, *J. Atmos. Sci*, *61*, 2919-2927.

Kuo YH., Wee TK, Sokolovskiy S, Rocken C, Schreiner W, Hunt D, and Anthes RA (2004), Inversion and error estimation of GPS radio occultation data, *J. Meteorol. Soc. Jpn., 82*,507–531.

Kursinski, E.R., G.A. Hajj, J.T, Schofield, R.P. Linfield and R.R.Hard (1997), Observing Earth's atmosphere with radio occultation measurements using the Global Positioning System. *J. Geophys. Res. 102*, 23,429– 23,465.

Lau, K.-M., and P. H. Chan (1985), Aspects of the 40–50 day oscillation during the northern winter as inferred from outgoing longwave radiation, Mon. Weather Rev., 113, 1889–1909.

Lieberman, R. S. and D.Riggin (1997), High resolution Doppler imagerobservations of Kelvin waves in the equatorial mesosphere and lower thermosphere, *J. Geophys. Res., 102*, 26 117–26 130,1997.

Lohmann, M.S (2007), Analysis of global positioning system (GPS) radio occultation measurement errors based on Satellite de Aplicaciones Cientificas- C (SAC-C) GPS radio occultation data recorded in open-loop and phase-locked-loop mode, *J. Geophys. Res. 112*: D09115, doi:10.1029/ 2006JD007764.

Madden, R. A., and P. R. Julian (1972), Description of global-scale circulation cells in the tropics with a 40–50 day period, *J. Atmos. Sci., 29*, 1109–1123.

Manabe, S., and B. G. Hunt (1968), Experiments with a stratospheric general circulation model, I, Radiative and dynamic aspects, Mon. Weather Rev., 96, 477-502.

Mapes, B. E. and J.R.A. Houze (1995) Diabatic divergence profiles in tropical mesoscale convective systems, *J. Atmos. Sci.*, *52*, 1807– 1828.

Mapes, B.E (1993), Gregarious tropical convection, *J. Atmos. Sci.*, *50*, 2026-2037.

Mehta, S. K., B. V. Krishna Murthy, D. N. Rao., M. V. Ratnam, K. Parameswaran, K. Rajeev, C. S. Raju, and K.G.Rao (2008), Identification of tropical convective tropopause and its association with cold point tropopause, *J. Geophys. Res.*, *113*, D00B04, doi:10.1029/2007JD009625

Meehl, G. A. (1994) Coupled land–ocean–atmosphere processes and the South Asian Monsoon Variability. *Science*, 266, (5183), 263–7.

Miyakawa. T., and T.Satomura (2006),Seasonal Variation and Environmental Properties of Southward Propagating Mesoscale Convective Systems over the Bay of Bengal, *SOLA, 2,* 088-091, doi:10.2151/sola.2006-023.

Mohanakumar, K. (2008), Stratosphere Troposphere Interactions -An Introduction, *Springer.*

Mohanakumar K, P.A.Pillai (2008) Stratosphere troposphere interaction associated with biennial oscillation of Indian summer monsoon, *J Atmos Terr Phys*, 70(5): 764–773

Mote, P. W., K. H. Rosenlof, M. E. McIntyre, E. S. Carr, J. C. Gille, J. R. Holton, J. S. Kinnersley, and H. C. Pumphrey (1996), An atmospheric tape recorder: The imprint

Narayana Rao D.,M.V.Ratnam, B.V.K.Murthy, V.V.M.J. Rao, S. K. Mehta, D. Nath, S.G Basha (2007). Identification of tropopause using bending angle profile from GPS radio occultation (RO): A radio tropopause, *Geophys. Res. Lett. 34*, L15809, doi:10.1029/2007GL029709.

Naujokat, B., (1986), An update of the observed quasi-bieenial oscillation of the stratospheric winds over the Tropics. J. Atmos. Sci., 43, 1873–1877.

Newell R.E, J.W.Kidson and D.G. Vincent (1969), Annual and biennial modulation in tropical Hadley cell circulation, *Nature, 222*, 76-78.

Newell, R. E., and B.C. Weare (1976a), Ocean temperatures and large-scale atmospheric variations, *Nature, 262*, 40-41.

Newell, R. E., and B.C. Weare (1976b), Factors governing tropospheric mean temperature, *Science, 194*, 1413-1414.

Newell, R. E., and S. Gould-Stewart (1981), A stratospheric fountain?, J. *Atmos. Sci., 38*, 2789–2796.

Pan LL, W.J.Rande, B.L.Gary, M.J.Mahoney, E.J.Hintsa, (2004), Definitions and sharpness of the extratropical tropopause: A trace gas perspective. *J. Geophys. Res. 109*, D23103. doi:10.1029/2004JD004982.

Plumb, R. A (1977), The interaction of two internal waves with the mean flow: Implications for the theory of the quasi-biennial oscillation, *J. Atmos. Sci*., *34*, 1847–1858.

Plumb, R. A., and R. C. Bell (1982), A model of the quasi-biennial oscillation on an equatorial beta-plane. Quart. J. Roy. Meteor. Soc., 108, 335–352.

Randel, W. J. and J.C Gille (1991), Kelvin wave activity in the upper stratosphere observed in SBUV ozone data, *J. Atmos. Sci., 48*, 2336–2349, 1991

Randel WJ, D.J.Seidel, L.L.Pan, (2007). Observational characteristics of double tropopauses. *J. Geophys. Res. 112* : D07309. doi: 10.1029/2006JD007904.

Randel, W. J. and F. Wu (2005), Kelvin wave variability near the equatorial tropopause observed in GPS radio occultation measurements, *J. Geophys. Res*., 110(D03102). doi:10.1029/2004JD005006.

Randel, W. J. and J.C. Gille (2000), Kelvin wave variability in the upper stratosphere observedin SBUV ozone data, *J. Atmos. Sci*., 17,971–17,982.

Randel, W. J., B.A.Boville, and J.C.Gille (1990), Observations of planetary mixed Rossby gravity waves in the upper stratosphere, J. Atmos. Sci., 47, 3092–3099.

Randel, W. J., F. Wu, and D. J. Gaffen (2000), Interannnual variability of the tropical tropopause derived from radiosonde data and NCEP reanalyses, *J. Geophys. Res.*, *105*(D12), 15,509–15,523.

Rao, P. B., A. R. Jain, P. Kishore, P. Balamuralidhar, S. H. Damle, and G. Viswanathan (1995), Indian MST radar 1. System description and sample vector wind measurements in ST mode, *Radio Sci., 30* , 1125-1138.

Rasmussen, E. M., and J. M. Wallace (1983), Meteorological aspects of the E1 Nino/Southern Oscillation, *Science, 222*, 1195-1202.

Rasool, S. I (1961)., Effets de l'activit6 solaire sur l'ozone atmosph6rique et la hauteur de la tropopause, *Pure Appl. Geophys., 48*, 93-101.

Ratnam M. V, T. Tsuda, S. Mori, T. Kozu (2006a), Modulation of tropopause temperature structure revealed by simultaneous radiosonde and CHAMPGPS measurements. *J. Meteor. Soc. Japan, 84*:, 6: 989-1003.

Ratnam M.V., T.Tsuda, M. Shiotani, and M. Fujiwara (2005), New Characteristics of the Tropical Tropopause Revealed by CHAMP/GPS Measurements, *SOLA.1*:185-188..

Ratnam, M. V., T. Tsuda, Y. Shibagaki, T. Kozu, and S. Mori (2006b), Gravity wave characteristics over equator observed during CPEA campaign using simultaneous multiple stations data, *J. Meteo. Soc. of Japan*, 84A, 239-257.

Reed, R.J., and C.L.Vlcek, (1969), The annual temperature variation in the lower tropical stratosphere. *J Atmos.Sci*., 26 ,163-167.

Reed, R. J.(1962), Evidence of geostrophic motion in the equatorial stratosphere, *Q. J. R. Meteorol. Soc.*, *88*, 324-327.

Reed, R. J (1964), A tentative model of the 26-month oscillation in tropical latitudes, *Q. J. R. Meteorol. Soc*., *90*, 441–466.

Reed, R. J (1967)., The structure and dynamics of the 26-month oscillation, in *Proceedings of the International Symposium on the Dynamics of Large-Scale Processes in the Atmosphere*, pp. 376–387, Russ. Acad. of Sci., Moscow.

Reed, R. J., W. J. Campbell, L. A. Rasmussen, and R. G. Rogers (1961), Evidence of a downward propagating annual wind reversal in the equatorial stratosphere, *J. Geophys. Res*., *66*, 813–818.

Reid, G. C., (1994), Seasonal and interannual temperature variations in the tropical stratosphere, ,*J. Geophys. Res*., *99*, 18923-18932.

Reid, G. C., and K. S. Gage (1981), On the annual variations in the height of tropopause, *J.Atmos. Sci*., *38*, 1928-1938.

Reid, G. C., and K. S. Gage (1985), Interannual variations in the height of tropical tropopause,*J. Geophys. Res*., *90*, 5629-5635.

Reid, G. C., and K. S. Gage (1996), The tropical tropopause over the western Pacific: Wave driving, convection, and the annual cycle, J. Geophys. Res., 101, 21,233–21,241.

Reigber , C.H. Luehr and P.Schwintzer (2002), CHAMP mission status, *Adv,Space Res., 30*(2), 129-134.

Revathy, K., S.R.P. Nayar, and B.V. Krishna Murthy (1996), Deduction of temperature profile from MST radar observations of vertical wind, *Geophys. Res. Lett*., *23*, 285–288.

Revathy, K., S.R.P. Nayar, and B.V. Krishna Murthy (1998), Estimation of error in the determination of temperature using MST radar,Ind. *J. Radio Space Phys*., *27*, 241–243.

Riehl, H., and J. S. Malkus (1958), On the heat balance of the equatorial trough zone. *Geophysica*, **6**, 503–538.

Robinson, G. D. (1980), The transport of minor atmospheric constituents between troposphere and stratosphere, Q. *J. R. Meteorol. Soc.*, *106*, 227–253.

Rosenlof, K. H., Seasonal cycle of the residual mean meridional circulation in the stratosphere, *J. Geophys. Res.,*100, 5173-5191, 1995.

Röttger, J., and C. H. Liu (1978), Partial reflection and scattering of VHF radar signals from the clear atmosphere, *Geophys. Res. Lett., 5*, 357-360.

Röttger, J., and M. F. Larsen (1990), UHF/VHF radar techniques for atmospheric research and wind profiler applications, Radar in Meteorology, ed., D. Atlas, 235-286.

Rottger,J., Reflection and scattering of VHF radar signal from refracivity strctures (1980), *Radio Sci*, *15*, 259.

Russell, J. M., III, L. L. Gordley, J. H. Park, S. R. Drayson, W. D. Hesketh, R. J. Cicerone, A. F. Tuck, J. E. Frederick, J. E. Harries, and P. J. Crutzen (1993), The Halogen Occultation Experiment, J. *Geophys. Res., 98*, 10,777–10,798.

Salby, M. L. and Garcia, R. R (1987) Transient response to localized episodic heating in the tropics, Part I: Excitation and short-time near-field behavior, *J. Atmos. Sci., 44*, 458–498.

Salby, M. L., D. L.Hartmann , P.L.Bailey, and J.C.Gille (1984), Evidence for equatorial Kelvin modes in Nimbus-7 LIMS, *J. Atmos. Sci*., *41(2)*, 220–235.

Santer BD, M.F.Wehner, T.M.L.Wigley, R.Sausen, G.A. Meehl, K.E.Taylor, C.Ammann, J.Arblaster, W.M.Washington, J.S.Boyle, W.Brüggemann (2003b), Contributions of anthropogenic and natural forcing to recent tropopause height changes, Science, 301: 479-483.

Santer BD, R.Sausen, T.M.L.Wigley, J.S.Boyle, R.K.Achuta, C.Doutriaux, J.E.Hansen, G.A Meehl E.Roeckner, R.Ruedy, G.Schmidt, K.E.Taylor (2003a). Behavior of tropopause height and atmospheric temperature in models, reanalysis, and observations: decadal changes. J. Geophys. Res. 108 :(D1). 4002. doi: 10.1029/2002JD002258.

Sasi, M. N., G. Ramkumar, and V. Deepa (1998), Nonmigrating diurnal tides in the troposphere and lower stratosphere over Gadanki (13.5_N, 79.2_E), *J. Geophys. Res.*, *103*, 19,485– 19,494.

Sasi, M. N., G. Ramkumar, and V. Deepa (2001), Tidal wind oscillations in the tropical lower atmosphere as observed by Indian MST Radar, *Ann. Geophys.*, *19*, 991–999.

Satheesan K., and B. V. Krishna Murthy (2005), A study of tropical tropopause using MST radar, *Ann. Geophys.*, *23*,2441-2448.

Sathiyamurthy V, K. Mohanakumar (2002) Characteristics of tropical biennial oscillation and its possible association with Stratospheric QBO, *Geophys Res Lett*, 7: 669–672

Sato, K., F. Hasegawa, and I. Hirota (1994), Short-period disturbances in the equatorial lower stratosphere, J. Meteor. Soc. Japan, 72, 859-872. [Reference therin, Sato,1989]

Sausen R, B.D.Santer (2003), Use of changes in tropopause height to detect human influences on climate. *Meteorol. Zeit. 12:* 131-136.

Schmauss A (1909),. Die obere Inversion, *Meteorol. Zeit. 26* ,251-258.

Schmidt T, Beyerle G. Heise S. Wickert J.Rothacher (2006). A climatology of multiple tropopauses derived from GPS radio occultations with CHAMP and SACC.*Geophys. Res. Lett. 33*,(4). doi: 10.1029/2005GL024600.

Schreiner, W., C. Rocken, S. Sokolovskiy, S. Syndergaard, and D. Hunt (2007), Estimates of the precision of GPS radio occultations from the COSMIC/FORMOSAT-3 mission. *Geophys. Res. Lett. 34*, L04808. doi:10.1029/2006GL027557.

Seidel D J, Randel WJ.2006. Variability and trends in the global tropopause estimated from radiosonde data.J. Geophys. Res. 111: D21101.doi:10.1029/2006JD007363.

Seidel D.J, R.J.Ross, J.K.Angell, G.C.Reid (2001). Climatological characteristics of the tropical tropopause as revealed by radiosonde, *J. Geophys. Res. 108*:7857-7878.

Selkirk H.B (1993), The tropopause cold trap in the Australian monsoon during STEP/AMEX 1987. J. Geophys. Res. 98,: 8591-8610.

Shepherd T.G (2002), Issues in Stratosphere-troposphere Coupling, *J. Meteorol. Soc. Jpn.*, *80*: 769-792.

Sherwood, S. C.(2000), A ‘‘stratospheric drain’’ over the Maritime Continent. Geophys. Res. Lett., 27, 677–680

Shimizu, A., and T. Tsuda (1997), Characteristics of Kelvin waves and gravity waves observed with radiosondes over Indonesia, *J. Geophys.Res., 102,* 26,159– 26,171

Shiotani, M., Gille, J. C., and Roche, A. E.: Kelvin waves in the equatorial lower stratosphere as revealed by cryogenic limb etalon spectrometer temperature data, J. Geophys. Res., 102(D22), 26 131–26 140, 1997.

Silverman R.A.(1956),Turbulent mixing theory applied to radio scattring, J. Appl. Physics, 27, 699, 1956.

Skolnik, M. I., (1980), Introduction to Radar Systems, 2nd ed., Auckland, McGraw-Hill.

Son, S.W., and S. Lee (2007), Intraseasonal variability of the zonal mean tropical tropopause height, J. Atmos. Sci., 64, 2695-2706.

Son, S.W., L.M. Polvani, D.W. Waugh, T. Birner, H. Akiyoshi, R.R. Garcia, A. Gettelman, D.A. Plummer, and E. Rozanov (2009), The Impact of Stratospheric Ozone Recovery on Tropopause Height Trends. *J. Climate, 22*, 429–445.

Srikanth, R. and D.A.Ortland (1998), Analysis of Kelvin Resolution Doppler Imager and Microwave Limb Sounder stratosphere measurements using a constrained least squares method, *J. Geophys. Res*., 103(D18), 23 131–23 151.

Staley, D. O (1957)., A study of tropopause formation, Contrib. Atmos. Phys., 29, , 290-316.

Stohl A, et al (2003). Stratosphere-troposphere exchange: A review and what have we learned from STACCATO? *J. Geophys. Res*. *108*: 8516. doi: 10.1029/2002JD002490.

Stranz, D (1959). Solar activity and the altitude of the tropopause near the equator, J. Atmos. Terr. Phys., 16, 180-182.

Straub, K. H. and G.N. Kiladis (2003) The observed structure of convectively coupled Kelvin waves: Comparison with simple models of coupled wave instability, *J. Atmos. Sci., 60*, 1655–1668.

Stutzman W.L., and G.A. Thiele (1981), Antenna theory and design, *Jhon Wiely and Sons*.

Sunil Kumar S.V., K.Parameswaran, B.V.Krishna Murthy (2003). Lidar observations of cirrus cloud near the tropical tropopause: General features. Atmos. Res. 66: 203-227.

Tapley B.D, S.Battadpu, J.C.Ries,P.F.Thomson, and M.M.Watkinins (2004a), Grace measurements of mass variability in the Earth system, *Science, 305*, 503-505.

Tapley B.D, S.Battadpu, J.C.Ries,P.F. and C. Reigber (2004b), The Gravity Recovery and Climate Experiment: Mission overview and early results, *Geophys. Res. Lett., 31*, L09607.

Tatarskii,V.I (1962) Scattering of electromagnetic waves by turbulent inhomoginitiesin the troposphere, IFA AN SSR, 4,147.

Tatarskii,V.I (1971), The effect of the turbulent atmosphere on wave propagation; *Nat. Tech. Inf. Svc. Springfiled*, Va.

Teitelbaum, H., M. Moustaoui, C. Basdevant and J. R. Holton (2000), An alternative mechanism explaining the hygropause formation in tropical regions, *Geophys. Res. Lett.*, 27, 221-224.

Thuburn, J., and C.G Craig (2002).: On the temperature structure of the tropical sub-stratopshere, J. Geophys. Res.,107, doi:10.1029/2001JD00048.

Tindall, J. C., J. Thuburn, and E.J.Highwood (2006a), Equatorial waves in the lower stratosphere. I: A novel detection method, *Q. J. Roy. Meteor. Soc*., *132*, 177–194, doi:10.1256/qj.04.152.

Tindall, J. C., J. Thuburn, and E.J.Highwood (2006b), Equatorial waves in the lower stratosphere. II: Annual and interannual variability, *Q. J. Roy. Meteor. Soc*., *132*, 195–212, doi:10.1256/qj.04.153, 2006.

Tsuda T, M.V.Ratnam , P.T.May, M.J.Alexander, R.A.Vincent, A.MacKinnon (2004), Characteristics of gravity waves with short vertical wavelengths observed with radiosonde and GPS occultation during DAWEX (Darwin Area Wave Experiment). *J. Geophys. Res. 109*, D20S03. doi:10.1029/2004JD004946.

Tsuda, T (1988), Lecture notes, Data acquisition and processing, International School on Atmospheic Rdaras, ed. S.Fukao, Kyoto, Nov. 24-28.

Tsuda T, Y.Murayama , H.Wiryosumarto, S W.B. Harijono, S. Kato (1994). Radiosonde observations of equatorial atmosphere dynamics over Indonesia.1.Equatorial waves and diurnal tides. *J.Geophys. Res. 99*,10491-10505.

Tsuda, T., M. Venkat Ratnam, T. Kozu, and S. Mori (2006), Characteristics of 10 day Kelvin wave observed with radiosondes and CHAMP/GPS occultation during CPEA campaign (April –May 2004), *J. Meteorol.Soc. Jpn., 84A*, 277–293, doi:10.2151/jmsj.84A.277.

Tsuda,T., P.T. May T Satio S Kato and S Fukao (1988), Simultaneous observations of eflection echoes and refractive index gradient in troposphere and lower stratosphere, *Radio Sci*, *23*, 655.

Veryard, R. G., and R. A. Ebdon (1961), Fluctuations in tropical stratospheric winds, *Meteorol. Mag*., *90*, 125–143.

Vomel, H., Oltmans, S.J., Johnson, B.J., Hasebe, F., Shiotani, M., Fujiwara, M., Nishi, N., Agama, M., Cornrjo, J., Paredes, F. and Enriquez, H. Balloon-borne observations of water vapor and Ozone in the upper troposphere and lower stratosphere, J.Geophys.Res., 107, NO.D14, 4210, 10.1029/2001JD000707, 2002.

Wallace, J. M. (1973), General circulation of the tropical lower stratosphere, *Rev. Geophys*., *11*, 191–222.

Wallace, J.M. and V.E. Kousky (1968a) Observational evidence of Kelvin waves in the tropical stratosphere, *J. Atmos. Sci., 25*, 900-907.

Wallace, J.M. and V.E. Kousky (1968b), On the relation between Kelvin waves and the Quasi-Biennial Oscillation, *J. Meteo. Soc. Japan, 46*, 496-502.

Wang P., M.P.rmick ,P.Minnis , G.S.Kent, K.M.Skeens (1996),. A study of the vertical structure of tropical 20S–20N optically thin clouds from SAGE II observations. *Atmos. Res. 48*: 599–614.

Ware et al (1996)., GPS sounding of the atmosphere for Low earth Orbit: Perminary results, Bull.Amer.Meteor. Soc., 77, 19-40.

Wheeler, M. and G.N. Kiladis, Convectively Coupled Equatorial Waves: Analysis of Clouds and Temperature in the Wavenumber-Frequency Domain, *J. Atmos. Sci*., 56, 374–399, 1999.

Wickemann, 1983;

Wallace, J. M (1973), General circulation of the tropical lower stratosphere, Rev. Geophys. Space Phys., 11, 191-222.

WMO (2003), Scientific Assessment of Ozone Depletion: 2002. Global Ozone Researchand Monitoring Project Report No. 47. World Meteorological Organization, Geneva , Switzerland

Woodman, R. F., and A. Guillen (1974), Radar Observations of Winds and Turbulence in the Stratosphere and Mesosphere, *J. Atmos. Sci., 31*, 491-505.

World Meteorological Organization.(1957). Meteorology—A three dimensional science, *WMO Bull. 6*, 34–138.

Yamamoto, M. K., M. Fujiwara, T. Horinouchi, H. Hashiguchi, and S. Fukao (2003), Kelvin-Helmholtz instability around the tropical tropopause observed with Equatorial Atmosphere Radar, *Geophys. Res. Lett., 30* (9), 1476, doi:10.1029/2002GL016685.

Yanai, M. and T. Maruyama (1966), Stratospheric wave disturbances propagating over theequatorial pacific, *J. Meteo. Soc. Japan, 44*, 291-294.

Yeh, K.C., and C.H. Liu (1972), Theory of ionospheric waves, Academic press New York, 1972.

Yulaeva, E., J. R. Holton, and J. M. Wallace (1994), On the cause of the annual cycle in tropical lower-stratospheric temperatures, J. Atmos. Sci., 51(2), 169–174.

Zhou, X. L (2000) The tropical cold point tropopause and stratospheric water vapor. Ph.D. dissertation, State University of New York at Stony Brook, 121 pp.

Zhou, X. L. M. A. Geller and M. H. Zhang (2001a), The cooling trend of the tropical cold point tropopause temperatures and its implications. *J. Geophys. Res., 106*, 1511–1522.

Zhou, X. L. M. A. Geller and M. H. Zhang (2001b), Tropical cold point tropopause characteristics derived from ECMWF reanalyses and soundings. *J. Climate*, 14, 1823–1838.

Zhou, X. L., and J. R. Holton (2002), Intraseasonal variations of tropical cold point tropopause temperatures. *J. Climate*, 15, 1460-1473.

Zhou, X. L. M. A. Geller and M. H. Zhang (2004), Temperature Fields in the Tropical Tropopause Transition Layer, *J. Climate*, 15, 2901–2908.

Publications

Under preparation

1. **Sanjay Kumar Mehta**, M.Venkat Ratnam, B.V. Krishna Murthy ; Modulation of the tropical tropopause by Equatorial wave during phase of quasi biennial oscillation , *J. Atmos. Sci*, 2010 (Manuscript under preparation) [Contents of chapter 7]

Submitted

2. **Sanjay Kumar Mehta**, M.Venkat Ratnam, B.V. Krishna Murthy; Longitudinal Characteristics of the tropical tropopause, *J. Geophys. Res.*, **2010**, (Submitted) [Contents of chapter 5]

Under revision

3. **Sanjay Kumar Mehta**, M.Venkat Ratnam, B.V. Krishna Murthy; Characteristics of the Multiple tropopause in the tropics, *QJRMS*, under revision, **2009**. [Contents of chapter 6]

4. T. K.Ramkumar, K. Niranjan kumar and **Sanjay Kumar Mehta**; MST radar observations of characteristics of lower atmospheric high frequency gravity waves passing through the tropical easterly jet, *J. Geophys. Res*., under review, **2009**

Published

5. **Sanjay Kumar Mehta**, M.Venkat Ratnam, B.V. Krishna Murthy; Variability of the Tropical Tropopause over Indian Monsoon Region, *J. Geophys. Res.*, Accepted, **2010**, paper in press. [Contents of chapter 4]

6. **Sanjay Kumar Mehta**, B.V. Krishna Murthy , D.Narayana Rao, M.Venkat Ratnam, K. Parameswaran, K. Rajeev, C. Suresh Raju, and Kusuma G Rao:Identification of tropical convective tropopause and its association with cold point tropopause,*J. Geophys. Res.*,*113*,D00B04,doi:10.1029/2007JD009625,**2008.** [Contents of chapter 3]

7. Sunilkumar S.V., K. Parmeshwaran, K. Rajeev, B.V. Krishna Murthy, S.Meenu, **Sanjay Kumar Mehta**, Asha Babu: Semitransparent cirrus clouds in the tropical tropopause layer during two contrasting seasons, *JASTP*, **2010**, 72, 745-762

8. Rao.D.N, M. V.Ratnam, B. V. Krishna Murthy, V.V.M.Jagannadha Rao, **Sanjay Kumar Mehta**, Debashis Nath and Ghouse Basha,:Identification of Tropopause using Bending Angle profile from GPS Radio Occultation (RO): A Radio Tropopause ,***Geophys Res. Lett.***,*34*,L15809,doi:10.1029/2007GL029709,**2007.**

9. Rao,D.N, M. Venkat Ratnam**, Sanjay Kumar Mehta**, Debashis Nath , Ghouse Basha, V. V. M. Jagannadha Rao,,B. V. Krishna Murthy,T. Tsuda and Kenji

Nakamura,Validation of the COSMIC data over Gadanki (13.48N, 79.2E): A tropical region ***Terr. Atmos. Ocean. Sci***., Vol. 20, No. 1, 59-70, doi: 10.3319/TAO.2008.01.23.01 (F3C)**, 2009.**

10. K. Rajeev, K.Parameswaran, S. Meenu, S.V. Sunilkumar, Bijoy V. Thampi, C. Suresh Raju,B. V. Krishna Murthy,K. S. Jagannath, **Sanjay Kumar Mehta**, D. Narayana Rao,Kusuma G. Rao:Observational assessment of the potential of satellite-based water vapour and thermal IR brightness temperatures in detecting semitransparent cirrus, *Geophys. Res. Lett.*,*35*,L08808,doi:10.1029/2008GL033393, **2008.**

11. **Sanjay Kumar Mehta**, D. Narayana Rao, B. V. Krishna Murthy, K.Parameshwaran, K.Rajeev, C.Suresh Raju, Kusuma G. Rao' S.C.Chakravarty, and K.S.Jagannath:Characteristics of cold and convective tropical tropopause using MST radar, *Proceedings of eleventh international conference on technical and scientific aspects of MST Radar (MST 11)*, pp 621-624, **2007.**

12. **Sanjay Kumar Mehta**, Debashis Nath, D.Narayana Rao and B.V.Krishna Murthy:Day-to-day variations of the tropical tropopause characteristics, *Proceedings of eleventh international conference on technical and scientific aspects of MST Radar (MST 11)* pp 759-762, **2007**.

13. **Sanjay Kumar Mehta**, B.V. Krishna Murthy, D. Narayana Rao, M. Venkat Ratnam, K. Parameswaran, K. Rajeev, C. Suresh Raju, Kusuma G. Rao, " Studies on Diurnal Variation of the tropical Tropopause using MST Radar," *CAWSES-India- Scientific Results* (Phase-1), 207-212, **2009**.

14. Parameswaran, K., S.V. Sunilkumar , Bijoy V Thampi , K. Rajeev , C. Suresh Raju , B.V. Krishna Murthy, **Sanjay Kumar Mehta**, D. Narayana Rao and Kusuma G Rao, "Properties of cirrus clouds in the Tropical Tropopause Layer", *CAWSES-India- Scientific Results* (Phase-1), 187-196, **2009**.

15. Rajeev, K., K.Parameswaran, S. Meenu, S.V. Sunilkumar, Bijoy V. Thampi, C. Suresh Raju, B. V. Krishna Murthy, K. S. Jagannath, **Sanjay Kumar Mehta**, D Narayana Rao, and Kusuma G. Rao, "Thin semitransparent cirrus clouds observed using KALPANA-1 VHRR and its inter-comparison with the Lidar-derived cirrus optical depth", *CAWSES-India- Scientific Results* (Phase-1), 197-306, **2009**.

16. Parameswaran K., S.V. Sunilkumar, K. Rajeev, C. Suresh Raju, D. Narayana Rao, **Sanjay Kumar Mehta**, B.V. Krishna Murthy, S.C. Chakravarthy, Kusuma G Rao, and K.S. Jagnath, Cirrus clouds in the Tropical Tropopause Layer, Proce. *MST 11*

Eleventh International Workshop on Technical and Scientific aspects of MST Radar (Ed. V K Anandan), Macmillan, 552-558, **2007**.

Conference presentations

1) 1st AP Science Congress-2008,held at Osmania University, during 14-16 Nov.2008 (Poster), [**Best Paper Award**]

2) 4th SPARC general assembly, Held at Bologna, Italy, 31Aug-5 sep 2008.(Poster)

3) XV National Space Science Symposium, National Radio Astronomy Center, Ooty, India,26-29 Febuary,2008. (both Poster and Oral)

4) GPS RO Work shop at National Atmospheric Research Laboratory during 10-11Jan 2008 (Oral)

5) CAWSES –India meetings, held at SPL, Tiruvandrum, during 7 Dec 2007 and at ISRO HQ ,Bangalore, during 8-9Jan 2008, (Oral)

6) GPS Radio Occultation Workshop-19th – 20th Apr. 2007 (Attended),Reunion Island International Symposium-2007 held at Saint Gilles, Reunion Island, France (Oral)

7) CAWSES –India workshop, 2007 (Oral)

8) User Scientist workshop, National Atmospheric Research Laboratory, India, Jun.2006 (Oral)

9) MST-11 Workshop, National Atmospheric Research Laboratory, India, Dec.2006 (Both Poster and Oral)

Supplemtary Figures

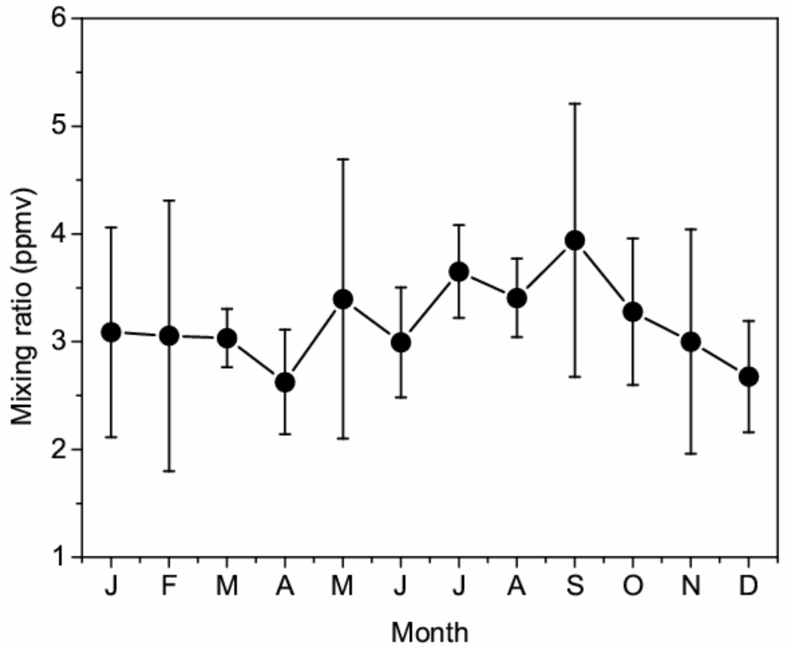

Figure S4.1: *Monthly mean variation of the saturation water vapor mixing ratio at cold point tropopause*

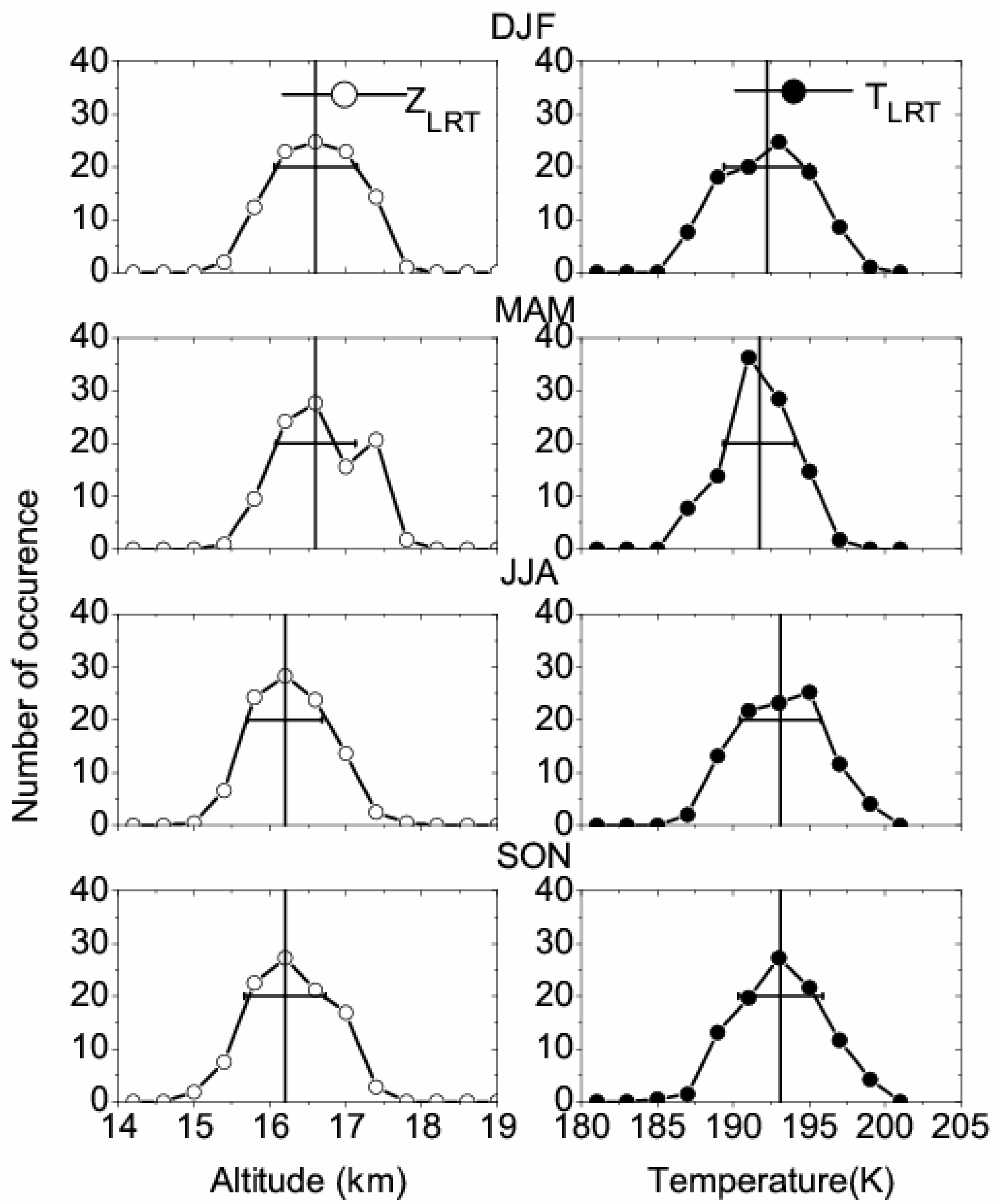

Figure S4.2: *Probability distribution of daily Z_{LRT} (left panels) with 0.4 km interval and T_{LRT} (right panels) with 2 K interval, observed in different seasons. The point at which the vertical line intersects the x-axis represents the mean Z_{LRT} (left panels) and T_{LRT} (right panels) while the length of horizontal bar represents the corresponding standard deviations associated with the respective parameters.*

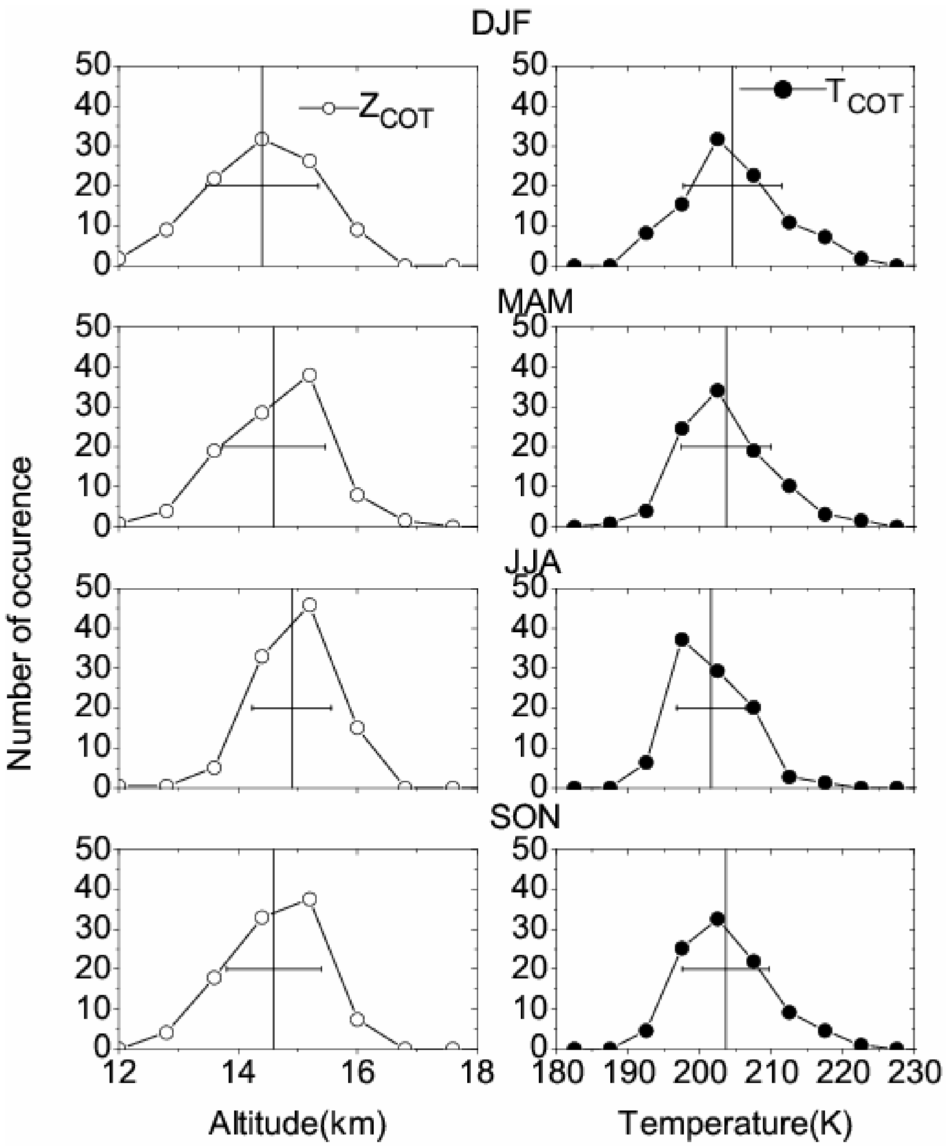

Figure S4.3: *Probability distribution of daily Z_{COT} (left panels) with 0.8 km interval and T_{COT} (right panels) with 5 K interval, observed in different seasons. The point at which the vertical line intersects the x-axis represents the mean Z_{COT} (left panels) and T_{COT} (right panels) while the length of horizontal bar represents the corresponding standard deviations associated with the respective parameters.*

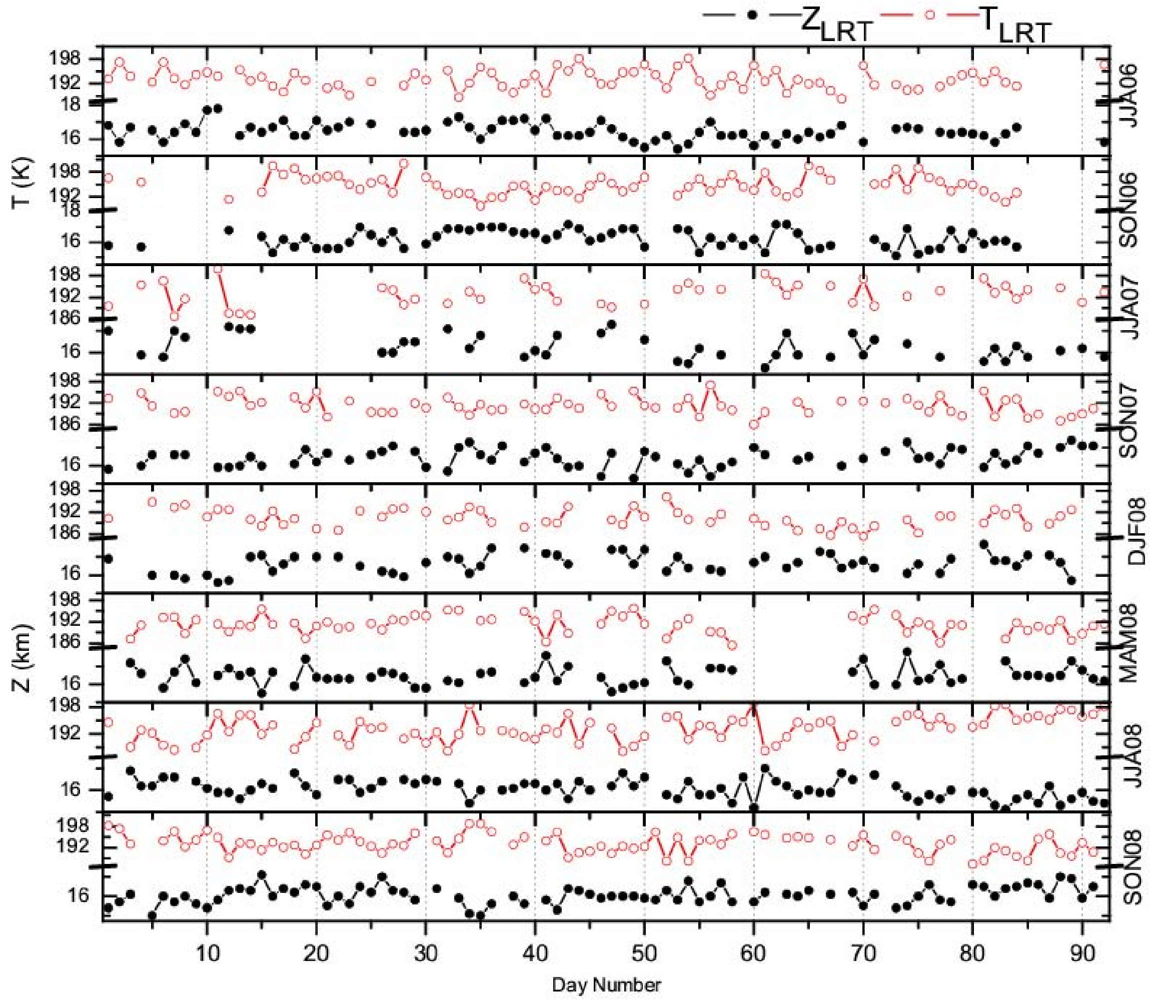

FigureS4.4: *The day-to-day variation observed in the Z_{LRT} and T_{LRT} during different seasons*

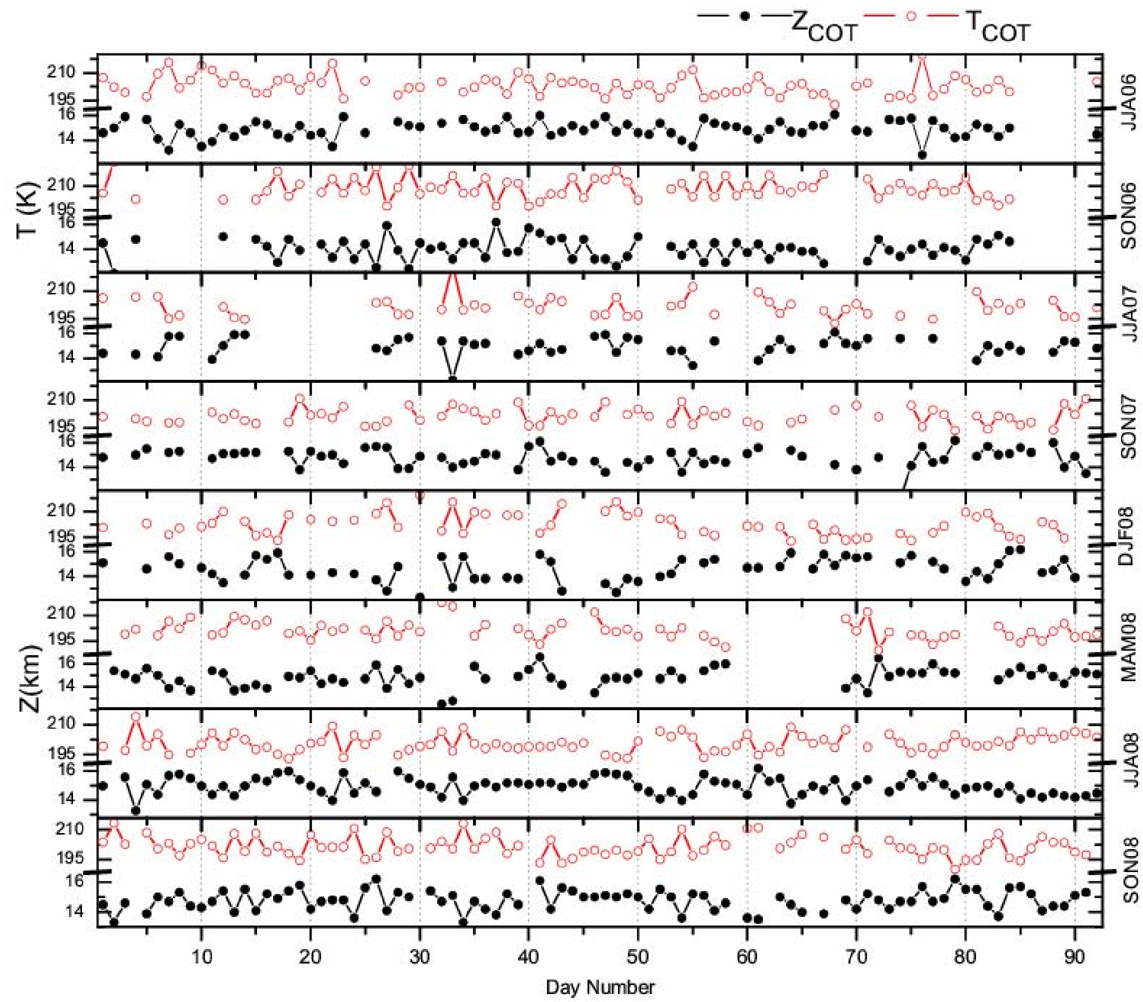

Figure S4.5: *Same as figureS4.4, but for Z_{COT} and T_{COT}*

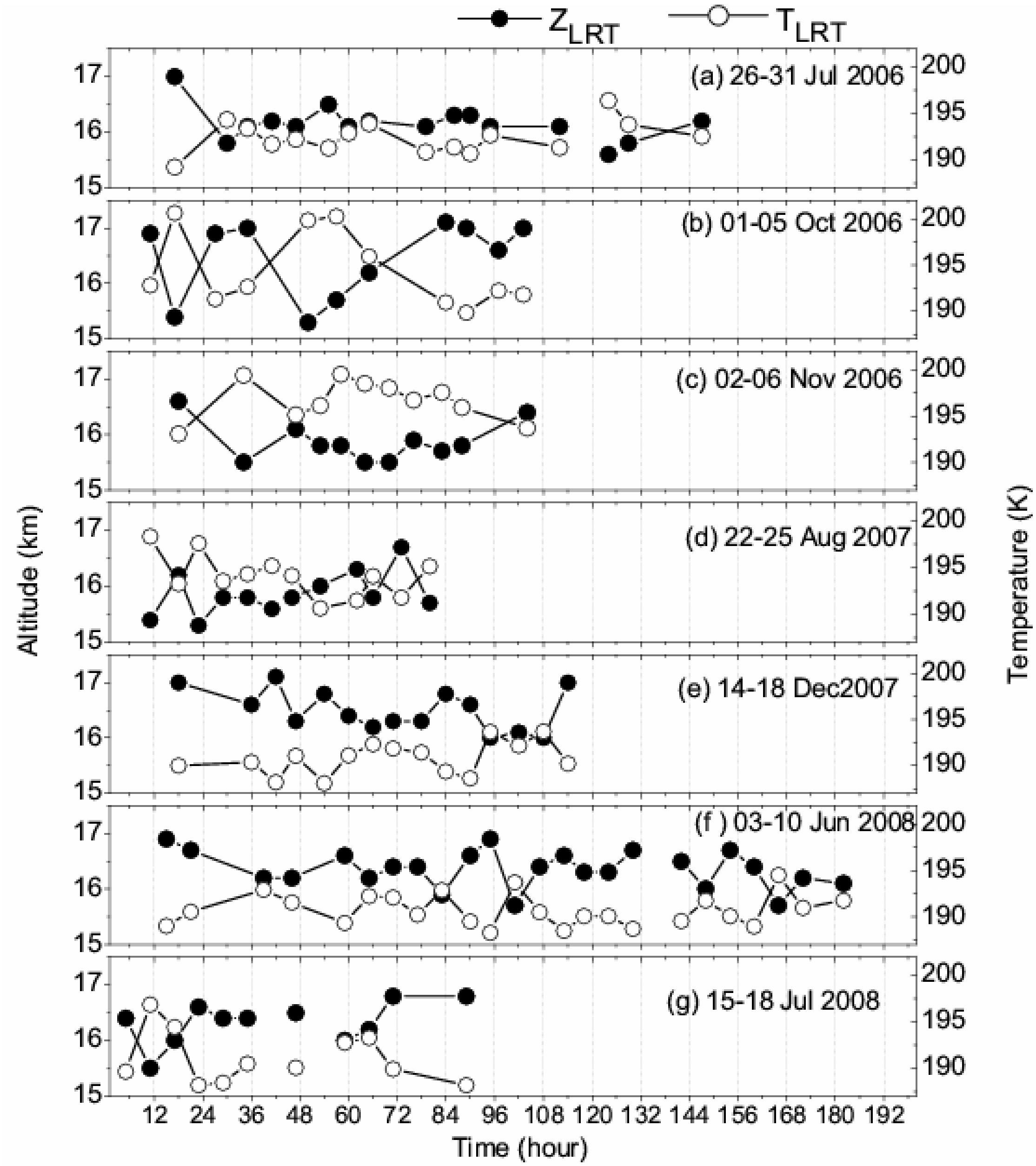

Figure S4.6: *Variation of the Z_{LRT} and T_{LRT} observed within a day in different seasons.*

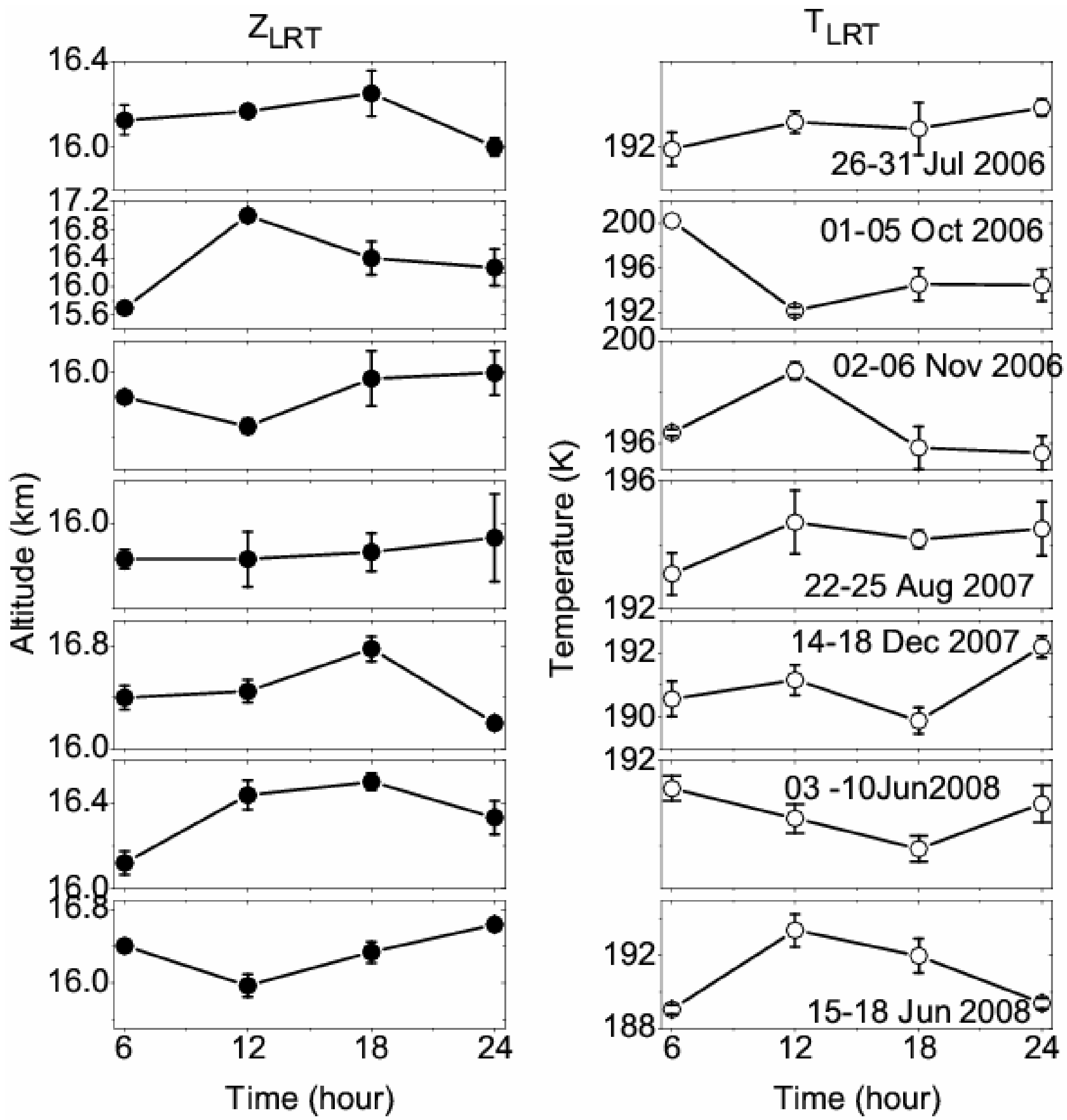

Figure S4.7: *Diurnal variation of the Z_{COT} and T_{COT} corresponding to the data shown in Figure S4.6*

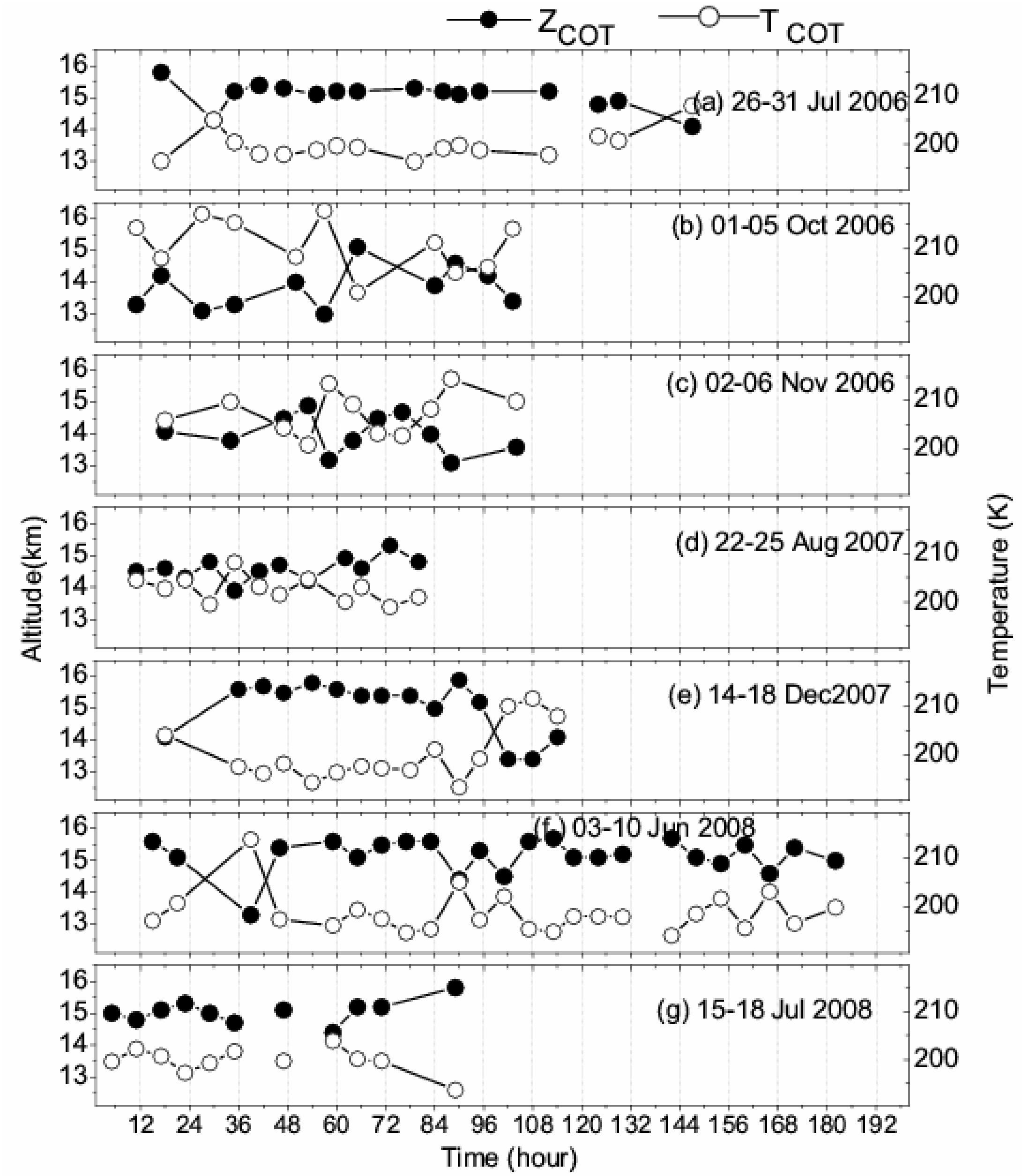

Figure S4.8: *Same as figure S4.6, but observed for Z_{COT} and T_{COT}.*

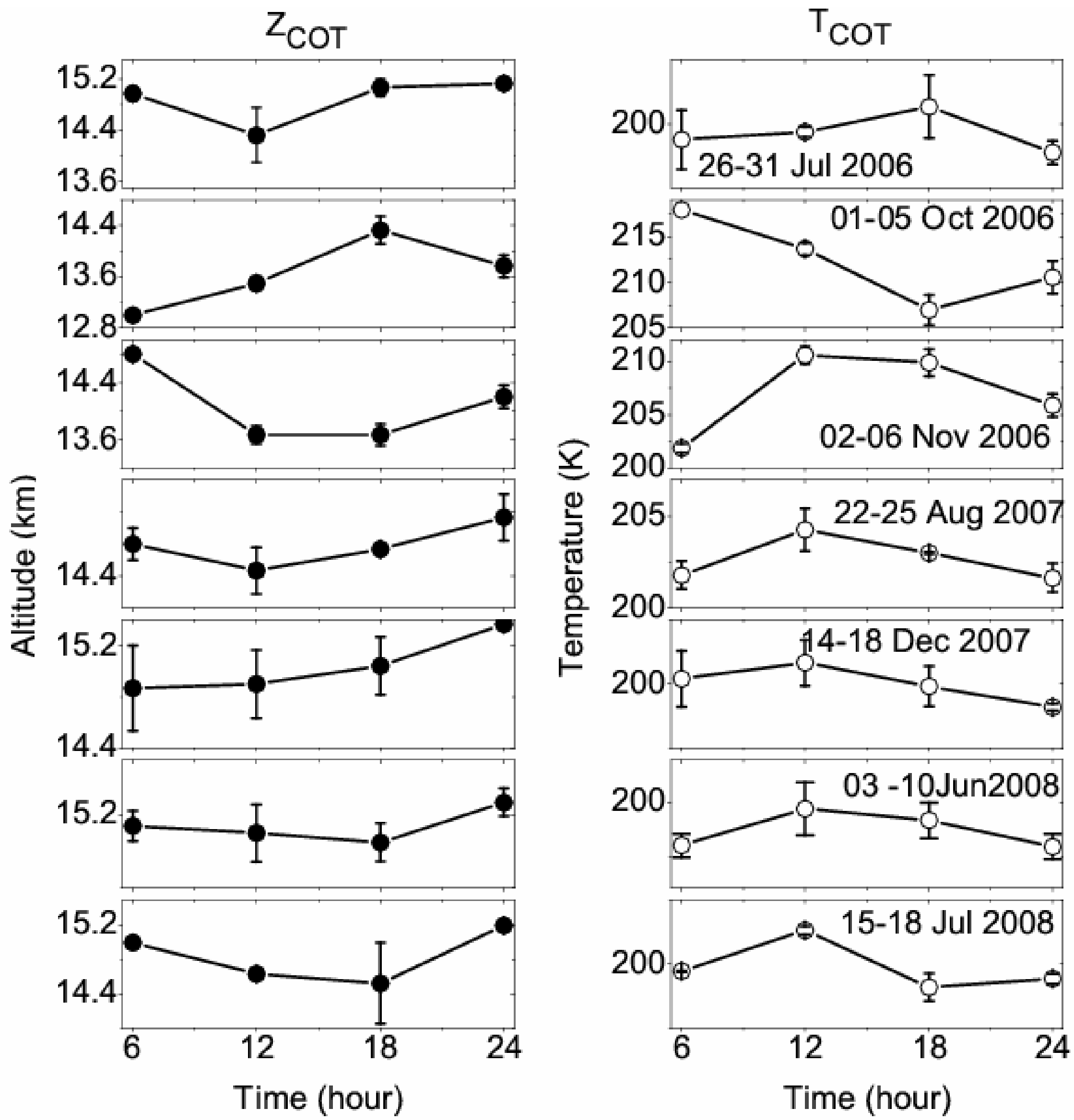

Figure S4.9: *Diurnal variation of the Z_{COT} and T_{COT} corresponding to the data shown in Figure S4.8.*

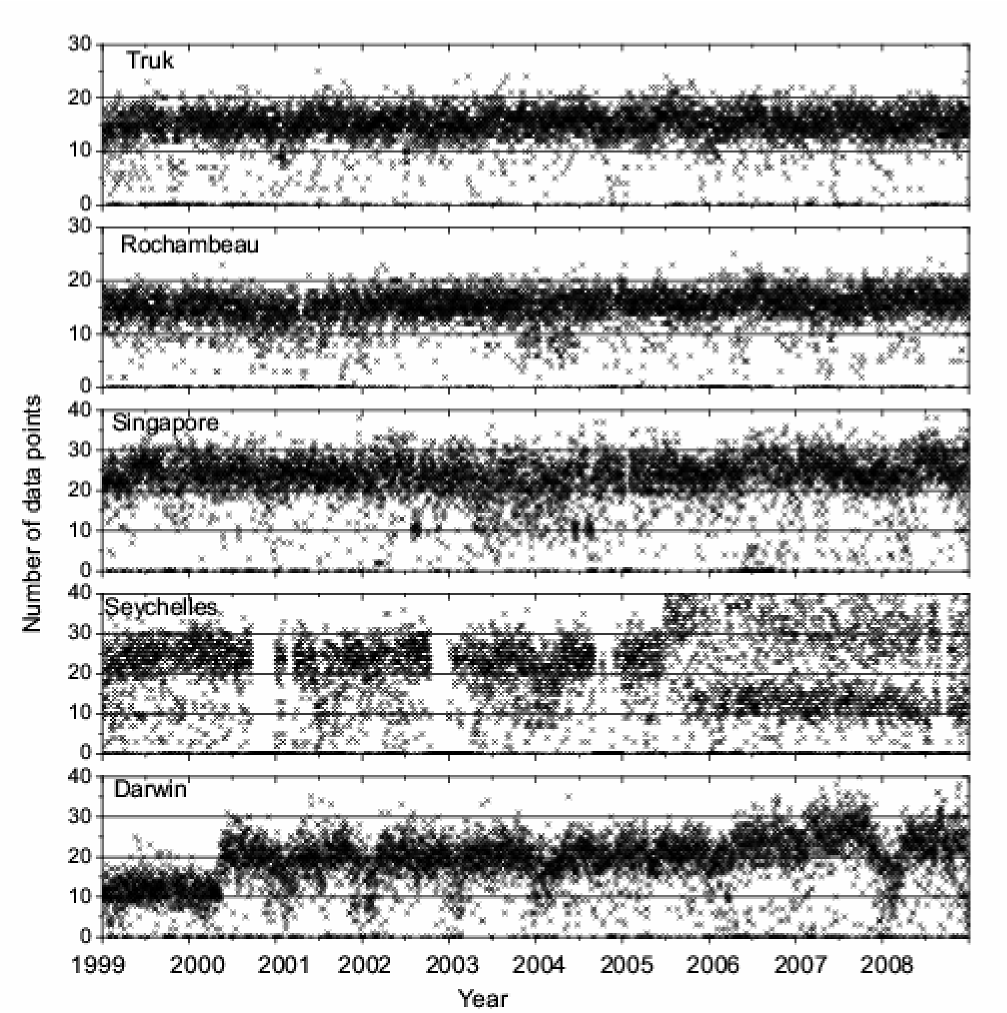

Figure S6.1: *Daily twice time series of the data levels available in the sounding observed over Truk, Rochambeau, Singapore, Seychelles and Darwin between 150-50 hPa (~14.2-20.5 km) for 10 years period 1999-2008*.

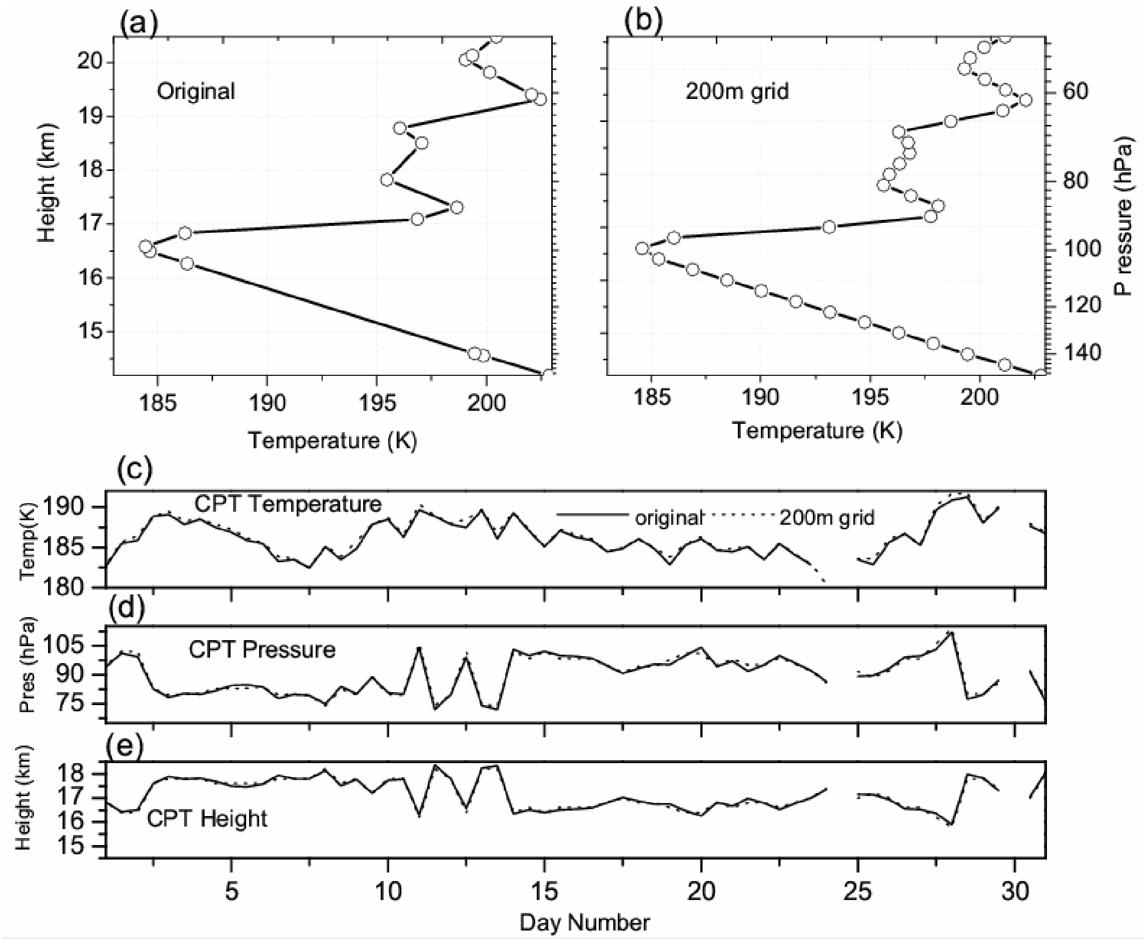

Figure 6.2: *(a) Typical original temperature profile observed over Singapore at 00UTC on January 1, 1999. (b) Corresponding temperature profile adjusted to 200 meter grid by linear fitting. (c) Time series of the cold point tropopause (CPT) temperature, pressure and height for the original (solid line) and 200 m grided data (dotted line) observed at Singapore during January 1999.*

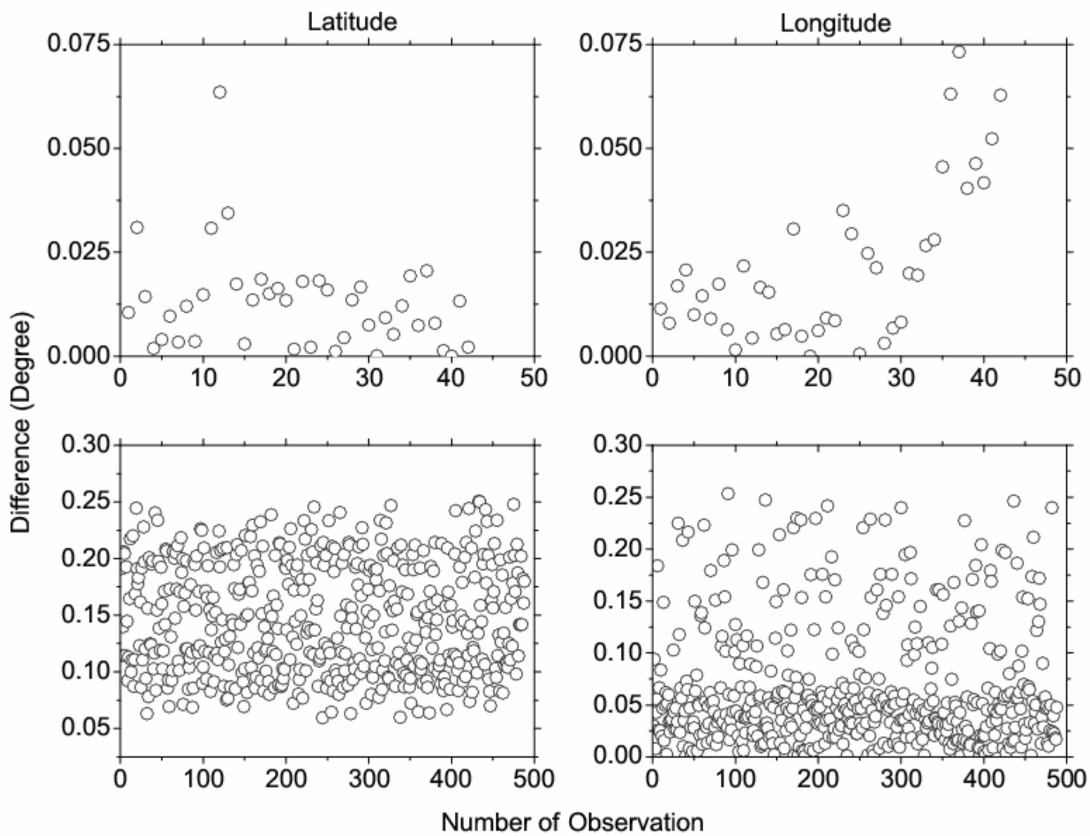

Figure S6.3: *The typical latitude and longitude difference (absolute) between 150-50 hPa for GPS Radiosonde observed over Gadanki during August 2008 (top panel) and GPS RO (COSMIC) data obtained over tropical region ±30^o on 1st Sep 2006 (bottom panel)*

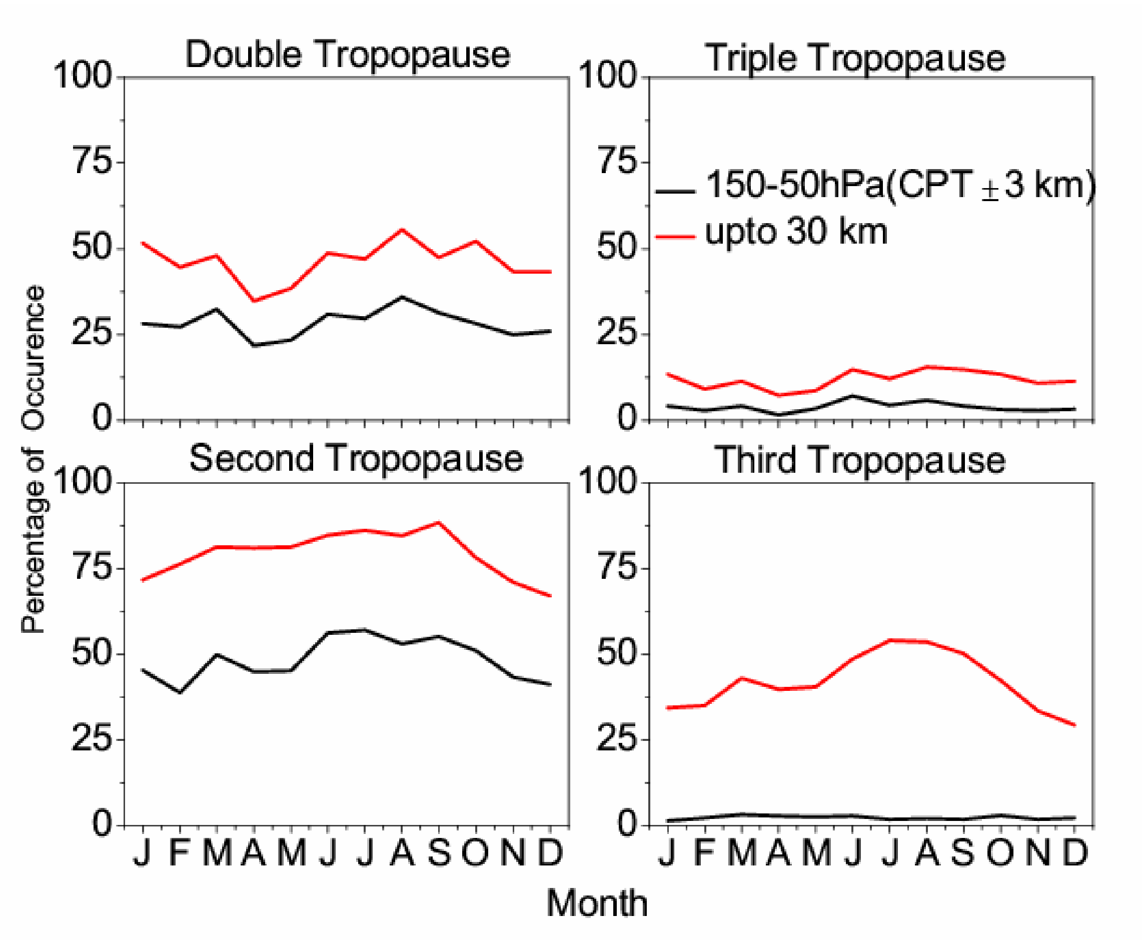

Figure S6.4: *Monthly percentage of occurrence of the MTs observed using WMO method (top panels) and present method (bottom panels) over Singapore during 1999-2008.*

---END---